National Library
of Canada

Acquisitions and
Bibliographic Services Branch

395 Wellington Street
Ottawa, Ontario
K1A 0N4

Bibliothèque nationale
du Canada

Direction des acquisitions et
des services bibliographiques

395, rue Wellington
Ottawa (Ontario)
K1A 0N4

Your file Votre référence

Our file Notre référence

NOTICE

The quality of this microform is heavily dependent upon the quality of the original thesis submitted for microfilming. Every effort has been made to ensure the highest quality of reproduction possible.

If pages are missing, contact the university which granted the degree.

Some pages may have indistinct print especially if the original pages were typed with a poor typewriter ribbon or if the university sent us an inferior photocopy.

Reproduction in full or in part of this microform is governed by the Canadian Copyright Act, R.S.C. 1970, c. C-30, and subsequent amendments.

AVIS

La qualité de cette microforme dépend grandement de la qualité de la thèse soumise au microfilmage. Nous avons tout fait pour assurer une qualité supérieure de reproduction.

S'il manque des pages, veuillez communiquer avec l'université qui a conféré le grade.

La qualité d'impression de certaines pages peut laisser à désirer, surtout si les pages originales ont été dactylographiées à l'aide d'un ruban usé ou si l'université nous a fait parvenir une photocopie de qualité inférieure.

La reproduction, même partielle, de cette microforme est soumise à la Loi canadienne sur le droit d'auteur, SRC 1970, c. C-30, et ses amendements subséquents.

Canada

A MULTINUCLEAR MAGNETIC RESONANCE STUDY OF THE STRUCTURES AND DYNAMICS OF La(III) COMPLEXES IN SOLUTION

By

ZHIGANG CHEN

A thesis presented to the University of Ottawa

in partial fulfilment of the requirements for the degree of

DOCTOR OF PHILOSOPHY

Christian Detellier

Research Supervisor

Zhigang Chen

Ph. D. Candidate

Department of Chemistry

University of Ottawa

Ottawa, Canada

ISBN 0-315-82581-2

UNIVERSITÉ D'OTTAWA
UNIVERSITY OF OTTAWA

ACKNOWLEDGEMENTS

First and foremost, I would like to thank my research supervisor, Professor Christian Detellier, for his great guidance and inspiration throughout my studies.

Dr. Heather Dettman, Mr. Raj Capoor, and Dr. Tony Williams of the NMR facility are thanked for their expert assistance.

I wish to thank my colleagues in our group and in this department. I have always appreciated their help.

The crystallographic analysis of the La(III) - crown ether complexes presented in this thesis was done by Dr. Corinne Bensimon. I would like to express my gratitude to her.

Finally, I would like to thank my family, in China and in Canada, for their support and patience. I would especially like to thank my wife, Zhanyun, for her constant support and encouragement throughout my studies. This thesis is dedicated to all of my family, and especially to my grandmother.

To my grandmother

To my wife, Zhanyun

ABSTRACT

The structural and dynamic behaviours of La(III) complexes in solution have been investigated by multinuclear magnetic resonance spectroscopy. In the aqueous solutions of lanthanum nitrate, chloride, and perchlorate, the ^{139}La NMR data were accounted for by the presence of 1:1 inner sphere complexes of La(III) with all three anions. The thermodynamic stability constants of formation of these ion pairs were determined by introducing activity coefficient effects to the data analysis. The quadrupolar relaxation mechanism of ^{139}La in the aqueous solutions of the lanthanum salts was discussed. The fast solvent exchange in the La(III) solvation shell is one of the major contributions to the ^{139}La quadrupolar relaxation. In the acetonitrile solution of $La(NO_3)_3$ 6 H_2O, a combined ^{139}La and ^{17}O NMR study revealed the existence of the following equilibrium:

$$\{La(NO_3)_3\ (AN)_x\} \quad + \quad H_2O \quad \rightleftharpoons \quad \{La(NO_3)_3\ H_2O(AN)_y\}$$

The NMR results have been quantitatively interpreted through this model. The detailed analysis of ^{17}O NMR spectra of H_2O allowed the indirect coupling constant between the ^{17}O of the coordinated water and ^{139}La to be estimated.

The main focus of the present work was given to the thermodynamic,

structural, and dynamic studies of La(III) complexes with crown ethers in non-aqueous solutions. In the methanol solution of $LaCl_3$ 7 H_2O, a 1:1 complex of La(III) with 18C6 was formed. The formation constant for the complex was determined from the full lineshape analysis of the experimental ^{139}La NMR spectra. In contrast, no complexation between La(III) and crown ether was detected by ^{139}La NMR in the system of $LaCl_3$ 7 H_2O - B15C5 - Methanol. The complexation of La(III) with crown ethers in the acetonitrile solutions of $La(NO_3)_3$ 6 H_2O was investigated through both cation and ligand nuclei NMR. Stable 1:1 cation : crown ether complexes were formed between La(III) and 18C6, B15C5, and 15C5. During the course of the complexation, the crown ethers entered to the first coordination shell of La(III) by replacing the coordinated water and most probably the solvent (AN) molecules. The crystals of these complexes were prepared and their structures were determined by X-ray crystallography. In all the cases, the La(III) cations were coordinated by the oxygen atoms from three bidentate nitrate anions and from the crown ethers.

Both cation and ligand exchanges are slow in the system $La(NO_3)_3$ 6 H_2O - 18C6 - AN. However, 18C6 chemical exchange was measurable by a magnetization transfer technique at high temperature. The rate constant for the exchange is $k = 0.15\ s^{-1}$ at 333 K. For the system involving B15C5, the cation chemical exchange was investigated by ^{139}La NMR. A dissociative exchange mechanism is one of the contributions to the La(III) exchange. This was confirmed

by the ^{13}C NMR kinetic study of the ligand exchange. The ligand (B15C5 and 15C5) exchange was studied by ^{13}C and ^{1}H NMR of the crown ethers. This two site exchange occurs only through a dissociative pathway, which is determined by the structures of the complexes. Since the ligand can not make contact with La(III) from both sides of the complexes, the dissociative mechanism must be the major contribution to the crown ether chemical exchange.

An exchange process involving coordinated B15C5 and/or 15C5 was detected by ^{1}H NMR spectra of the ligands. Detailed ^{1}H NMR observations were made on the system involving 15C5. A model involving "inner" and "outer" proton exchange was postulated to account for the ^{1}H NMR experimental data. The mechanistic study showed that the dissociative pathway is responsible for the coordinated 15C5 exchange.

The activation parameters for B15C5 and 15C5 chemical exchanges were determined through temperature variation studies. Although the ligand exchange occurs through a dissociation process, a large negative entropy of activation was obtained. This may be interpreted by a strong solvation of the transition state, during the dissociative process.

The structures of La(III) complexes with crown ethers in solution and in the solid state were compared. It might be concluded that the structures of these complexes in solution are very similar to that in the solid state.

TABLE OF CONTENTS

LIST OF FIGURES AND SCHEMES

Figures:

Schemes:

LIST OF TABLES

SYMBOLS AND ABBREVIATIONS

AN	acetonitrile
15C5	15-crown-5
B15C5	benzo-15-crown-5
18C6	18-crown-6
DB24C8	dibenzo-24-crown-8
CN	coordination number
k_1	rate constant for complex formation
k_{-1}	rate constant for complex dissociation
k_2	rate constant for metal cation associative exchange
k_2'	rate constant for ligand associative exchange
K_{th}	thermodynamic stability constant for ion pair formation
K_p	equilibrium constant for ion pair formation
K_f	equilibrium constant for complex formation

$\Delta G^{\neq}$	free energy of activation
$\Delta H^{\neq}$	enthalpy of activation
$\Delta S^{\neq}$	entropy of activation
Ln(III), Ln^{3+}	lanthanide metal cation
M	metal cation
C	crown ether
X^{-1}	Cl^{-1}, ClO_4^{-1}, or NO_3^{-1}
(M C)	lanthanum(III) complex
$[La(III)]_o$, $[La(III)]_T$	total concentration of La(III)
$[C]_o$, $[C]_T$	total concentration of crown ether
$(M X)^{2+}$	ion pair
ρ	$[C]_o$ / $[La(III)]_o$
R	$[La(III)]_o$ / $[C]_o$
τ_c	correlation time
τ_A	life time of site A
τ_B	life time of site B
τ_{mix}	mixing time
η	macroscopic viscosity
f_R	microviscosity factor
k_B	Boltzmann constant
h	Planck constant

T	temperature
R	gas constant
γ	gyromagnetic ratio
γ	mean activity coefficient
a	activity
I	ionic strength
Q, eQ	electric quadrupole moment
q, eq	electric field gradient
ω	Larmor frequency
δ	chemical shift
δ_s , δ_f	chemical shift for solvated site
δ_c	chemical shift for complexed site
δ_p	chemical shift for ion pair
B_o	magnetic field
I	spin quantum number
$k_a + k_b$	pseudo-first order rate constant for cation exchange
$k_a' + k_b'$	pseudo-first order rate constant for ligand chemical exchange
P_A	population of site A
P_B	population of site B

$\upsilon_{1/2}$	linewidth at half height
T_1^{-1}	spin-lattice or longitudinal relaxation rate
T_2^{-1}	spin-spin or transverse relaxation rate
$(T_2^{-1})_{obs}$	observed transverse relaxation rate
$(T_2^{-1})_{ex}$	exchange contribution to the transverse relaxation rate
$(T_2^{-1})_{inh}$	inhomogeneity contribution to the transverse relaxation rate
FID	free induction decay
HETCOR	heteronuclear chemical shift correlation
AT	acquisition time
J_{gem}	geminal proton - proton coupling constant
J_{trans}	trans proton - proton coupling constant
J_{cis}	cis proton - proton coupling constant
σ	screening constant
υ_A , υ_a	chemical shift of species A (in Hz)
υ_B , υ_b	chemical shift of species B (in Hz)

Chapter 1

Introduction

Tripositive lanthanide cations (Ln^{3+}) constitute the longest series of chemically similar metal ions. Fifteen members of lanthanide cations have a common electronic configuration, $4f^n\ 5s^2\ 5p^6$. Because the f orbitals are shielded by the filled 5s and 5p orbitals, very small crystal field splittings are expected. Their coordination properties are thus more similar to those of alkali and alkaline earth metal ions than to those of transition metal ions. The chemistry of the lanthanide series has been studied in great depth over the last forty years[1]. One of the reasons to carry out this kind of study is that lanthanide cations can be used as spectroscopic probes.

1.1, Lanthanide Cations as Spectroscopic Probes

Lanthanide cations are well known as shift and/or relaxation reagents in NMR spectroscopy. The lanthanide induced shift (LIS) method has been widely used to solve NMR problems, ranging from qualitative spectral simplification, proof of molecular stereochemistry, quantitative analysis of dynamic solution structures, to applications in magnetic resonance imaging[2]. All of these applications are based upon the specific physical and chemical properties of the lanthanide cations, their Lewis acid characteristics, unpaired f electrons, and their tendency to form complexes with high coordination numbers. When a Lewis base interacts with a lanthanide cation, any NMR active nucleus within that base molecule "feels" the presence of those unpaired f electrons. This leads to paramagnetic relaxation or broadening of that resonance plus, in some cases, a shift to a different NMR frequency.

Another outstanding application of lanthanide cations is their use as spectroscopic probes in biological systems, especially for calcium-containing biological materials. Some alkaline earth metal ions play key roles in biological systems. However, it is difficult to investigate these systems extensively from the metal ion point of view because the metal ions are optically inert. Even metal ion NMR experiments which have shown their powerful application in the cases of alkali metal ions are difficult to perform since the active nuclei of the alkaline earth metals have very low natural abundances (for example, ^{43}Ca, which has an abundance of 0.145% and a receptivity of 5.27×10^{-2} relative to ^{13}C, is a quite insensitive

nucleus). Lanthanide ions, on the other hand, occur in only trace amounts in organisms and do not seem to play any significant biological role. They can, however, substitute the alkaline earth metal ions in biological materials which, along with their paramagnetic and spectroscopic properties, make them very informative substitution probes. Most reported substitutions were for Ca(II) in calcium-containing biological materials. There are several similar properties between Ln(III) and Ca(II) which are the key points allowing Ca(II) replacement by Ln(III) without or with little perturbation of biological material activity:

a, Their ionic radius is about the same. For example, La(III) has an ionic radius of 1.16 Å and the radius for calcium cation is 1.12 Å at coordination number of eight. Moreover, there are fifteen members in the lanthanide cation series, and the ionic radius decreases slightly from La(III) to Lu(III). It is always possible to find one lanthanide cation which has a radius very close to Ca(II);

b, Both Ln(III) and Ca(II) are hard acids and prefer ligands with hard base donor atoms, such as oxygen;

c, In aqueous solution, Ln(III) and Ca(II) show very similar static and kinetic properties: coordination numbers are the same, 9 for Ca(II)[3] and 8 - 9 for Ln(III)[4]; solvent exchanges are fast for both cases, log k, the rate constant for the exchange of water molecules, are 8.4 and 8.7 for Ca(II) and Tb(III)[5] respectively.

In some cases, the Ca(II) substitution by Ln(III) is indeed perfectly isomorphous[6]. Using lanthanide cations as substitutional probes can provide a variety of types of information, including identification and characterization of metal

ion binding sites, measurements of binding constants and the distances between the metal ion binding sites, quantization of the numbers of coordinated water molecules, structural elucidation of the biological material in solution, and aid for NMR resonance assignments[7-11]. The work related to this area has been reviewed by several authors[10, 12-22].

Another lanthanide chemistry area which has recently attracted considerable interest is the complexes of lanthanide cations with macrocyclic ligands (synthetic ionophores).

1.2, Lanthanide Cation Complexes with Macrocyclic Ligands

Natural ionophores are receptor molecules which can form stable, lipophilic complexes with charged hydrophilic species. The formation of complexes of ionophores with alkali metal cations is a typical example. It is well known that the natural ionophores play a key role in the metal ion transfer processes in biological systems. For example, the presence of ionophores will facilitate the transport of sodium and potassium cations across membranes by serving as a carrier or forming a channel. There are two types of natural-occurring ionophores: those which are cyclic such as valinomycin and enniatin and those are not cyclic such as monensin and lasalocid. In either case the resulting complex is characterized by a cation completely or partially surrounded by the ionophore ligand. To understand better these biological processes, detailed investigations of the interactions between these

metal cations and ligands is needed. The successful synthesis of macrocyclic compounds, such as crown ethers[23], cryptands[24], and spherands[25], has opened a new field of coordination chemistry[26]. These macrocyclic ligands are structurally related to the natural ionophore and can reproduce one or some of the features of the natural ionophores. This discovery makes the investigation of the complexation between metal cations and macrocyclic ligands a very active research area. The early work in this area was focussed mainly upon alkali metal cations[27] and soon extended to lanthanide cations[28]. One kind of macrocyclic molecules, crown ethers, will be considered in the following discussion since they were the main ligands used in the present work.

The formation of complexes between lanthanide cations and crown ethers was originally observed by C. J. Pedersen in 1967[23,29]. The first crystalline complexes of Ln(III) with crown ethers were isolated in 1973[30]. Since then, numerous reports involving the synthesis and crystal structure determination of such complexes have appeared[28,31-34]. Different stoichiometries of the isolated complexes with metal:ligand ratios from 2:1, 3:2, 4:3, 1:1, to 1:2 have been reported[35]. There are several factors which determine the stoichiometry of the complex, such as the ratio of the ionic diameter to the cavity of the macrocyclic ligands, the coordination ability of the counteranions, the flexibility of the ligands, and the number of coordination atoms available in the ligands. The first two factors appear to be more important than others. For example, if the Ln(III) cation is larger than the cavity of the ligand, a sandwich-type complex is expected. A 1:1 complex is most likely when the diameter

of the metal ion is smaller than or similar to the size of the ligand cavity since in this case, the metal ion can locate in the centre of the ligand. A typical example of how the counteranion coordination ability affects the complex formation is the complexation of crown ethers with lanthanide nitrate. Since nitrate is a strong coordinating anion, only 1:1 complexes for the cases involving nitrate as the counteranions were found, regardless which kind of crown ether was used. Although a complex with metal ion to ligand ratio of 4:3 has been reported for $La(NO_3)_3$ with 18C6[36,37], one of the metal ions was found to be coordinated only by the nitrate anions in the complexes.

Studies of Ln(III) complexation with crown ethers have also been carried out in solution. The investigations were mainly focussed upon showing the evidence of the complex formation and determining the stability constants of the complexes. Several techniques have been applied for the investigations of the interactions between Ln(III) and crown ethers, such as electronic absorption spectroscopy[38], luminescence spectroscopy[39], NMR spectroscopy[34], potentiometry[40], and calorimetry[41]. Measurements of stability constants have been made for many complexes. It has been found that the complexation constants in solution depend on many factors. Besides those mentioned previously for the complex in the solid state, the nature of the solvent is another factor which will dramatically affect the Ln(III)-crown ether complex formation. For example, log K, the formation constant for La(III)-18C6 complex, is 8.75 in propylene carbonate whereas it is 3.29 in the case of methanol.

The above briefly reviewed literature indicates that the complexation of lanthanide cations by crown ethers has been quite extensively investigated. However, many aspects of this research area are still unclear. For example, there is almost no information available about the kinetics and the structure of the Ln(III)-crown ether complexes in solution. This kind of information indeed is very useful for understanding the nature of the interaction between Ln(III) cations and macrocyclic ligands and could be further used in understanding the biological activities of the natural ionophores with cations. Moreover, the applications of lanthanide cations as spectroscopic probes described in section 1.1 also requires the detailed studies of Ln(III) complexes in solution.

Since metal ion nuclear magnetic resonance which has been proven to be a powerful technique in the study of alkali metal cation-macrocyclic ligand complexes[42] and since ^{1}H as well as ^{13}C NMR of the ligands can provide detailed information about the nature of cation complexations, it is logical to extend the multinuclear magnetic resonance method to the investigation of the interaction between Ln(III) and crown ethers in solution. This kind of study constitutes the main part of the present thesis.

1.3, Nuclear Magnetic Resonance Spectroscopy

Nuclear magnetic resonance (NMR) spectroscopy is a very important analytical technique. The development of modern Fourier Transform (FT) NMR

spectrometers and related techniques has made all the active nuclei of the periodic table available for NMR observations. Therefore, applications of the NMR technique have been extended to many areas of research. The investigation of the interaction between a metal cation and various ligands in solution is one example. NMR can directly provide information about the structure and, in suitable cases, about the dynamics of the ionic coordination shell in solution through its three parameters: chemical shifts, longitudinal and transverse relaxation rates.

1.3.1 Chemical Shift

The NMR chemical shift reflects the electronic environment of an observed magnetic nucleus[43,44]. When an active nucleus ($I \rangle 0$) is placed in a magnetic field its energy states will no longer be degenerate. The energy difference (υ) between different spin states depends on the gyromagnetic ratio γ and the applied magnetic field B_o.

$$\upsilon = (\gamma/2\pi) B_o \qquad (1.1)$$

The observation of the transition between those spin states produces the NMR spectrum. In equation 1.1, γ is determined by the nuclear characteristic properties. Therefore, for a given nucleus, the resonance frequency υ is proportional to the magnetic field B_o. A variation of resonance frequency (chemical shift) will be

observed when perturbation of B_o occurs, arising from the motion of the electrons surrounding the nucleus. In a magnetic field, electrons will be induced to circulate around the nucleus. Since electrons are charged particles their circulations will generate a local magnetic field opposing the applied field. The effects of electronic motion on B_o are called the nuclear shielding, and are described by σ, the screening constant. If σ is taken into account, equation 1.1 becomes[43,44]:

$$\upsilon = (\gamma/2\pi)\, B_o\, (1-\sigma) \qquad (1.2)$$

There are two major contributions to the nuclear shielding: a diamagnetic contribution arising from the electron circulation described above, and a paramagnetic one, understood in terms of many elements, such as the presence of other nuclei, which hinder rotation of the electrons around the nucleus. Because of the dependence of υ on the effective magnetic field ($B_e=B_o(1-\sigma)$), same type of nuclei in different electronic environments will resonance at different frequencies. During a complexation process, central cations vary from their solvated states (M, state "A") to the complexed ones (MC, state "B"), as expressed in equation 1.3. Since the coordination spheres of the metal ions are different in those two sites, NMR signals characterized by different chemical shifts are expected to be observed. Thermodynamic information about the complex formation and structural information about the complex can be obtained by observations of the changes of chemical shift during a complexation process.

$$M + C \rightleftharpoons MC \qquad (1.3)$$

(A) (B)

NMR is a relatively slow spectroscopic technique. The exchange rate of metal ions between their different states has to be considered for the analyses of the chemical shift results. For example, if the metal ions are in fast exchange between sites A and B expressed in equation 1.3, only one NMR signal is observed and the observed chemical shift is the average of the contributions from both sites as expressed:

$$\delta_{obs} = \delta_A P_A + \delta_B P_B \qquad (1.4)$$

Where δ_{obs} is the observed chemical shift, and δ_A and δ_B are those of sites A and B respectively. P_A and P_B represent the population of the metal ions respectively in A and B sites. This property has been used to study the interactions of La(III) with anions in aqueous and non-aqueous solutions by ^{139}La NMR. The results will be presented in the chapter 3 of this thesis.

When metal ion exchange is very slow on the NMR time scale, separated peaks respectively corresponding to solvated and complexed species will be observed. The complexation of La(III) with 18C6 in methanol and in acetonitrile gives such a case. In this situation, the thermodynamic information about the complex formation can still be obtained by performing lineshape analysis of the ^{139}La NMR spectra. A detailed discussion on those systems will be given in Chapter 4.

1.3.2 Longitudinal and Transverse Relaxation Rates

Longitudinal and transverse relaxation rates are two other important NMR parameters. They have been widely used for the kinetic study of alkali metal cation - crown ether complexation[42].

Like any other form of spectroscopy, NMR spectroscopy may be defined as the interaction between matter and electromagnetic radiation such that energy is either emitted or absorbed. The conventional approaches to the NMR experiment are described in a number of books. Basically, FT NMR measurements are initiated by applying a radiofrequency pulse perpendicular to the applied magnetic field which forces the net z magnetization, M_z, of the observed nucleus to turn to the x-y plane or the x'-y' plane of the rotating frame. This process can be understood in terms of nuclear excitation. Following a 90^0 pulse, a signal will be received by a receiver coil placed in the y' direction. A plot of the intensity of the received signal against time is referred to as a *free induction decay* (FID). Fourier transformation of the FID will produce an NMR spectrum[45-47].

Once the pulse has stopped, the magnetization will tend to realign with B_o and a Boltzmann equilibrium of the magnetization will be slowly restored by relaxation. This process involves the nuclei going from their excited state to the ground state and is referred to as longitudinal relaxation. Since, during the process, the excited nuclei have to lose their energy to the surroundings, the process is also named as spin-lattice relaxation. The rate of the process is described by a first order

rate constant, T_1^{-1}, in Bloch equation[48].

$$d(M_z-M_o) / dt = -(M_z-M_o) / T_1 \qquad (1.5)$$

Where t is the time, M_o and M_z are the initial magnetization and the magnetization on the z axis at time t, and T_1 is a constant characterizing the relaxation process.

Following the 90^0 pulse, there is another relaxation process involved. T_2^{-1} is used to describe this process in Bloch equation[48].

$$d(M_{x \text{ or } y}) / dt = -(M_{x \text{ or } y}) / T_2 \qquad (1.6)$$

This process causes the net $M_{x \text{ or } y}$, the magnetization on x or y axis, to be zero by dephasing the initially coherent magnetization in the x'-y' plane. T_2 is known as the transverse relaxation time. Because the energy flow occurs between different spin systems in this process T_2 is also called the spin-spin relaxation time. T_1^{-1} is always $\leq T_2^{-1}$ and under condition of extreme narrowing, which is normal for a mobile liquid, T_1 is equal to T_2. The transverse relaxation rate constant, T_2^{-1}, is related to the linewidth at half height of a Lorentzian shaped NMR peak[49].

$$\upsilon_{1/2} = (\pi \quad T_2)^{-1} \qquad (1.7)$$

The NMR relaxation involves many mechanisms[43]. For a nucleus with spin

) 1/2, the quadrupolar mechanism is a dominant contribution to the relaxation. It arises from the interaction between the electric quadrupolar moment (eQ) of the nucleus and the electric field gradient (eq) caused by an asymmetric charge distribution around the nucleus. In the condition of extreme narrowing ($\omega^2 \tau_c^2 \ll 1$, ω is the Larmor frequency of the observed nucleus and τ_c is the motional correlation time of the entire molecule), T_q^{-1} , the quadrupolar relaxation rate, can be approximately expressed as[50]

$$T_q^{-1} = (3\pi^2/10)\ \chi^2\ \tau_c\ (2I + 3) /\ (\ I^2\ (2I-1)\ ) \qquad (1.8)$$

Where I is the spin number of the nucleus and χ is referred to as the quadrupolar coupling constant ($\chi = e^2Qq / h$) which is related to the electric quadrupole moment (eQ) of the nucleus and the electric fieid gradient (eq) at the nucleus.

The relaxation rate of a quadrupolar nucleus is a good measurement of the symmetry of the metal cation coordination sphere, as reflected in the electric field gradient (eq). Lower symmetry will result in a larger value of $T_{2,q}^{-1}$. Consequently, a broader NMR peak will be obtained (see equation 1.7). Since, as for the chemical shifts, cations in a specific environment will have their own characteristic relaxation rates, the observation of linewidth variations will also provide the thermodynamic and structural information about the complexes if the symmetry of the charge distribution around the metal ion is different for the two species described in equation 1.1. In this thesis, linewidth measurements have been made for ^{139}La NMR

spectra. The results can be found in Chapters 3, 4, and 6.

Kinetic information about the exchange of metal ions between different sites may be obtained from lineshape analyses of NMR spectra[51, 52]. A chemical exchange of nuclei in different sites will provide another pathway for transverse relaxation whereas it will not affect T_1^{-1}, the longitudinal relaxation rate. Since T_2^{-1} is proportional to the linewidth, the variation of transverse relaxation rates will alter the lineshape of the experimental NMR spectra. In suitable cases, which will be discussed below, the rate constants of the exchange may be derived from the measurements of $T_{2,e}^{-1}$, the chemical exchange contribution to T_2^{-1} .

The chemical exchange effects upon the transverse relaxation rates can be divided into several types which depend on the relative rate of the exchange on the NMR chemical shift timescale. To discuss those different situations, let us take a two-site exchange as an example.

$$\text{M (A)} \underset{k_b}{\overset{k_a}{\rightleftharpoons}} \text{M (B)} \qquad (1.9)$$

If the exchange is very fast or extremely slow on the NMR chemical shift timescale, no effects on T_2^{-1} will be observed. In the former case, a single peak characterizing the population average of two sites will be observed, while for the latter case, two separated signals corresponding respectively to sites A and B will be obtained. The kinetic information is available only when the exchange rate is

between these two limits. Since the chemical exchange will cause line broadening in this region, the exchange rate constants k_a and k_b expressed in equation 1.9 can be obtained either by linewidth measurements or by full lineshape analyses of the observed NMR spectra[53]. The detailed discussion of this kind of study will be given in Chapter 6 of this thesis.

1.4 ^{139}La NMR

NMR and its possible applications to the study of metal cation complexes in solution was discussed in the previous section with the main focus on the metal cation nuclei. The principles described above are indeed suitable for any nucleus. Therefore, similar information can also be obtained by looking at the nuclei associated with the ligands. Most of the work presented in this thesis was done by multinuclear (^{139}La, ^{17}O, ^{1}H, and ^{13}C) magnetic resonance spectroscopy. Since ^{139}La is the only metal cation nucleus used in the present work, the characteristics of its NMR spectroscopy will be discussed in this section.

In the series of trivalent lanthanide cations, only lanthanum and lutetium are diamagnetic. ^{175}Lu (I=7/2) has a very large quadrupolar moment ($Q = 5.68 \times 10^{-28}$ m^2) and very broad lines are expected for its NMR spectra unless the nucleus is in a high symmetric environment. These characteristics make this nucleus useless in practice for high resolution NMR observations[54]. Therefore, the ^{139}La nucleus is the only possible choice among the lanthanide cation nuclei. Table 1.1 gives the nuclear properties of the nucleus ^{139}La[54, 55].

Table 1.1 The Nuclear properties of ^{139}La

Spin (I)	Natural Abundance (%)	Receptivity to ^{13}C	Quadrupolar Moment (10^{-28} m^2)	Resonance Frequency (7 Tesla) (MHz)	Typical T_1 values (s)
7/2	99.91	342	0.22	42.37	10^{-3}

^{139}La is also a quadrupolar nucleus with a quadrupolar moment of 0.22 x 10^{-28} m^2 which sometimes leads to broad resonances as a consequence of quadrupolar relaxation. However, with its natural abundance of 99.91% and its receptivity of 342 relative to ^{13}C, ^{139}La is a good candidate for the metal ion NMR study. In fact, ^{139}La NMR has been used in the studies of La(III) solution chemistry. The first ^{139}La NMR experiment was performed as early as 1949[56, 57]. Thereafter, a number of ^{139}La studies have been reported[58-64]. The earlier work mainly focussed upon the nature of the outer- or inner- sphere of lanthanum complexes formed by a variety of small ligands and anions in aqueous solution. A few papers dealing with La(III) ion

coordination properties in non-aqueous solutions have recently appeared in the literature[65-70] .

Based on these investigations, it has been found that ^{139}La NMR has a very large range of chemical shifts (*ca.* 1200 ppm). The origin of the ^{139}La NMR chemical shifts, however, is far from being understood. One suggestion is that the shifts mainly resulted from the "paramagnetic" term. There is partial electron transfer from the ligand to the metal ions when the complexes are formed and those transferred electrons are mainly non-paired which will lead to some deshielding of the observed nucleus. The chemical shifts of $^{139}La(III)$ therefore depend strongly on the extent of covalency in La(III) - ligands interaction.

Another characteristic of ^{139}La NMR spectroscopy is that the NMR lines are usually broad. For the nucleus ^{139}La (I = 7/2), equation 1.8 shown previously becomes:

$$T_q^{-1} = (2 / 49)\, \pi^2\ \chi^2\ \tau_c = \pi\, \upsilon_{1/2} \qquad (1.10)$$

Since ^{139}La has a quite large quadrupolar moment, small variations of the symmetry of the electron clouds around La(III) will result in large changes of relaxation rates, increasing strongly the linewidth of the observed NMR spectra. Linewidths of 130 Hz for lanthanum perchlorate in aqueous solution and several thousands Hz for La(III) complexes with organic ligands have been reported[65]. The advantage of this characteristic is the sensitivity of linewidths to the dissymmetry of La(III)

coordination shell.

In this thesis, both chemical shift and linewidth of ^{139}La NMR were used to provide information about the La(III) complexes with a variety of ligands, mainly crown ethers, in solution from the metal cation point of view. The individual result can be found in the related chapters. As mentioned previously, this kind of study has not yet been reported.

Chapter 2

Experimental Methods

2.1 Materials

2.1.1 Salts

$La(NO_3)_3$ 6 H_2O (Aldrich, 99.999%) and $LaCl_3$ 7 H_2O (Aldrich, 99.999 %) were used without further purification. Lanthanum perchlorate was made by dropping perchloric acid (BDH AnalaR) into a mixture of lanthanum oxide (Aldrich 99.999%) with small amount of water. When the pH was about 6, the resulting solutions were filtered and were then evaporated at reduced pressure. The remaining solids were dried under vacuum. The lanthanum content in all lanthanum salts was determined by titration with EDTA using xylenol orange as indicator[71].

2.1.2 Crown Ethers

18C6 (Aldrich 99%) was recrystallized following the procedure described by Gokel *et al*[72], and vacuum dried over P_2O_5 at 50 °C. The complete removal of acetonitrile from the recrystallized crown ether was checked by ^1H NMR. DB24C8 (Aldrich 98%) was recrystallized from acetonitrile and cyclohexane and was dried under vacuum over P_2O_5 for at least 24 hours just prior to use. B15C5 (Aldrich 98%) and was recrystallized from hexanes. The recrystallized B15C5 was vacuum dried over P_2O_5 for a minimum of 24 hours prior to use. 15C5 (Aldrich 98%) was distilled under vacuum and was kept over 3 Å molecular sieves.

2.1.3 Solvents

Water was doubly distilled and was kindly supplied by Prof. B. E. Conway's lab in this department. Acetonitrile (BDH assured) was dried under reflux, over calcium hydride (CaH_2) for at least 3 hours, distilled under nitrogen and stored under argon. Methanol (BDH assured) was dried by refluxing over magnesium metal for a minimum of 3 hours, distilled under N_2 and stored under argon. Deuterated acetonitrile CD_3CN (Aldrich 99.5% D) was dried over 3 Å molecular sieves.

2.2 Sample Preparation

Samples for ^{139}La NMR measurements were prepared by weighing the appropriate amount of crown ether directly into volumetric flasks and filling up with stock solutions of the desired lanthanum salt concentration. In the concentration study where the concentration of lanthanum salts was varied, dilutions were done. Whenever the pH of the solution had to be controlled, the pH value of the stock solutions was adjusted by adding very small amounts of concentrated HCl or NaOH solutions. Samples for ^{13}C NMR measurements were prepared by weighing the desired amount of lanthanum salt directly into 5.0 ml flask and adding an appropriate

amount of stock crown ether solutions of known concentration in the desired solvent. The solution samples for both ^{139}La and ^{13}C NMR measurements were transferred into 10 mm NMR tubes which were sealed under argon with Parafilm. Samples for ^{1}H NMR measurements were prepared by a procedure similar to ^{13}C sample preparation except that deuterated solvent and 5 mm tubes were used.

2.3 NMR Measurements

2.3.1 ^{139}La NMR measurements

^{139}La NMR spectra were recorded, unlocked, on a Varian XL-300 spectrometer at 42.37 MHz. Typical spectral width was 50 kHz. Since the relaxation rates of ^{139}La are very fast, very short acquisition time and no delay between two pulses were used. The 90° pulse width was typically 16 μs. ^{139}La NMR chemical shifts were referred to 0.10 M $La(NO_3)_3$ 20% D_2O aqueous solution. The transverse relaxation rates, T_2^{-1} , were obtained directly from the linewidths at half height of the ^{139}La NMR spectra ($T_2^{-1} = \pi \nu_{1/2}$) if the obtained spectra had a Lorentzian shape. The longitudinal relaxation time, T_1 , was determined by using the inversion-recovery pulse sequence, 180° - τ - 90° - Acquisition, and a three parameter nonlinear regression analysis. At least nine different τ values were used for each T_1 determination. The number of transients for normal spectra was from several thousands to 10^6 depending on the concentration of La(III) and the linewidth of the ^{139}La NMR spectra.

2.3.2 ^{13}C NMR Measurements

^{13}C NMR spectra were recorded on a Varian XL-300 NMR spectrometer at a frequency of 75.429 MHz under proton - noise - decoupling conditions. No lock was used for the samples which did not contain deuterated solvents. The chemical shifts were referred to the solvent line and corrected to TMS. The number of transients was

from a few hundreds to 10^5 depending on the concentration of crown ethers and the purpose of the investigations. For example, if the obtained spectra were further used for kinetic analysis, a higher ratio of signal to noise was necessary and a large number of accumulations for each spectrum was needed.

2.3.3 ^{17}O NMR Measurement

Natural abundance ^{17}O NMR spectra were measured at 40.66 MHz on a Varian XL-300 spectrometer. Typical spectral width was 50 kHz. Acquisition time was 0.1 second and no delay between pulse cycles was used. 100% D_2O was used as an external chemical shift reference. Number of scans for each measurement was from 10^5 to 10^7 depending on the concentration of $La(NO_3)_3$ 6 H_2O in the samples. Longitudinal relaxation rates were determined by using a inverse - recovery procedure and under conditions of broad band proton decoupling.

2.3.4 ^1H NMR measurement

Normal proton spectra were acquired on a Varian XL-300 spectrometer by a routine procedure. The chemical shifts were referred to the solvent signal and corrected to TMS.

Saturation transfer measurements were done for some samples. Low power homonuclear decoupling was centered at the frequency of saturated line. In order to minimize the effect of decoupling power on the observed spectral line, a measurement was also made by centering the homonuclear decoupling frequency at the position which was equal to the difference between saturated and observed spectral lines but at opposite direction (see figure 2.1). A difference spectrum of these two measurements was used for further analysis. The longitudinal relaxation times (T_1^{sat}) were determined using inversion recovery pulse sequences with the presence of a saturating rf field. The intensities of the ^1H NMR peaks were obtained by integration.

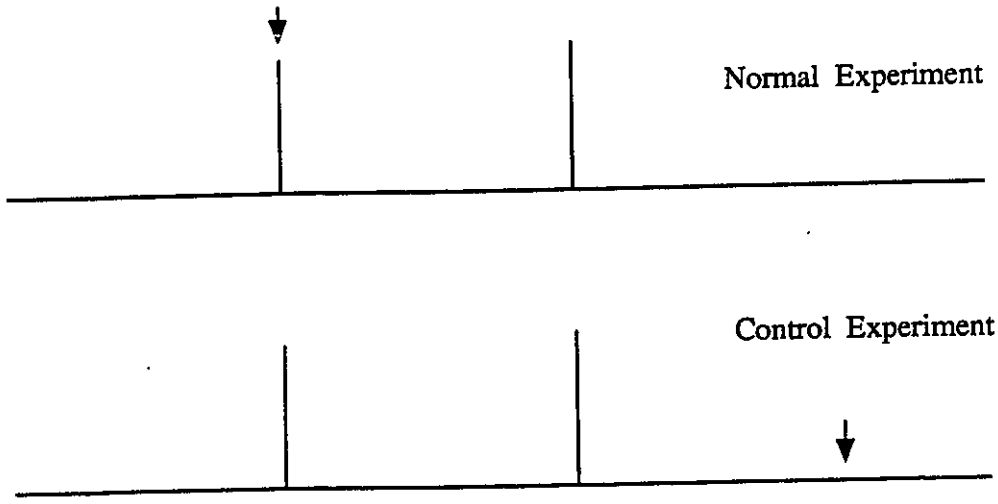

Figure 2.1: Representation of saturation transfer experiment. The arrows indicate the positions in which the saturating rf are centered.

The inversion transfer technique was applied to the system of $La(NO_3)_3\ 6H_2O$ - 18C6 - Acetonitrile in which the ligand 18C6 exchanged slowly between free and complexed sites. Since only two singlet ^1H NMR lines representing free and complexed 18C6 were involved in the exchange process, a relatively simple pulse sequence was used in the experiments instead of the DANTE pulse sequence. Selectively inverting one peak was accomplished by using three 90° nonselective pulses[73,74].

$$(90_x^\circ - t_1 - 90_x^\circ - \tau_{mix} - 90_x^\circ - \text{Acquisition} - RD)_n$$

Here, t_1 is equal to half the reciprocal of the chemical shift difference between complexed and free 18C6 ^1H NMR lines; τ_{mix} is a variable called "mixing time" during which spin exchange between the two 18C6 sites occurs; RD is a relaxation delay which was set to be $RD > 5 \times T_1$; n is the number of scans.

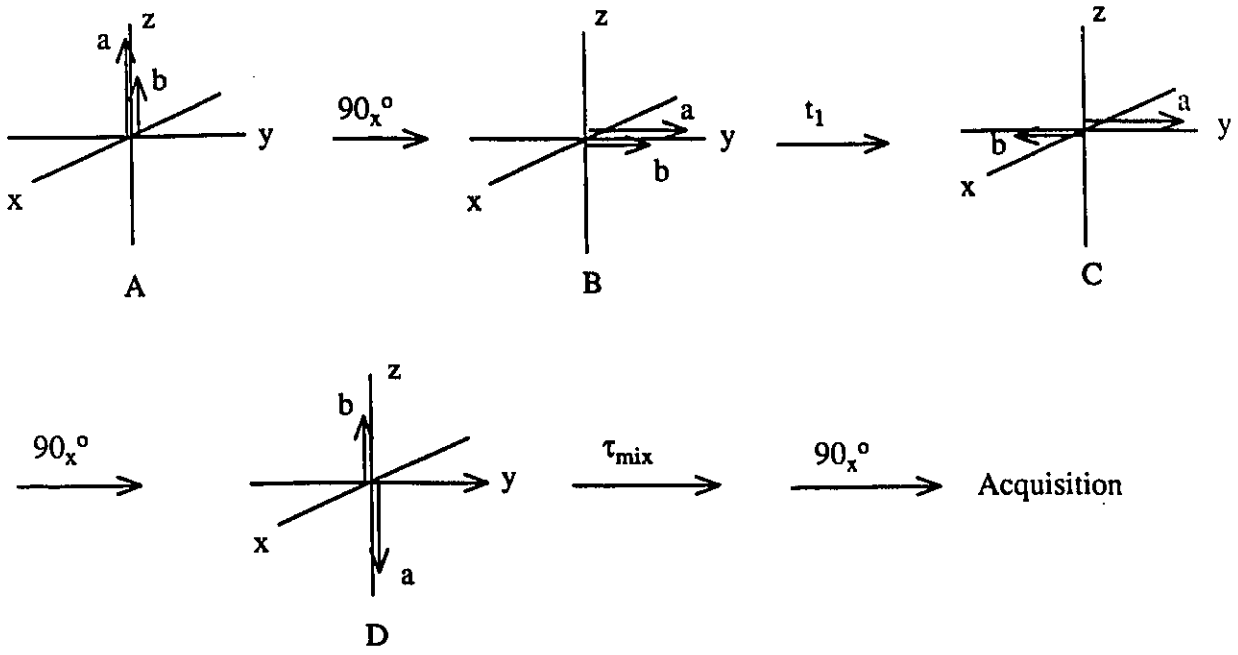

Figure 2.2[75]: Vector diagram for the inversion transfer experiment. (A) Equilibrium. (B) Both a and b vectors are aligned with y axis after first 90° pulse. (C) After t_1, vector a will remain in the y axis and vector b will align with -y. (D) Another 90° pulse inverses the population of a with its vector in the -z direction. Following the mixing time, the third 90° pulse allows to monitor the effect of exchange between two sites on the b signal.

2.3.5, NMR Probe Temperature Control

The temperature of the probe was measured with a thermocouple submerged in pure solvents (water or acetonitrile) in non-spinning NMR tubes (5 or 10 mm). The measurements were done periodically. Whenever the temperature variation experiments were done, the temperature of the probe would be recalibrated. The temperature of the samples was estimated to be reliable to ± 0.5 K. Unless otherwise stated, the NMR experiments in this thesis were run at 300 ± 0.5 K.

2.4 Data Analyses

2.4.1 Full Lineshape Analysis

When the obtained spectrum was a single Lorentzian line, a full lineshape analysis was made on the XL-300 spectrometer computer using curve fitting software. Other analyses of the spectral lineshapes were performed on an Amdahl mainframe computer. Digitized spectral data for the analyses were first transferred from XL-300 NMR spectrometer to an IBM compatible PC by using Kermit software and Varian "magical" software (*Varian Magnetic Moments*, **3**, 12, 1987). The obtained data files were then transferred to the mainframe through a Sytek line for further analysis(non-linear regression or simulation). Full lineshape analyses of ^{139}La NMR spectra were carried out by using a non-linear least-squares regression with a program developed from SAS (Statistical Analysis Systems)[76] routines. In the cases of overlapping Lorentzian signals and when linewidths were very large, a phase correction was also included in the calculation because the obtained spectra were not perfectly phased. ^{13}C NMR lineshape analyses were done by simulations. The program for the simulations was originally written by Dr. R. E. D. McClung (Department of Chemistry at University of Alberta), and kindly given to us by Prof. M. J. McGlinchey (Department of Chemistry at McMaster University). This PC program was written in FORTRAN 77 language and suitable for multiple site exchange without coupling. Some modifications were made so that the program could be run on the Amdahl mainframe. ^{1}H NMR and ^{17}O NMR spectra simulations were carried out using the DNMR3 program[77] which was originally written in FORTRAN 4 language and kindly supplied by Prof. J-L. Roustan (Chemistry Department of University of Ottawa). We loaded this program on to the Ottawa University mainframe and made some modifications (from FORTRAN 4 to FORTRAN 77) so that the program could be run on the mainframe computer. The simulations were performed by comparing

the calculated spectra which could be modified by varying the parameters with experimental ones until a best match was reached. The output of the simulation programs was data points. A plot or diagram was created through SAS graphic software[78] from the digitized data so that the comparison could be made. Figure 2.3 is an example of simulation of ^1H NMR spectrum.

2.4.2 Other Data Analysis

Like full lineshape analyses, all other data analyses were also carried out by either non-linear or linear regressions on the Ottawa University mainframe computer. The programs for the regressions were developed from SAS routines. The equations involved in the non-linear regression will be described in relevant chapters.

2.5 Error Analysis

If a single Lorentzian peak was observed, the error on the chemical shift measurement was visually estimated by fitting the spectrum on the computer of the XL-300 NMR Spectrometer (see figure 2.4). The error in the transverse relaxation rate determinations was taken to be twice the error in the chemical shift measurements. The error in the T_1 determinations was given as two standard deviations (2 σ) from the non-linear regression analysis. When a full lineshape analysis was performed for a two site population weighted spectrum without exchange, the errors in the chemical shifts and T_2^{-1} were given as one standard deviation from the non-linear regression.

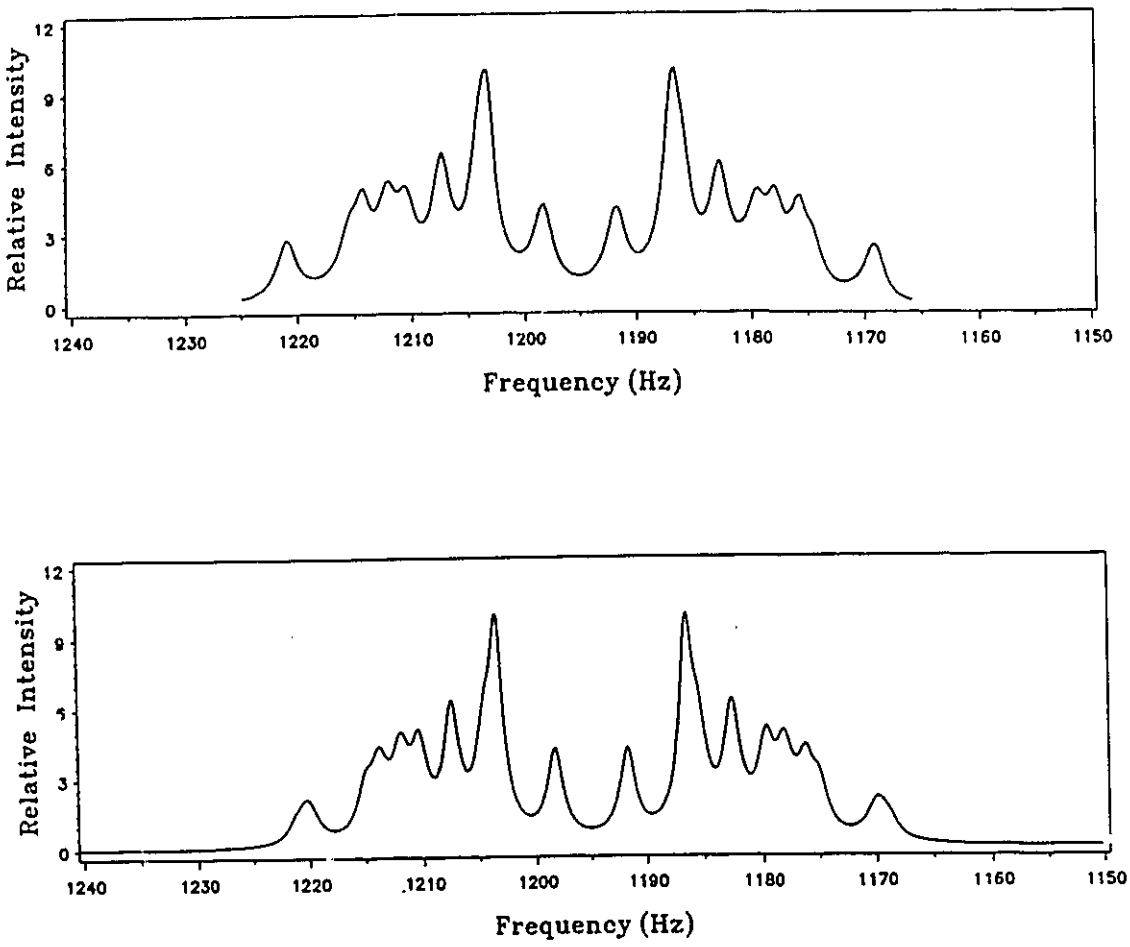

Figure 2.3. Experimental and simulated ^1H NMR spectra of 15C5 coordinated to La(III) in AN solution. Lower, experimental spectrum recorded at 239 K, $[15C5]_o = 0.0032$ M, and $R = [La(III)]_o / [15C5]_o = 1.08$. Upper, the corresponding spectrum simulated by DNMR3 program.

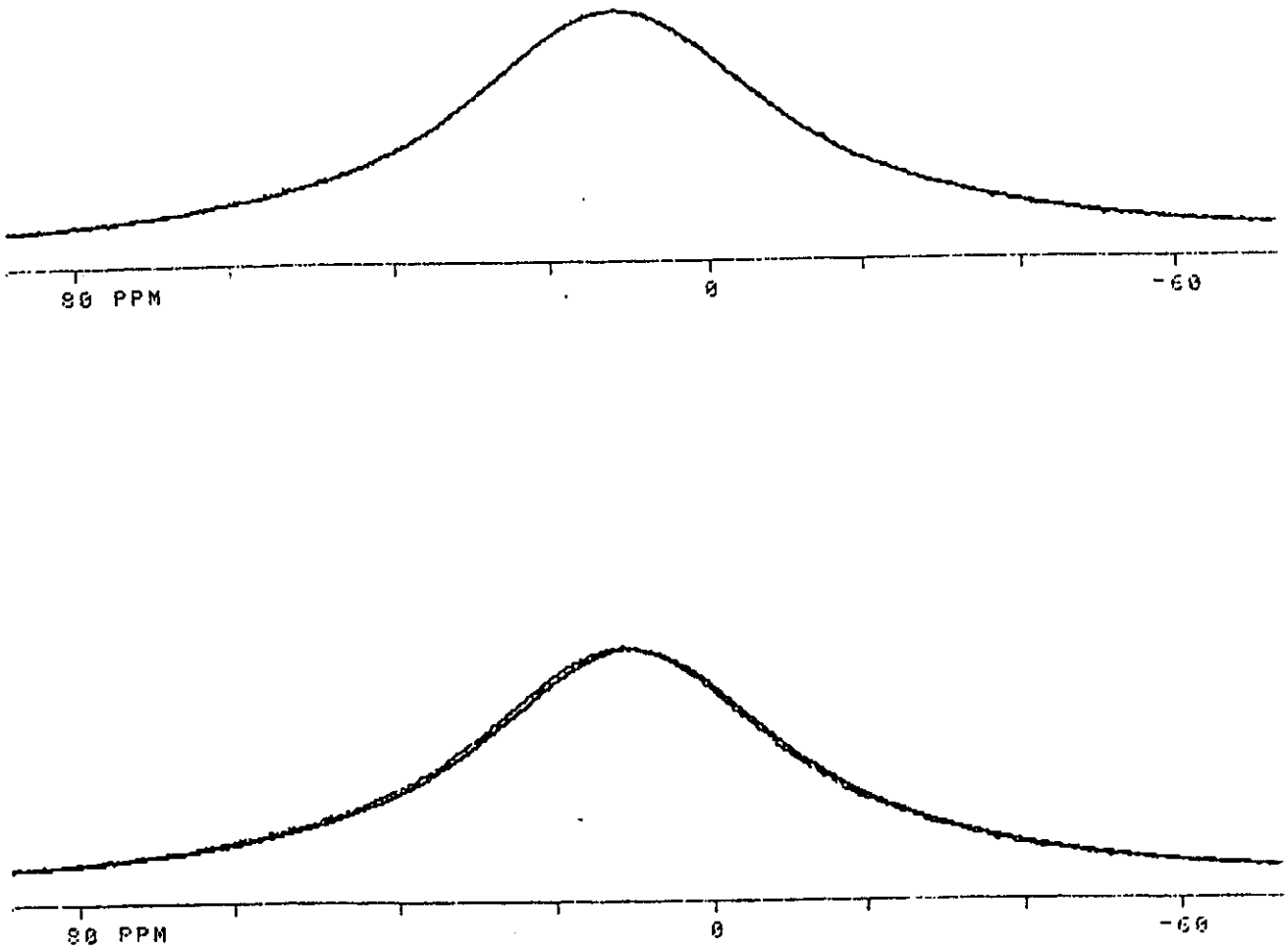

Figure 2.4. ^{139}La NMR spectra of $La(NO_3)_3$ 6 H_2O solution in AN. [La(III)] = 0.100 M. Upper, superpositioned experimental spectrum and its best fit by the computer of the XL-300 NMR Spectrometer. Lower, the computer fitted spectrum was artificially shifted -0.50 ppm from the best fitting position. An obvious difference between the experimental and its fitting spectra was observed. Therefore, the error on the chemical shift was estimated to be ± 0.50 ppm.

In the cases of other data analyses which were performed by either non-linear or linear regressions, the error in the variables was calculated by a computer and reported as one standard deviation. If a spectrum simulation procedure was used to get the exchange rate constant, the error reported for ($k_a + k_b$) was visually estimated by comparing the best fitting spectrum with the one of parameters being slightly varied.

The kinetic parameters $\Delta S^{\neq}$ and $\Delta H^{\neq}$ were reported with $\pm \sigma$ as the error. The free energy of activation, $\Delta G^{\neq}$ was directly calculated from the measured rate constants[9]

$$\Delta G^{\neq} = - RT \ln (k\, h / k_B\, T)$$

where k is the rate constant and k_B is the Boltzmann constant. The errors on $\Delta G^{\neq}$ were calculated using the following equation[51],

$$\frac{\Delta\Delta G^{\neq}}{\Delta G^{\neq}} = \frac{\{[\Delta T/T(\ln(k_B T/kh) + 1)]^2 + (\Delta\, k/k)^2\}^{1/2}}{\ln(k_B T/kh)}$$

The errors on the chemical shift measurements of ^{13}C and ^{1}H NMR spectra were taken from their theoretical digital resolutions (DR=2 SW / NP). The errors related to the sample preparations, such as ρ and *R*, were neglected.

Chapter 3

NMR Study of Lanthanum Salts in Aqueous and Non-Aqueous Solutions

3.1 Ionic Interactions in Aqueous Solutions of Lanthanum Salts. A ^{139}La NMR Study

3.1.1 Introduction:

As mentioned in the introduction, the complexation properties of lanthanide ions in solution have attracted considerable interest. However, the nature and the structure of the chemical species in solutions of rare earth salts are not clearly known. For example, the coordination of the Ln^{3+} ions in aqueous solution is one of the most controversial questions of lanthanide chemistry. The main argument has two aspects. One is about the coordination number (CN) of the lanthanide ions. The other deals with the nature of the interaction between the cation and counteranion. The coordination number of lanthanide ions in aqueous solution is now believed to be 8 or 9. However, it is still unclear whether or not CN change occurs along the series[4,5].

In solid state of hydrated lanthanide salts, a hydration number of nine is very common. In aqueous solution, Spedding and his co-workers[79-81]suggested that the CN changed from 9 (lighter lanthanide) to 8 (heavy ones) in order to interpret the non-regular change in lanthanide aqua-ion partial molar volumes along the series. This hypothesis was supported by X-ray and neutron diffraction studies of Ln^{3+} aqueous

solutions[82,83]. However, this description is far from being fully accepted. As pointed out by Wertz and coworkers[84] and by Breen and Horrocks [85], a constant CN of 8 along the series was found when the formation of chlorocomplexes was taken into account. Moreover, a ^{17}O NMR chemical shift study was also consistent with a constant CN along the series[86].

The controversy about the presence of the counteranion in the inner coordination shell of the lanthanide cations, to form contact ion pairs, still remains, especially in the cases of lanthanide chloride and perchlorate. Recently, several spectroscopic techniques, including UV - Visible[87], luminescence[85,88], ultrasonic relaxation[89], X-ray[82] and neutron diffraction[83], have been used to characterize the nature of the complexes formed between lanthanide cations and various anions in aqueous solution. According to them, no inner-sphere complexes were formed with perchlorate, the formation of a 1 : 1 complex $\{Ln(NO_3)\}^{2+}$ was concluded for nitrate and an inner- sphere ion pair may or may not be formed in the case of chloride. The presence of mono- and dinitrate complexes was deducced from $^{15}NO_3^-$ NMR spectra in solutions of Lu(III) in water-acetone-d_6-freon-12 mixtures[90] at very low temperature. Under the same conditions a similar conclusion was reached from ^1H, ^{35}Cl, and ^{89}Y NMR spectra of Y(III) solutions[91], and direct evidence for the anion entering the first coordination shell of La(III) was provided in the case of lanthanum nitrate by ^1H, ^{35}Cl, and ^{139}La NMR spectra[70].

It has been shown that metal cation NMR of quadrupolar nuclei in solution is a powerful probe of the nature of the immediate environment of the metal cation[92]. Among the lanthanide series, ^{139}La is almost the only candidate which is amenable to this kind of study. The NMR technique has been used to investigate the coordination properties of lanthanide salts in aqueous, aqueous mixture, and nonaqueous solvents[59-62, 70, 90-92]. The use of a metal cation as an NMR spectroscopic probe was established by ^{139}La. Several reports related to investigation of aqueous solutions of

lanthanum salts have appeared in the literature[58, 59, 63, 64]. The formation of inner-sphere ion pairs in the case of NO_3^-, which was detected by other techniques, was confirmed by the significant ^{139}La NMR chemical shift and linewidth variations with the concentration of $La(NO_3)_3$ in aqueous solution. Such a strong variation was not observed for perchlorate at low concentration and a significant variation was obtained only for the chemical shift in the case of chloride. Therefore, it is not clearly known whether or not interaction between cation and anion occurs in the aqueous solutions of lanthanide chloride and perchlorate. Moreover, only either linewidth or chemical shift variation of ^{139}La NMR with lanthanum salt concentration was considered and no quantitative interpretation of the ^{139}La NMR results has so far been reported in the literature. It is worth reinvestigating the nature of the lanthanum salts in aqueous solution by the ^{139}La NMR technique.

As part of this chapter, the ^{139}La NMR chemical shifts and linewidths were measured as a function of the concentrations of La(III) in aqueous solutions of $La(NO_3)_3$, $LaCl_3$, and $La(ClO_4)_3$ at a constant pH. A quantitative treatment of the experimental data was given by calculating the formation constants of the complexes of La(III) with these three anions, taking into account the appropriate activity coefficient effects.

3.1.2: Results and discussions.

The ^{139}La NMR spectra of aqueous solutions of lanthanum nitrate, chloride, and perchlorate consist of a single Lorentzian line. Figure 3.1 shows a series of ^{139}La NMR spectra at various concentrations of $La(NO_3)_3$, ranging from 0.005 to 1.50 M. Figure 3.2 gives the chemical shift variation with the concentration of La(III) for the three salts. The chemical shifts of $La(NO_3)_3$ and $La(ClO_4)_3$ move upfield as the concentration of La(III) increases. The variations are about 12 ppm for nitrate and 3 ppm for perchlorate in the range of the La(III) concentrations of 0.01 - 1.50 M.

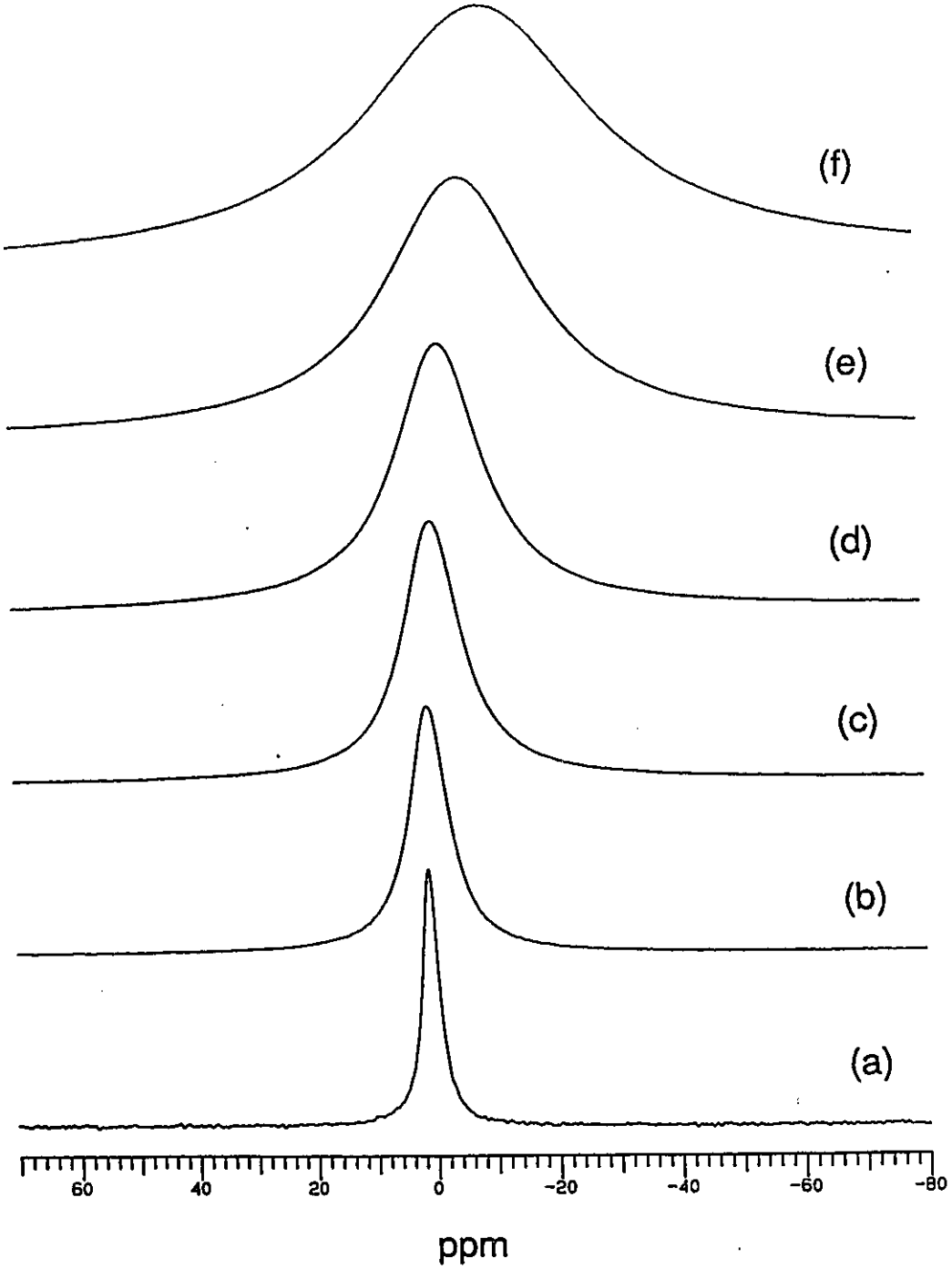

Figure 3.1: A series of ^{139}La NMR spectra at various concentrations of $La(NO_3)_3$ in aqueous solution. Bottom to top [La(III)] = (a) 0.0050, (b) 0.100, (c) 0.250, (d) 0.500, (e) 1.00, and (f) 1.500 M. T = 300 K.

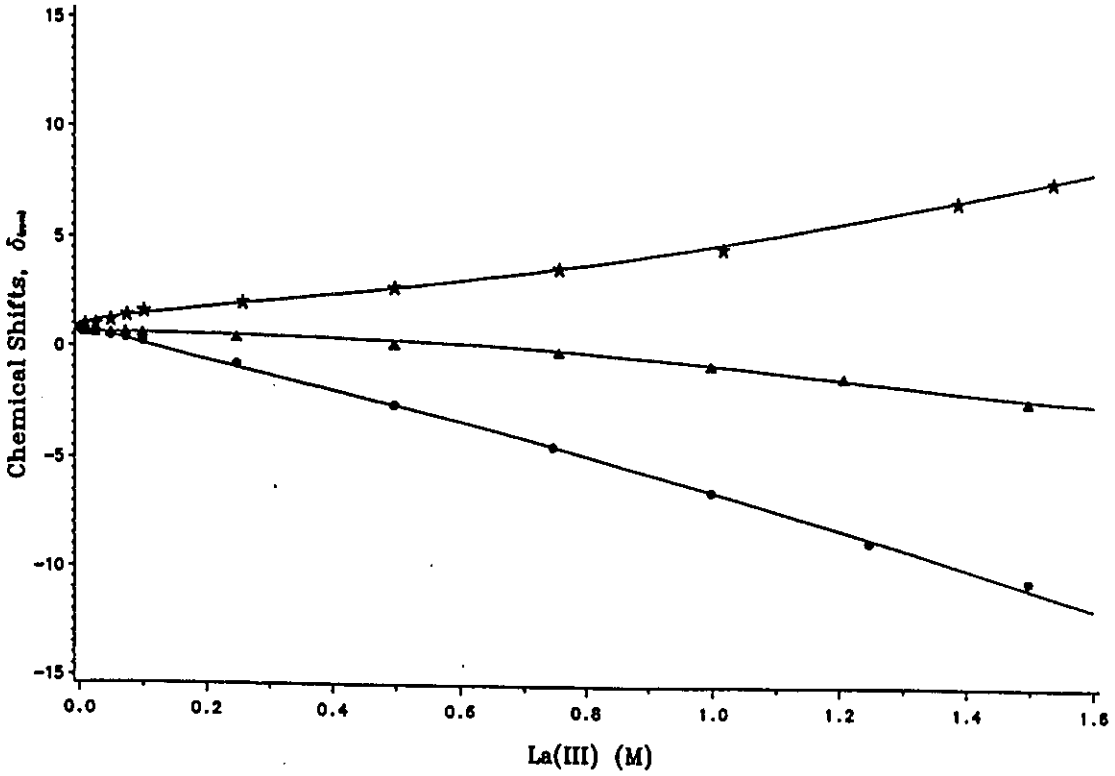

Figure 3.2: ^{139}La NMR chemical shifts as a function of lanthanum concentration for three lanthanum salts in aqueous solution. (★) chloride, (▲) perchlorate, and (●) nitrate. T = 300 K. pH = 5.5 ± 0.1. The data points are experimental and the curve is calculated (see the text).

In the case of $LaCl_3$, The ^{139}La NMR signals were shifted downfield. The ^{139}La NMR chemical shift of 1.54 M $LaCl_3$ aqueous solution is 7.78 ppm compared to the external reference, 0.10 M solution of $La(NO_3)_3$ in D_2O : H_2O 20 : 80. The magnitude and the direction of the ^{139}La NMR chemical shift variations observed in this work are in good agreement with those reported in the literature[63,64].

As expected, the linewidths of ^{139}La NMR spectra increased as the concentration of La(III) increased. The transverse relaxation rates of ^{139}La NMR, T_2^{-1}, which are directly obtained from the linewidths at half height of the ^{139}La NMR spectra ($T_2^{-1} = \pi \times \nu_{1/2}$), vary significantly in the case of $La(NO_3)_3$, from 0.50 kHz to 5.9 kHz in the range of concentration of La(III) 0.01 - 1.50 M. Similar variations are observed, but to a lesser extent, for the cases of $LaCl_3$ and $La(ClO_4)_3$. In the investigated concentration range, T_2^{-1} varies from 0.33 to 0.88 kHz for chloride and from 0.33 to 1.14 kHz for perchlorate. Figure 3.3 shows the transverse relaxation rates of ^{139}La NMR as a function of La(III) concentration for nitrate, chloride, and perchlorate aqueous solutions at pH = 5.5.

Since ^{139}La is a quadrupolar nucleus, it is possible that both chemical shifts and linewidths of ^{139}La NMR provide information about the La(III) species existing in solution. The ^{139}La nucleus has a relatively large quadrupole moment ($Q=0.21 \times 10^{-28}$ m^2). Therefore, the relaxation mechanism is governed by the quadrupolar interaction[59,63]. In aqueous solution, similar to the equation 1.10 given in Chapter 1, the ^{139}La linewidth at half height can be approximately expressed as

$$\nu_{1/2} = (3\pi\,(2I + 3)/10\,I^2\,(2I - 1)) \times (e^2Qq_{zz} / h)^2\,\tau_c \qquad (3.1)$$

$$\text{or } \nu_{1/2} = 2/49 \times \chi^2\,\tau_c \qquad (3.2)$$

Where $\chi = e^2Qq_{zz}/ h$ is the quadrupolar coupling constant and τ_c is the correlation time responsible for the quadrupolar interaction.

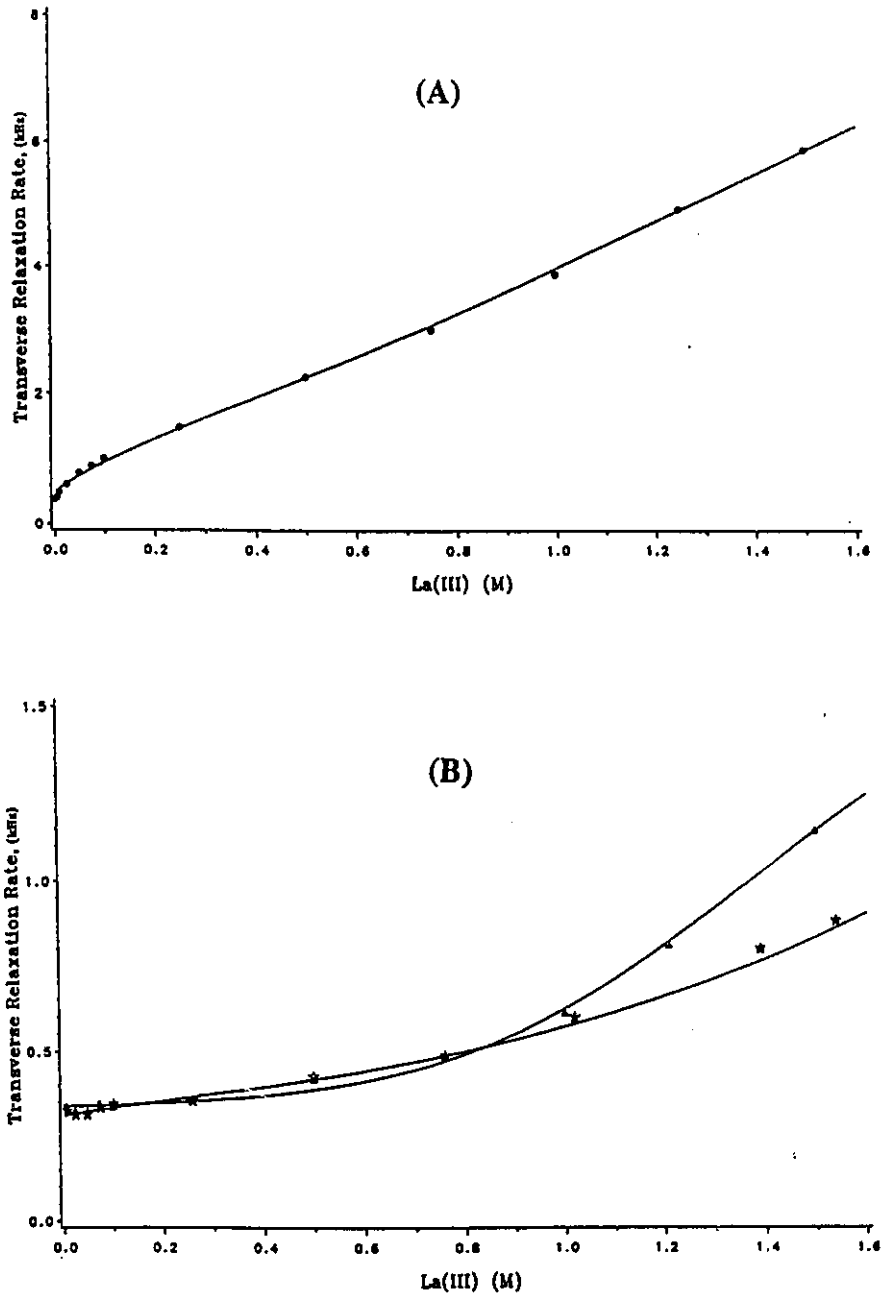

Figure 3.3: ^{139}La NMR transverse relaxation rates as a function of lanthanum concentration for three lanthanum salts in aqueous solution. (A) nitrate, (B), (▲) perchlorate and (★) chloride. T = 300 K. pH = 5.5 ± 0.1. The data points are experimental and the curve is calculated (see the text).

The relaxation of the ^{139}La nucleus is thus related to two factors, the chemical environment (reflected in the magnitude of χ) and the microdynamic behavior (reflected in τ_c). Assuming that the complex involving La(III) can be regarded as a rigid sphere with a radius of a and that the correlation time is the reorientation time of the molecule in solution, τ_c is thus related to the viscosity of the solution and given by

$$\tau_c = 4 \pi a^3 \eta \ / 3 k T \qquad (3.3)$$

If the linewidth is divided by the macroscopic viscosity of the solution, the viscosity reduced linewidths should be related only to the chemical environment of the nucleus. Nakamura and Kavamura[58] utilized this approach in the investigation of the solutions of lanthanum nitrate, chloride, and perchlorate. They arrived at the conclusion that in solutions of $La(NO_3)_3$ inner - sphere complexes were formed. In the cases of chloride and perchlorate, the viscosity reduced linewidths of ^{139}La NMR first decreased and then increased with an increase of the La(III) concentration. In order to interpret their results they postulated that two different kinds of hydrated La(III) coexisted, $La(H_2O)_8$ and $La(H_2O)_9$, in the cases of chloride and perchlorate. $La(H_2O)_8$ has higher symmetry than $La(H_2O)_9$ and the population of octa-hydrated species increased with an increase of the La(III) concentration. The variation of $(\upsilon_{1/2} / \eta)$ with the concentration would be due to a shift of the equilibrium between these two species rather than to the cation - anion interactions. This postulate, however, was not confirmed by other investigations[86,59,93]. In 1975, Reuben[59] investigated the longitudinal relaxation rate, T_1^{-1}, of ^{139}La in aqueous solutions of lanthanum salts. He found that outer - sphere La(III) - ClO_4^- and inner - sphere La(III) - NO_3^- ion pairs formed. The explanation of his results also supported the constancy of the La(III) coordination number. Tarasov *et al*[64] studied the aqueous solutions of lanthanum salts by ^{139}La NMR spectroscopy in 1982. Based on their data, they concluded that La(III) formed inner sphere complexes

with both nitrate and perchlorate anions and the complexation with chloride anion occurred at higher concentration.

The above-mentioned reports show that the experimental results obtained by different groups are similar. Different interpretations of the results, however, lead to different conclusions. Our results were interpreted quantitatively.

Since the ^{139}La chemical shifts are directly related to the chemical environment of the La(III) species, the variation of ^{139}La NMR chemical shift with La(III) concentration is evidence that different La(III) species exist in solution and the exchange among these species is very fast. The observed chemical shifts, therefore, will be the weighted sum of those for these La(III) species. We measured the ^{139}La NMR parameters of $La(NO_3)_3$ solutions at pH 6.5, 5.5, and 4.0. Figures 3.4 and 3.5 are respectively the results of ^{139}La NMR chemical shifts and transverse relaxation rates as a function of lanthanum nitrate concentration at these pH's. One can see from figures 3.4 and 3.5 that the same results for both chemical shifts and linewidths are obtained at different pH. The independence of the chemical shifts and of linewidths on pH variation excludes, in that range of pH, any lanthanum ion hydrolysis. The variation of the ^{139}La NMR spectra with La(III) concentration has to come from cation - anion interactions. The quantitative treatment of the results was done, on the basis of the ion-pair model of equation 3.4 ($X = NO_3^-, Cl^-, ClO_4^-$).

$$La(III) + X^- \rightleftharpoons LaX^{2+} \qquad (3.4)$$

Considering the range of La(III) salt concentration used, activity coefficient effects have to be taken into account. The thermodynamic stability constants (K_{th}) are used instead of ion pair formation constants K_p for the calculation. The relationship between K_{th} and K_p can be expressed as[68]:

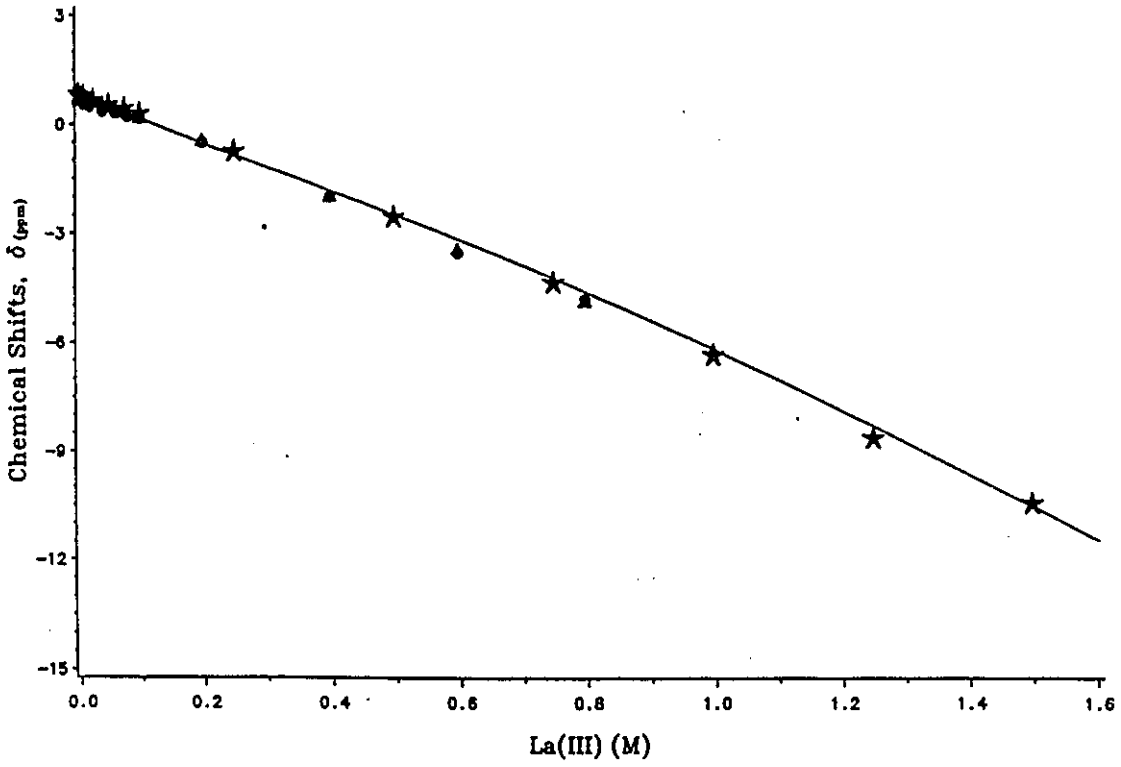

Figure 3.4: ^{139}La NMR chemical shifts as a function of lanthanum concentration for lanthanum nitrate in aqueous solution at different pH values. (•) pH = 6.5 ± 0.1, (★) pH = 5.5 ± 0.1, and (▲) pH = 4.0 ± 0.1. T = 300 K.

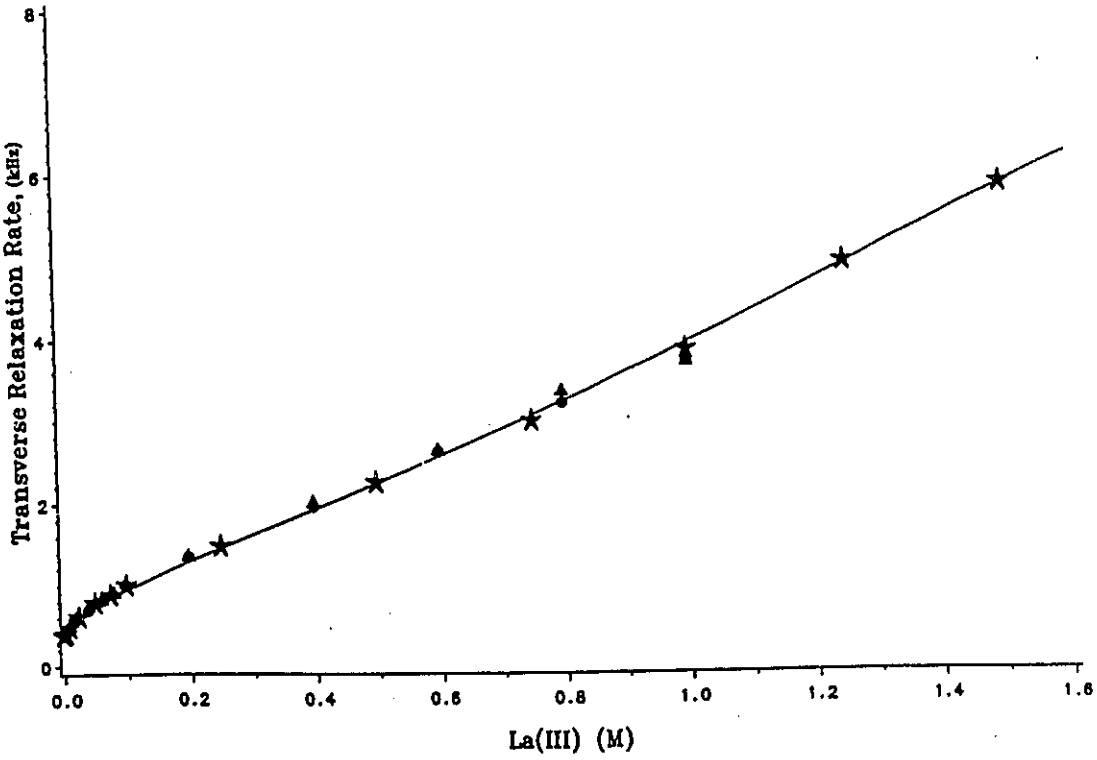

Figure 3.5: ^{139}La NMR transverse relaxation rates as a function of lanthanum concentration for lanthanum nitrate in aqueous solution at different pH values. (•) pH = 6.5 ± 0.1, (★) pH = 5.5 ± 0.1, and (▲) pH = 4.0 ± 0.1. T = 300 K.

$$K_{th} = a_{[LaX]}/(a_{[La]}a_{[X]}) = K_p/\gamma_{\pm} \quad (3.5)$$

where $K_p = [(LaX)^{2+}]/[La(III)]\,[X^-]$ and $\gamma_{\pm}$ is the mean activity coefficient of the lanthanum salts.

The analytical concentration of the ion-paired species is given by equation 3.9, derived from equations 3.5 to 3.8, with $[La(III)]_T$ being the total concentration of La(III).

$$[La(III)] = [La(III)]_T - [(LaX)^{2+}] \quad (3.6)$$

$$[X^-] = 3\,[La(III)]_T - [(LaX)^{2+}] \quad (3.7)$$

$$Q = 4\,[La(III)]_T + (K_{th}\gamma_{\pm})^{-1} \quad (3.8)$$

$$[(LaX)^{2+}] = 0.5\,Q - (0.25\,Q^2 - 3\,[La(III)]_T^2)^{0.5} \quad (3.9)$$

The highest concentration of La(III) used in the experiment is 1.5 M. The general Debye-Hückel equation cannot be used to get the mean activity coefficient, $\gamma_{\pm}$, for such high concentrated solution. The Bromley method was used to get $\gamma_{\pm}$[94,95]. We chose the Bromley method to calculate the $\gamma_{\pm}$ for two reasons. One is that this method is valid until quite high concentration (I = 6 M). The other is that Bromley parameter, B, for all three lanthanum salts can be found in the literature[95]. The Bromley method for the $\gamma_{\pm}$ calculation is indicated in equation 3.10, where B, I, and A are the Bromley parameter, the ionic strength, and the Debye-Hückel constant respectively.

$$\log \gamma_{\pm} = -A|z_+z_-|I^{0.5}/(1+I^{0.5}) + (0.06+0.6B)|z_+z_-|I/(1+1.5I/|z_+z_-|)^2 + BI \quad (3.10)$$

The observed ^{139}La NMR chemical shifts (δ_{obs}; equation 3.11) are population-averaged on the chemical shifts of the two sites, solvated (δ_s) and ion-paired La(III) (δ_p), of equation 3.4.

Table 3.1:

Thermodynamic equilibrium constants for ion-pair formation and NMR parameters characteristic of the La(III) species in aqueous solution (pH=5.5; T=300 K)

Anion	δ_s[a] (ppm)	δ_p[b] (ppm)	K_{th}[c]	$(T_2^{-1})_s$[d] (kHz)	$(T_2^{-1})_p$[e] (kHz)	K_{th}[f]
NO_3^-	1.09±0.07	-25 ± 2[g]	0.41±0.04	0.47±0.03	11.2±0.5	0.50±0.04
Cl^-	1.04±0.06	22 ± 2	0.23±0.04	0.31±0.01	5 ± 2	0.06±0.03
ClO_4^-	0.64±0.04	-3.1±0.2	0.04±0.01	0.34±0.01	1.65±0.07	0.022±0.003

a, ^{139}La NMR chemical shifts of solvated La(III) (at infinite dilution);

b, ^{139}La NMR chemical shifts of ion-paired La(III) (see equations 3.4 and 3.11);

c,f, Thermodynamic equilibrium constants of $(LaX)^{2+}$ formation, determined from chemical shift variation(c) and from linewidth variation(f);

d, ^{139}La NMR transverse relaxation rates of solvated La(III);

e, ^{139}La NMR transverse relaxation rates of ion-paired La(III);

g, All errors are given as one standard deviation, σ, from the non-linear regression.

$$\delta_{obs}\,[La(III)]_T = \delta_s\,[La(III)] + \delta_p\,[(LaX)^{2+}] \qquad (3.11)$$

Using δ_s, δ_p, and K_{th} as the adjustable parameters and with B = 0.0868, 0.0818 and 0.2513 for lanthanum nitrate, chloride and perchlorate respectively[95], the observed ^{139}La chemical shifts were fitted to equations 3.4 to 3.11 by a three-parameter non-linear regression procedure[96]. The data points in Figure 3.2 are experimental and the lines are calculated from the values of the adjustable parameters reported in Table 3.1

The same procedure was applied to the transverse relaxation rates(T_2^{-1}) of ^{139}La by using $(T_2^{-1})_s$, $(T_2^{-1})_p$, and K_{th} as the adjustable parameters. The observed ^{139}La NMR relaxation rates$(T_2^{-1})_{obs}$ (equation 3.12) are population-weighted on the relaxation rates of the two sites, solvated$(T_2^{-1})_s$ and ion-paired$(T_2^{-1})_p$, of equation 3.4.

$$(T_2^{-1})_{obs}\,[La(III)]_T = (T_2^{-1})_s\,[La(III)] + (T_2^{-1})_p\,[(LaX)^{2+}] \qquad (3.12)$$

Figure 3.3 gives the variation of the ^{139}La NMR transverse relaxation rates as a function of La(III) concentrations. Again, in figure 3.3, the points are experimental and the curves are calculated from the parameters given in table 3.1 and through equations 3.4 to 3.10 and equation 3.12.

The ^{139}La NMR parameters at infinite dilution are solely determined by the solvent molecules. Therefore, the ^{139}La NMR chemical shifts and linewidths of the solvated La(III) species will be same for nitrate, chloride, and perchlorate. This is shown in our results. The ^{139}La NMR chemical shifts of solvated La(III) are about 1 ppm compared to the reference. The transverse relaxations rates are in average 370 Hz, which is identical to the value reported in the literature[63]. The agreement of ^{139}La NMR chemical shift and transverse relaxation rate of solvated La(III) species in the cases of three lanthanum salts is a good support for the model. The ^{139}La NMR

chemical shifts obtained for the ion-paired La(III) species are quite different, depending upon the nature of the anions: -25 ± 2 ppm for nitrate, 22 ± 2 ppm for chloride, and -3.1 ± 0.2 ppm for perchlorate. The variation is also shown in the transverse relaxation rates, 11.2 ± 0.5 kHz for nitrate, 5 ± 2 kHz for chloride, and 1.65 ± 0.07 kHz for perchlorate. The ^{139}La NMR chemical shifts of the hexanitrato lanthanum $\{La(NO_3)_6\}^{3-}$ and of hexachloro $\{LaCl_6\}^{3-}$ complexes in acetonitrile were reported to be respectively -60 and 851 ppm[65]. Although the reported chemical shift data are not directly comparable to our results, because the solvent used and the lanthanum species are different, the shifts of -25 ppm for $\{LaNO_3\}^{2+}$ and 22 ppm for $\{LaCl\}^{2+}$ are indications of the presence of NO_3^- and Cl^- in the first coordination sphere of La(III). The quality of the regression can be further checked by the values of the thermodynamic equilibrium constants: K_{th} obtained from ^{139}La NMR chemical shifts and transverse relaxation rates, two different and independent series of data, are the same in the error limits for nitrate and perchlorate, and are in the same order of magnitude for chloride.

The thermodynamic stability constants of formation of LaX^{2+} decrease in the order of $NO_3^- > Cl^- > ClO_4^-$. By fluorescence lifetime measurements, Breen and Horrocks[85] obtained complexation constants of 0.13 and 1.41 respectively for $EuCl^{2+}$ and $EuNO_3^{2+}$ in aqueous solution. By the same technique, Bunzli and Yersin[88] obtained a stability constant of 0.3 for $EuNO_3^{2+}$. Formation constants of 0.53[93], 0.54[96] for $DyNO_3^{2+}$ and 0.66[97] for $PrNO_3^{2+}$ were reported in the literature. Inner sphere complexes of Pr(III), Gd(III), and Yb(III) with ClO_4^- were characterized by Kasabov *et al*[98] by an electromigration method. The authors reported formation stability constants of 0.01, 0.03, and 0.045, respectively. All these values, with all three anions, are in fair agreement with the results obtained in the present work.

The K_{th} values for $LaCl^{2+}$ and $LaClO_4^{2+}$ are relatively small, for example 0.03 in the case of lanthanum perchlorate. Such small amounts of inner-sphere complexes

could plausibly not be detected by less sensitive methods, such as fluorescence lifetime measurements[85,88]. This may be the explanation of the controversial nature of the ion-pairing in these two systems. However, modern FT NMR instruments allow the observation of the ^{139}La NMR parameter variations in these systems since the parameters are sensitive to the electronic distribution at the site of the La(III) cation. In the present work, both chemical shift and transverse relaxation rate measurements can be interpreted by the formation of contact ion pairs (inner sphere coordination complexes) of La(III) in aqueous solutions, for all three anions.

Finally, one should note that the transverse relaxation rates used to account for the model of equations 3.4 to 3.10 are not viscosity corrected, which give results in good agreement with the values obtained from chemical shift data. The results of transverse relaxation rates divided by the relative viscosity of the solution are shown in figure 3.6. The viscosity reduced T_2^{-1} are almost horizontal lines in the concentration of 0.01 - 1.5 M in the cases of chloride and perchlorate. In the case of nitrate, the viscosity corrected transverse relaxation rate is quite different from the non-corrected T_2^{-1} in the concentration dependence. The (T_2^{-1}/η) data of nitrate have been analyzed by a procedure similar to T_2^{-1}. The regression curve is given in figure 3.6. The obtained stability constant, 4.8 ± 0.5, is more than one order of magnitude larger than the value obtained from chemical shifts (see table 3.1) and reported in the literature for similar systems[85,88,93-97]. This indicates that the linewidth of ^{139}La may not be directly related to the viscosity of the solution. In other words, the quadrupolar relaxation mechanism of ^{139}La does not originate from reorientational time fluctuations. Therefore, the correlation time responsible for the $^{139}La(III)$ quadrupolar relaxation in aqueous solutions must be characteristic of other time fluctuation of the electric field gradient at the nucleus, such as rapid internal reorganization of the solvation shell, or rapid solvent molecule exchange in this solvation shell. Cossy *et al*[86] have recently reported an ^{17}O NMR kinetic study of water exchange on the lanthanide(III) aqua ions. They found an increase of the water exchange rate in going from heavier (Yb^{3+}; 4.1×10^7 s^{-1}) to

lighter (Tb^{3+}; 5.0×10^8 s^{-1}) cations in the series. The trend is confirmed by a previously determined value for Gd^{3+} (1.1×10^9 s^{-1})[99] and by a lower limit value of 10^9 s^{-1} estimated for the exchange on Nd^{3+}[100]. Assuming that the trend also holds for the lighter lanthanides, by linear extrapolation from the data reported by Cossy *et al.*[86], one can estimate a water exchange rate of 6.3×10^{10} s^{-1}, or a residence time of water in the first coordination sphere of 16 ps, for La^{3+}, a value falling in the reorientational time scale. From the estimated molecular volume of the aquated cation (based on neutron diffraction data[83]) and the measured solution viscosity, the reorientational correlation time τ_c can be calculated from the Debye-Stokes-Einstein equation (3.13) (similar to that mentioned previously; equation 3.3), in which a is the molecular radius of the reorientating entity, estimated to be 4Å, η is the viscosity of the solution, and f_R is a microviscosity coefficient[101]. Depending upon the value chosen for f_R, τ_c can be calculated to be between 65 ps ($f_R = 1$) and 11 ps ($f_R = 1/6$). The value usually taken in the case of solute and solvent molecules of similar size is $f_R = 1/6$[101]. These estimated values of reorientational times are very reasonable, since a value of 70 ps was previously reported for proton relaxation rates in dilute $GdCl_3$ solutions[102]. Assuming that the relaxation process is controlled by water exchange in the first solvation shell, 1.5×10^{10} s^{-1} (the exchange rate corresponding to a residence time of 65 ps) is a *lower* limit value for the exchange rate of water in the solvation shell of La^{3+}. This is in good agreement with the extrapolated value of 6.3×10^{10} s^{-1} obtained from reference 86, as discussed above (for $f_R = 1/6$, $\tau_c = 11$ ps and the exchange rate would be 9.1×10^{10} s^{-1}).

$$\tau_c = 4/3\ \pi\ a^3\ (\eta/kT)\ f_R \qquad (3.13)$$

In the cases of chloride and perchlorate, the variation of T_2^{-1}/η with the La(III) concentration was too small to allow any regression to be made which could have allowed such a comparison with the chemical shift data. However, the fact that the

parameters determined from chemical shifts and, independently, from viscosity-uncorrected relaxation rates are in good agreement, suggests that in these two cases also, as for nitrate, the quadrupolar relaxation is controlled by water exchange in the solvation shell.

In conclusion, the chemical shifts and the transverse relaxation rates (linewidths) of ^{139}La NMR in the aqueous solutions of nitrate, chloride, and perchlorate, have been measured as a function of La(III) concentration. The experimental data could be accounted for by the presence of 1 : 1 inner sphere complexes of La(III) with these three anions. The thermodynamic stability constants of formation of these ion pairs were determined by introducing activity coefficient effects to the data analyses. They are 0.4 - 0.5 for nitrate, 0.1 - 0.2 for chloride, and 0.02 - 0.04 for perchlorate.

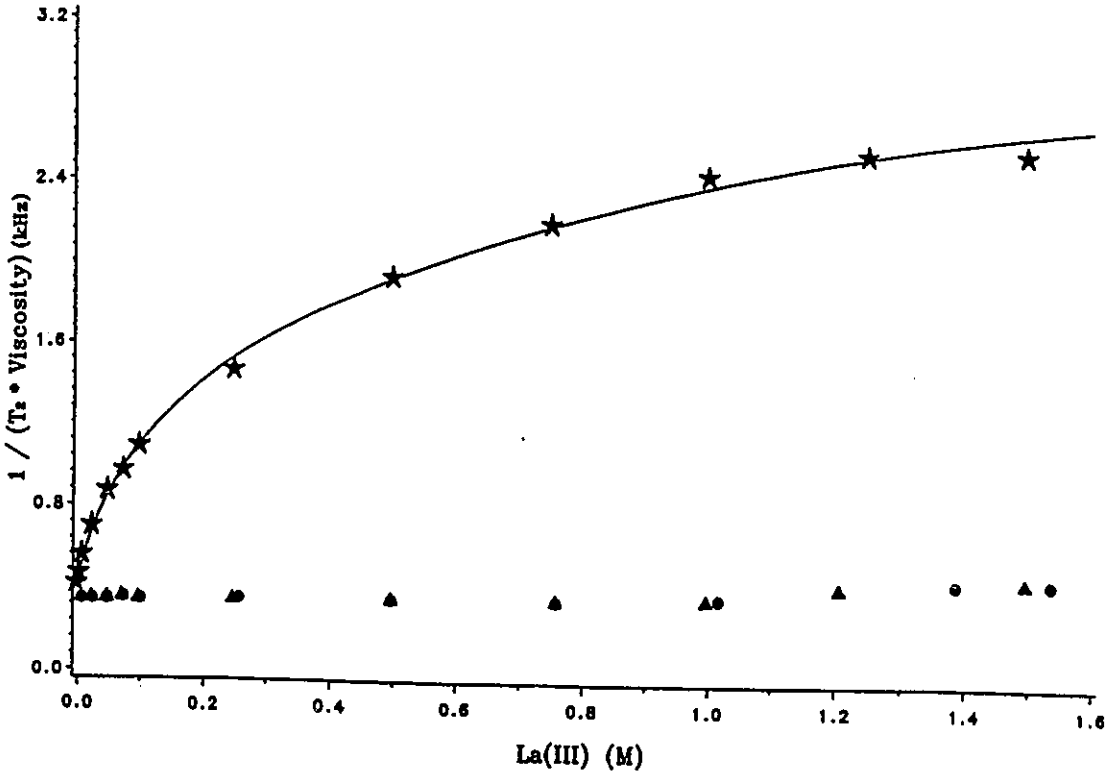

Figure 3.6: Viscosity corrected ^{139}La NMR transverse relaxation rates as a function of lanthanum concentration for lanthanum nitrate, perchlorate, and chloride in aqueous solution. (★) nitrate, (●) perchlorate, and (▲) chloride. pH = 5.5 ± 0.1. T = 300 K.

3.2: *The Nature of the La(III) First Coordination Sphere in Acetonitrile Solutions Studied by ^{139}La and ^{17}O NMR Spectroscopy*

3.2.1 Introduction:

In the preceding section, the formation of ion pairs was detected by ^{139}La NMR in the aqueous solutions of lanthanum salts. It is expected that ion pairs will be formed more easily in poorly coordinating solvents. However, information on such interactions is rather scarce[4,5]. Bunzli et al has investigated the interactions between lanthanoid cations and perchlorate anions in anhydrous acetonitrile solutions by FTIR spectroscopy. They found that inner sphere complexes of Ln^{3+} with ClO_4^- were formed in these systems[103,104]. The nature of the solutions of lanthanide chloride in methanol and methanol-water mixtures has been studied by several techniques, including X-ray diffraction[61,105], NMR spectroscopy[61,62,68], ultrasonic absorption measurements[106], and UV-Visible spectroscopy[87]. On the basis of these studies, evidence was found to show that contact ion pairs are formed between Ln^{3+} and Cl^- in water-methanol solutions. As methanol replaces water, the degree of Ln-Cl inner sphere coordination increases. Inner sphere complexes of Ln^{3+} with nitrate and perchlorate anions were also found to be formed in methanol-water solutions[87].

We are mainly interested in the complexation of lanthanoid cations with crown ethers in non-aqueous solutions. As a first step, some basic knowledge of the coordination behavior of these metal ions alone in solution is needed. In this part of the thesis, the nature of the La^{3+} coordination sphere was investigated by means of ^{139}La and ^{17}O NMR spectroscopies when the salt $La(NO_3)_3\ 6H_2O$ was dissolved in anhydrous acetonitrile. These NMR techniques permit one to characterize the competition between small amounts of water and bulk solvent molecules for the occupation of the La(III) first coordination shell. A model is proposed, and a quantitative interpretation of the results is given, allowing the calculation of the equilibrium constant of formation of the monohydrated species, $La(NO_3)_3.H_2O$.

3.2.2 Results and Discussions.

The chemical shifts and linewidths of the ^{139}La NMR spectra have been measured as a function of the $La(NO_3)_3.\ 6H_2O$ concentration in acetonitrile. In the range of concentrations studied, the ^{139}La NMR spectra consist of a single Lorentzian line. Figure 3.7 shows a series of ^{139}La NMR spectra for various concentrations, ranging from 0.010 M to 0.100 M. Because the variations of the ^{139}La NMR chemical shifts and linewidths with concentration were small, the chemical shift and linewidth for each spectrum of ^{139}La were obtained by a complete lineshape analysis of the experimental Lorentzian lines. The ^{139}La NMR signals shift downfield, from 7.9 ppm to 12.0 ppm, as the concentration of La(III) increases from 0.0050 M to 0.10 M. The linewidths values decrease from 2750 Hz to 1930 Hz with an increase of the La(III) concentration from 0.0050 M to 0.10 M.

These results indicate that at least two different La(III) species, with different chemical environments, coexist and exchange rapidly in the solution. The formation of these different La(III) solution sites can be the results of interaction of La(III) with nitrate anion, water, and/or solvent molecules.

The ^{17}O NMR spectra proved useful in showing which kind of interaction is dominant in the solution. Two ^{17}O peaks were observed: at 428 ppm, corresponding to the nitrate anion (Figure 3.8), and at higher fields, in the range -10 to 10 ppm, corresponding to water (Figure 3.9). The ^{17}O NMR chemical shifts and linewidths of the nitrate anion are independent of the $La(NO_3)_3.6H_2O$ concentrations, in the limits of the experimental errors. The ^{17}O NMR chemical shifts of water, on the other hand, vary with the concentrations of hydrated lanthanum nitrate, from -2.26 ppm to 10.6 ppm in the La(III) concentration range of 0.005 M to 0.10 M. Figure 3.8 and 3.9 show a series of ^{17}O NMR spectra for various concentrations of $La(NO_3)_3.6H_2O$.

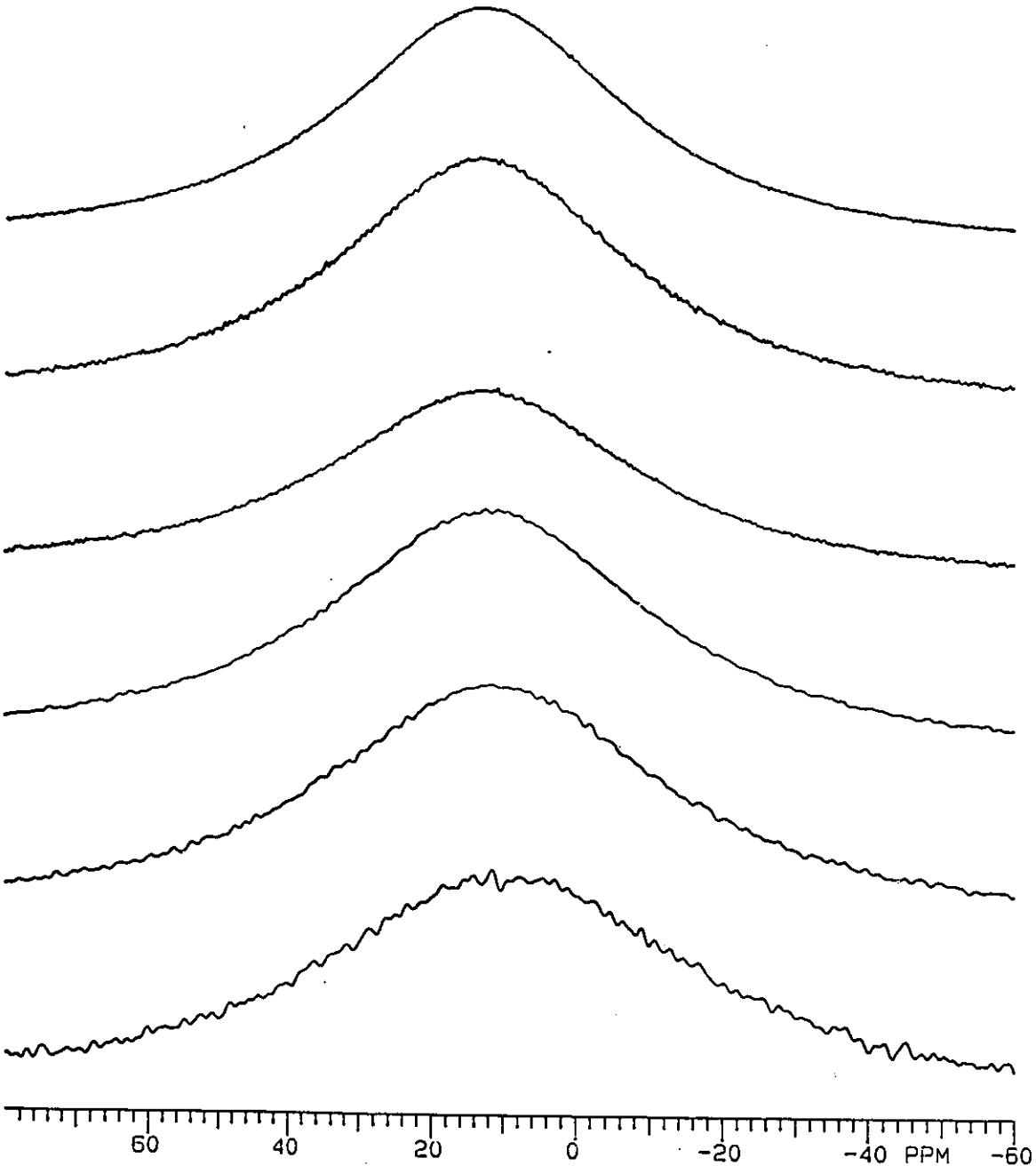

Figure 3.7: A series of ^{139}La NMR spectra at various concentrations of $La(NO_3)_3$ 6 H_2O in AN. Top to bottom [La(III)] = 0.100, 0.050, 0.040, 0.030, 0.020, and 0.010 M. T = 300 K.

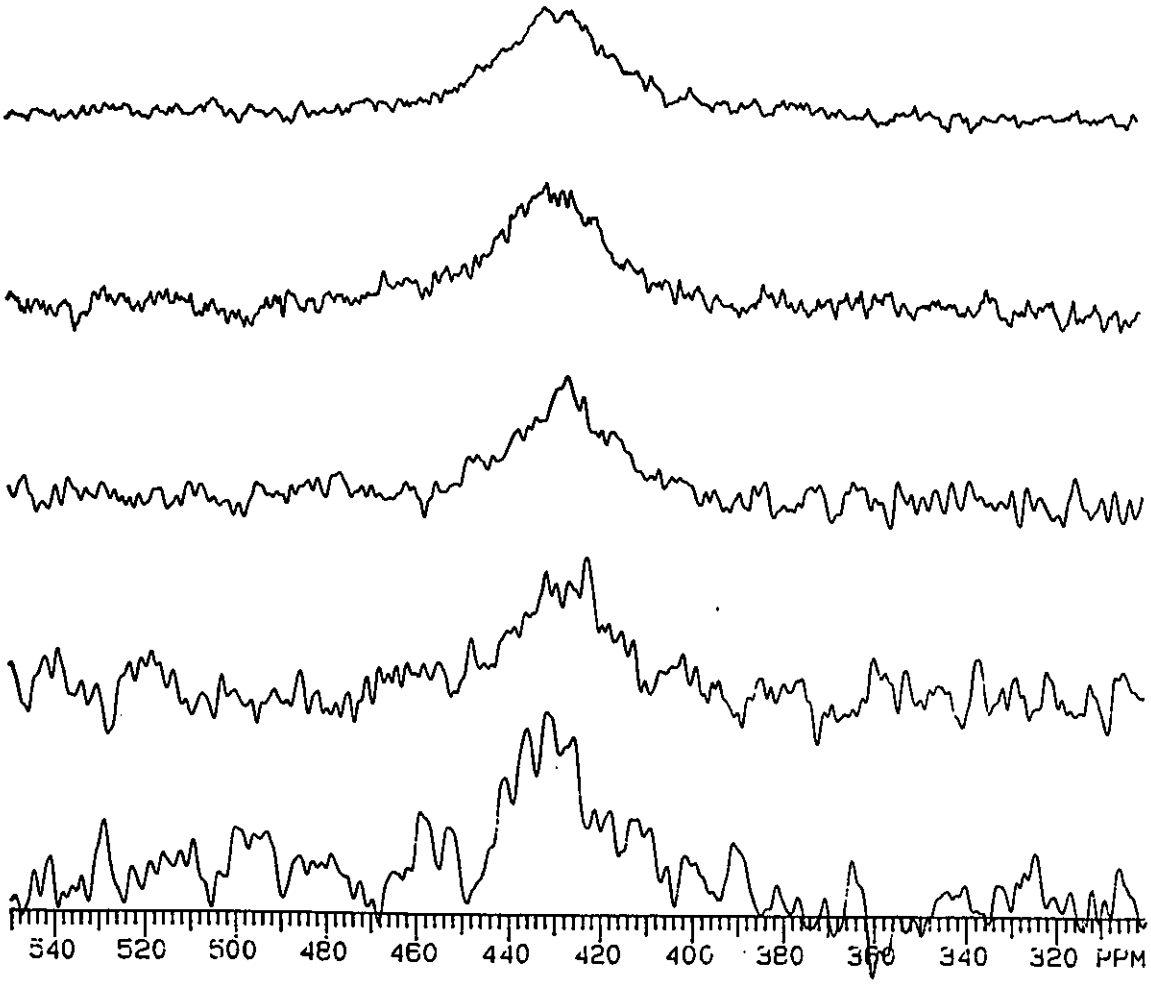

Figure 3.8: ^{17}O NMR spectra of $N^{17}O_3^-$ for $La(NO_3)_3$ 6 H_2O solution in AN. Top to bottom [La(III)] = 0.090, 0.070, 0.050, 0.025, and 0.015 M. T = 300 K.

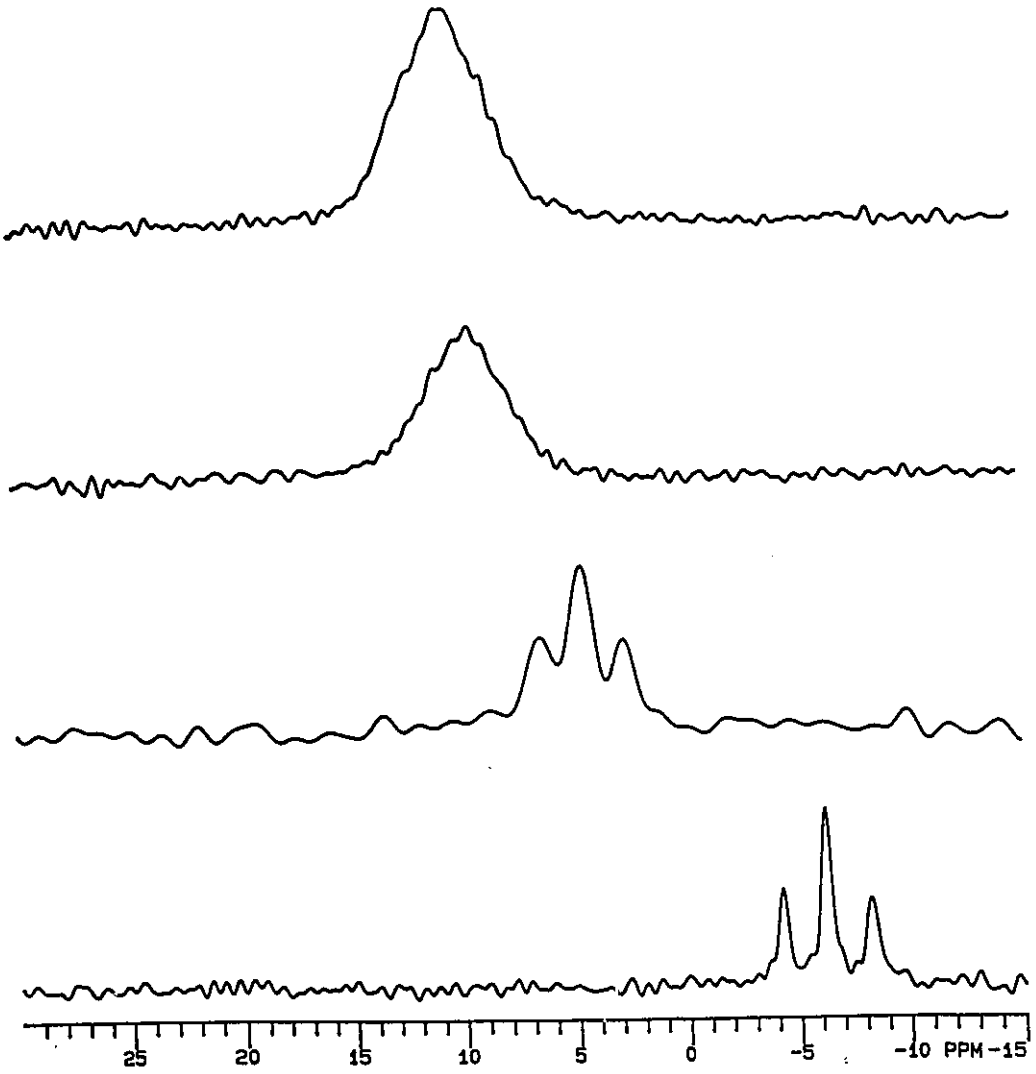

Figure 3.9: ^{17}O NMR spectra of $H_2{}^{17}O$ for $La(NO_3)_3$ 6 H_2O solution in AN. Top to bottom [La(III)] = 0.090, 0.070, and 0.025 M. The bottom spectrum is free water in AN ([H_2O] = 0.090 M). T = 300 K.

These characteristics indicate the presence of only one type of NO_3^- and of at least two types of water molecules. As it has been shown by several studies[65,106,107], all three nitrate anions are expected to be coordinated to the La(III) cation, while a variable number of water molecules is expected to be in the first coordination sphere of La(III). The different La(III) sites, which are observed on the ^{139}La NMR spectra, are thus attributed to chemical species characterized by a different number of water molecules coordinated to La(III). The following model is proposed, and accounts for the experimental data (Equations 3.14-3.21).

$$\{La(NO_3)_3 \, x \, H_2O\} + \{H_2O\} \rightleftharpoons \{La(NO_3)_3 \, (x+1) \, H_2O\} \qquad (3.14)$$

Let $[A] = [La(NO_3)_3 \, x \, H_2O]$ and $[B] = [La(NO_3)_3 \, (x+1) \, H_2O]$

$$K = [B]/[H_2O]/[A] \qquad (3.15)$$

$$[A] = [La]_o - [B] \qquad (3.16)$$

$$[H_2O] = (6 - x) \times [La]_o - [B] \qquad (3.17)$$

$$C = (7 - x) \times [La]_o + 1 / K \qquad (3.18)$$

$$D = (6 - x) \times [La]_o^2 \qquad (3.19)$$

$$[B] = 0.5 \times C - (0.25 \times C^2 - D)^{1/2} \qquad (3.20)$$

Where $[La]_o$ is the initial (or total) concentration of La(III).

$$\delta_{obs} = \delta_A \times (1 - [B]/[La]_o) + \delta_B \times [B] / [La]_o \qquad (3.21)$$

δ_A and δ_B are the chemical shifts for site A ($\{La(NO_3)_3 \times H_2O\}$) and site B ($\{La(NO_3)_3 (x+1) H_2O\}$), respectively.

Using δ_A, δ_B, and K (equilibrium constant) as adjustable parameters, the observed ^{139}La NMR chemical shifts (δ_{obs}) were fitted through equations 3.14 to 3.21 by a three-parameter nonlinear regression procedure[96]. The regressions were done with different x values. The results are reported in Table 3.2. Figure 3.10 shows the observed ^{139}La NMR chemical shifts (δ_{obs}) as a function of $La(NO_3)_3$ 6 H_2O concentrations in acetonitrile solutions, in which the points are experimental and the line is calculated from the values of the adjustable parameters with x = 0 reported in Table 3.2.

A similar treatment was made for linewidths($\nu_{1/2}$).

$$(\nu_{1/2})_{obs} = (\nu_{1/2})_A \ (1 - [B]/[La]_o) + (\nu_{1/2})_B \ [B]/[La]_o \qquad (3.22)$$

$(\nu_{1/2})_A$, $(\nu_{1/2})_B$, the linewidths respectively for site A and site B, and K are used as adjustable parameters. The results are also given in Table 3.2. Figure 3.11 gives the variations of $(\nu_{1/2})_{obs}$ with the concentration of hydrated lanthanum nitrate, in which the points are experimental and the curve is calculated, based on the values of the parameters of Table 3.2 with x = 0.

The regressions were done for all the values of x between 0 and 4. From the results reported in Table 3.2, it appears that the ^{139}La NMR chemical shifts and linewidths results can be accounted for by a model such as the one of equation 3.14. However, the quality of the ^{139}La NMR data, particularly the small range of variations, precludes a fine analysis to be successful in determining x, the number of coordinated water molecules. There is a strong covariance between x and the equilibrium constant K in the non-linear regression procedure. Figure 3.10 and 3.11 are the regression curves with x = 0 for the chemical shifts and linewidths, respectively. Very similar regression curves, which are not shown, were obtained with other x values.

Table 3.2:

Equilibrium constants and ^{139}La NMR parameters characterizing the La(III) species in acetonitrile solutions of $La(NO_3)_3\ 6H_2O$ (T=300 K)

X[a]	δ_A[b] (ppm)	δ_B[c] (ppm)	Log K[d]	$(\nu_{1/2})_A$[e] (kHz)	$(\nu_{1/2})_B$[f] (kHz)	Log K[g]
0	5.8±0.6	12.9±0.2	1.1±0.4[h]	2.92±0.05	1.60±0.06	0.8±0.2
1	5.7±0.7	13.0±0.2	1.2±0.4	2.93±0.05	1.60±0.06	0.9±0.2
2	5.7±0.7	13.0±0.3	1.4±0.5	2.94±0.06	1.59±0.06	1.0±0.3
3	5.6±0.7	13.0±0.3	1.5±0.6	2.94±0.06	1.57±0.07	1.1±0.5
4	5.2±0.9	13.1±0.3	1.8±0.9	2.96±0.06	1.53±0.07	1.3±0.7

a, Number of water molecules in the first coordination shell of La(III);

b, ^{139}La NMR chemical shift of species A ($\{La(NO_3)_3 \times H_2O\}$);

c, ^{139}La NMR chemical shift of species B ($\{La(NO_3)_3\ (x+1)H_2O\}$);

d,g, Equilibrium constants (equation 3.15) determined from chemical shift variation (*d*) and from linewidth variation (*g*);

e, ^{139}La NMR linewidth of species A ($\{La(NO_3)_3 \times H_2O\}$);

f, ^{139}La NMR linewidth of species B ($\{La(NO_3)_3\ (x+1)H_2O\}$);

h, All errors are given as one standard deviation, σ, for the nonlinear regression.

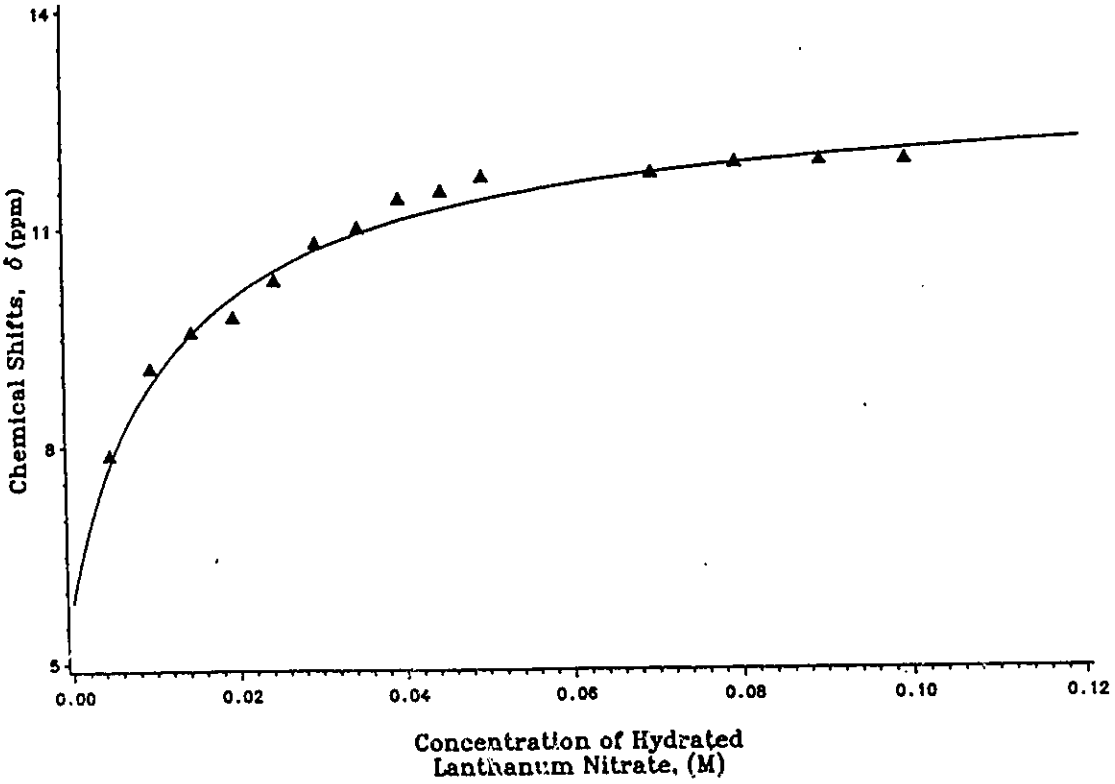

Figure 3.10: ^{139}La NMR chemical shifts as a function of $La(NO_3)_3$ 6 H_2O concentration in AN. The data points are experimental and the curve is calculated from the values of the adjustable parameters reported in table 3.2 with x = 0.

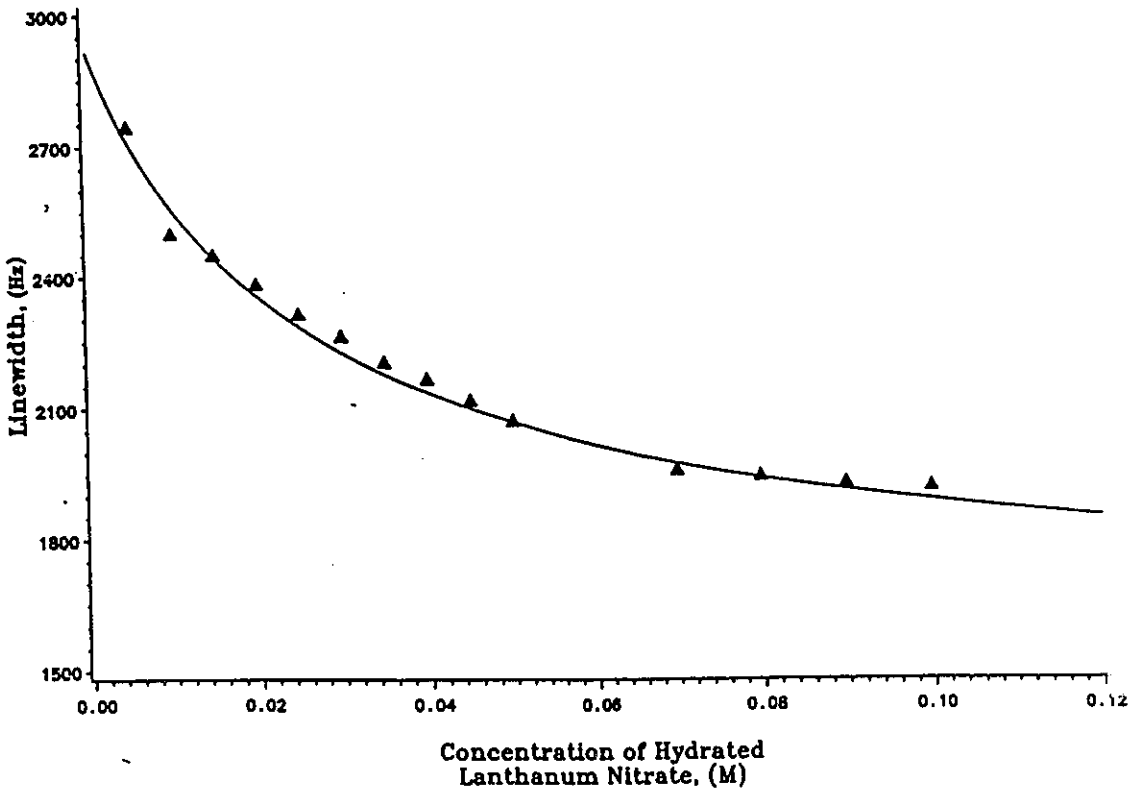

Figure 3.11: ^{139}La NMR transverse relaxation rates as a function of $La(NO_3)_3$ 6 H_2O concentration in AN. The data points are experimental and the curve is calculated from the values of the adjustable parameters reported in table 3.2 with x = 0.

The ^{17}O NMR chemical shifts of water were then considered. On the basis of the model of Equations 3.14 to 3.21, and assuming that all the complexed water molecules have the same ^{17}O NMR chemical shift, the observed ^{17}O NMR chemical shifts is the weighted sum of the characteristic chemical shifts of coordinated and free (or solvated) water.

$$\delta_{obs} = \delta_f [H_2O]_f / 6 [La]_o + \delta_c [H_2O]_c / 6 [La]_o \quad (3.23)$$

$$[H_2O]_c = x [La]_o + [B] \quad (3.24)$$

$$[H_2O]_f = 6 [La]_o - [H_2O]_c \quad (3.25)$$

Where [B] and $[La]_o$ are the same as described previously. δ_f and δ_c are the ^{17}O chemical shifts for free and complexed water, respectively.

The ^{17}O NMR chemical shifts of free water have been measured by adding given amounts of water to anhydrous acetonitrile. Only a very slight dependence of δ_f upon the water concentration could be observed. At water concentrations of 0.62 and 0.31 M, shifts of -5.92 ppm and -6.10 ppm were respectively observed and we chose -6.00 ppm as the value of δ_f for the non-linear regression analysis. The observed ^{17}O NMR chemical shifts of water for $La(NO_3)_3$ 6 H_2O acetonitrile solutions were then fitted through equations 3.14 to 3.21 and 3.23 to 3.25 using δ_c, K, and x as the adjustable parameters. The result of this regression is reported in Table 3.3. In Figure 3.12, the points are the experimental values of the ^{17}O NMR chemical shifts of water and the curve is calculated from the parameters reported in Table 3.3. The non-linear regression gives a value for x (see Equation 3.14) of zero. It is worth stressing that the K values obtained from ^{17}O NMR chemical shift data and from both ^{139}La NMR chemical shift and linewidth data are in good agreement. This is strong support for the proposed model.

Table 3.3:

Equilibrium constant and $H_2{}^{17}O$ NMR parameters of characterizing the La(III) chemical species in acetonitrile solutions of $La(NO_3)_3\ 6H_2O$ (T=300 K)

X[a]	δ_f[b](ppm)	Log K[c]
-0.01±0.06[d]	120±5	0.9±0.3

a, Number of water molecules in the first coordination shell of La(III);

b, ^{17}O NMR chemical shift of the water molecule coordinated to La(III);

c, Equilibrium constant (equation 3.15) determined from the water ^{17}O NMR chemical shift variation;

d, All errors are given as one standard deviation, σ, from the nonlinear regression.

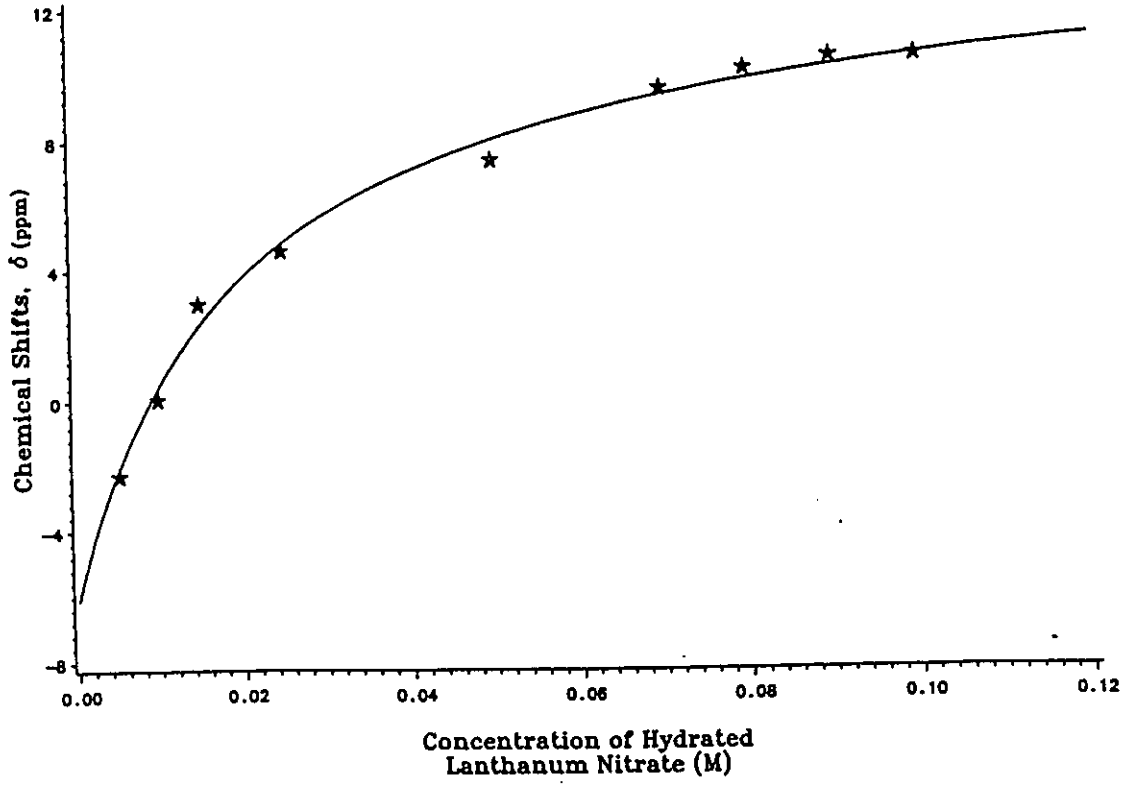

Figure 3.12: ^{17}O NMR chemical shifts of H_2O as a function of $La(NO_3)_3$ 6 H_2O concentration in AN. The data points are experimental and the curve is calculated from the values of the adjustable parameters reported in table 3.3 with $\delta_f = -6.00$ ppm.

The ^{139}La NMR chemical shift of $La(NO_3)_3$ in acetonitrile is 5.8 ± 0.6 ppm (x=0; Table 3.2). Evans and Missen[21] have investigated the interactions between NO_3^- and La(III) by progressively adding $(NBu_4)(NO_3)$ to the anhydrous acetonitrile solution of lanthanum perchlorate. They found that both chemical shift and linewidth of ^{139}La NMR first increased then decreased as the ratio of NO_3^- : La(III) increased. At the ratio of 3:1 (NO_3^-/La(III)), the observed ^{139}La NMR chemical shift was 10 ± 2 ppm (see reference 65, Figure 3). This value is comparable with our result although the systems involved are not identical.

The ^{139}La NMR chemical shift of $La(NO_3)_3.H_2O$, 12.9 ± 0.2 ppm, is higher than that of $La(NO_3)_3$. The shift is caused by the replacement of acetonitrile molecule(s) by a water molecule in the first coordination shell of La(III). A similar result was reported by Evans and Missen[65]. They showed that the progressive addition of water to an anhydrous $La(ClO_4)_3$ solution in acetonitrile caused the ^{139}La NMR signals to shift downfield.

The calculated ^{139}La NMR linewidths for $La(NO_3)_3$ and $La(NO_3)_3.H_2O$ are 2.9 kHz and 1.6 kHz, respectively. Again, the calculated linewidth value of $La(NO_3)_3$ is of the same order of magnitude as that reported by Evans and Missen[65]($\nu_{1/2} \sim 3.8 \pm 0.2$ kHz at NO_3^- : La(III) of 3 : 1, estimated from Figure 3 of reference 65). It is interesting that the ^{139}La linewidth value for $La(NO_3)_3.H_2O$ is smaller than that for $La(NO_3)_3$. This indicates a higher symmetry of the electronic charge distribution around the ^{139}La nucleus in $La(NO_3)_3.H_2O$ than in $La(NO_3)_3$, when an oxygenated ligand (water) replaces one or several acetonitrile molecules in the first coordination sphere of La(III).

The ^{17}O NMR chemical shift of free water in acetonitrile is about -6 ppm. This shift is understood on the basis of hydrogen bond breaking, resulting in an increased shielding of the ^{17}O nucleus[108]. Values of -11.3 ± 0.6 ppm and -6.8 ppm have been reported in the literature[107,109] for the ^{17}O chemical shift of water in acetonitrile.

The ^{17}O NMR chemical shift of a water molecule coordinated to the lanthanum

cation is 120 ± 4 ppm. Paramagnetic lanthanide cations have been used as "shift reagents" in ^{17}O NMR measurements[108], but, unfortunately, there is no any ^{17}O NMR data on water coordinated to diamagnetic lanthanide cation available in the literature, and so a direct comparison of the δ_c (^{17}O) obtained in the present work is impossible. However, ^{17}O NMR chemical shifts of coordinated water of +6 ppm in $Al(H_2O)_6^{3+}$ [110], -131.8 ppm in $Pd(H_2O)_4^{2+}$ [111], and 126 ppm in *cis*-$Co(en)_2(H_2O)_2^{2+}$ [112] have been reported. Even in diamagnetic systems, the ^{17}O NMR chemical shift of water varies widely upon complexation, and is very dependent upon the nature of the metal cation.

Finally, from Figure 3.9, one should note that the ^{17}O signal of coordinated water is considerably broadened, compared to the signal of non-coordinated water. In the case of free water, the linewidth of ^{17}O and coupling constant ($J(^{17}O - ^{1}H)$) are 25 Hz and 80 Hz respectively. Since the chemical exchange between free and complexed water is very fast, the observed ^{17}O NMR spectra will be the population averaged of free and complexed water in these two sites. Assuming that the ^{17}O - ^{1}H coupling constant is also 80 Hz for the complexed water, the obtained ^{17}O NMR spectra will be the weighted sum of two triplets with different linewidths. From the data of table 3.3, and on the basis of equation 3.14, a simulation of the various ^{17}O spectra as a function of the total water concentration was performed by using the linewidth for the complexed water as a variable. Examples of the simulations are given in figure 3.13, for the cases of figure 3.9. The characteristic water ^{17}O linewidth of the species $La(NO_3)_3 . H_2O$ could be determined from the simulations: it is equal to 400 ± 50 Hz as an average value.

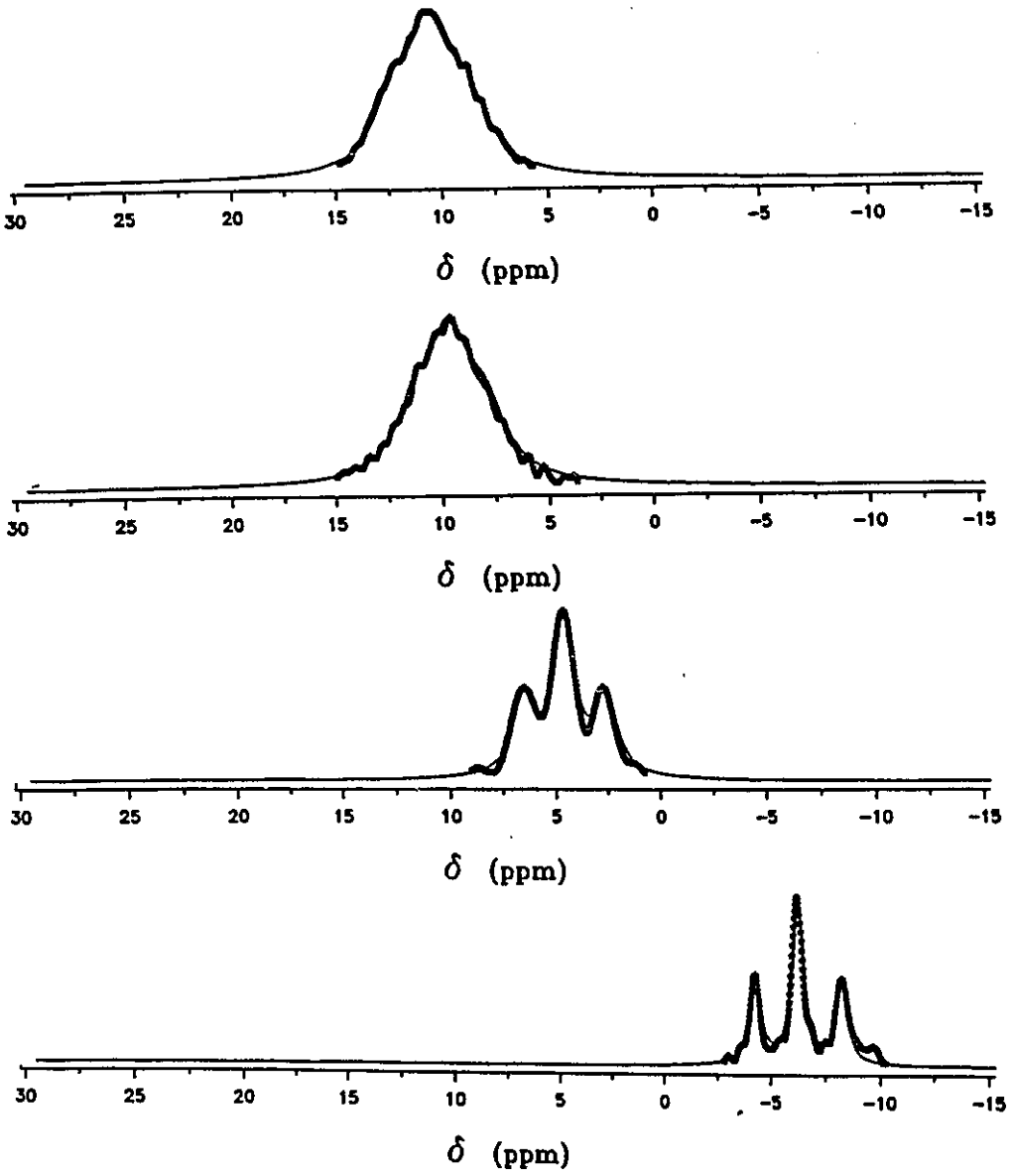

Figure 3.13: Calculated ^{17}O NMR spectra of $H_2{}^{17}O$ for $La(NO_3)_3$ 6 H_2O solution in AN. These spectra are respectively corresponding to the cases shown in figure 3.9. The data points are experimental.

There are several possible contributions to the ^{17}O NMR line broadening when the water coordinates to the La(III) cation. One is the water chemical exchange between its free and coordinated sites. To verify this contribution, we recorded ^{17}O NMR spectra of two samples ([$La(NO_3)_3$ 6 H_2O] = 0.050 and 0.090 M) on a 500 MHz Spectrometer. The experiments were done with proton decoupling. The ^{17}O NMR results, obtained respectively at 40.66 MHz (7.05 T NMR Spectrometer) and at 67.77 MHz (11.75 T NMR Spectrometer) are reported in table 3.4.

Table 3.4:

^{17}O NMR parameters of H_2O in the acetonitrile solutions of $La(NO_3)_3$ 6 H_2O

[La][a](M)	δ^b(ppm)	$\nu_{1/2}{}^b$(Hz)	δ^c(ppm)	$\nu_{1/2}{}^c$(Hz)
0.050	7.40	76	7.12	67
0.090	10.48	80	10.22	74

a, The concentrations of $La(NO_3)_3$ 6 H_2O in acetonitrile;

b, ^{17}O chemical shift and linewidth of H_2O observed at 40.66 MHz;

c, ^{17}O chemical shift and linewidth of H_2O observed at 67.77 MHz.

From the data reported in table 3.4, one can see that, for a given $La(NO_3)_3$ 6 H_2O concentration in AN, the same linewidth was observed at different resonance frequencies. This excludes the contribution of chemical exchange to the linewidth since the line broadening caused by a chemical exchange depends on the applied magnetic field as expressed in equation 3.26.

$$(\nu_{1/2})_{ex} = 4\, P_f\, P_c\, \pi\, (\nu_f - \nu_c)^2\, (k_a + k_b)^{-1} \qquad (3.26)$$

Where $(\nu_{1/2})_{ex}$ is the chemical exchange contribution to the linewidth. P_f and P_c are the populations of water molecules respectively in free and coordinated states. ν_f and ν_c are the ^{17}O chemical shifts (in Hz) of the water in these two sites. $k_a + k_b$ is the sum of the pseudo-first order rate constants characterizing the water chemical exchange.

Since ^{17}O is a quadrupolar nucleus (I = 5/2, Q = 0.026 × 10^{-28} m^2), the broadened ^{17}O NMR signal of the complexed H_2O could be the result of the direct quadrupolar interaction (the interaction of the electric field gradient with the quadrupolar moment of ^{17}O), due to the increase of the electric field gradient at the ^{17}O nucleus when a water molecule coordinates to the La(III) cation. This contribution to the ^{17}O linewidth is defined as $(\pi T_{2Q})^{-1}$ in the following discussion. Furthermore, since ^{139}La has a natural abundance of 99.91 %, the line broadening of the coordinated water ^{17}O signal could result also from the indirect quadrupolar interaction between ^{17}O and ^{139}La nuclei (^{17}O - ^{139}La coupling). This kind of interaction is referred to as a scalar relaxation of the second kind, which occurs when a nucleus (nucleus I) couples to another nucleus (nucleus S) which relaxes rapidly. This will have a significant effect on the T_2 of nucleus I in a manner analogous to the effects of a chemical exchange. It appears that it is the case for the interaction between ^{17}O and ^{139}La in this system. Since the transverse relaxation rate of ^{139}La(III) in the species $La(NO_3)_3$. H_2O is about 5,000 Hz (see Table 3.2), and since the system is under extreme narrowing conditions

($T_1 = T_2$), very plausibly, from the known values of coupling constants involving the ^{17}O nucleus[113], $T_1^{-1}(^{139}La) >> |^1J(^{139}La\ -^{17}O)|$. An indirect coupling between ^{139}La and ^{17}O cannot be directly observed under these very fast relaxation conditions because the multiplets caused by the coupling would be entirely collapsed[114]. Under the condition of $T_1^{-1}(^{139}La) >> |^1J(^{139}La\ -^{17}O)|$, the contribution of the indirect coupling between ^{17}O and ^{139}La to the ^{17}O linewidth, $(\nu_{1/2})_J$, is[115]

$$(\nu_{1/2})_J = 4/3\ \pi\ J^2\ T_1(^{139}La)\ I\ (I+1) \qquad (3.27)$$

Where $T_1(^{139}La)$ is the ^{139}La longitudinal relaxation time and I is the nuclear spin number for ^{139}La.

Combining the contributions from the direct quadrupolar interaction and the scalar relaxation of the second kind, the ^{17}O linewidth for the complexed H_2O can be expressed as

$$(\nu_{1/2})_c = (\pi(T_{2Q})_c)^{-1} + 21\ \pi\ J^2\ T_1(^{139}La) \qquad (3.28)$$

Here $(\pi(T_{2Q})_c)^{-1}$ and $21\ \pi\ J^2\ T_1(^{139}La)$ respectively are the ^{17}O quadrupolar relaxation and the indirect coupling contributions to the ^{17}O linewidth of the coordinated water.

Under extreme narrowing conditions, $T_{1Q} = T_{2Q}$ for ^{17}O and $T_1 = T_2$ for ^{139}La, so that

$$(\nu_{1/2})_c = (\pi(T_{1Q})_c)^{-1} + 21\ \pi\ J^2\ T_2(^{139}La) \qquad (3.29)$$

$$\text{or } (T_2^{-1})_c = (T_{1Q}^{-1})_c + 21\ \pi^2\ J^2\ T_2\ (^{139}La) \qquad (3.30)$$

$$21\ \pi\ J^2\ T_2\ (^{139}La) = ((T_2^{-1})_c - (T_{1Q}^{-1})_c) \qquad (3.31)$$

To calculate the value of J, we measured the ^{17}O longitudinal relaxation time $(T_1)_{obs}$, which is 5.18×10^{-3} seconds for the $La(NO_3)_3$ 6 H_2O concentration of 0.090 M. Since $(T_1^{-1})_{obs} = P_f(T_1^{-1})_f + P_c(T_1^{-1})_c$, where P is the population of free or complexed water, and since $T_1 = T_2$ for free water, $(T_1^{-1})_c$ can be calculated from the results obtained from the nonlinear regression analyses of the ^{17}O NMR data. At $La(NO_3)_3$ 6 H_2O concentration of 0.090 M, $(T_1^{-1})_{obs} = 193\ s^{-1}$, $P_c = 0.1332$, and $P_f = 0.8668$. Since for free water $(T_1)_f^{-1} = (T_2)_f^{-1} = 78.5$ Hz, $(T_1^{-1})_c$ is equal to 938 Hz. The ^{17}O linewidth of coordinated water has been given previously ($\nu_{1/2}$ = 400 Hz). On the basis of equation 3.31 and taking the $T_2(^{139}La)$ value for the species {$La(NO_3)_3$ H_2O} from table 3.2, one can eventually calculate the coupling constant between ^{17}O and ^{139}La, J, which is 88 ± 13 Hz.

In conclusion, the ^{139}La and ^{17}O NMR chemical shifts and linewidths have been measured as a function of $La(NO_3)_3$ 6 H_2O in acetonitrile. The results have been quantitatively interpreted through a chemical equilibrium model, in which two La(III) species, $La(NO_3)_3$ and $La(NO_3)_3$ H_2O , coexist and exchange rapidly in solution. The variation of the ^{139}La and ^{17}O NMR parameters with the concentration of $La(NO_3)_3$ 6 H_2O results from the population increase of the species $La(NO_3)_3.H_2O$. The detailed analysis of ^{17}O NMR spectra allows the evaluation of the indirect coupling constant between ^{17}O of coordinated water and ^{139}La, $^1J(^{17}O - ^{139}La)$.

Chapter 4

The Complexes of La(III) with Crown Ethers in Non-Aqueous Solutions

4.1 Introduction:

The study of crown ether-metal complexes has been an active area of research since Pedersen first reported these multidentate ligands in 1967[23]. Macrocyclic ligands such as crown ethers were first designed as synthetic models to mimic the properties of the natural ionophores towards alkali and alkaline earth metal cations. Therefore, the complexation between crown ethers and those cations has been extensively investigated. This kind of research has recently been extended to the lanthanide cations[35], which was mainly motivated by their analogy with alkali and alkaline earth cations and their uses as spectroscopic probes for the study of biological systems.

A brief review of the literature about the complexation of lanthanide cations with crown ethers has been given in the section 1.2 of chapter 1. As mentioned in that section, although a number of solid Ln^{3+} - crown ether complexes have been

synthesized and their crystal structures have been determined, the studies of their properties in solution are rather scarce[35, 38-41].

Nuclear Magnetic Resonance Spectroscopy has showed its significant advantages in the elucidation of thermodynamic and kinetic properties of alkali metal cation complexes with crown ethers in solution[116]. In the present work, this technique has been applied to La(III) - crown ether systems. The results related to the structure and formation of La(III) complexes with crown ethers in non-aqueous solution are reported in this chapter.

Table 4.1 lists the systems which have been investigated. Figure 4.1 shows the crown ethers used in the present work. The formation of La(III) complexes with crown ethers was studied by multinuclear magnetic resonance (^{1}H, ^{13}C, ^{17}O, and ^{139}La). The structural information of these complexes in the solution phase will also be discussed.

Table 4.1 Systems investigated

Salts	Solvents	Ligands	Nuclei*
$LaCl_3$ 7 H_2O	Methanol	18C6	^{139}La
$LaCl_3$ 7 H_2O	Methanol	B15C5	^{139}La
$La(NO_3)_3$ 6 H_2O	Acetonitrile	18C6	^{139}La, ^{1}H, ^{13}C, ^{17}O
$La(NO_3)_3$ 6 H_2O	Acetonitrile	DB24C8	^{139}La, ^{13}C, ^{17}O
$La(NO_3)_3$ 6 H_2O	Acetonitrile	B15C5	^{139}La, ^{1}H, ^{13}C, ^{17}O
$La(NO_3)_3$ 6 H_2O	Acetonitrile	15C5	^{1}H and ^{13}C

*, The NMR observations were made on those nuclei.

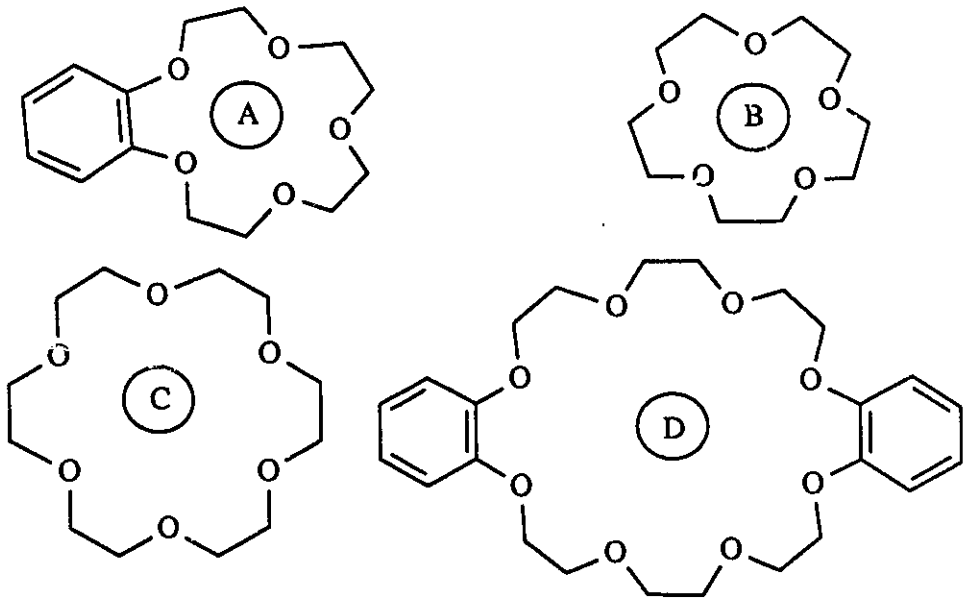

Figure 4.1: Crown Ethers, A, B15C5; B, 15C5, C, 18C6, and D, DB24C8.

4.2 Complexation of La(III) with Crown Ethers:

4.2.1: $LaCl_3$ 7 H_2O and 18C6 in Methanol

The ^{139}La NMR spectrum of a $LaCl_3.7H_2O$ solution in methanol consists of a single, broad, Lorentzian line. The addition of 18C6 to the solution resulted in the appearance of a much broader line resonating at lower frequency. The lineshapes were almost invariant with temperature variations (300 K < T < 330 K). This is the indication of two species in very slow exchange on the chemical shift time scale. Figures 4.2 to 4.4 show series of the ^{139}La NMR spectra of hydrated lanthanum chloride solutions in methanol in the presence of 18C6. Since the crown ether is known to form a 1:1 complex with La(III) in methanol[117], the simplest interpretation for the observed spectra is that they result from the superposition of two Lorentzian absorption

lines corresponding to the uncomplexed La(III) solvated cation, and to the 1:1 La(III) : 18C6 complex.

The spectrum resulting from the superposition of two Lorentzian signals can be described by equation 4.1[118,51], which is the two-site slow exchange case ($k \rightarrow 0$) of the general equation given by Gold and Zdunek[119] for an imperfectly phase-corrected spectrum.

$$I(\nu)=C[(M+N)\cos\phi + (P+Q)\sin\phi] + B \qquad (4.1)$$

$$M=T_{2A}P_A / (1+4\pi^2 T_{2A}^2(\nu_A-\nu)^2)$$
$$N=(1-P_A)T_{2B} / (1+4\pi^2 T_{2B}^2(\nu_B-\nu)^2)$$
$$P=T_{2A}^2P_A(\nu_A-\nu) / (1+4\pi^2 T_{2A}^2(\nu_A-\nu)^2)$$
$$Q=(1-P_A)T_{2B}^2(\nu_B-\nu) / (1+4\pi^2 T_{2B}^2(\nu_B-\nu)^2)$$

T_{2A}, T_{2B} and ν_A , ν_B correspond to the transverse relaxation times and the chemical shifts of the solvated (A) and complexed (B) sites respectively. C is a scaling factor. P_A is the population of site A (here, uncomplexed ^{139}La(III)). It was difficult to adequately adjust the phase and baseline of the broad, overlapping peaks. Consequently, the simulation of these spectra required phase angle (ϕ) and baseline (B) parameters to be included in the lineshape equation.

Table 4.2 gives the results of the deconvolution of the observed spectra on the basis of equation 4.1, for three La(III) total concentrations at several values of the ratio $\rho = [18C6]_o / [La(III)]_o$. The transverse relaxation rate characterizing the solvated site, T_{2A}^{-1}, was found to be a constant, within experimental error, for a given total La(III) concentration: 6.8 kHz (0.20 M), 6.3 kHz (0.10 M), and 5.1 kHz (0.050 M). The decrease of the relaxation rate as the concentration decreases is an indication of ionic association. This is further confirmed by the variation of the chemical shift for the solvated La(III): 165, 194 and 230 ppm, respectively for [La(III)] = 0.20, 0.10, and

0.050 M. In the previous chapter, we have shown the formation of ion pairs in $LaCl_3$ aqueous solutions. It is expected that this kind of reaction will be stronger in MeOH solution. A similar variation of the ^{139}La chemical shifts with a variation of the $LaCl_3$ concentration was observed for the complexed species: 130, 150, 167 ppm. These observations point to the participation of the chloride anion in the first coordination sphere of the lanthanum cation, both in the solvated and in the complexed species. This has been shown recently to be the case in the solid state for a hydrated gadolinium chloride complex with 18C6[32]. McCain[62] has studied concentrated solutions of $LaCl_3$ in methanol, water, and binary mixtures of methanol and water, by ^{139}La and ^{35}Cl NMR. The ^{139}La chemical shift of a 1.45 M $LaCl_3$ solution in methanol was found to be 293 ppm, and the linewidth was 3800 Hz. These values are in the same order of magnitude with these of the present study. In the binary mixtures, there was evidence for the formation of La-Cl inner sphere complex when the percentage of methanol was > 66%. The interaction between La^{3+} and Cl^- in methanol solutions is also confirmed by ultrasonic absorption experiments[106], X-ray investigation[120,121], and ^{139}La NMR measurements[68].

Despite the fact that the nature of the coordinating atoms (oxygens) is the same in the solvated and in the macrocyclic ligand, substantial chemical shift differences between the solvated and the complexed cations can be observed. This is an indication that, in methanol solution, the crown ether occupies the first coordination sphere of the La(III) cation. The ^{139}La NMR signals of the La(III) complexed species were so broad that only an estimate could be made for the value of the transverse relaxation rate of the complexed $^{139}La(III)$. They are 65, 54, and 28 kHz respectively for $[La(III)]_o$ = 0.200, 0.100 and 0.050 M. These very large values reflect a large quadrupolar coupling constant resulting from a strong dissymmetry of the electric charge distribution around the first coordination shell of the La(III) cation. Again, this is in good agreement with direct coordination of the crown ether on the La(III).

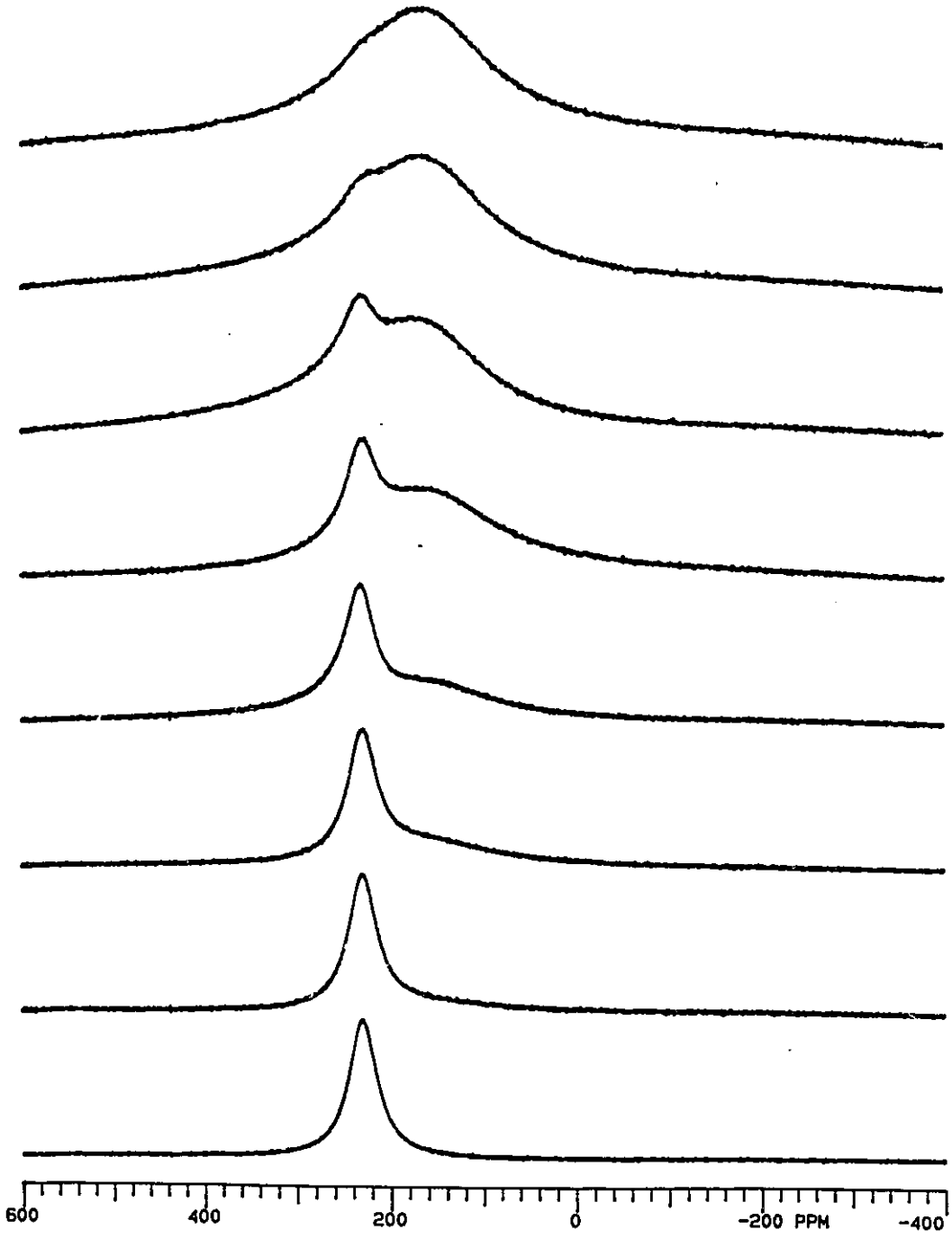

Figure 4.2: ^{139}La NMR spectra of $LaCl_3$ 7 H_2O solutions in methanol in the presence of 18C6 for various values of ρ. $[La(III)]_o$ = 0.050 M. T = 300 K. Top to bottom, ρ (= $[18C6]_o$ / $[LaCl_3$ 7 $H_2O]_o$) = 1.40, 1.20, 1.00, 0.90, 0.70, 0.50, 0.30, 0.00.

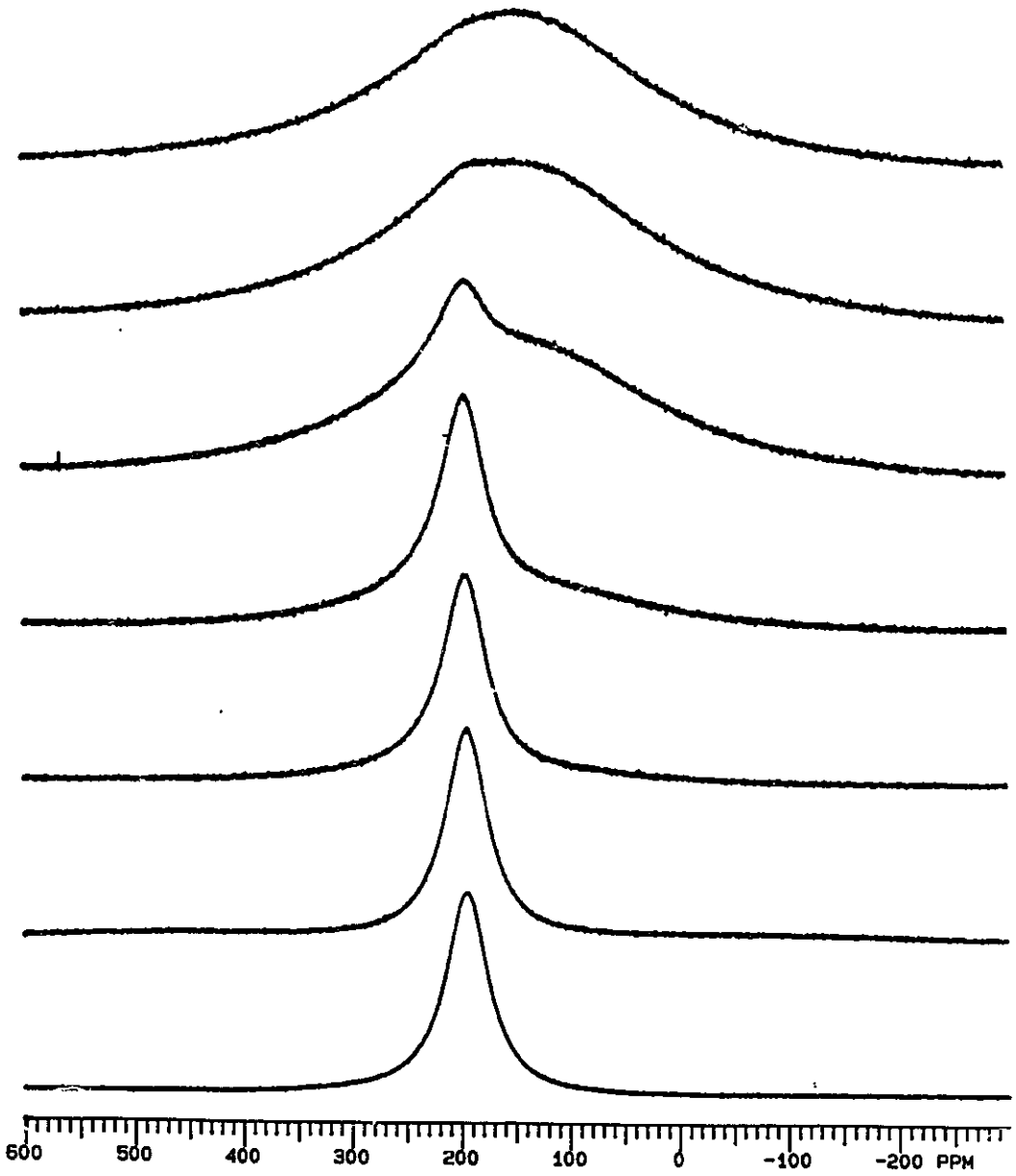

Figure 4.3: ^{139}La NMR spectra of $LaCl_3$ 7 H_2O solutions in methanol in the presence of 18C6 for various values of ρ. $[La(III)]_o$ = 0.100 M. T = 300 K. Top to bottom, ρ (= $[18C6]_o$ / $[LaCl_3$ 7 $H_2O]_o$) = 1.40, 1.20, 1.00, 0.70, 0.50, 0.30, 0.00.

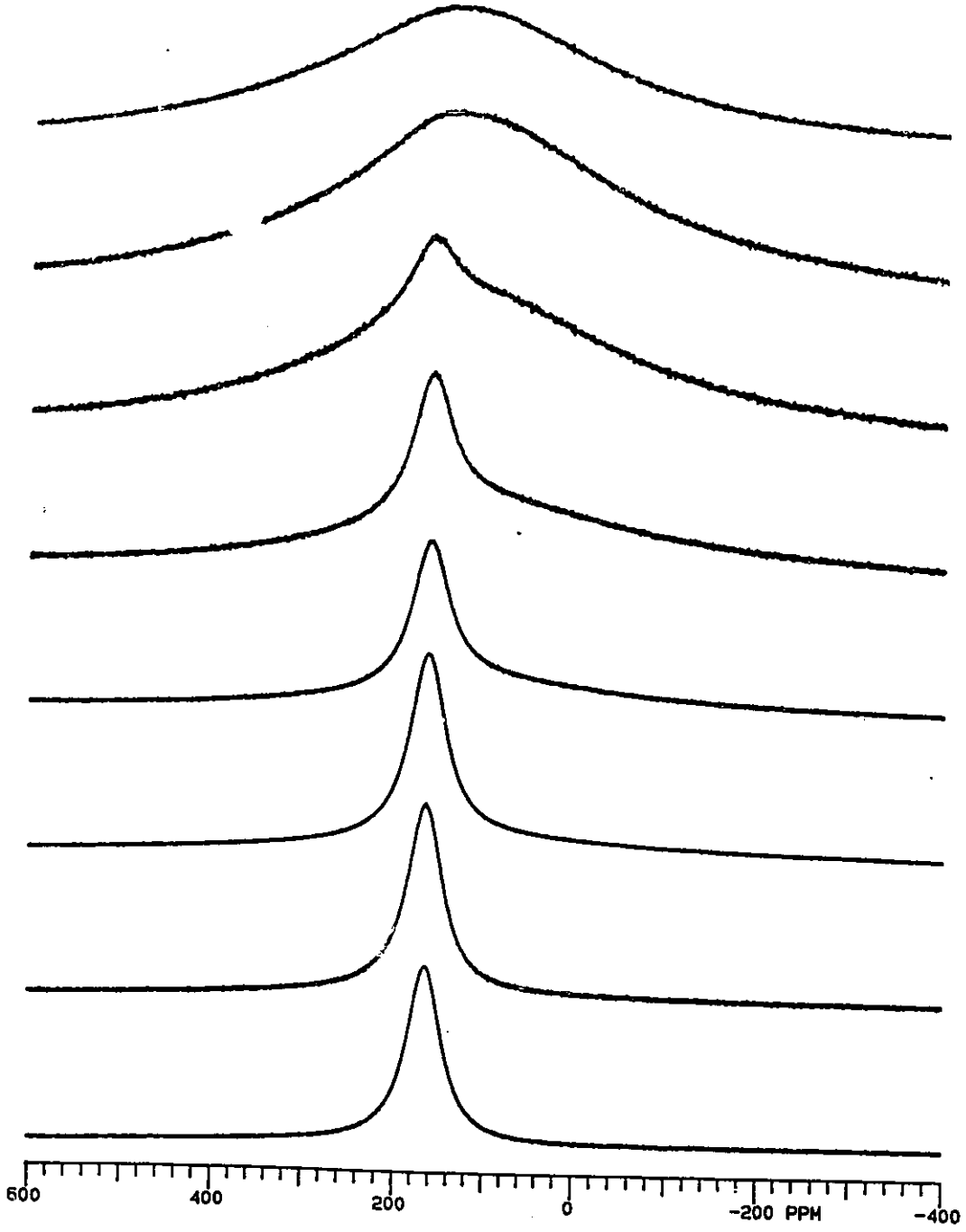

Figure 4.4: ^{139}La NMR spectra of $LaCl_3$ 7 H_2O solutions in methanol in the presence of 18C6 for various values ρ. $[La(III)]_o$ = 0.200 M. T = 300 K. Top to bottom, ρ (= $[18C6]_o$ / $[LaCl_3$ 7 $H_2O]_o$) = 1.40, 1.20, 1.00, 0.90, 0.70, 0.50, 0.30, 0.00.

Table 4.2

^{139}La NMR parameters of La(III) and its complex with 18C6 in methanol solution

$[La]_o$	ρ^a	$P_A{}^b$	$(T_2^{-1})_A{}^c$	$\delta_A{}^d$	$\delta_B{}^e$
0.200	0.00	1.00	6.1±0.3	165	----
0.200	0.50	0.43±0.07	6.5±0.5	165	130
0.200	0.70	0.33±0.02	6.7±0.5	165	130
0.200	0.90	0.19±0.01	7 ± 1	165	130
0.200	1.00	0.06±0.01	7 ± 1	165	130
0.200	1.40	----	----	----	130
0.100	0.00	1.00	6.1±0.3	194	----
0.100	0.50	0.46±0.09	6.4±0.5	194	150
0.100	0.70	0.31±0.02	6.4±0.5	194	150
0.100	1.00	0.07±0.01	7 ± 1	194	150
0.100	1.40	----	----	----	150
0.050	0.00	1.00	4.8±0.3	230	----
0.050	0.50	0.45±0.01	4.8±0.5	230	167
0.050	0.70	0.34±0.01	4.8±0.5	230	167
0.050	0.90	0.16±0.01	5.0±0.5	230	167
0.050	1.00	0.12±0.01	6 ± 1	230	167
0.050	1.40	----	-----	----	167

a, $[18C6]_o / [La(III)]_o$;

b, Normalized population of uncomplexed La(III), determined from the spectra deconvolution;

c, ^{139}La transverse relaxation rates (kHz) of uncomplexed La(III) (site A);

d, ^{139}La NMR chemical shifts (ppm) of uncomplexed La(III);

e, ^{139}La NMR chemical shifts (ppm) of La(III) complex with 18C6.

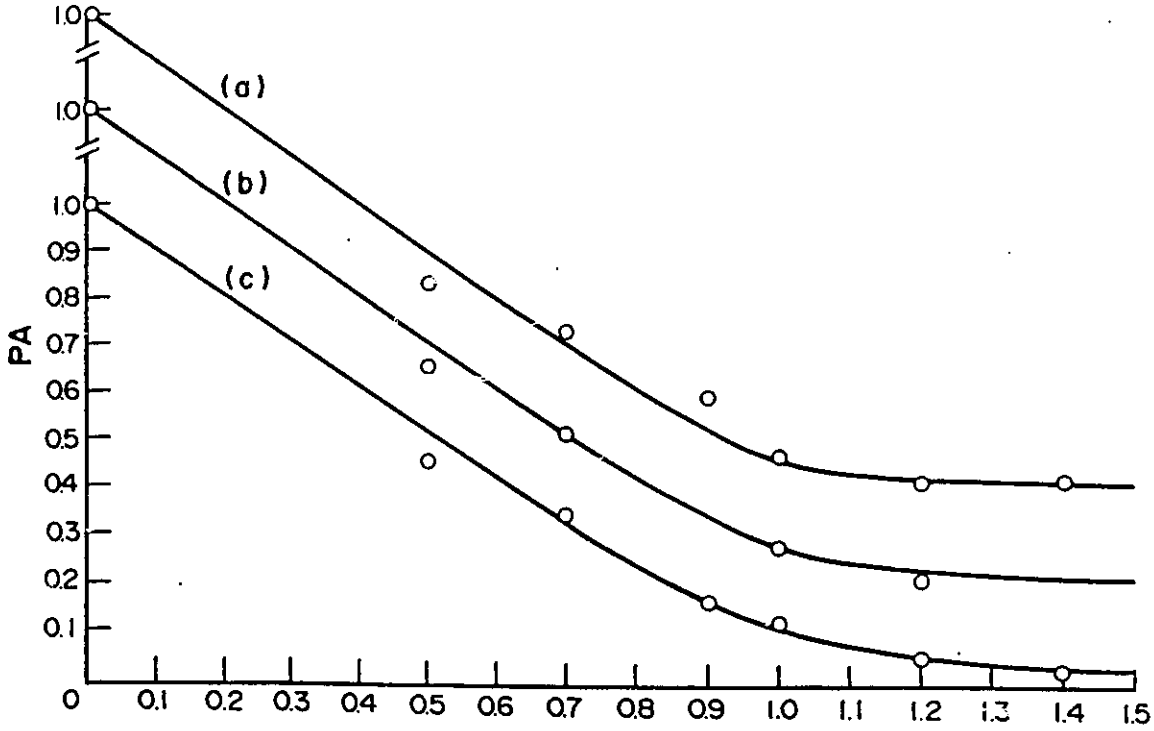

Figure 4.5: Normalized population of uncomplexed La(III) as a function of ρ. T = 300 K. The data points were obtained from the non-linear regression analysis of the experimental ^{139}La NMR spectra and the solid lines were calculated on the basis of log K_f = 3.2. $[La(III)]_o$ = (a) 0.200, (b) 0.100, and (c) 0.050 M.

From the normalized populations of the solvated (see Table 4.2) and of the complexed lanthanum cation, it was possible to calculate an equilibrium constant of formation for the 1:1 La(III) : 18C6 complex. A mean value of log $K_f = 3.2 \pm 0.5$ was obtained. This value is in excellent agreement with the result given by Izatt *et al.* on the same system[117], using titration calorimetry (log $K_f = 3.29$). Recently, Ohyoshi and Kohata[122] reinvestigated this system using a spectrophotometric procedure. They obtained a value of log $K_f = 3.89 \pm 0.8$ for the stability constant of La(III)-18C6 complex. The value of 3.25 for log K_f on the same system was also reported in the literature[123]. Once again, the results obtained in the present work are in very good agreement with literature values. Figure 4.5 shows the normalized population of the solvated La(III) as a function of the ratio $[18C6]_o$ / $[La(III)]_o$. In figure 4.5, the data points are experimental and the solid lines have been calculated from the value of log $K_f = 3.2$.

4.2.2: <u>$LaCl_3$ 7 H_2O and B15C5 in Methanol;</u>

In this system, a single Lorentzian line was observed in the presence and in the absence of B15C5 in the solutions. Figure 4.6 shows a series of ^{139}La NMR spectra with different ratios of B15C5 : La(III) for this system. The ^{139}La NMR spectrum was located at 229 ppm with a linewidth of 1.6 KHz in the case of a 0.050 M $LaCl_3$ 7 H_2O solution in methanol. The spectra were not affected by the addition of B15C5 into the solutions. These results indicate that there is no observable complexation occurring between B15C5 and La(III) in MeOH.

As shown in the last section, the complexation of La(III) with 18C6 was observed in the same system, the B15C5, however, could not replace the methanol molecules or counterion(s) to form a similar complex with La(III). The results obtained by ^{139}La NMR in the cases of 18C6 and B15C5 confirm that the stability of the lighter lanthanide complexes with 18C6 is much higher than with other crown ethers. This was

previously explained by the close similarity between the cation ionic radius and the radius of the internal cavity of the macrocyclic polyethers[124]. The complexes between metal cations and crown ethers are of the host - guest type. For this kind of complex, a size match between the host and the guest is an important factor for the stabilization of the complex. Especially in the above two systems, the size compatibility between La(III) and crown ethers is the main factor affecting the stability of the complexes since the counterion and the solvent used are the same. From the known values of La(III) ionic radius (2.43 Å, CN = 9) and of the cavity diameters of the crown ethers (2.5 Å for 18C6 and 1.9 Å for 15C5)[35], it is expected that the complex of La(III) with 18C6 be more stable than with B15C5.

An outer sphere complexation between La(III) and B15C5 might occur, but with less probability, since both ^{139}La chemical shift and linewidth were invariant with the B15C5 concentration variations in the solution.

Finally, as will be discussed later in section 4.2.5, the formation of the La(III) complex with B15C5 has been observed in the system of $La(NO_3)_3$ 6 H_2O - B15C5 - AN. No observable complexation occuring between La(III) and B15C5 in MeOH indicates that the properties of solvent molecules have a strong effect on the complexation of La(III) with crown ethers.

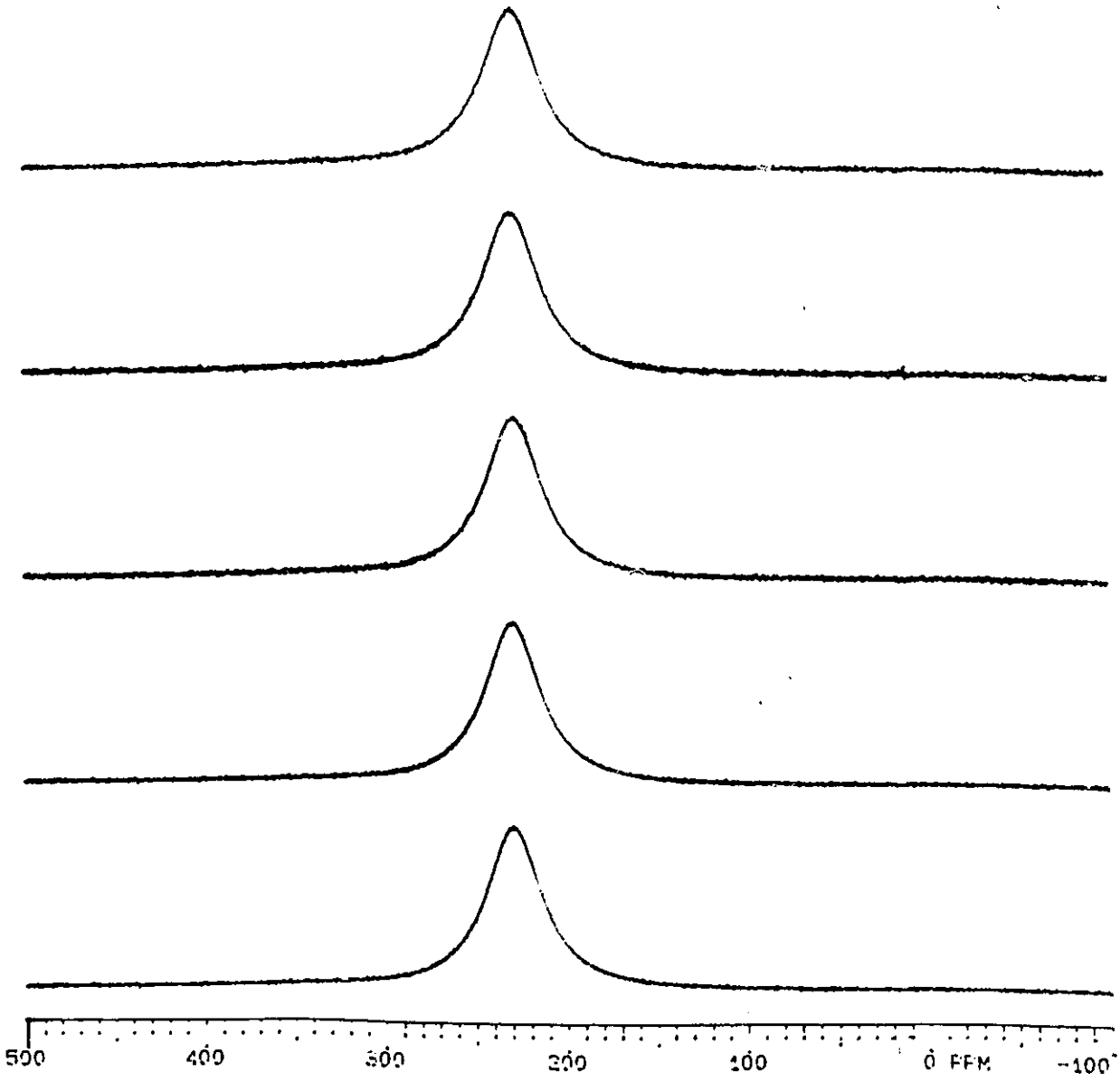

Figure 4.6: ^{139}La NMR spectra of $LaCl_3$ 7 H_2O solutions in methanol in the presence of B15C5 for various values of ρ. $[La(III)]_o$ = 0.010 M. T = 300 K. Top to bottom, ρ (= $[B15C5]_o$ / $[LaCl_3\ 7\ H_2O]_o$) = 1.40, 1.00, 0.70, 0.50, 0.00.

4.2.3: $La(NO_3)_3.6H_2O$ and 18C6 in Acetonitrile Solution

Acetonitrile was used as the solvent for the rest of work in this thesis since it has a low viscosity and is a good ionizing solvent; in addition, it coordinates relatively weakly to the La(III) cation.

Figure 4.7 shows a series of ^{139}La NMR spectra for a series of ρ values ($\rho = [18C6]_o / [La]_o$) in the case of total La(III) concentration ($[La]_o$) of 0.015 M. At $\rho = 0$ there is no crown ether present and the ^{139}La NMR spectrum of a 0.015 M solution of $La(NO_3)_3 .6H_2O$ in acetonitrile was characterized by a chemical shift of 9.6 ppm and a linewidth of 2.5 kHz. This ^{139}La NMR signal results from a equilibrium involving $\{La(NO_3)_3 (AN)_x\}$ and $\{La(NO_3)_3 H_2O (AN)_y\}$ species as described in section 3.2.2 (see equation 3.14 with x = 0). When $\rho > 0$, another ^{139}La NMR signal corresponding to the 18C6 complexed species appeared at lower frequency , with a chemical shift of -139 ppm and a linewidth of 4.4 kHz. In the region of $0 < \rho < 1$, the resonances characterizing the free and the complexed La(III) species coexist and the temperature variations ($300< T < 335$) do not affect the ^{139}La NMR lineshape, indicating that the exchange of La(III) between its free and crown ether complexed sites is very slow on the ^{139}La NMR timescale. At $\rho > 1$, the NMR signal of free lanthanum disappeared and, except for the one located in -139 ppm, no other ^{139}La resonances were observed. These observations are an indication that a 1:1 complex between La(III) and 18C6 is formed.

To evaluate the formation constant of the complex {La(III) 18C6}, the procedure described previously in section 4.2.1 (see equation 4.1) was also applied to the full lineshape analysis of the spectra, except that ν_a, the chemical shift of solvated La(III), was used as an adjustable parameter. The deconvolution results for the observed spectra of two solutions, [La(III)]=0.015 M and 0.010 M, with several ρ values, are reported in table 4.3. Figure 4.8 shows the relationship between ρ and the

normalized population of the uncomplexed La(III) species. The linearity of the plot in figure 4.8 is an indication that the formation of the complex is quantitative where the formation constant can be estimated to be greater than 10^4. Bunzli, *et al.*[34] investigated the same system by means of ^1H NMR. They obtained the formation constant of log $K_f = 4.4$ for the complex by integration of the signals of the free and coordinated crown ether and assuming a 1:1 stoichiometry[34]. The quantitative formation of a 1 : 1 Pr^{3+} complex with 18C6 in acetonitrile was also concluded from electronic absorption measurements[34]. Stoichiometries of 4 : 3 and 1 : 1 for the La(III) : 18C6 complexes have been reported in solid sate[36,37]. In the case of the 4 : 3 stoichiometry, one of the La(III) was found to be coordinated only by the nitrate anions in the complex. When dissolved in acetonitrile, a 4 : 3 La(III) : 18C6 complex dissociated to result in ($La(NO_3)_3$ 18C6) and ($La(NO_3)_3$) species present in the solution[34].

The large differences of chemical shifts and linewidths between solvated and complexed La(III) sites suggest that 18C6 occupies the La(III) first coordination sphere in the complexed species. Compared to the free La(III), a much higher value of T_2^{-1} was observed for the complexed species. This reflects a lowering of the overall symmetry about La(III) in the La(III) - 18C6 complex. It is worth mentioning that the chemical shifts and linewidths of the solvated La(III) species varied with ρ. This indicates that the equilibrium involving different solvated La(III) species expressed in equation 3.14 is shifted while there is formation of the La(III) complex with 18C6. The detailed discussion of this effect will be given in the section 4.3 of this chapter.

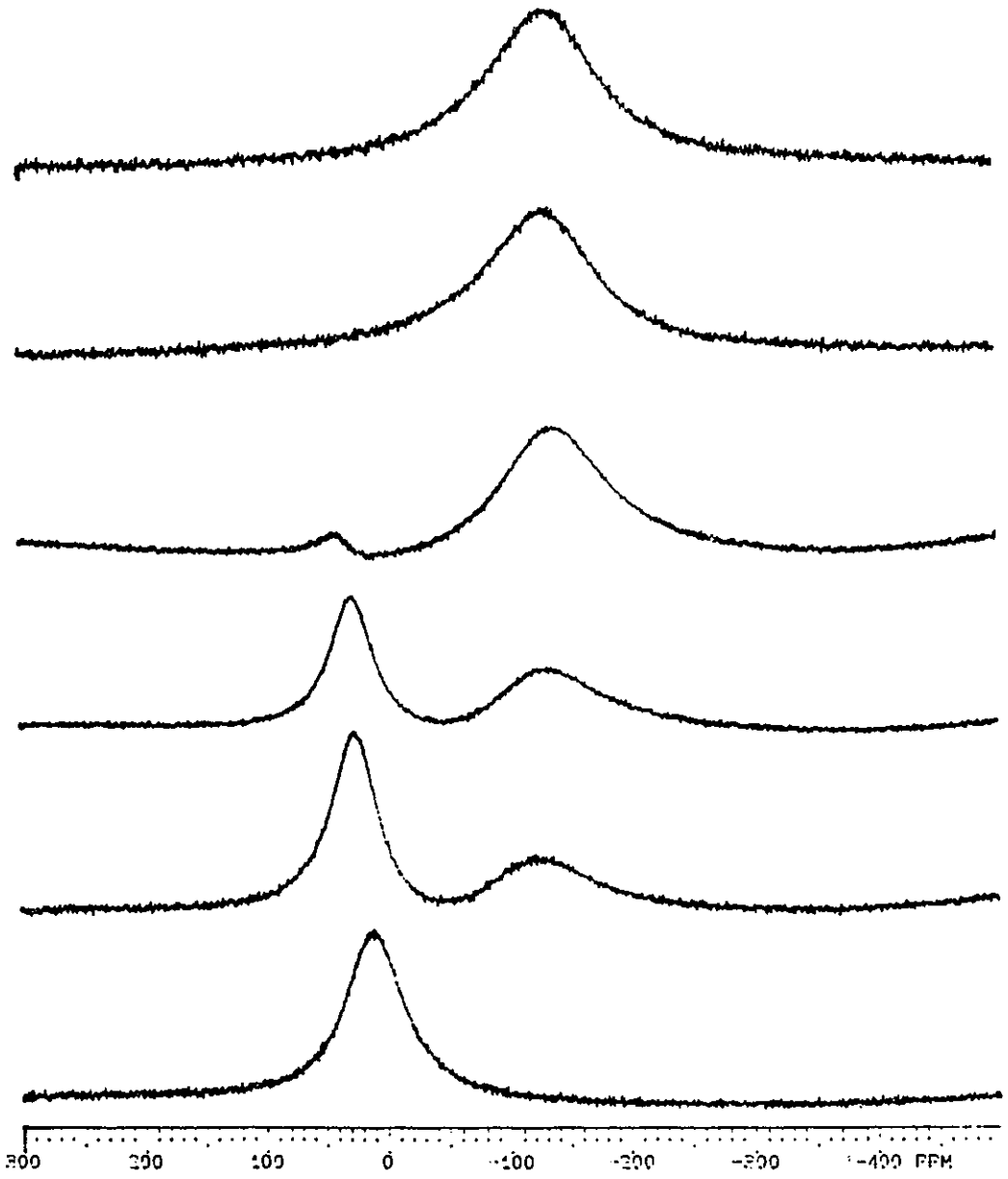

Figure 4.7: ^{139}La NMR spectra of $La(NO_3)_3$ 6 H_2O solutions in acetonitrile in the presence of 18C6 for various values of ρ. $[La(III)]_o$ = 0.015 M. T = 300 K. Top to bottom, ρ (= $[18C6]_o$ / $[La(NO_3)_3$ 6 $H_2O]_o$) = 1.20, 1.00, 0.90, 0.70, 0.50, 0.00.

Table 4.3.

^{139}La NMR parameters of $La(NO_3)_3$ 6 H_2O in acetonitrile solutions in the presence of different amount of 18C6

$[La]_o$ (M)	ρ^a	$P_A{}^b$	$(T_{2A}{}^{-1})^c$ (kHz)	$(T_{2B}{}^{-1})^c$ (kHz)	$\delta_A{}^d$ (ppm)	$\delta_B{}^d$ (ppm)
0.015	0.00	1.00	7.4±0.3	-----	9.6±0.5	-----
0.015	0.48	0.52±0.05	5.7±0.4	16 ± 1	22 ± 1	-----
0.015	0.61	0.42±0.04	5.4±0.5	15 ± 1	24 ± 1	-----
0.015	0.93	0.05±0.03	3.8±0.5	14 ± 1	27 ± 1	-----
0.015	1.00	-----	-----	12 ± 1	-----	-139±1
0.015	1.45	-----	-----	13 ± 1	-----	-139±1
0.010	0.00	1.00	7.6±0.3	-----	8.6±0.5	-----
0.010	0.50	0.52±0.04	6.3±0.5	14 ± 1	21 ± 1	-----
0.010	0.70	0.31±0.02	5.9±0.5	13 ± 1	25 ± 1	-----
0.010	0.90	0.12±0.03	4.2±0.5	13 ± 1	32 ± 1	-----
0.010	1.00	-----	-----	14 ± 1	-----	-132±1
0.010	1.30	-----	-----	13 ± 1	-----	-132±1

a, $\rho = [18C6]_o / [La(III)]_o$;

b, The normalized population of uncomplexed La(III) determined from the lineshape analysis of the spectra;

c, $T_{2A}{}^{-1}$ and $T_{2B}{}^{-1}$ were the ^{139}La transverse relaxation rates of solvated La(III) (site A) and complexed La(III) (site B), respectively;

d, δ_A and δ_B were defined as the chemical shifts of ^{139}La NMR for site A and site B respectively.

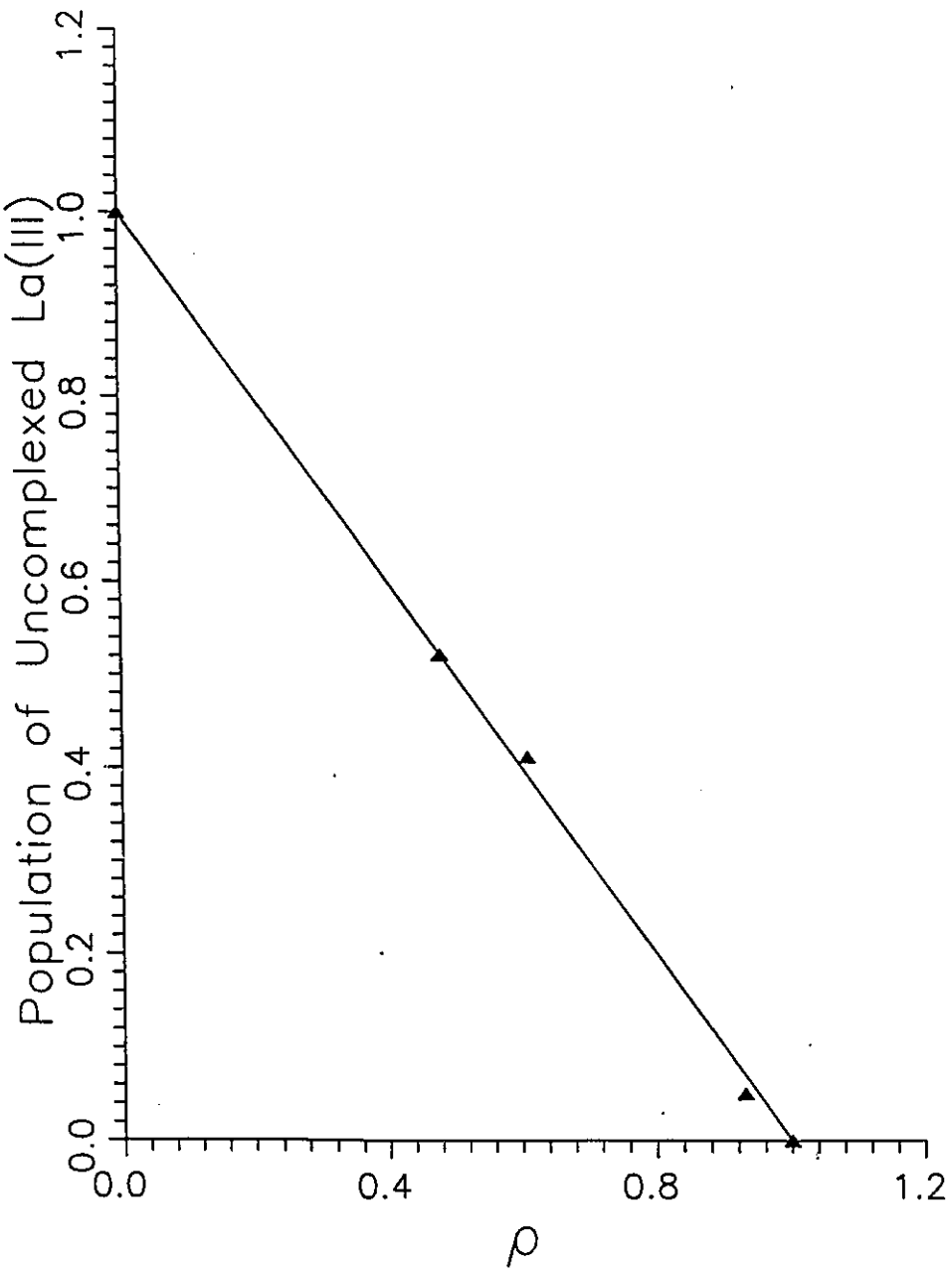

Figure 4.8: Normalized population of uncomplexed La(III) as a function of ρ. T = 300 K. The data points were obtained from the non-linear regression analysis of the experimental ^{139}La NMR spectra. $[La(III)]_o = 0.015$ M.

^{1}H and ^{13}C NMR provide another way to investigate the complexation between La^{3+} and crown ethers. The ^{1}H and ^{13}C NMR spectra of the ligand 18C6 were recorded under a constant ligand concentration, while varying the amounts of $La(NO_3)_3$ 6 H_2O in acetonitrile solutions. Figure 4.9 gives a series of 18C6 ^{1}H NMR spectra with different R (= $[La(III)]_o$ / $[18C6]_o$) values. As expected, a single peak was observed for free 18C6 since all its protons are equivalent due to symmetry. The ^{1}H chemical shift is 3.502 ppm for a 0.0032 M solution of 18C6 in CD_3CN. The addition of lanthanum nitrate into the solution resulted in the appearance of another single peak located at higher frequency (δ = 3.838 ppm), attributed to the 18C6 complexed to La(III). This downfield shift is induced by the coordination of 18C6 to the La^{3+} cation. When $0 < R < 1$, two peaks, corresponding to the free and to the complexed 18C6, were obtained. The integrations of these ^{1}H NMR signals indicated that a 1:1 complex of 18C6 and La(III) was quantitatively formed. Those results are in agreement with that reported in the literature[34] and are a good support for the results obtained by the ^{139}La NMR lineshape analysis.

Figure 4.10 shows the ^{13}C NMR spectra of 18C6 for various values of R. The ^{13}C NMR spectra of 18C6 have the characteristics similar to the protons. When $R = 0$, a single peak with a chemical shift of 70.79 ppm was observed, characterizing the 18C6 in the solvated site. In the case of $R > 1$, all the 18C6 molecules present in the solution being complexed, a single signal located at 71.06 ppm was found. In the region of $0 < R < 1$, these two peaks coexisted.

The ^{13}C and ^{1}H NMR spectra are characteristic of a very slow ligand exchange on the two respective chemical shift time scales. Furthermore, in the case of complexed 18C6, only one single signal was observed on the ^{1}H and ^{13}C NMR spectra, indicating that all the protons and all the carbons of the complexed 18C6 are equivalent or averaged by a fast exchange. This is not the case for the lanthanum complexes with 15C5 and B15C5 as it will be shown later in section 4.2.5 and 4.2.6.

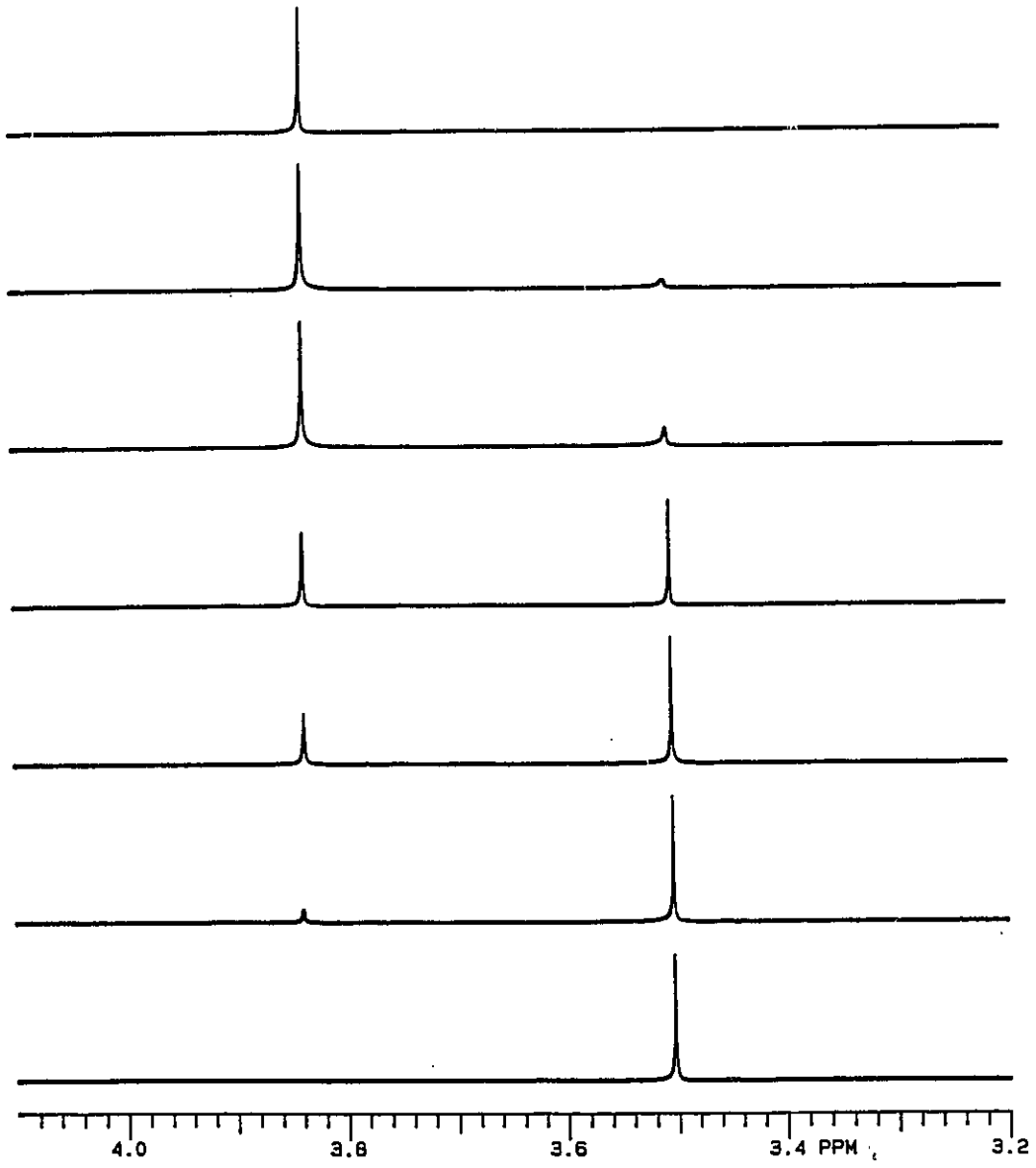

Figure 4.9: ^1H NMR spectra of 18C6 solutions in acetonitrile in the presence of $La(NO_3)_3$ 6 H_2O for various values of *R*. $[18C6]_o$ = 0.0032 M. T = 300 K. Top to bottom, *R* (= $[La(NO_3)_3$ 6 $H_2O]_o$ / $[18C6]_o$) = 1.00, 0.85, 0.75, 0.50, 0.35, 0.15, 0.00.

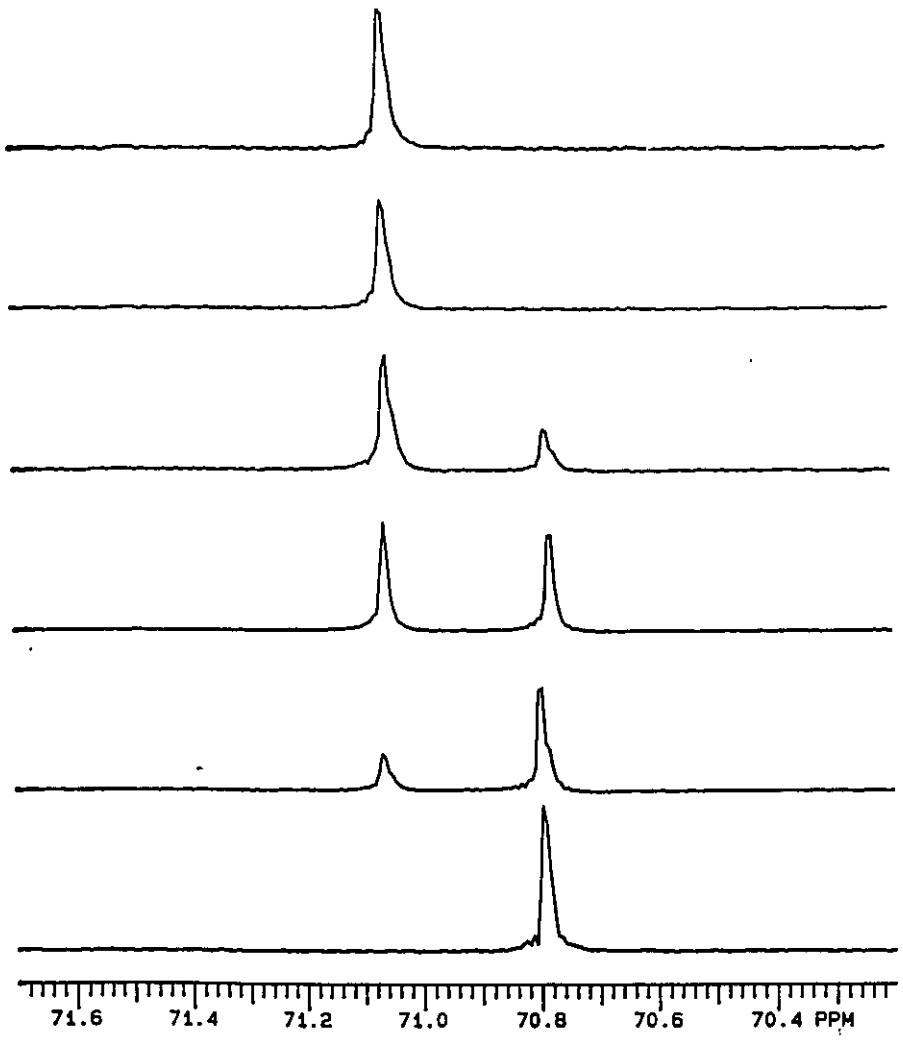

Figure 4.10: ^{13}C NMR spectra of 18C6 solutions in acetonitrile in the presence of $La(NO_3)_3\ 6\ H_2O$ for various values of *R*. $[18C6]_o = 0.021$ M. T = 300 K. Top to bottom, *R* (= $[La(NO_3)_3\ 6\ H_2O]_o / [18C6]_o$) = 1.20, 1.00, 0.79, 0.51, 0.23, 0.00.

4.2.4: $La(NO_3)_3$ 6 H_2O and DB24C8 in Acetonitrile

Figure 4.11 shows a series of ^{139}La NMR spectra of a 0.10 M $La(NO_3)_3$ 6 H_2O solution in acetonitrile in the presence of various amounts of DB24C8. A single peak was observed on the ^{139}La NMR spectra for all ρ (= $[\text{crown ether}]_o$ / $[La(III)]_o$, as defined previously) values. The ^{139}La linewidths increased with the increase of ρ, from 1.9 kHz for ρ = 0.0 to about 7.2 kHz in the case of ρ = 1.40. The chemical shifts of ^{139}La varied slightly with ρ. Table 4.4 gives the ^{139}La NMR results for this system. The characteristics observed on the ^{139}La NMR spectra could result from two possibilities: a fast La(III) exchange between solvated and complexed sites and the co-location of two peaks corresponding respectively to the La(III) cation in these two sites. The latter case is less plausible since we carefully analyzed the ^{139}La NMR spectra and Lorentzian lineshapes were found for all of them. Therefore, the characteristics of the ^{139}La NMR spectra in this system indicate that the La(III) cation exchanges rapidly between different states in the solution.

In the previous section, it has been shown that the La(III) cation exchange between its solvated site and the site complexed by 18C6 is slow. The different behaviors of La(III) species exhibited in the system involving DB24C8 are attributed to the coordination property differences between 18C6 and DB24C8. Because of the presence of dibenzo-substituents, the basicity of the oxygen atoms of DB24C8 decreases due to the electron-withdrawing effect of the phenyl rings. The substitution also causes an increase of the ligand rigidity. Consequently, the phenyl substitution on the polyether will depress the complexation. It has been reported that the presence of the t-butyl-phenyl substituent on 15C5 causes a large decrease, approximately of three orders of magnitude, of the stability constant for the Ln(III) - crown ether complexes and the destabilization provided by the t-butyl-phenyl substituent is found to be larger for the 18-membered systems than the 15-membered polyether[35]. Since there are two

phenyl substituents in DB24C8, the weaker interactions between La(III) and the oxygen atoms of DB24C8 are expected. It has been reported that in non-aqueous solvents DB24C8 can wrap around a sodium cation and expel the conjugate anion (tetraphenylborate) and the solvent molecules from the cation coordination sphere[125-128]. However, the similar "wrap around" structure is not expected for the La(III) - DB24C8 complex since the nitrate anions which have a strong coordination property should occupy the first coordination sphere of the La(III) cation. Therefore, it is reasonable to interpret these results by a second sphere coordination of the lanthanum cation by DB24C8. The first sphere, on the other hand, should be occupied by the nitrate anions and residual solvent molecules, water and/or AN. As it will be shown later in this chapter, the coordinated water molecule remains in the inner sphere during the course of the La(III) complexation by DB24C8. Another example for this case is the complex $\{Gd(NO_3)_3\ 18C6\ (H_2O)_3\}$ in the solid state[37]. The crystal structure of this complex indicates that Gd(III) is coordinated by three bidentate nitrates and by three water molecules while the 18C6 is held in the lattice by weak hydrogen bonds from coordinated water. The above interpretation is also supported by the ^{139}La NMR chemical shift results. Table 4.4 shows that the ^{139}La chemical shifts vary only slightly in the presence of DB24C8 in the solutions, about 7 ppm from $\rho = 0.0$ to $\rho > 1$. Compared to the corresponding values obtained in the case of the La(III) - 18C6 complex (~ 150 ppm), such a small variation in the chemical shifts cannot lead to the conclusion of formation of an inner sphere complex between La(III) and DB24C8.

The ^{139}La linewidths, on the other hand, vary strongly with the amounts of DB24C8 present in the solutions, T_2^{-1} increasing from 6.0 kHz for $\rho = 0$ to ~ 23 kHz for $\rho = 1.4$. Besides the effect of macroscopic viscosity of the solution, the increase of the ^{139}La linewidths can also be the result of the volume difference between free and complexed La(III) species. The ^{139}La linewidth depends on two factors (as shown in equation 3.1): one is the quadrupolar coupling constant which is related to the symmetry of the La(III) coordination environment; the other is the entire volume of the

La(III) complex which is reflected in the correlation time as indicated in equation 4.2. The correlation time, τ_c, is proportional to the cube of a, the diameter of a La(III) complex. Although a very small variation on the ^{139}La chemical shifts with ρ suggests that DB24C8 may not directly coordinate to the metal cation, the size of the La(III) complex coordinated by DB24C8 is expected to be larger than that of the solvated one, which will lead to the increase of the ^{139}La linewidth.

$$\tau_c = 4/3\ \pi\ a^3\ (\eta/kT)\ f_R \qquad (4.2)$$

Since the chemical shift variation with ρ is very small and since the linewidths are too large (for instance, $\Delta\nu_{1/2} \sim 7$ kHz when $\rho > 1$) to be measured accurately in the cases of $\rho >$ and ~ 1, it is impossible to determine precisely the stoichiometry of the La(III) - DB24C8 complex from the ^{139}La NMR results.

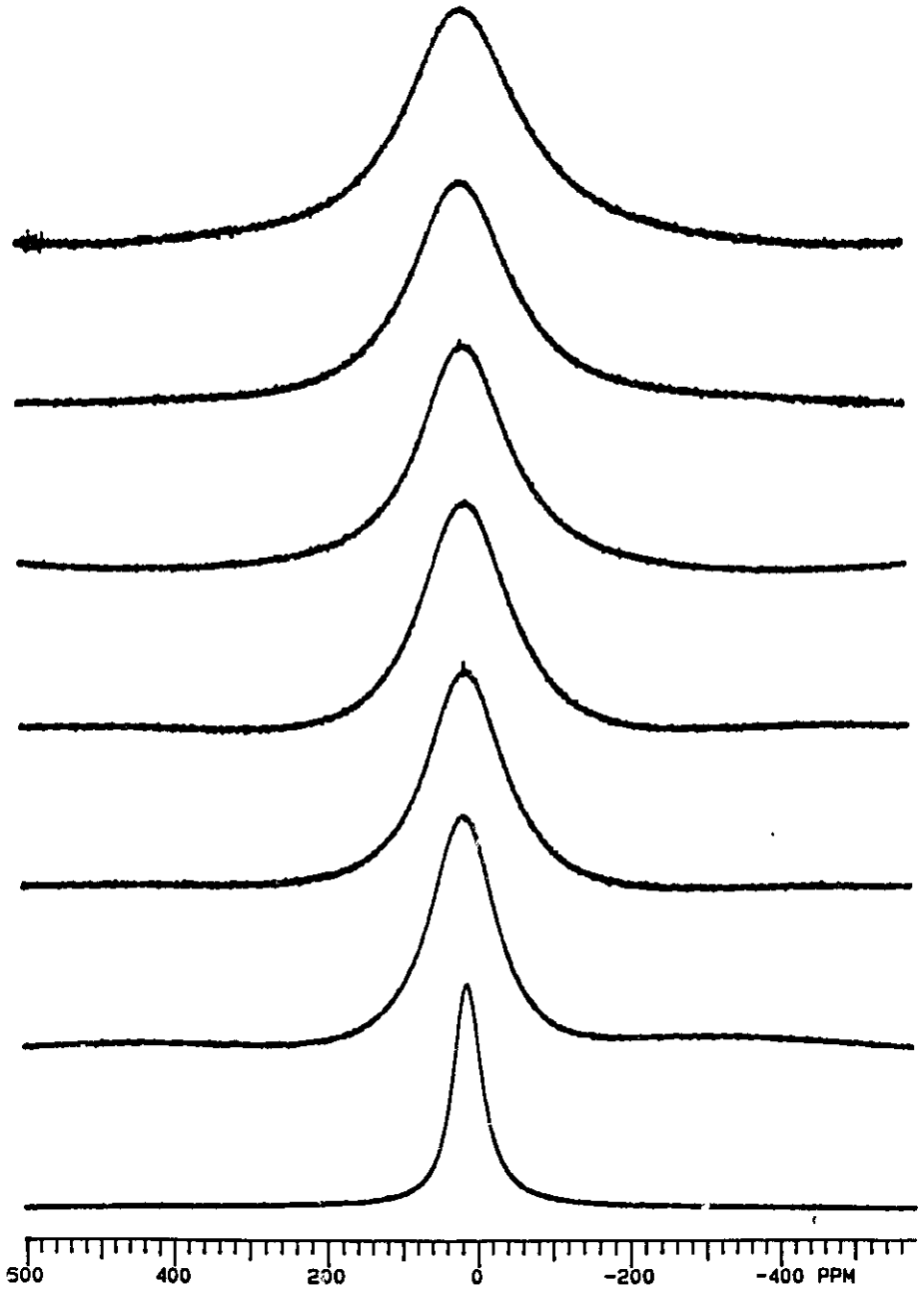

Figure 4.11: ^{139}La NMR spectra of $La(NO_3)_3$ 6 H_2O solutions in acetonitrile in the presence of DB24C8 for various values of ρ. $[La(III)]_o$ = 0.100 M. T = 300 K. Top to bottom, ρ (= $[18C6]_o$ / $[La(NO_3)_3$ 6 $H_2O]_o$) = 1.40, 1.20, 1.00, 0.88, 0.60, 0.40, 0.00.

Table 4.4:

The ^{139}La NMR experimental data of a 0.10 M $La(NO_3)_3$ 6 H_2O solution in AN in the presence of DB24C8, for various values of ρ

ρ[a]	δ(ppm)[b]	(T_2^{-1})[c](kHz)
0.00	11	6.0
0.42	9	13
0.59	9	16
0.77	8	18
0.88	7	20
1.00	4	21
1.20	4	22
1.40	4	23

a, The ratio of $[DB24C8]_o$ / $[La(III)]_o$;

b, The ^{139}La chemical shifts, errors are estimated to be ±1 to ±5 ppm;

c, The transverse relaxation rates, errors are estimated to be ±0.3 to ±1 kHz.

The complexation of La(III) with DB24C8 in acetonitrile was also observed by ^{13}C NMR of the ligand. Figure 4.12 shows the ether region of the DB24C8 ^{13}C NMR spectra with the presence of different amounts of $La(NO_3)_3$ 6 H_2O in the AN solutions. Because of two phenyl substituents, the ether carbons of DB24C8 are no longer equivalent. As a result, three signals were observed on the ^{13}C NMR spectra of the DB24C8. For a 0.012 M DB24C8 solution in acetonitrile, these three peaks are respectively at 71.26, 70.16, and 69.42 ppm. The assignments of the ^{13}C NMR peaks for the DB24C8 ether ring have been done by HETCOR technique in CD_3NO_2 solution[129]. The carbon closer to the benzene ring has the lowest chemical shift (highest field resonance). When lanthanum nitrate was added to the crown ether solutions, shifts were observed on the ^{13}C NMR signals, indicating the complexation between DB24C8 and La(III). The fact that no additional peaks could be observed on the ^{13}C NMR spectra when different amounts of $La(NO_3)_3$ 6 H_2O were present in the solutions, shows that the ligand exchange is also fast on the ^{13}C NMR chemical shift time scale. These results are consistent with that obtained by ^{139}La NMR spectra shown previously. Furthermore, the ^{13}C chemical shifts changed monotonically with R ($[La(III)]_o$ / $[crown\ ether]_o$) in a range of $0 \leq R \leq 1.4$. This may indicate that a complex with a higher ratio of La(III) : DB24C8, such as 2 : 1, was formed, which needs to be verified by recording the ^{13}C NMR spectra of DB24C8 at higher R values. A plot of ^{13}C chemical shifts as a function of R is given in figure 4.13.

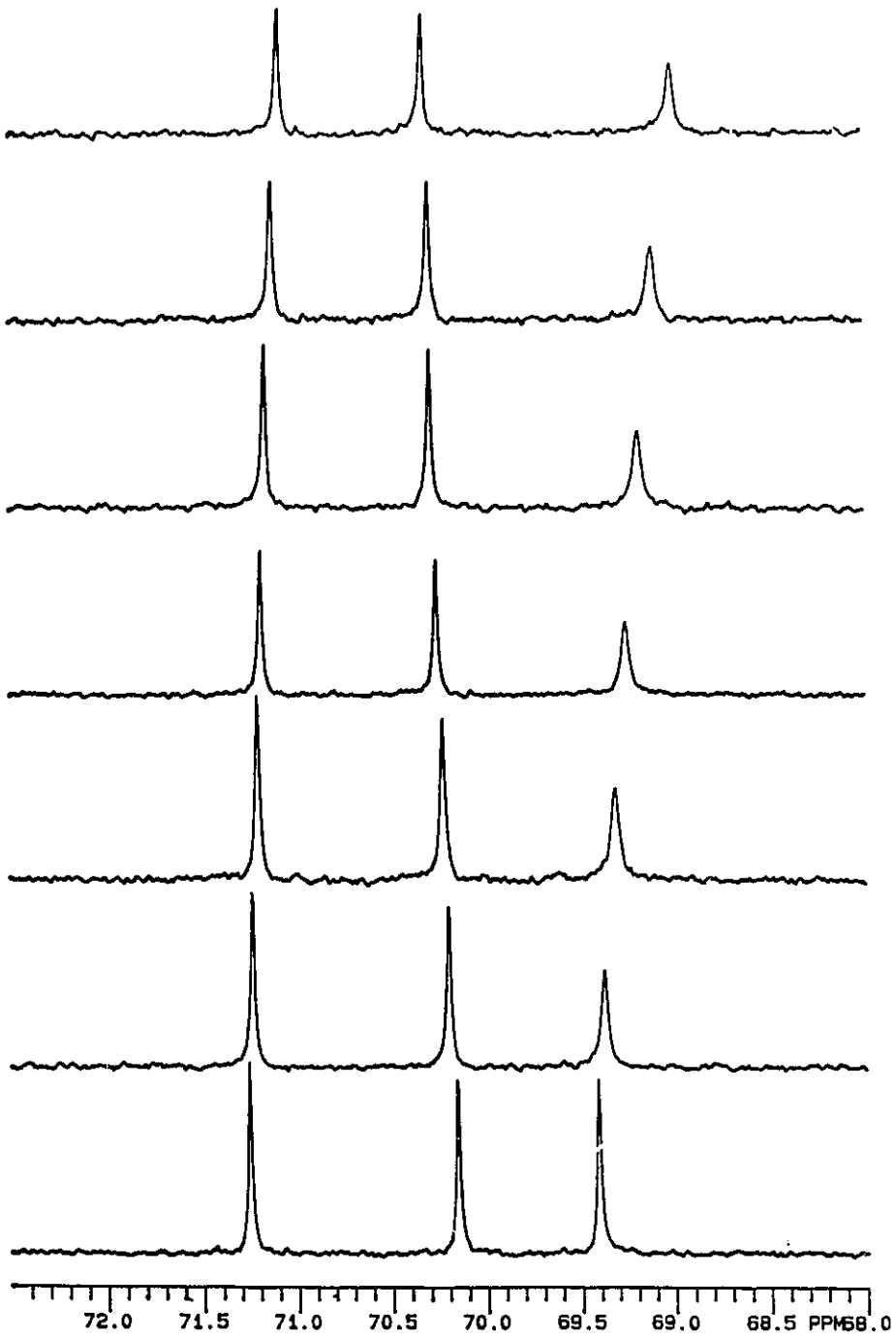

Figure 4.12: ^{13}C NMR spectra of DB24C8 solutions in acetonitrile in the presence of $La(NO_3)_3$ 6 H_2O for various R values. $[DB24C8]_o$ = 0.012 M. T = 300 K. Top to bottom, R (= $[La(NO_3)_3\ 6\ H_2O]_o$ / $[DB24C8]_o$) = 1.47, 1.05, 0.84, 0.63, 0.42, 0.21, 0.00.

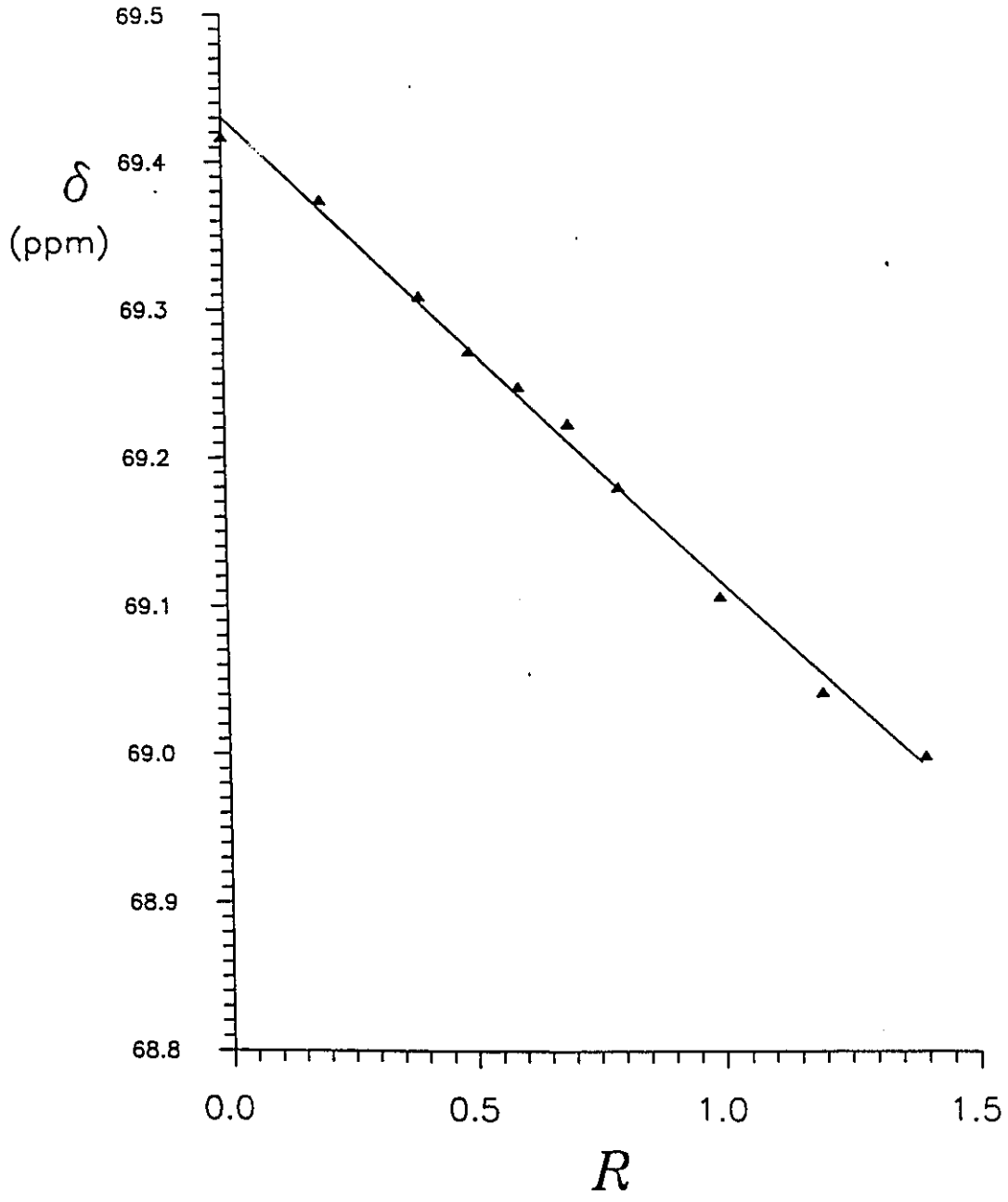

Figure 4.13: ^{13}C NMR chemical shifts of DB24C8 (the resonance at highest field shown in figure 4.12) as a function of R ($R = [La(NO_3)_3 6H_2O]_o / [DB24C8]_o$).

4.2.5 $La(NO_3)_3$ 6 H_2O and B15C5 in Acetonitrile:

Figure 4.14 shows a series of ^{139}La NMR spectra of a 0.020 M $La(NO_3)_3$ 6 H_2O solution in AN in the presence of various amounts of B15C5. A single ^{139}La NMR peak was observed in all the cases. The chemical shifts decreased with the increase of ρ, from 11 ppm for $\rho = 0$ to -46 ppm for $\rho > 1$. The linewidths varied with the values of ρ as well, but in a different manner compared to the chemical shift variation. The observed linewidths were around 2 kHz for both $\rho = 0$ and $\rho > 1$. The largest value of the linewidths was about 4 kHz which appeared in the cases of $0 < \rho < 1$. The longitudinal relaxation rates, T_1^{-1}, were measured for some samples. Differences between T_2^{-1} and T_1^{-1} were found in the cases of $0 < \rho < 1$. The ^{139}La NMR data are reported in table 4.5. All these results point to a limited fast chemical exchange between La(III) solvated and complexed species. Contrary to the present case, it was shown in section 4.2.3 that the La(III) exchange is slow in the system involving 18C6. This may be ascribed to the structural differences between the La(III) complexes with the two ligands, 18C6 and B15C5. The detailed discussions on the structure of the La(III) complexes with crown ethers will be given later in this chapter and in chapter 5. The kinetic study related to the present system can be found in chapter 6 of this thesis. It should be mentioned that the La(III) complex with B15C5 has a low solubility in AN, precipitation occurring when $\rho > 0.35$. As a consequence, the stoichiometry of the La(III) complex with B15C5 in the solution can not be accurately determined.

At a lower $La(NO_3)_3$ 6 H_2O concentration ($[La(III)]_o = 0.0050$), separated signals corresponding respectively to the solvated and complexed La(III) were observed on the ^{139}La NMR spectra in the cases of $0 < \rho < 1$. This indicates that the La(III) chemical exchange in this case is slower compared to the case of $[La(III)]_o$ = 0.020 M. The dependence of the chemical exchange rate on the total concentration of the cation is directly related to the mechanism of the exchange reaction. The detailed discussions about this point will be given in chapter 6. Figure 4.15 shows a series of

the ^{139}La NMR spectra recorded for a 0.0050 M $La(NO_3)_3$ 6 H_2O solution in AN in the presence of B15C5. The disappearance of the solvated La(III) signal on the ^{139}La NMR spectra at $\rho \geq 1$ is an indication that a 1 : 1 La(III) : B15C5 complex is quantitatively formed. The formation of a stable 1 : 1 complex between La(III) and B15C5 is also detected by the B15C5 proton NMR observations. These results will be shown later in this section.

In both cases, $[La(III)]_o$ = 0.020 M and 0.0050 M, the same chemical shift was observed for the complexed La(III) (-46 ppm). This relatively large upfield shift upon the complex formation indicates that the ligand B15C5 participates in the first coordination sphere of La(III) in the complex. A solid 1 : 1 complex of $La(NO_3)_3$ with B15C5, {$La(NO_3)_3$ B15C5}, was isolated from acetone[30,126]. It was found that both nitrate and B15C5 coordinated directly to the La(III) cation. Crystals of this complex were prepared and its structure determination was done. These results will be shown in the next chapter of this thesis.

The ^1H NMR spectra of B15C5 were recorded for a 0.0061 M crown ether solution in CD_3CN in the presence of $La(NO_3)_3$ 6 H_2O. Figure 4.16 shows the spectra for various values of R (R = $[La(III)]_o$ / $[crown\ ether]_o$). Because of the phenyl substitution, multiple signals corresponding to the ether protons were observed. When R = 0, there is no lanthanum nitrate present in the solution, the ^1H NMR spectrum of B15C5 consists of two 4-spin AA'BB' and one 4-spin AA'XX' patterns. One of the 4-spin AA'BB' patterns is at highest frequency attributed to the aromatic protons. The other 4-spin AA'BB' pattern and the 4-spin AA'XX' pattern are at lower frequency, and correspond to the methylene protons of the B15C5. When lanthanum nitrate was introduced to the solution, these proton peaks lost their high resolution feature and their chemical shifts varied with R. This is an indication that chemical exchange of the ligands in different states is moderately fast on the ^1H NMR time scale.

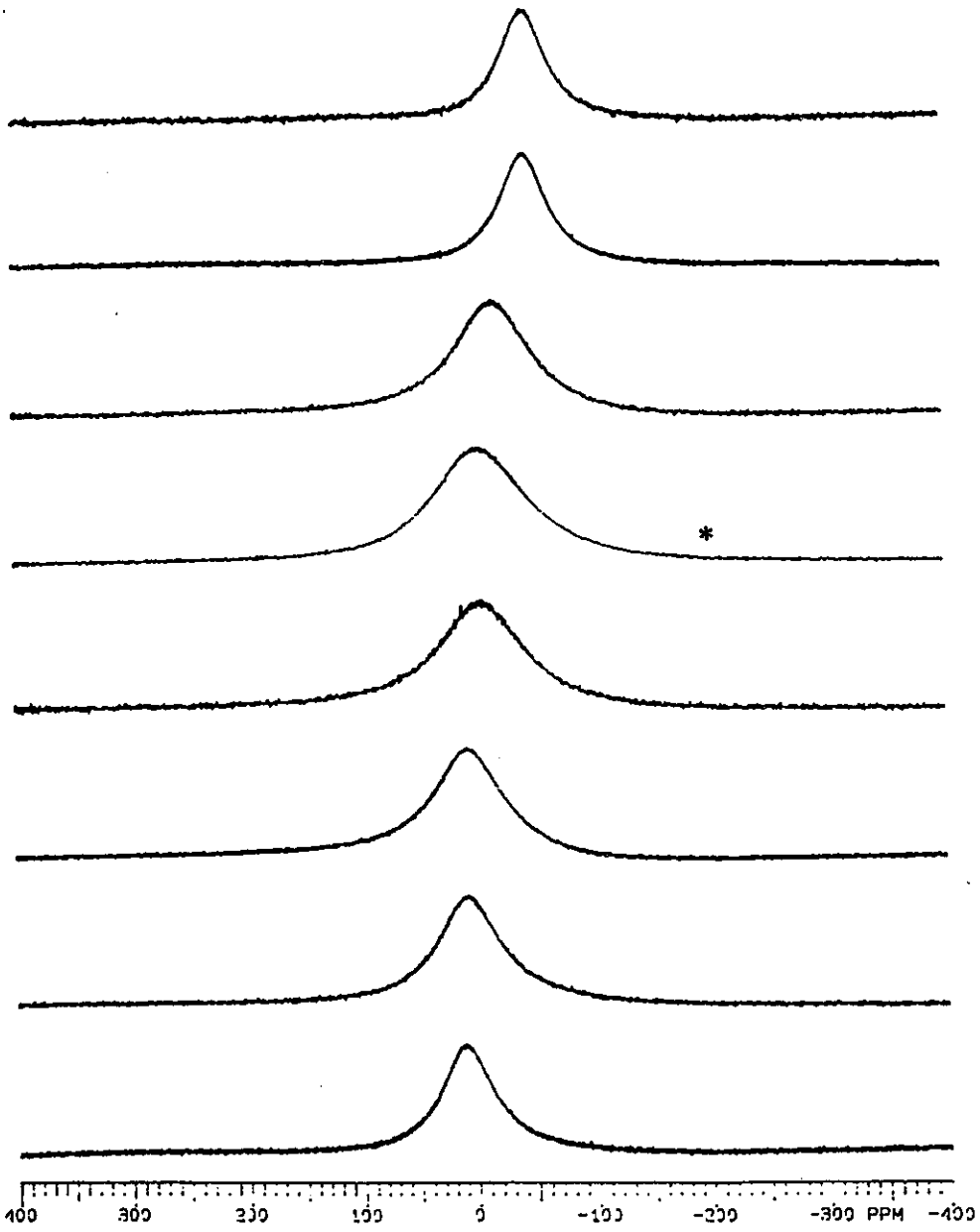

Figure 4.14: ^{139}La NMR spectra of $La(NO_3)_3$ 6 H_2O solutions in acetonitrile in the presence of B15C5 for various values of ρ. $[La(III)]_o$ = 0.020 M. T = 300 K. Top to bottom, ρ (= $[B15C5]_o$ / $[La(NO_3)_3$ 6 $H_2O]_o$) = 1.30, 1.05, 0.80, 0.50, 0.35, 0.20, 0.10, 0.00. *, the precipitation occurred from ρ = 0.50 to higher ρ values.

Table 4.5:

^{139}La NMR experimental data of 0.020 M $La(NO_3)_3$ 6 H_2O in the presence of B15C5 in AN solutions for various ρ values

ρ[a]	δ(ppm)[b]	(T_1^{-1})[c](kHz)	(T_2^{-1})[d](kHz)
0.00	10.0	6.5±0.2	6.8
0.10	7.9	6.8±0.7	8.4
0.15	7	6.5±0.4	8.9
0.20	4	-----	9.5
0.25	0	6.7±0.3	10.1
0.30	-2	6.8±0.7	10.1
0.35	-9	-----	11.5
0.50[e]	-6	-----	9.9
0.65	-14	-----	9.4
0.80	-25	-----	8.4
1.05	-44	-----	5.3
1.30	-46	-----	5.0

a, The ratio of $[B15C5]_o$ / $[La(III)]_o$;

b, Chemical shifts, errors are estimated to be ±1 to ±2 ppm;

c, Longitudinal relaxation rates;

d, Transverse relaxation rates, errors are estimated to be ±0.2 to ±0.6 kHz;

e, The precipitation occurred from this point to higher ρ values.

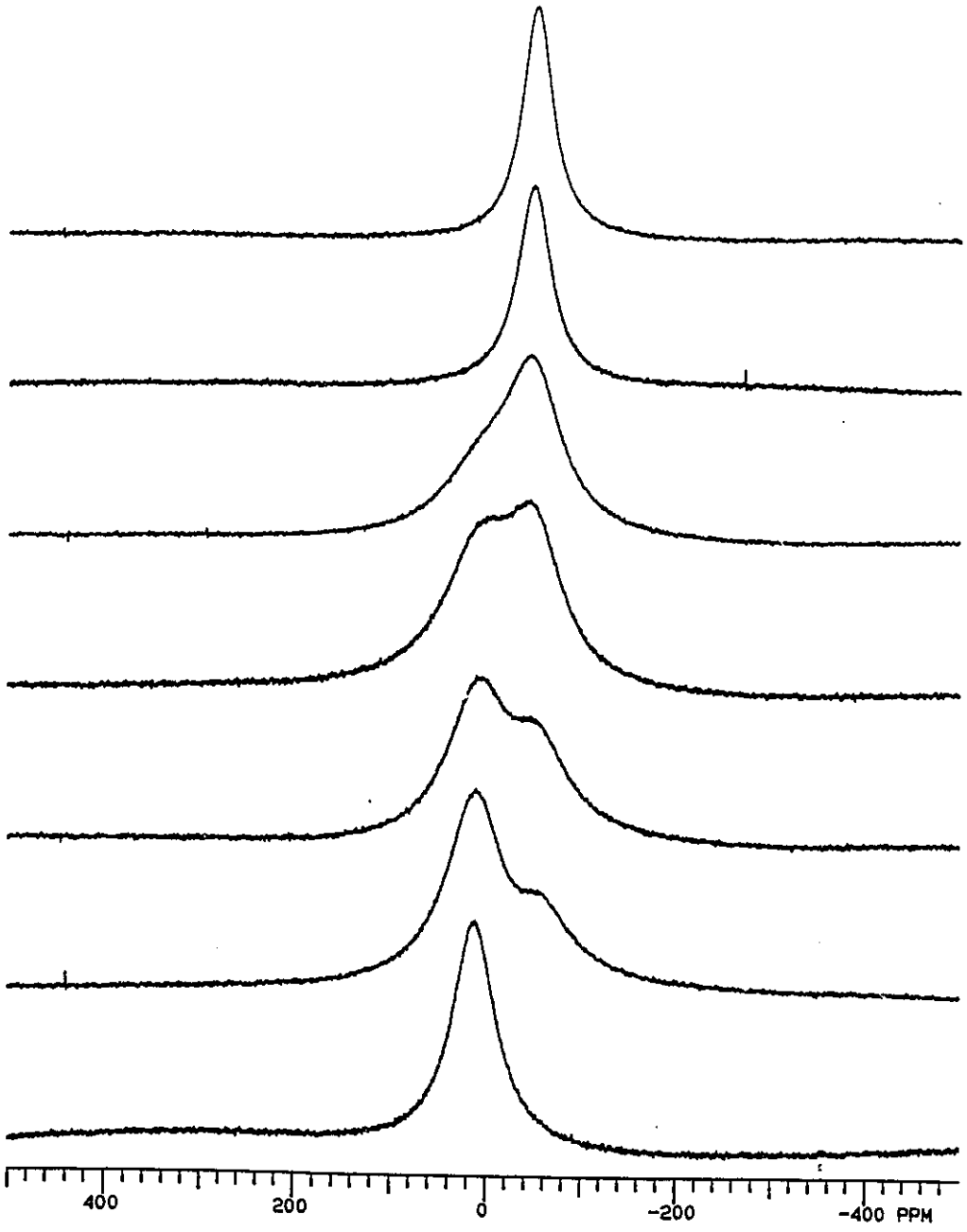

Figure 4.15: ^{139}La NMR spectra of $La(NO_3)_3$ 6 H_2O solutions in acetonitrile in the presence of B15C5 for various values of ρ. $[La(III)]_o$ = 0.0050 M. T = 300 K. Top to bottom, ρ (= $[B15C5]_o$ / $[La(NO_3)_3$ 6 $H_2O]_o$) = 1.20, 1.03, 0.60, 0.40, 0.30, 0.18, 0.00.

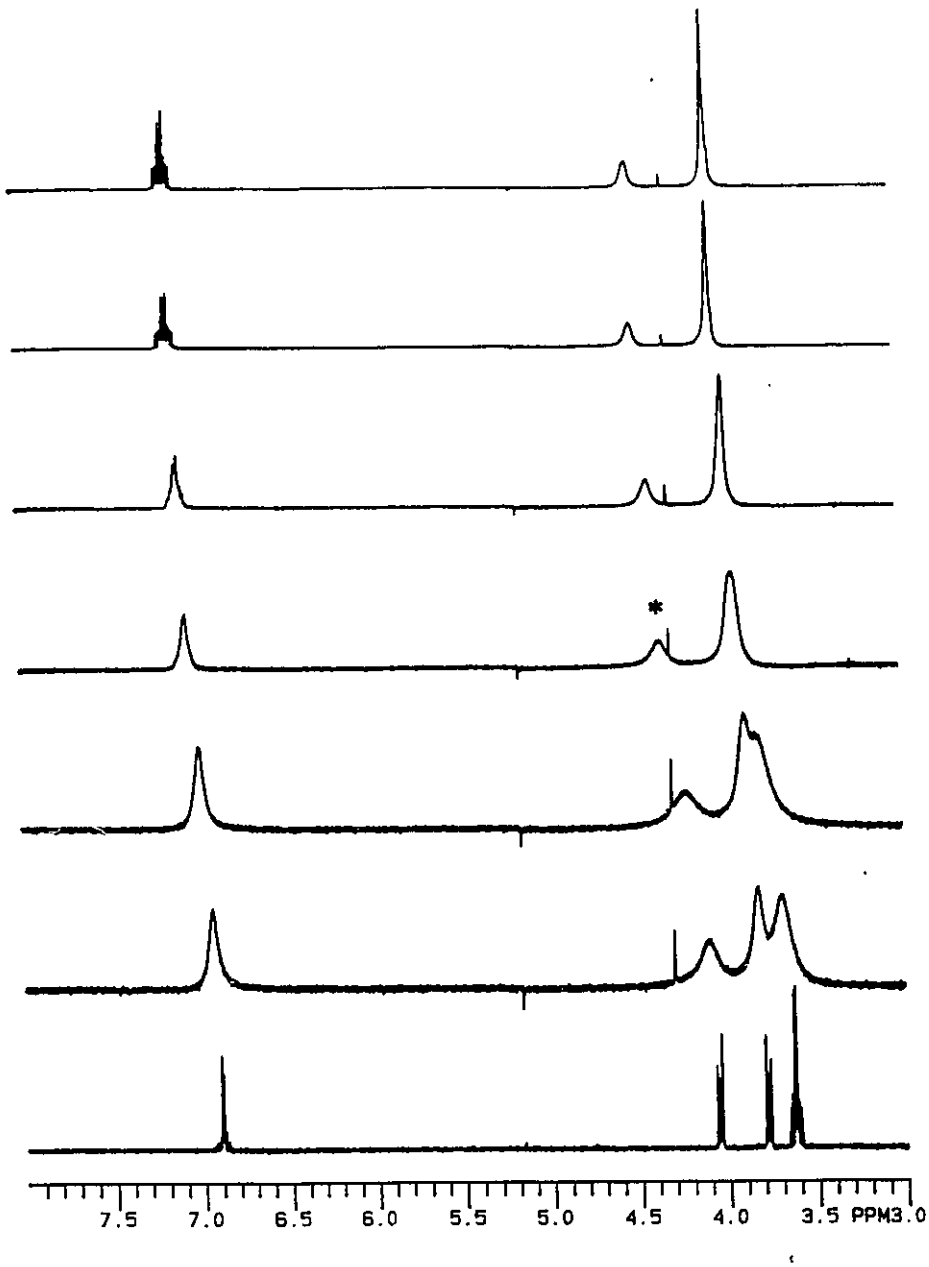

Figure 4.16: ^{1}H NMR spectra of B15C5 solutions in acetonitrile in the presence of $La(NO_3)_3$ 6 H_2O for various values of *R*. $[B15C5]_o$ = 0.0061 M. T = 300 K. Top to bottom, *R* (= $[La(NO_3)_3$ 6 $H_2O]_o$ / $[B15C5]_o$) = 1.23, 1.06, 0.85, 0.63, 0.42, 0.21, 0.00.

From figure 4.16, it can be seen that one ^{1}H peak (with a * in the figure) is well separated from the others in the ether region. The chemical shift of this peak varied with R in the cases of $0 < R < 1$ and was constant when $R \geq 1$. A similar characteristics is also shown by the aromatic proton peaks. A plot the ^{1}H chemical shifts of this peak as a function of R is shown in figure 4.17. From the plot, one may conclude that a stable 1 : 1 La(III) : B15C5 complex is formed in the solution. A 1 : 1 strongly bound lanthanide-B15C5 complex has been detected by Simon *et al.*[39] in a lanthanide perchlorate solution in acetonitrile.

Proton decoupled ^{13}C NMR spectra of the B15C5 in this system exhibit characteristics similar to the proton ones. The ^{13}C NMR observations were made for a 0.015 M B15C5 solution in AN in the presence of $La(NO_3)_3$ 6 H_2O. The ^{13}C NMR spectra of B15C5 in the ether region are shown in figure 4.18 for various values of R. As expected, four peaks were observed for free B15C5. When different amounts of $La(NO_3)_3$ 6 H_2O were added to the solution, these ^{13}C signals changed their positions and their lineshapes. These observations are an indication that the B15C5 exchange between its solvated site and the site complexed by La(III) is also moderately fast on the ^{13}C NMR time scale. When $R \geq 1$, four ^{13}C peaks with equal intensities appeared again but with different chemical shifts compared to those obtained in the case of R = 0. This is further evidence that the complex of La(III) with B15C5 in a ratio of 1 : 1 is quantitatively formed. Again, because of the low solubility of the complex La(III)-B15C5 in AN, some precipitation was also found in some of ^{13}C NMR samples.

Finally, it is noteworthy that different features were observed for the aromatic and methylene protons of the B15C5 on the ^{1}H NMR spectra in the cases of $R \geq 1$. The NMR spectra of the aromatic protons have high resolution characteristics. However, this is not the case for the methylene protons. The different observed behaviors of these protons can be interpreted by an exchange process involving the coordinated B15C5, which will be discussed in detail in chapter 6.

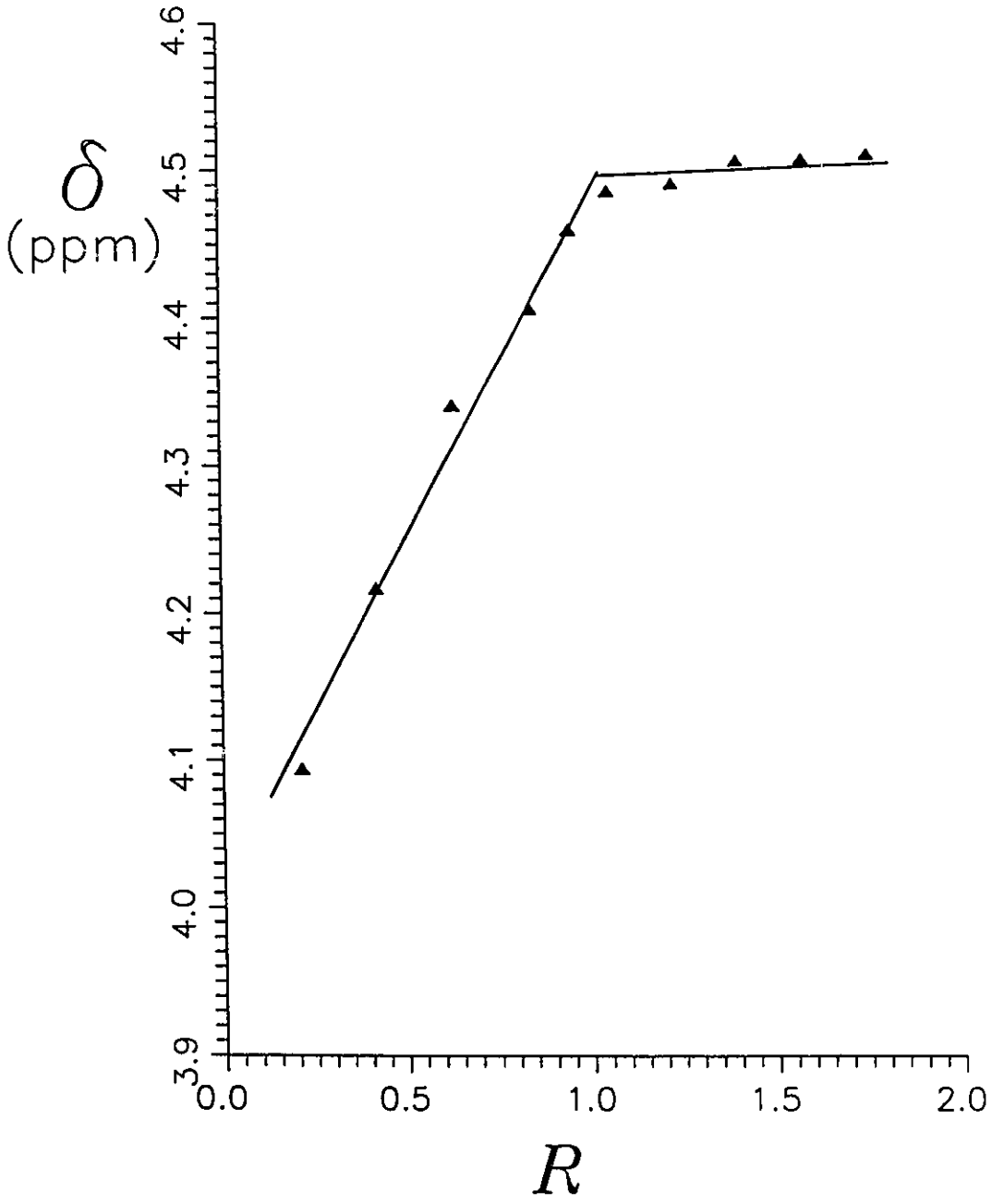

Figure 4.17: ^{1}H NMR chemical shifts of B15C5 (the resonance indicated by * in figure 4.16) as a function of R (= $[La(NO_3)_3 6H_2O]_o$ / $[B15C5]_o$).

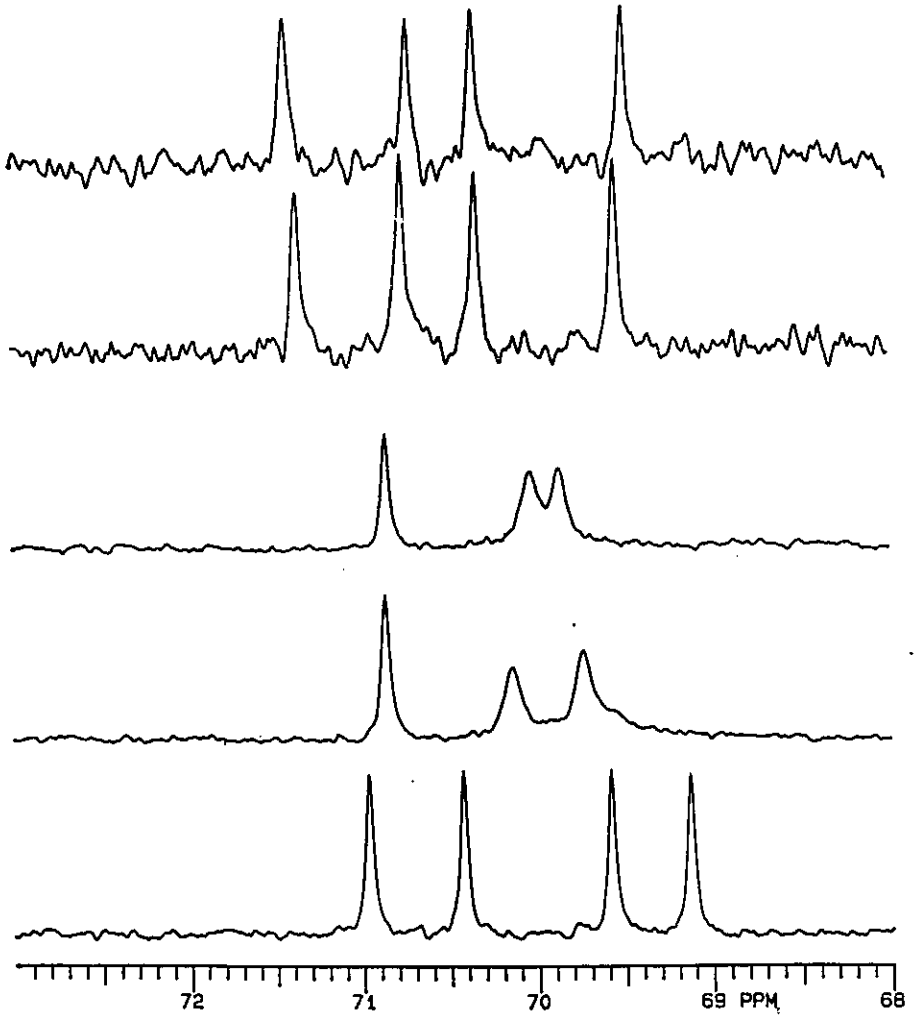

Figure 4.18: ^{13}C NMR spectra of B15C5 solutions in acetonitrile in the presence of $La(NO_3)_3$ 6 H_2O for various values of *R*. $[B15C5]_o$ = 0.015 M. T = 300 K. Top to bottom, *R* (= $[La(NO_3)_3\ 6\ H_2O]_o$ / $[B15C5]_o$) = 1.20, 1.00, 0.40, 0.20, 0.00.

4.2.6 $La(NO_3)_3\ 6\ H_2O$ and 15C5 in AN

Because the complex La(III)-15C5 has a very low solubility in acetonitrile, the ^{139}La NMR measurements were not made on this system. The complexation between La(III) and 15C5 was investigated by the ^1H and the ^{13}C NMR of the ligand. The ^1H and ^{13}C NMR spectra were recorded in a constant 15C5 concentration in CD_3CN whereas the concentrations of lanthanum nitrate in the solutions were varied. The ^1H NMR spectra of a 0.0032 M 15C5 solution in CD_3CN are shown in figure 4.19. When $R = 0$, the ^1H NMR spectrum of 15C5 exhibits a single peak with a chemical shift of 3.575 ppm characterizing the solvated 15C5. In the cases of $0 < R < 1$, this peak remains at its position but with line broadening. In addition, another group of ^1H peaks can be observed at higher frequency in the proton spectra. These ^1H signals correspond to the complexed 15C5. When R increases, the intensity of the solvated 15C5 signal decreases whereas the intensity of the complexed 15C5 increases. Those observations show clearly that complexation between La(III) and 15C5 occurs. The ligand exchange between its solvated and complexed sites is relatively slow on the ^1H NMR time scale. When $R \geq 1$, the ^1H peak corresponding to the solvated 15C5 disappears and, except for the peaks of complexed 15C5, no additional signals were observed. This is an indication that the complex formed has a 1 : 1 stoichiometry and that the complex formation is quantitative, which was also confirmed by the integrations of the ^1H peaks.

In the previous section, it has been shown that the NMR spectra of the ether protons of the complexed B15C5 have no high resolution features. This characteristic was also observed on the ^1H NMR spectra of the complexed 15C5. Again, this feature of the complexed 15C5 proton NMR spectra can be interpreted by an exchange process involving the coordinated ligand as will be described and discussed in chapter 6.

The complexation between 15C5 and La(III) was also shown by the ^{13}C NMR spectra. Figure 4.20 shows a series of ^{13}C NMR spectra of a 0.0043 M 15C5 solution in

CD_3CN in the presence of hydrated lanthanum nitrate. In contrast with the ^1H NMR spectra shown above, a single peak was observed for all the samples. The position and linewidths of this peak varied with R in the range of $0 < R < 1$ and were unchanged in the cases of $R \geq 1$. In the range of $0 < R < 1$, the ^{13}C NMR chemical shifts decreased linearly with the concentration of La(III). The linewidths varied also with the variation of R. The maximum linewidth was observed in the case of half equimolar of lanthanum nitrate being added into the sample. All these results show typical characteristics of a ligand undergoing a moderately rapid chemical exchange between two sites, on the ^{13}C chemical shift time scale.

A plot of the ^{13}C chemical shifts as a function of R is given in figure 4.21. The plot can be accounted for by the formation of a stable 1 : 1 complex, which is consistent with the result obtained from the ^1H NMR observations. A solvent free complex $La(NO_3)_3$-15C5 with a stoichiometry of 1 : 1 has been isolated in the solid state[34,36]. The single crystal structure analysis for this complex has also been reported in the literature[131].

The variation of ^{13}C linewidths with R will provide kinetic information about the 15C5 exchange. They will be described in chapter 6.

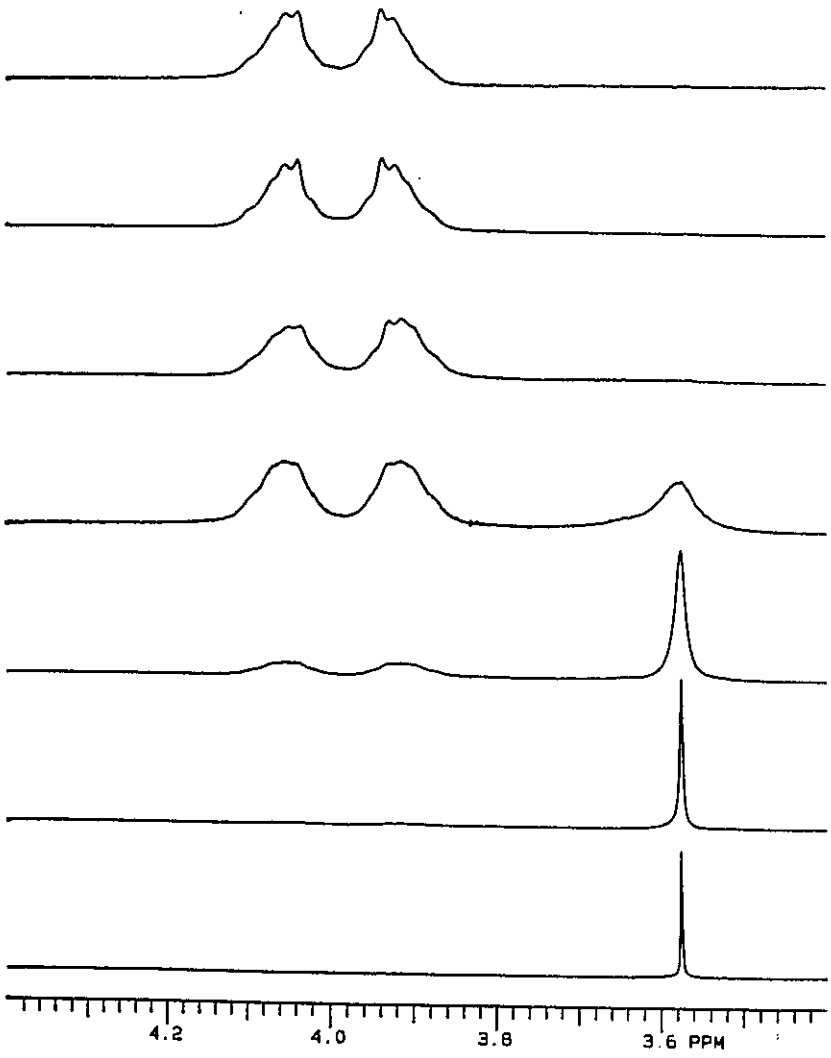

Figure 4.19: ^{1}H NMR spectra of 15C5 solutions in acetonitrile in the presence of $La(NO_3)_3$ 6 H_2O for various values of *R*. $[15C5]_o$ = 0.0032 M. T = 300 K. Top to bottom, *R* (= $[La(NO_3)_3\ 6\ H_2O]_o$ / $[15C5]_o$) = 1.18, 1.00, 0.81, 0.62, 0.43, 0.19, 0.00.

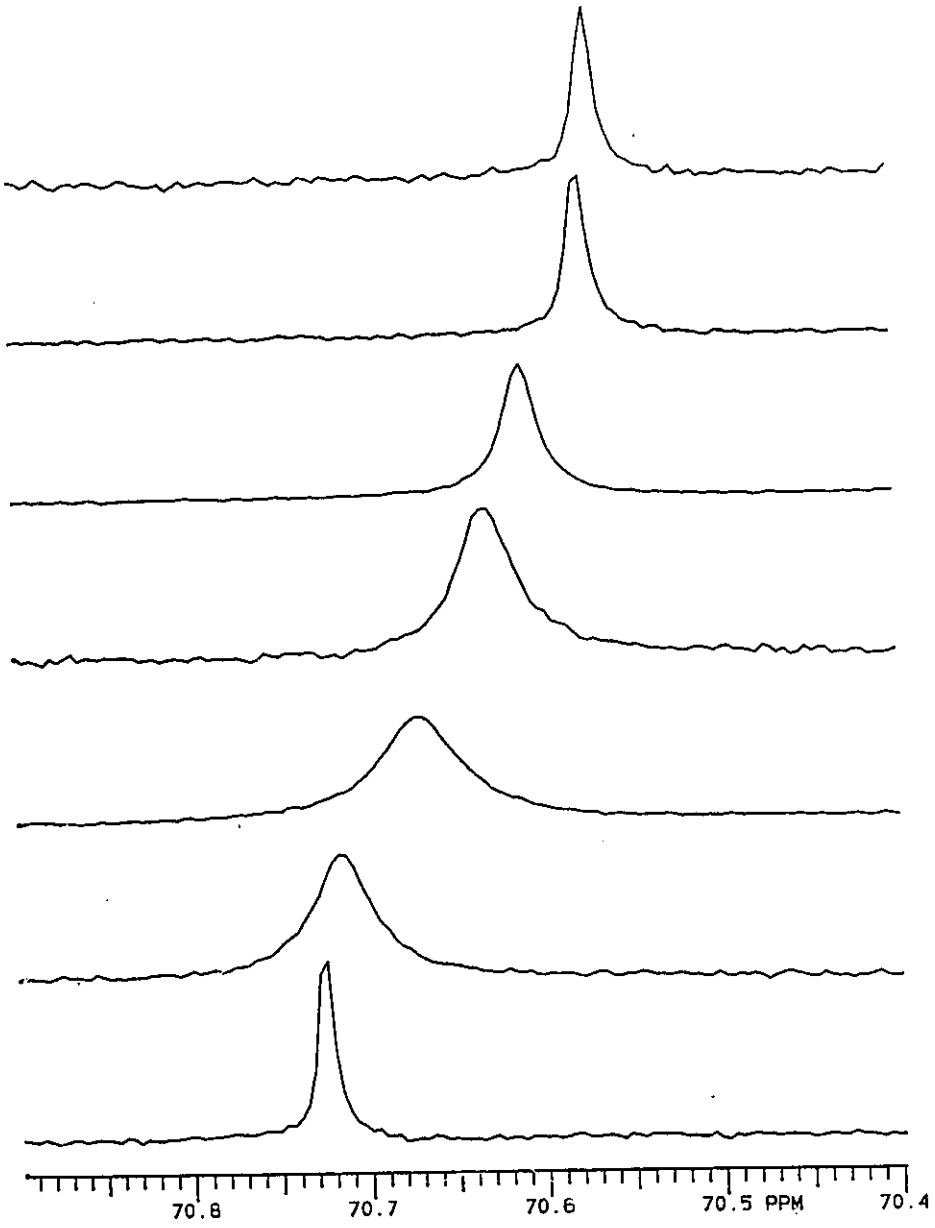

Figure 4.20: ^{13}C NMR spectra of 15C5 solutions in acetonitrile in the presence of $La(NO_3)_3$ 6 H_2O for various values of *R*. $[15C5]_o = 0.0043$ M. T = 300 K. Top to bottom, *R* (= $[La(NO_3)_3\ 6\ H_2O]_o$ / $[15C5]_o$) = 1.33, 1.04, 0.76, 0.59, 0.30, 0.14, 0.00.

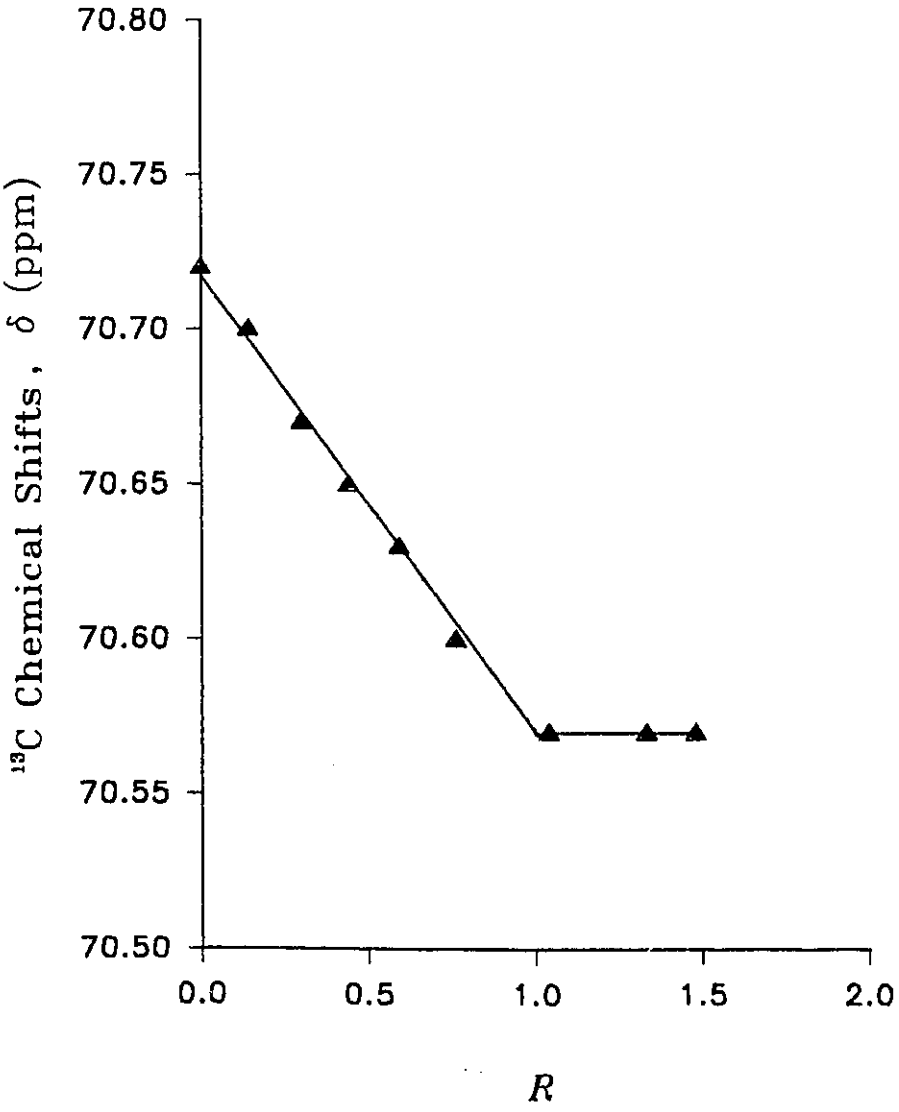

Figure 4.21: ^{13}C NMR chemical shifts of 15C5 as a function of R (= $[La(NO_3)_36H_2O]_o$ / $[15C5]_o$).

4.3. The structure of the La(III) coordination shell in lanthanum crown ether complexes.

In section 4.2, complexations between La(III) and crown ethers have been shown by the results obtained from multinuclear magnetic resonance spectroscopy. We hope to gain insight into which elements actually participate in the first coordination sphere of the La(III) in those complexes. Considering the systems investigated, the following species may be involved in the competition for the La(III) coordination sphere: crown ethers, NO_3^- , H_2O, and CH_3CN. In the previous chapter, the equilibrium given in equation 4.2 has been used to interpret the ^{139}La NMR data of the $La(NO_3)_3$ 6 H_2O solutions in acetonitrile.

$$\{La(III)\ (NO_3^-)_3\ (AN)_x)\} + H_2O \rightleftharpoons \{La(III)\ (NO_3^-)_3\ (AN)_y)\ H_2O\} \qquad (4.2)$$

When crown ethers were introduced into the solution, the formation of complexes between La(III) and crown ethers was observed. If the complexation has an inner sphere characteristic, some of the species present in the first coordination shell of the solvated La(III) must be substituted. In order to verify which those species are, we recorded the ^{17}O NMR spectra for the samples containing various amounts of crown ethers in the $La(NO_3)_3$ 6 H_2O acetonitrile solutions.

The observations of ^{17}O NMR were made on a 0.015 M hexhydrated lanthanum nitrate solution in acetonitrile in the presence of different amounts of B15C5. Only water peaks were obtained on the ^{17}O NMR spectra. No signals corresponding either to B15C5 or to NO_3^- anions were observed, which might be because the natural abundance of the ^{17}O nucleus is low and the concentration of the solutions was also relatively low. The ^{17}O chemical shifts of H_2O varied with ρ (= $[B15C5]_o$ / $[La(III)]_o$) within $0 \leq \rho \leq 1$, from 2.98 ppm ($\rho = 0$) to -6.20 ppm ($\rho = 1$), whereas it was constant in the cases of $\rho \geq 1$ (-6.20 ppm). This value is consistent with the ^{17}O chemical shift of

free H_2O, which has been checked by the ^{17}O NMR spectrum of an acetonitrile solution containing 0.09 M water (the water concentration corresponding to 0.015 M of $La(NO_3)_3$ 6 H_2O). Those results indicate clearly that the water molecules in the first coordination shell of the solvated La(III) are replaced by B15C5 during the course of the La(III) - crown ether complexation. Figure 4.22 shows the ^{17}O chemical shifts of H_2O as a function of ρ.

At present, we have no information on the coordination states of the nitrate anions, because their signals were not observed on the ^{17}O NMR spectra. However, the non-conductivity behavior of the lanthanide crown ether complexes in nonaqueous solutions reported in the literature[30,36,130] indicate that all the nitrate anions remain in the La(III) first coordination sphere for the complexed La(III) species. The presence of the three NO_3^- ions in the inner sphere of the La(III) was also found in the complex with phenanthroline[107]. Considering the fact that water has a stronger coordination ability to the La(III) than acetonitrile molecules, it is reasonable to assume that the solvent molecules (AN) are also replaced upon the crown ether complex formation and the inner sphere of the La(III) are only occupied by B15C5 and NO_3^- ions. Therefore, the coordination number of the La(III) complexed by B15C5 will be 11 if the bound nitrate ions are bidentate. The absence of water and solvent molecules (here AN) in the B15C5 - lanthanum nitrate complex agrees well with the corresponding compound in the solid state[30,130] and with the single crystal structure of the complex which will be shown in the next chapter.

That water was completely expelled from the inner coordination sphere of La(III) by B15C5 was found in the cases of $\rho \geq 1$. This is another evidence that the 1 : 1 La(III):B15C5 complex is quantitatively formed in solution. The same conclusion was reached in section 4.2.5.

As expected, the crown ether complexation will also affect the equilibrium of the solvated La(III) species (see equation 4.2). This effect has been shown in section

4.2.3 by the variations of ^{139}La chemical shifts and linewidths of the solvated La(III) with ρ in the system involving 18C6 (see table 4.3). Since only water was released upon the formation of the complex, it might be assumed that the effect is simply to shift the equilibrium described in equation 4.2. On the basis of this assumption and of the equation 4.2, the following relationships between water species and ρ can be obtained.

$$K = [B] / [H_2O]_f / [A] \qquad (4.3)$$

Where B and A represent {La(III) $(NO_3^-)_3$ $(AN)_x$)} and {La(III) $(NO_3^-)_3$ $(AN)_y$) H_2O} respectively, and $[H_2O]_f$ is the concentration of water in the free site.

Since water does not participate in the inner sphere of the complexed La(III), the complexed La(III) species are not involved in the equilibrium described in equation 4.2. Therefore,

$$[A] = [La(III)]_o - [B] - \rho \times [La(III)]_o \qquad (4.4)$$

$$[H_2O]_f = 6 \times [La(III)]_o - [B] \qquad (4.5)$$

$$[H_2O]_c = [B] = 0.5 \times C - (0.25 \times C^2 - D)^{1/2} \qquad (4.6)$$

Where, $C = 1 / K + (7 - \rho) \times [La(III)]_o$ and $D = 6 \times (1 - \rho) \times [La(III)]_o^2$, and $[H_2O]_c$ is the concentration of water in the complexed site.

$$\delta_{cal}(^{17}O) = (\delta_f \times [H_2O]_f + \delta_c \times [H_2O]_c) / 6 / [La(III)]_o \qquad (4.7)$$

On the basis of equation 4.7 and by using a value of -6.20 ppm for δ_f (chemical shift of free water) and taking the K and δ_c values from table 3.3 of Chapter 3, δ_{cal}, the

water ^{17}O chemical shifts for the solutions in the presence of B15C5, were calculated. The results are shown in figure 4.22 as a solid line. The calculated chemical shifts and the experimental data are in good agreement, indicating that the above assumption is reasonable. It should be mentioned that precipitation of the solid complex was found in some samples. Since no water molecules were present in the B15C5 - La(III) complex both in solution and in the solid state, that some of the complex precipitated out of the solution does not affect the treatment of the water ^{17}O NMR results described above.

The replacement of the water present in the inner sphere of La(III) in the solvated state by B15C5 upon the formation of the crown ether complexes was also observed by the water proton NMR observations. The water ^{1}H NMR peak was monitored for the B15C5 AN-d_3 solutions in the presence of various amounts of $La(NO_3)_3$ 6 H_2O. In the cases of $R \leq 1$ (R = $[La(NO_3)_3\ 6\ H_2O\ ]_o$ / $[B15C5]_o$), no chemical shift variation was found on the ^{1}H peak of water. If the conclusion given previously is correct, this result is obvious since all water molecules are in their free state in this range of R. When R is greater than 1, a substantial variation of the ^{1}H chemical shift on the water peak was observed, indicating that some water molecules begin to join the inner sphere of the solvated La(III). Figure 4.23 shows the water ^{1}H chemical shifts as a function of R.

The ^{17}O and ^{1}H NMR observations were also made on the system involving 18C6. Compared to the B15C5 system, identical water ^{17}O NMR spectra and ^{1}H NMR results were obtained, indicating that 18C6 also participated and replaced water molecules in the La(III) inner sphere when the crown ether complex was formed. For 15C5, a similar conclusion can be reached from the water ^{1}H NMR observations made on the corresponding system. Those results are not shown. Different results, however, were obtained on the system containing DB24C8. No variations of the ^{17}O chemical shifts of the water signals was found for different ρ values, showing that DB24C8 did not compete with water molecules for the La(III) inner sphere. This result may suggest

that the discussion given in section 4.2.3 on the DB24C8 system is correct, that is, the DB24C8 forms a secondary coordinated complex with La(III) (an outer-sphere complex).

Based on the results obtained from the water ^{17}O and ^{1}H NMR measurements, one might conclude that the nature of the species present in the inner sphere of the La(III) cations, complexed by 18C6, B15C5, and 15C5, is the same in all these systems: the crown ethers and the nitrate ions. From the ^{1}H NMR results of these ligands, further discussion about the complex structures may be made. Unequivalent characteristics of the methylene protons has been observed on the ^{1}H NMR spectra for the 15C5 complexed to La(III) (see figure 4.19). Similar characteristics were also found in the ^{1}H NMR spectra of the complexed B15C5 (see figure 4.16). Those unequivalent protons in the ether ring must reflect the position of the crown ether present in the La(III) complexes. It is known that the internal cavity of a 15-membered crown ether is smaller than the ionic diameter of the La(III) cation, the former is 1.9 Å[132] (for 15C5) and the latter is 2.43 Å estimated upon CN = 9[133]. As a consequence, when it forms a complex with 15C5 or with B15C5, the La(III) cation can only stay outside the cavity of those crown ethers. The "sandwich" type complexes of lanthanum with 15C5 have been isolated for the counteranions of ClO_4^-[134] and PF_6^-[135]. However, only a 1 : 1 15C5 complex with lanthanum nitrate can be formed because NO_3^-, associated with a stronger coordination ability than ClO_4^- and PF_6^-, will occupy the first coordination shell of the La(III). Therefore, it might be expected that in the complex, the crown ether will be found on one side of the La(III) coordination shell and nitrates will lie on the other. This is exactly what is found in the crystal structure of the La(III) - 15C5 complex[131] (which will also be described in the next chapter). If the structures of the complex in solution and in the solid state are the same or very similar, the unequivalent behavior of the protons for the complexed 15C5 will be logical since the protons are in the different environment due to the effect of La(III) cation. The same thing will be true for the B15C5 - La(III) complex. The proton NMR spectra for the complexed 15C5 and

B15C5 might indicate that the arrangement of the coordination components around La(III) cation in the complex is also the same in solution and in the solid state. This point will be further discussed in chapters 5 and 6.

The situation is different in the case of 18C6. The cavity of 18C6[136] (2.5 Å) is slightly larger than the ionic diameter of La(III) cation. In the complex, the La(III) cation is expected to stay in the center of the crown ether. This is found to be the case in the crystal structure of the lanthanum nitrate complex with 18C6[37]. Since the effect of La(III) cation for each of them is the same, the protons of the 18C6 will also be equivalent in the complexed site. This characteristic was observed in the 18C6 ^{1}H NMR spectra shown in figure 4.9, in which single ^{1}H peaks were observed for both free and complexed 18C6.

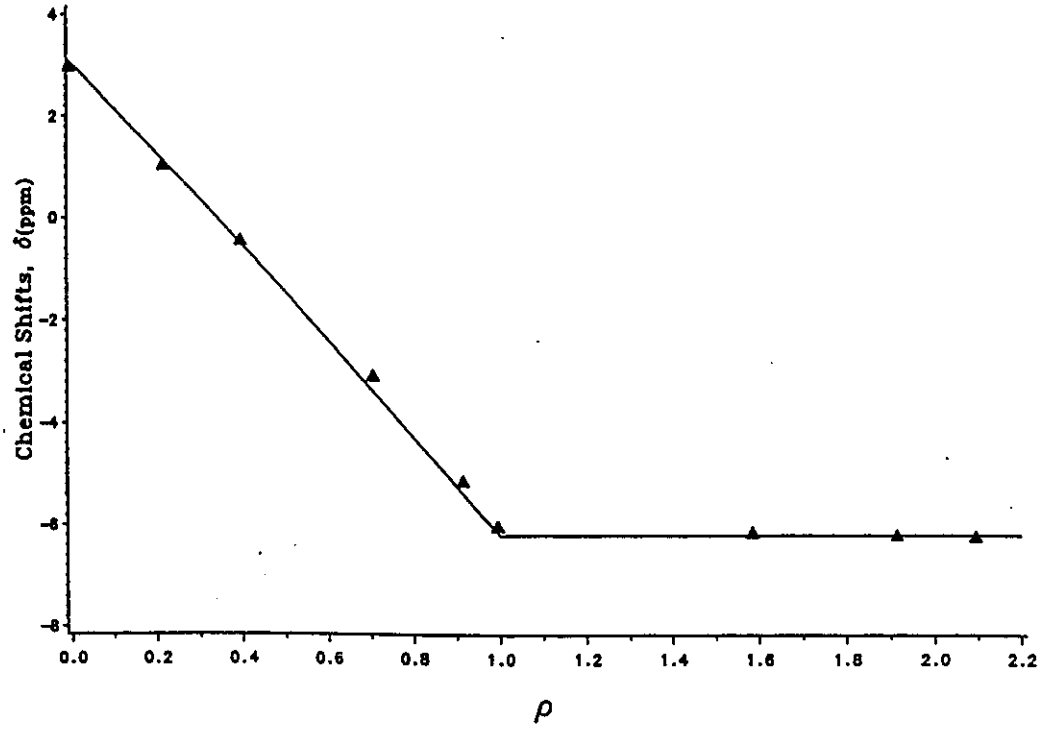

Figure 4.22: ^{17}O NMR chemical shifts of $H_2{}^{17}O$ for $La(NO_3)_3$ 6 H_2O solution in AN in the presence of B15C5 as a function of ρ. The data points are experimental and the solid line is calculated on the basis of equations 4.3 to 4.8.

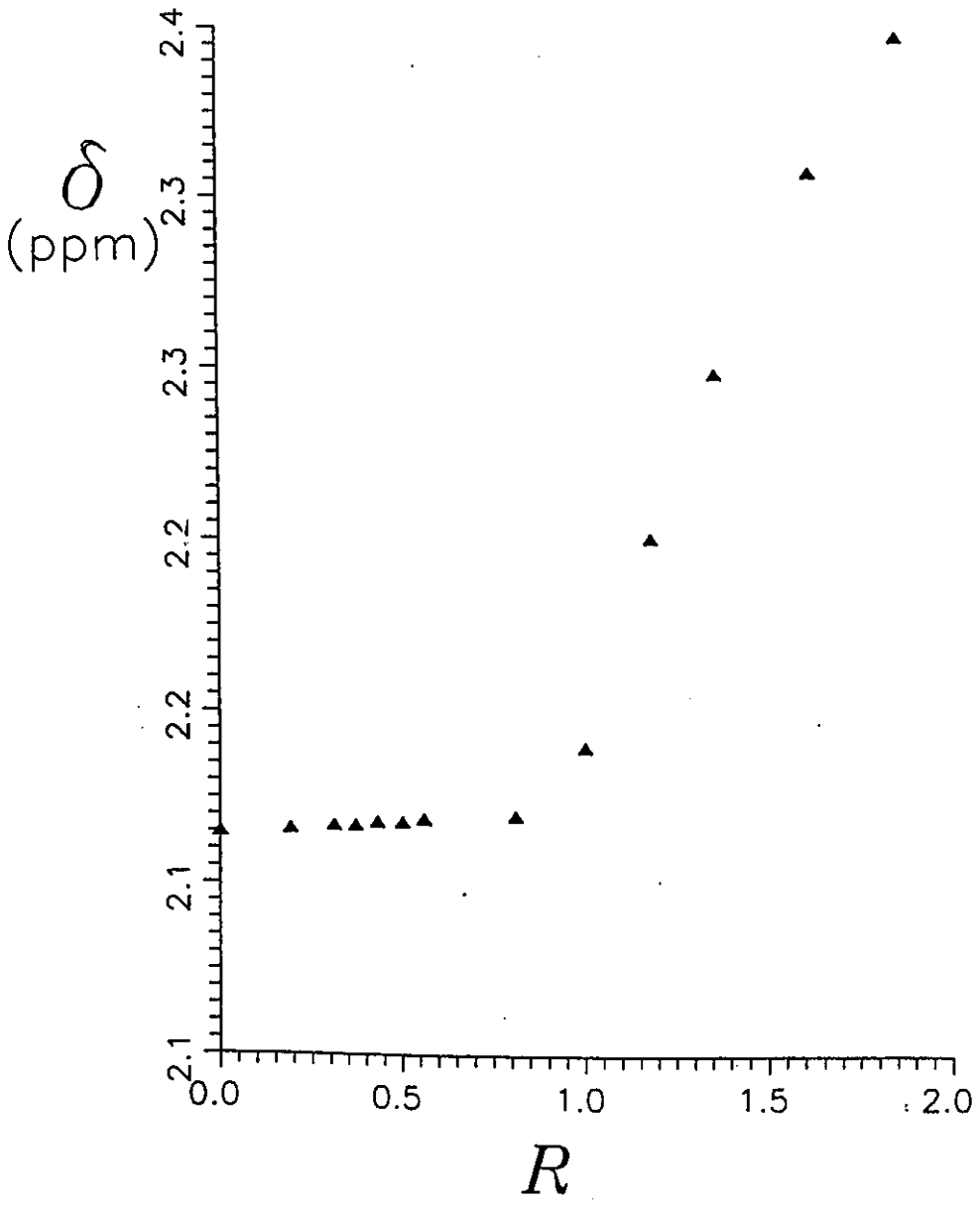

Figure 4.23: Water proton NMR chemical shifts as a function of R ($R = [La(NO_3)_3\ 6\ H_2O]_o / [B15C5]_o$).

Chapter 5

Crystal Structures of the La(III) Complexes with B15C5, 15C5, and 18C6

In order to compare the structures of the La(III) - crown ether complexes in solution and in the solid state, the crystals of those complexes were prepared. Their structures were determined by X-ray diffraction. These results are given in this chapter.

5.1. Experimental

5.1.1. Synthesis of the La(III) - crown ether complexes.

An equal molar quantity of B15C5 was added to a 15 mL 0.015 M $La(NO_3)_3$ 6 H_2O solution in anhydrous acetonitrile. The reaction mixture was shaken until B15C5 was dissolved. The resulting solution was stored at room temperature for a week. During that time, crystals suitable for an X-ray diffraction study formed. The crystals were isolated by decantation of the solvent and dried with a stream of argon. The crystal for an X-ray study was selected under a microscope and mounted in a glass

capillary tube sealed under argon.

Similar procedures were used for the preparation of the 18C6 and 15C5 complexes except for the concentration of the hydrated lanthanum nitrate. For 18C6, the concentration of La(III) in AN solution was 0.030 M. In the case of 15C5, $[La(III)]_o$ = 0.010 M.

5.1.2. Crystallographic analysis.

{La $(NO_3)_3$ B15C5} CH_3CN.

A crystal of dimensions 0.30 × 0.40 × 1.0 mm was used for X-ray crystallographic analysis. The crystal was orthorhombic. The diffracted intensities were collected with M_o K_α radiation on a Nonius diffractometer using $\omega/2\theta$ scan technique with profile analysis[137]. The space group was determined from the systematic absences. Unit cell parameters were obtained from 24 reflections by least-squares refinement with 2θ in the range of 40.00 - 45.00°. Lorentz and polarization factors were applied. An absorption correction was made with an empirical Ψ scan method. The minimum and maximum transmission factors are 0.808749 and 0.999623 respectively.

The structure was solved by the direct method. The refinement was done by a full matrix least-squares with counting statistical weight. Because of the small ratio of reflection to variable, the carbon atoms were not refined anisotropically. Almost all the hydrogen atoms were found by different Fourier maps. All the calculations were performed with the NRCVAX Crystal Structure Program[138]. The absolute configuration was determined with the approach developed in reference (139). The last least-squares cycle was calculated with 58 atoms, 265 parameters, and 2436 out of the unique 2526 reflections. The residuals on significant reflections are R_f = 0.031 and R_w = 0.033 with GoF = 9.15. For all reflections, both R_f and R_w are 0.033, where $R_f = \Sigma$

$(F_o - F_c) / \Sigma F_o$,

$R_w = [\Sigma (w (F_o - F_c)^2) / \Sigma (w (F_o)^2]^{1/2}$, and GoF = $[\Sigma (w (F_o - F_c)^2) /$ (No. of reflns - No. of params.)$^{1/2}$. The maximum shift and σ ratio in the final least-squares cycle was 1.902. The details of data collection parameters are given in table 5.1.

{La $(NO_3)_3$ 18C6}

For this complex, data were collected on a Rigaku diffractometer. No correction was made for absorption. The rest of the procedures are similar to those used for the B15C5 complex. A summary of data collection for this compound is given in table 5.2.

{La $(NO_3)_3$ 15C5}

The crystallographic analysis of this complex was also done on a Rigaku diffractometer. The procedures involved in the X-ray study of {$La(NO_3)_3$ 15C5} are the same as those applied for B15C5 complex. Table 5.3 is a summary of data collection for this compound.

Table 5.1.

Crystallographic Data and Collection Parameters for $\{La(NO_3)_3$ B15C5$\}CH_3CN$

Formula	$LaC_{16}H_{23}N_4O_{14}$
Molecular weight	634.27
Crystal dimensions (mm)	$0.2 \times 0.4 \times 1.0$
Crystal system	orthorhombic
Space group	$P2_12_12_1$
Lattice parameters:	
a, Å	12.823(3)[a]
b, Å	13.6694(9)
c, Å	13.7780(9)
β, degree	90
Cell vol. Å^3	2415.0
Z, (molecules/cell)	4
F(000), electrons	1303.76
d_{calc}, g/cm^3	1.745
Linear absorption coeff. (μ) mm^{-1}	1.85
Radiation	Mo K_α (λ=0.70930 Å)
2 θ (max), degree	44.8
No. reflections measured	2849
No. unique reflections	2526
No. unique refl. $I_{net} > n\sigma(I_{net})$	2438
Last least sq. cycle calcd. with	58 atoms, 264 parameters and 2435 reflections
R_f (sig. refl.)	0.031
R_w (sig. refl.)	0.033
Goodness of fit	9.5
R_f (all refl.)	0.033
R_w (all refl.)	0.033
Max. shift/σ	1.902
Last D-map:	
deepest hole, e/ Å^3	-0.690
highest peak, e/ Å^3	0.560
Sec. ext.coeff.	0.746638

a, Estimated standard deviations are given in parentheses and referred to the last digit printed.

Table 5.2.

Crystallographic Data and Collection Parameters for $\{La(NO_3)_3\ 18C6\}$

Formula	$LaC_{12}H_{24}N_3O_{15}$
Molecular weight	589.23
Crystal dimensions (mm)	$0.2 \times 0.4 \times 0.4$
Crystal system	orthorhombic
Space group	Pbca
Lattice parameters:	
a, Å	15.637(4)[a]
b, Å	21.893(10)
c, Å	12.266(11)
β, degree	90
Cell vol. Å^3	4199(4)
Z, (molecules/cell)	8
F(000), electrons	2415.58
d_{calc}, g/cm^3	1.864
Linear absorption coeff. (μ) mm^{-1}	2.12
Radiation	Mo K_α (λ=0.70930 Å)
2 θ (max), degree	46.9
No. reflections measured	3094
No. unique reflections	3094
No. unique refl. $I_{net} > n\sigma(I_{net})$	2234
Last least sq. cycle calcd. with	55 atoms, 281 parameters and 2233 reflections
R_f (sig. refl.)	0.027
R_w (sig. refl.)	0.031
Goodness of fit	4.59
R_f (all refl.)	0.057
R_w (all refl.)	0.031
Max. shift/σ	3.025
Last D-map:	
deepest hole, e/ Å^3	-0.590
highest peak, e/ Å^3	0.380
Sec. ext.coeff.	0.567011

a, Estimated standard deviations are given in parentheses and referred to the last digit printed.

Table 5.3.

Crystallographic Data and Collection Parameters for {$La(NO_3)_3$ 15C5}

Formula	$LaC_{10}H_{20}N_3O_{14}$
Molecular weight	545.18
Crystal dimensions (mm)	$0.2 \times 0.2 \times 0.2$
Crystal system	monoclinic
Space group	$P2_1/c$
Lattice parameters:	
a, Å	9.3456(9)[a]
b, Å	14.6670(13)
c, Å	13.6647(9)
β, degree	95.574(7)
Cell vol. Å^3	1864.2(3)
Z, (molecules/cell)	4
F(000), electrons	1239.78
d_{calc}, g/cm^3	1.943
Linear absorption coeff. (μ) mm^{-1}	2.39
Radiation	Mo K_α (λ=0.70930 Å)
2 θ (max), degree	44.8
No. reflections measured	2957
No. unique reflections	2768
No. unique refl. $I_{net} > n\sigma(I_{net})$	2311
Last least sq. cycle calcd. with	48 atoms, 334 parameters and 2311 reflections
R_f (sig. refl.)	0.024
R_w (sig. refl.)	0.019
Goodness of fit	2.82
R_f (all refl.)	0.037
R_w (all refl.)	0.019
Max. shift/σ	0.095
Last D-map:	
deepest hole, e/ Å^3	-0.460
highest peak, e/ Å^3	0.580
Sec. ext.coeff.	0.866466

a, Estimated standard deviations are given in parentheses and referred to the last digit printed.

5.2 Description of the Structures of the Complexes

{$La(NO_3)_3$ B15C5} CH_3CN:

In this complex, the cation La(III) is coordinated to five oxygen atoms of the B15C5 and to the oxygen atoms of three bidentate nitrate anions. Therefore, the coordination number is 11. Table 5.4 gives the atomic parameters for this compound. Figure 5.1 shows an ORTEP drawing with its atomic numbering scheme. In the complex, B15C5 is on one side of the La(III) coordination sphere and three nitrate anions occupy the other side. Since the internal cavity of B15C5 is smaller than the ionic radius of La(III), this arrangement of the ligands allows the metal ion to achieve its high coordination number and to contact closely with the oxygen atoms of both crown ether and nitrates. Some bond lengths and angles of interest are reported in table 5.5. The distances between La(III) and ether oxygens are in a range of 2.599 to 2.754 Å, with an average of 2.691 Å. This is in very good agreement with the average bond length reported for other lanthanide nitrate - 15-membered crown ether complexes[35]. The six La-O(nitrate) distances are also different, from 2.559 to 2.657 Å. The average bond length of La-O's(nitrate) is 2.591 Å. Compared to the La-O(ether), the distance of La-O(nitrate) is shorter, which may indicate that the interaction of La(III) with B15C5 is weaker than with nitrate.

No water or solvent molecules were found in the first coordination sphere of La(III). This is in agreement with the results given in the previous chapter on the structure in solution. One acetonitrile molecule was held in the lattice by a hydrogen bond formed between CH_3CN and the oxygen atom of one coordinated nitrate anion. Table 5.6 gives the distances between the acetonitrile molecule and the nitrate in close contact.

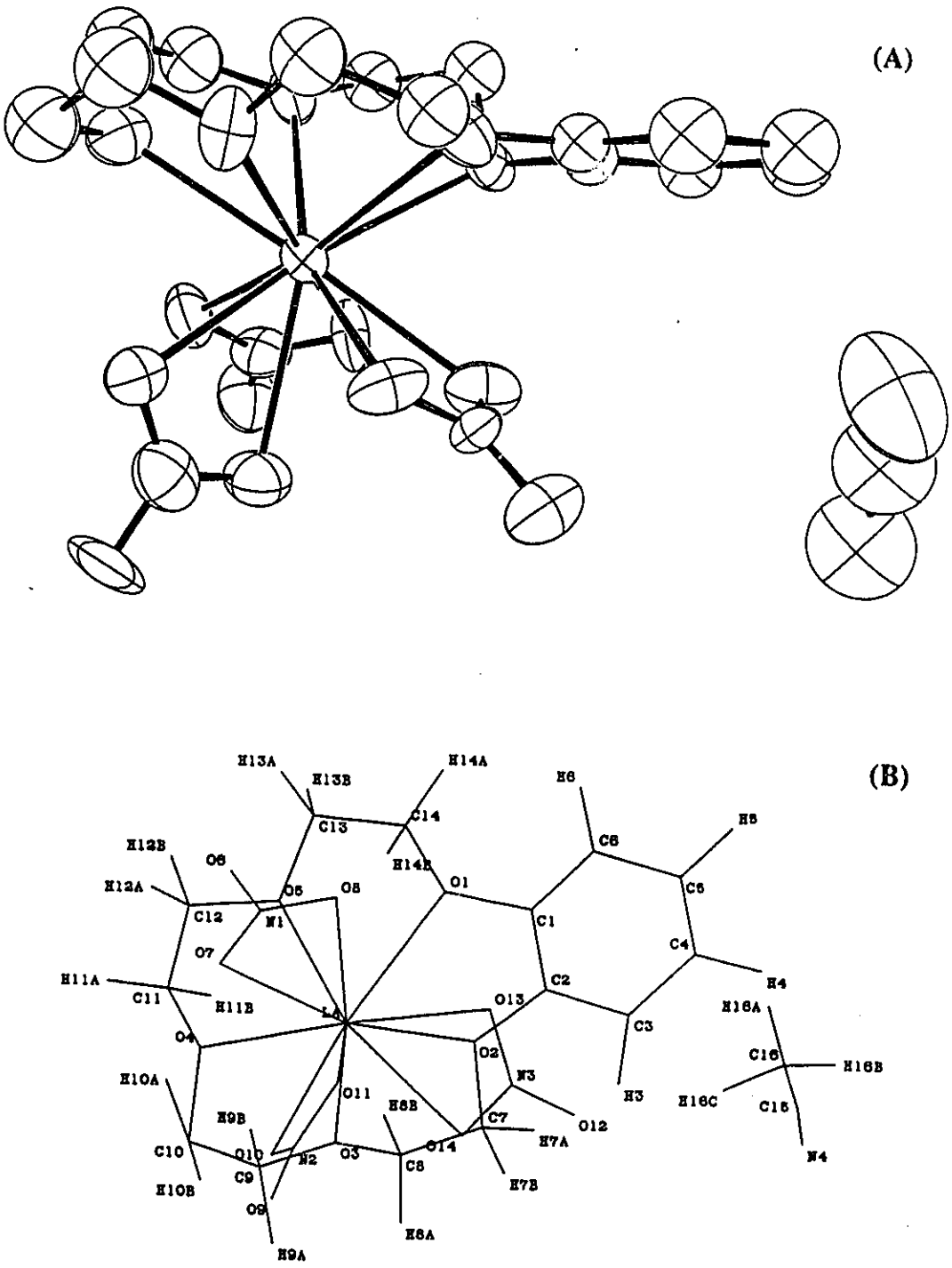

Figure 5.1:

ORTEP drawing (A) and numbering scheme (B) of {La $(NO_3)_3$ B15C5} CH_3CN complex.

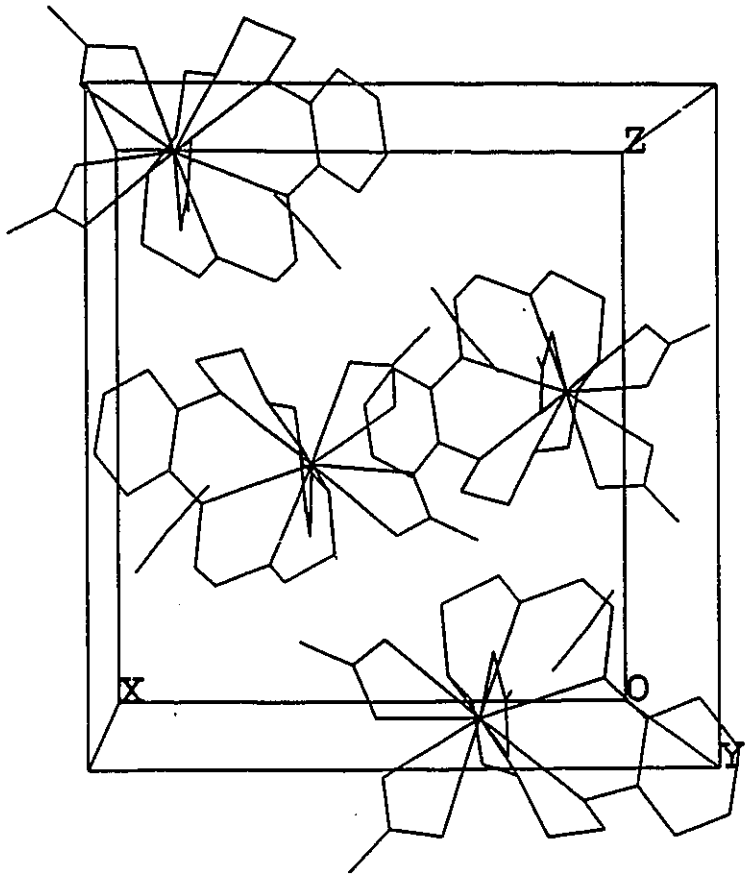

Figure 5.2:

Cell-packing diagram for {La $(NO_3)_3$ B15C5} CH_3CN complex.

Table 5.4.

Non-Hydrogen Atom Coordinates and Biso[a] for $\{La(NO_3)_3$ B15C5$\}CH_3CN$

Atoms	x	y	z	Biso
La	0.87102(10)	0.60847(8)[b]	0.93771(9)	3.01(5)
N1	1.0202(17)	0.6221(17)	1.1052(13)	4.1(10)
N2	1.0818(18)	0.5465(18)	0.8523(17)	4.8(12)
N3	0.8509(14)	0.3940(14)	0.8894(17)	3.9(10)
N4	0.5694(22)	0.185(3)	0.7782(22)	10.5(20)
O1	0.7077(9)	0.5792(9)	1.0581(11)	3.4(6)
O2	0.6731(11)	0.5659(12)	0.8734(10)	4.1(7)
O3	0.7967(13)	0.6815(11)	0.7673(10)	4.7(8)
O4	0.9085(12)	0.7931(11)	0.8866(11)	4.3(8)
O5	0.7953(11)	0.7493(11)	1.0421(11)	5.2(8)
O6	1.0872(12)	0.6176(15)	1.1686(12)	6.2(9)
O7	1.0274(12)	0.6801(12)	1.0348(11)	4.9(8)
O8	0.9383(12)	0.5695(11)	1.1086(10)	4.4(7)
O9	1.1640(12)	0.5241(13)	0.8161(18)	7.3(11)
O10	1.0264(12)	0.6164(12)	0.8187(11)	4.8(8)
O11	1.0459(12)	0.5036(11)	0.9260(12)	4.9(8)
O12	0.8513(16)	0.3077(11)	0.8677(14)	6.8(11)
O13	0.8423(13)	0.4245(11)	0.9753(11)	4.6(8)
O14	0.8634(15)	0.4594(10)	0.8239(11)	4.3(8)
C1	0.6318(19)	0.5061(14)	1.0267(14)	3.7(4)
C2	0.6163(17)	0.5011(13)	0.9294(15)	3.7(4)
C3	0.5427(22)	0.4353(19)	0.8905(18)	5.5(6)
C4	0.4917(20)	0.3753(18)	0.9580(18)	5.6(6)
C5	0.5065(18)	0.3795(18)	1.0518(17)	5.1(5)
C6	0.5815(19)	0.4478(18)	1.0917(15)	4.7(5)
C7	0.6583(19)	0.5682(18)	0.7682(16)	4.8(6)
C8	0.6937(21)	0.6604(20)	0.7317(18)	5.4(6)
C9	0.8259(22)	0.7726(21)	0.7307(21)	6.0(7)
C10	0.9177(22)	0.8027(21)	0.7783(19)	5.9(6)
C11	0.8594(23)	0.8696(19)	0.9356(23)	6.7(6)
C12	0.8455(20)	0.8427(18)	1.0347(17)	5.7(6)
C13	0.7459(20)	0.7260(17)	1.1339(17)	4.9(5)
C14	0.6619(22)	0.6551(21)	1.1121(21)	4.4(6)
C15	0.619(3)	0.1554(25)	0.839(3)	8.1(9)
C16	0.688(3)	0.120(3)	0.912(3)	10.2(11)

a, Biso is the mean of the principal axes of the thermal ellipsoid.
b, Estimated standard deviations are given in parentheses and referred to the last digit printed.

Table 5.5.

Selected bond lengths and angles for $\{La(NO_3)_3\ B15C5\}CH_3CN$

Bond Lengths (Å)			
La-O1	2.714(8)[a]	La-O2	2.754(8)
La-O3	2.730(9)	La-O4	2.660(9)
La-O5	2.599(8)	La-O7	2.592(9)
La-O8	2.559(8)	La-O10	2.577(8)
La-O11	2.657(8)	La-O13	2.582(9)
La-O14	2.580(8)		

Bond Angles (degree)			
O1-La-O10	172.2(3)	O1-La-O14	101.3(3)
O1-La-O13	66.68(25)	O1-La-O3	108.5(3)
O1-La-O8	70.1(3)	O1-La-O2	56.39(24)
O1-La-O4	117.56(24)	O1-La-O11	126.3(3)
O1-La-O7	110.2(3)	O1-La-O5	59.99(22)
O10-La-O14	71.5(3)	O10-La-O13	105.8(3)
O10-La-O3	73.1(3)	O10-La-O8	109.8(3)
O10-La-O2	121.0(3)	O10-La-O4	70.0(3)
O10-La-O11	48.5(3)	O10-La-O7	73.7(3)
O10-La-O5	127.7(3)	O14-La-O13	48.5(3)
O14-La-O3	76.3(3)	O14-La-O8	113.7(3)
O14-La-O2	66.4(3)	O14-La-O4	127.7(3)
O14-La-O11	64.6(3)	O14-La-O7	129.8(3)
O14-La-O5	155.5(3)	O13-La-O3	118.6(3)
O13-La-O8	70.3(3)	O13-La-O2	74.4(3)
O13-La-O4	175.6(3)	O13-La-O11	66.8(30
O13-La-O7	111.5(3)	O13-La-O5	124.0(3)
O3-La-O8	170.0(3)	O3-La-O2	58.4(3)
O3-La-O4	59.6(3)	O3-La-O11	116.4(3)
O3-La-O7	125.4(3)	O3-La-O5	94.0(3)
O8-La-O2	124.0(3)	O8-La-O4	111.8(3)
O8-La-O11	70.3(3)	O8-La-O7	49.1(3)
O8-La-O5	76.7(3)	O2-La-O4	106.7(3)
O2-La-O11	130.0(3)	O2-La-O7	163.1(3)
O2-La-O5	89.3(3)	O4-La-O11	110.0(3)
O4-La-O7	68.8(3)	O4-La-O5	60.4(3)
O11-La-O7	65.3(3)	O11-La-O5	138.5(3)
O7-La-O5	74.2(3)		

a, Estimated standard deviations are given in parentheses and referred to the last digit printed.

Table 5.6. Intramolecular contact between the acetonitrile molecule and a coordinated nitrate anion for $\{La(NO_3)_3\ B15C5\}CH_3CN$

Atoms	Distance (Å)
H(16A) - O(12)	3.4879
H(16C) - O(12)	2.4054
H(16C) - O(13)	3.9887
C(16) - O(12)	3.3654

$\{La(NO_3)_3$ 18C6$\}$:

The crystal structure of this complex has been reported in the literature[37]. In this previous report, the complex of $\{La(NO_3)_3$ 18C6$\}$ was synthesized in acetone solution. Since our purpose is to compare the structures of the complex in solution and in the solid state, it is better to obtain the crystal under the conditions in which the solution NMR investigations were performed. Therefore, $\{La(NO_3)_3$ 18C6$\}$ was prepared in acetonitrile solution and its crystal structure was determined. The results obtained in the present work are very similar to those reported in the literature.

In this complex, the La(III) was 12-coordinated by 6 ether oxygen atoms and by 6 oxygen atoms of three nitrate anions. Figure 5.3 shows the molecular structure for this complex. The selected bond lengths and angles are reported in table 5.7.

The nitrate anions coordinating to the La(III) are also bidentate. The major difference between this complex and the complex involving B15C5 is the ligand arrangement. The La(III) cation is located in the center of the 18C6 ring whereas three nitrates are found on both sides of the crown ether ring. Again, the crystal structure found for $\{La(III)\ (NO_3)_3$ 18C6$\}$ is a good model for the interpretation of the NMR results in solution.

Table 5.7.

Selected bond lengths and angles for {$La(NO_3)_3$ 18C6}

Bond Lengths (Å)			
La-O1	2.714(8)[a]	La-O2	2.745(5)
La-O3	2.664(6)	La-O4	2.660(9)
La-O5	2.721(6)	La-O6	2.633(6)
La-O7	2.647(6)	La-O8	2.682(7)
La-O10	2.671(6)	La-O11	2.680(6)
La-O13	2.656(6)	La-O14	2.678(6)

Bond Angles (degree)			
O1-La-O2	60.07(11)	O1-La-O3	87.67(11)
O1-La-O4	103.38(11)	O1-La-O5	60.30(11)
O1-La-O6	157.65(12)	O1-La-O7	124.32(11)
O1-La-O9	135.24(11)	O1-La-O10	127.62(12)
O1-La-O12	70.19(12)	O1-La-O13	72.62(12)
O2-La-O3	61.60(21)	O2-La-O4	117.26(11)
O2-La-O5	136.42(18)	O2-La-O6	119.27(20)
O2-La-O7	71.06(18)	O2-La-O8	67.04(21)
O2-La-O10	115.02(19)	O2-La-O11	160.09(18)
O2-La-O13	101.60(21)	O2-La-O14	62.30(20)
O3-La-O4	60.10(11)	O3-La-O5	119.41(20)
O3-La-O6	178.39(18)	O3-La-O7	112.49(19)
O3-La-O8	70.32(19)	O3-La-O10	66.43(20)
O3-La-O11	108.78(20)	O3-La-O13	111.75(20)
O3-La-O14	69.91(21)	O4-La-O5	60.65(11)
O4-La-O6	71.07(11)	O4-La-O7	115.73(11)
O4-La-O9	109.27(11)	O4-La-O10	66.27(11)
O4-La-O12	120.36(12)	O4-La-O13	169.91(13)
O5-La-O6	61.08(19)	O5-La-O7	69.52(18)
O5-La-O8	72.91(19)	O5-La-O10	101.87(19)
O5-La-O11	63.23(18)	O5-La-O13	115.05(19)
O5-La-O14	160.88919)	O6-La-O7	69.11(18)
O6-La-O8	111.21(19)	O6-La-O10	112.02(19)
O6-La-O11	69.95(19)	O6-La-O13	66.88(19)
O6-La-O14	109.15(20)	O7-La-O8	47.52(18)
O7-La-O10	169.87(19)	O7-La-O11	128.00(19)
O7-La-O13	123.04(18)	O7-La-O14	124.46(18)
O8-La-O10	125.88(19)	O8-La-O13	166.39(19)
O8-La-O14	125.85(20)	O10-La-O11	42.23(19)
O10-La-O13	64.91(19)	O10-La-O14	65.23(20)
O11-La-O13	64.42(19)	O11-La-O14	98.43(19)
O13-La-O14	47.56(20)		

a, Estimated standard deviations are given in parentheses and referred to the last digit printed.

(A)

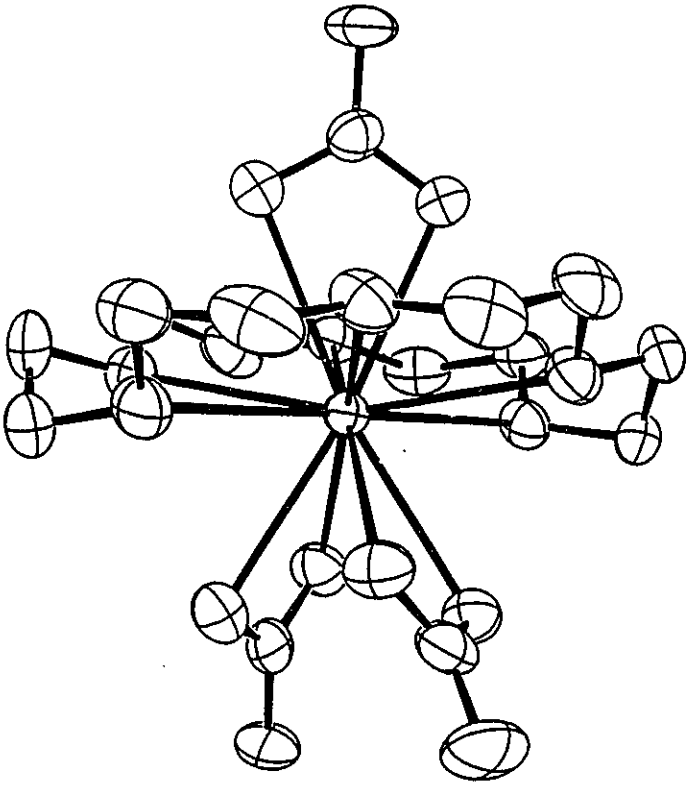

(B)

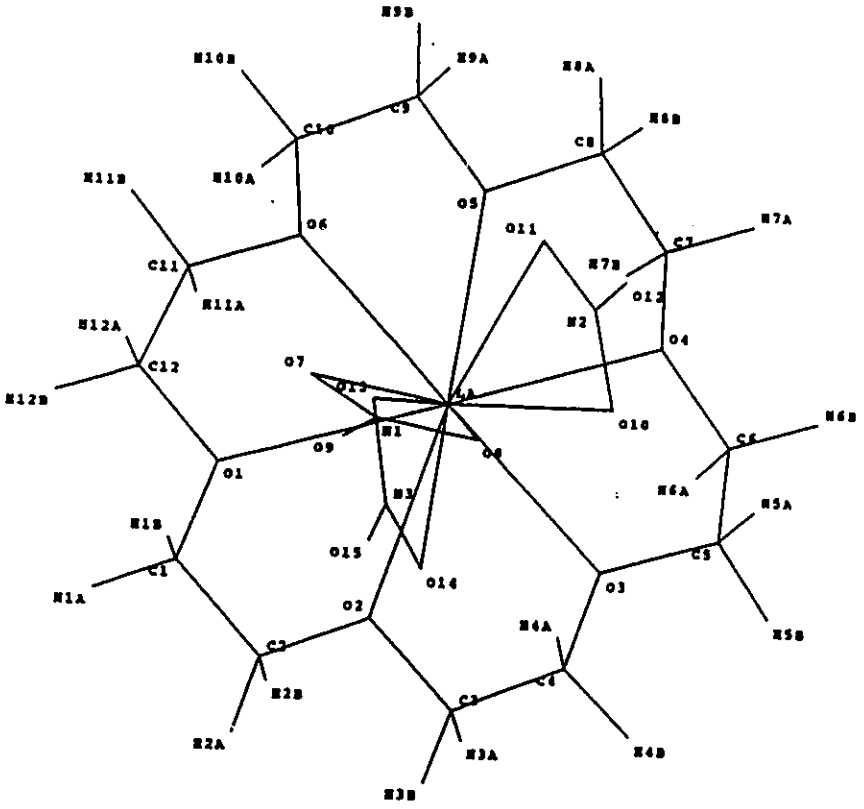

Figure 5.3:

ORTEP drawing (A) and numbering scheme (B) of {La $(NO_3)_3$ 18C6} complex.

{La(III) $(NO_3)_3$ 15C5}:

The crystal structure of this complex was also previously reported in the literature[131]. For the same reasons mentioned in the case of 18C6, the crystals of {La(III) $(NO_3)_3$ 15C5} were prepared from acetonitrile solution and its structure was determined. The results obtained in the present work are very similar to those reported in reference 131. Table 5.8 gives the selected bond lengths and angles for {La(III) $(NO_3)_3$ 15C5}. Figure 5.4 shows its molecular structure.

The crystal structure of {La(III) $(NO_3)_3$ 15C5} is very similar to that of the complex involving B15C5. The lanthanum cation is 11-coordinated with 15C5 on one side and three nitrates on the other side of the La(III) coordination shell. The average La-O(ether) distance is 2.689 Å, the same as the one found in the case of B15C5 (2.691 Å). The variation of the La-O(ether) bond lengths is 0.096 Å (from 2.630 Å to 2.726 Å) which is smaller than that observed in the B15C5 complex (0.155 Å). This may indicate that, because of the benzo-substitution, the B15C5 has to be more distorted than the 15C5 in their complexes to minimize the interligand repulsion. Another difference found in the crystal structures of these two complexes is that no solvent molecules (here acetonitrile) are found in the lattice for the case of 15C5.

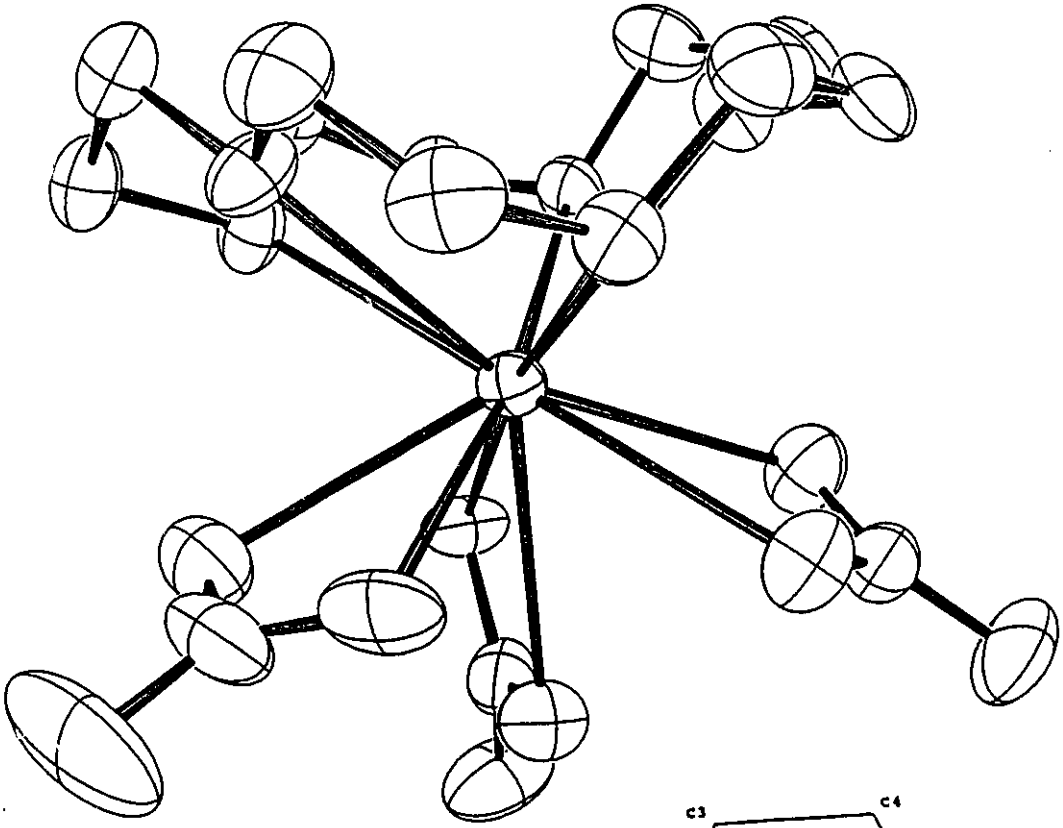

(A)

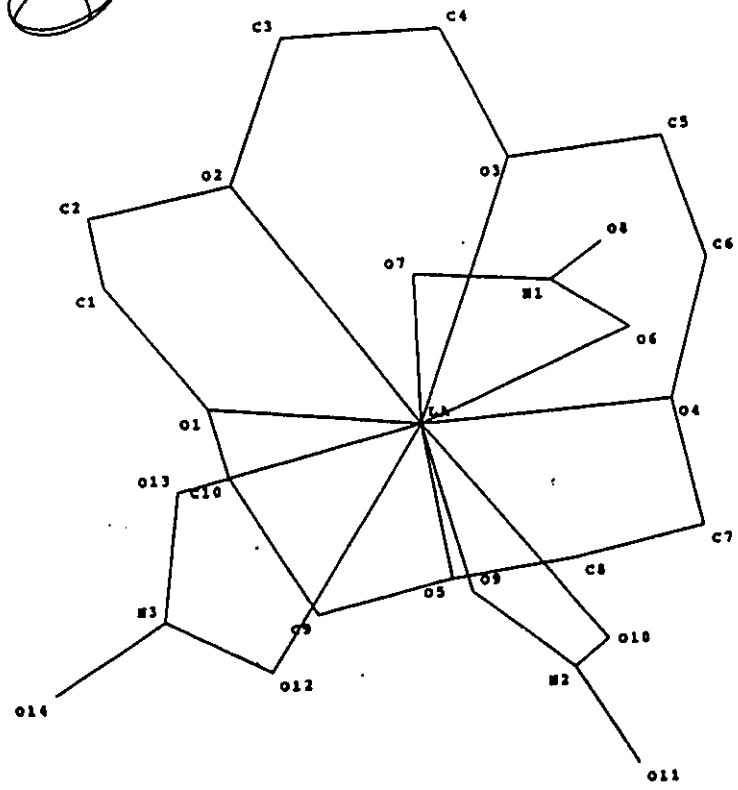

(B)

Figure 5.4:

ORTEP drawing (A) and numbering scheme (B) of {La $(NO_3)_3$ 15C5} complex.

Table 5.8.

Selected bond lengths and angles for {$La(NO_3)_3$ 15C5}

Bond Lengths (Å)			
La-O1	2.713(3)[a]	La-O2	2.726(3)
La-O3	2.632(4)	La-O4	2.699(3)
La-O5	2.677(4)	La-O6	2.607(4)
La-O7	2.633(4)	La-O9	2.657(4)
La-O10	2.588(3)	La-O12	2.614(4)
La-O13	2.565(4)		

Bond Angles (degree)			
O1-La-O2	60.07(11)	O1-La-O3	87.67(11)
O1-La-O4	103.38(11)	O1-La-O5	60.30(11)
O1-La-O6	157.65(12)	O1-La-O7	124.32(11)
O1-La-O9	135.24(11)	O1-La-O10	127.62(12)
O1-La-O12	70.19(12)	O1-La-O13	72.62(12)
O2-La-O3	59.26(11)	O2-La-O4	117.26(11)
O2-La-O5	116.88(11)	O2-La-O6	102.36(12)
O2-La-O7	67.15(11)	O2-La-O9	124.15(11)
O2-La-O10	171.57(11)	O2-La-O12	109.59(12)
O2-La-O13	69.25(13)	O3-La-O4	60.10(11)
O3-La-O5	99.92(12)	O3-La-O6	70.68(12)
O3-La-O7	79.94(12)	O3-La-O9	135.19(12)
O3-La-O10	121.30(11)	O3-La-O12	157.56(12)
O3-La-O13	127.94(13)	O4-La-O5	60.65(11)
O4-La-O6	71.07(11)	O4-La-O7	115.73(11)
O4-La-O9	109.27(11)	O4-La-O10	66.27(11)
O4-La-O12	120.36(12)	O4-La-O13	169.91(13)
O5-La-O6	127.44(11)	O5-La-O7	175.29(11)
O5-La-O9	111.84(11)	O5-La-O10	71.54(12)
O5-La-O12	66.42(12)	O5-La-O13	109.90(13)
O6-La-O7	48.01(12)	O6-La-O9	65.03(12)
O6-La-O10	71.06(12)	O6-La-O12	131.70(12)
O6-La-O13	116.16(13)	O7-La-O9	65.86(11)
O7-La-O10	104.45(12)	O7-La-O12	115.18(13)
O7-La-O13	73.50(13)	O9-La-O10	48.69(11)
O9-La-O12	67.17(12)	O9-La-O13	69.90(12)
O10-La-O12	72.82(13)	O10-La-O13	108.44(14)
O12-La-O13	49.70(14)		

a, Estimated standard deviations are given in parentheses and referred to the last digit printed.

5.3. *Comparison of the complex structures in solution and in the solid state*

The solution NMR results given in the previous chapter indicate that the crown ether enter into the first coordination sphere of the La(III) cation while the water and most probably the acetonitrile solvent molecules are expelled from the La(III) inner sphere during the course of the lanthanum - crown ether complex formation. This corresponds to the solid state structures of these complexes.

The structural similarities of the La(III) - crown ether complexes in solution and in their solid state can also be found in the ligand arrangement around the La(III) cation. The ^{1}H NMR spectra of the complexed 18C6 show a single peak, indicating that all the protons of the complexed 18C6 are equivalent. This requires that La(III) has to sit in the center of the 18C6 ring and that the nitrates are located on both sides of the crown ether ring, as shown in its crystal structure. The fast conformational exchanges of the crown ether make the protons of the complexed 18C6 not distinguishable by NMR methods. In contrast to the case of 18C6, multiple NMR resonances were found on the ^{1}H NMR spectra of the 15C5 crown ether coordinated to the La(III) cation. If the ligand arrangement around the lanthanum inner sphere for La(III) - 15C5 complex in solution is the same as that shown in its solid state, the interpretation of the proton NMR results should be straightforward since the protons close to the central cation are different from those further away from the La(III). For each O-CH_2-CH_2-O segment of the 15C5, the protons are an AA'BB' system. This is further confirmed by the kinetic study of the complexed 15C5 chemical exchange. A model involving the 'inner' (close to La(III)) and 'outer' (apart from the La(III)) proton exchange successfully accounts for the experimental NMR observations. This model is indeed proposed based on the solid structure of the La(III) - 15C5 complex. Those results will be discussed in detail in the next chapter of this thesis. The crystal structure of lanthanum complex with 15C5 can also be used to interpret the ^{13}C NMR spectra of the coordinated 15C5. As shown

in the previous chapter, a single peak was observed in the ^{13}C NMR spectra of the complexed 15C5 ligand. Since the arrangement of the ligands around the inner sphere of the La(III) does not affect the carbons of the complexed 15C5 crown ether, it is expected that all of them will be equivalent in the complex in solution. The discussions related to the 15C5 crown ether are also suitable for the case of B15C5. Furthermore, the La(III) - B15C5 complex structure in the solid state can be used to interpret the benzo-proton NMR spectra of the coordinated B15C5. It was shown in the previous chapter that, in contrast to the ether protons, the benzo-proton NMR spectra of the complexed B15C5 had a high resolution feature. Again, if the structures of this complex in solution and in the solid state are the same, these ^{1}H NMR observations can be logically understood since the coordinated B15C5 chemical exchange will not affect those benzo-protons.

Chapter 6

Kinetic Study of La(III) - Crown Ether Complexes

6.1 Introduction:

A full understanding of the lanthanide cation complexation with macrocyclic ligands requires detailed investigations of the structure, thermodynamics, and kinetics of those complexes. The thermodynamic and structural studies of La(III) complexes with several crown ethers have been described in the chapters 4 and 5 of this thesis. The kinetic behaviours of those complexes are discussed in this chapter.

In comparison with the investigations of the synthesis and the structure determination of Ln(III) - macrocyclic complexes, very few studies have been devoted to their kinetics and mechanisms[35,140-143]. One reason may be that the dissociation processes for the complexes of Ln(III) with macrocyclic molecules are usually slow. For instance, the dissociation rate constant of the Eu(III) cryptate (2,2,1) complex in aqueous solution is about 10^{-7} s^{-1}[144]. Concerning the systems involving crown ethers, only lanthanum perchlorate with 12C4[145] and lanthanide nitrate with 18C6[34,37] in acetonitrile solutions have been investigated kinetically. For both cases, the ligand exchange rate constants have been calculated. However, more detailed kinetic studies,

such as the mechanisms of the exchange processes, have not yet been carried out. In Chapter 4 of this thesis, the chemical exchange effects on the NMR spectra have been observed for several cases of La(III) complexes with crown ethers in acetonitrile solutions. The detailed kinetic investigations of these systems are given in this chapter.

As mentioned in chapter 1, kinetic information about lanthanide complexation with crown ethers may be obtained through NMR observations. The theoretical basis is that the exchange between different sites of the investigated nuclei will contribute to the transverse relaxation process, so that the lineshapes of the resulting NMR spectra are affected. Therefore, the kinetic parameters related to the exchange process can be obtained from lineshape analyses of these NMR spectra. The availability of this method depends on the magnitude of the exchange rate relative to the transverse relaxation constant, T_2^{-1}. Different NMR techniques or different treatments of the spectra may be used for various situations. They will be discussed in detail in the following sections

6.2 NMR Kinetic Studies of La(III) Complexes with Crown Ethers

6.2.1 La(III) Exchange Between the Solvated Site and the Site Complexed by B15C5. ^{139}La NMR Investigations.

Since only 1 : 1 complexes of La(III) with crown ethers were detected in the systems studied in the present work (see chapter 4), the corresponding chemical exchange of La(III) involves two sites and can be described by the following simple equation:

$$\underset{(A)}{(La(III))_s} \underset{k_b}{\overset{k_a}{\rightleftharpoons}} \underset{(B)}{(La(III))_c} \qquad (6.1)$$

Where $(La(III))_s$ and $(La(III))_c$ represent respectively the La(III) cation in the solvated site and in the site complexed by a crown ether. k_a (= $1 / \tau_A$) and k_b (= $1 / \tau_B$)

are the reciprocal life time of the La(III) cation respectively in these two sites.

The ^{139}La NMR spectra shown in chapter 4 indicate that the La(III) exchange is very fast in the case of DB24C8 (on the ^{139}La NMR chemical shift time scale). This system will not be further discussed because kinetic information about the exchange reaction is not available from NMR observations.

The ^{139}La NMR spectra on the system involving B15C5 are characterized by the La(III) cation undergoing an exchange between sites A and B of equation 6.1 at a "moderately rapid" rate. In the case of $[La(III)]_o$ = 0.020 M, one Lorentzian peak resulting from the population average of the two sites was observed on the ^{139}La NMR spectra, and some line broadening appeared in the range $0 < \rho < 1$ ($\rho = [B15C5]_o / [La(III)]_o$). In this situation, the transverse relaxation of ^{139}La contains contributions from the quadrupolar interaction, the inhomogeneity of the magnetic field, and the La(III) cation chemical exchange. Since under conditions of extreme narrowing $T_2^{-1} = T_1^{-1}$, the overall transverse relaxation rate, $(T_2)^{-1}_{obs}$, can be expressed as:

$$(T_2^{-1})_{obs} = T_1^{-1} + (T_2^{-1})_{inh} + (T_2^{-1})_{ex} \qquad (6.2)$$

$(T_2^{-1})_{obs}$ is directly related to the linewidth of the observed NMR peak. $(T_2^{-1})_{inh}$ is the difference of T_1^{-1} and T_2^{-1} in the absence of chemical exchange. For the nucleus ^{139}La, characterized by a large quadrupole moment, $(T_2^{-1})_{inh}$ is negligible. Therefore, the chemical exchange contribution to the transverse relaxation rate, $(T_2^{-1})_{ex}$, can be obtained from the linewidth and the relaxation rate measurements.

$$(T_2^{-1})_{ex} = (T_2^{-1})_{obs} - T_1^{-1} \qquad (6.3)$$

Figure 6.1 shows $(T_2^{-1})_{obs}$, obtained directly from the linewidth ($\pi \nu_{1/2}$), and T_1^{-1}, measured independently, as a function of ρ. The difference between $(T_2^{-1})_{obs}$ and T_1^{-1} is $(T_2^{-1})_{ex}$.

If $4\pi^2 (\nu_A - \nu_B)^2 >> (T_{2A}^{-1} - T_{2B}^{-1})^2$, which is the case for the present system (see table 4.5), the relationship between the exchange contribution and the sum of the pseudo-first order constants, $k_a + k_b$, can be described by the following equation[146,147].

$$(T_2^{-1})_{ex} = 4 P_A P_B \pi^2 (\nu_A - \nu_B)^2 (k_a + k_b)^{-1} \qquad (6.4)$$

Where P_A and P_B represent the populations of La(III) respectively in site A and in site B (see equation 6.1). ν_A and ν_B are the ^{139}La chemical shifts expressed in Hz for these two sites.

Since La(III) and B15C5 form a stable 1 : 1 complex in solution, P_A and P_B can be taken directly from ρ ($P_B = \rho$ and $P_A = 1 - \rho$). ν_A and ν_B were measured from the ^{139}La NMR spectra recorded respectively at $\rho = 0$ and $\rho > 1$ (10 ppm and -46 ppm respectively). Therefore, an evaluation of $k_a + k_b$ can be obtained from $(T_2^{-1})_{ex}$. These results are reported in table 6.1. One should note that a relatively large error is attached to the measured T_1 values. This is because the ^{139}La relaxation is so fast that it reaches the instrumental limitation for such measurements. As a result, the $k_a + k_b$ given in table 6.1 should be considered only as approximate values.

At a lower La(III) concentration ($[La(III)]_o$= 0.0050 M), separated signals were observed, corresponding respectively to the free and the complexed La(III) cations (see figure 4.15). In this case, full lineshape analyses of the ^{139}La NMR spectra have to be done to obtain the rate constants of the lanthanum exchange. The equations used in the lineshape analysis can be found in Appendix I. The chemical shift and linewidth of the complexed La(III) were measured from the ^{139}La experimental NMR spectrum at $\rho >$ 1. These NMR parameters were used as constants in the non-linear regression for the lineshape analysis. The chemical shift and linewidth for the solvated La(III) cation were calculated by taking into account the effect of the complex formation on the equilibrium established between different solvated La(III) species.

Table 6.1

Kinetic Data for La(III) Exchange in Acetonitrile[a]

ν^b_a (Hz)	$\nu_b{}^c$ (Hz)	$P_B(\rho)$	T_1^{-1} (kHz)	T_2^{-1} (kHz)	$k_a + k_b{}^d$ ($\times 10^4$ s^{-1})
423.7	-1949	0.10	6.8±0.7	8.4±0.2	1.3
		0.15	6.5±0.4	8.9±0.2	1.2
		0.25	6.7±0.3	10.1±0.2	1.3
		0.30	6.8±0.7	10.1±0.2	1.5

a, Crown ether = B15C5, $[La]_o$= 0.020 M, T = 300 K;

b, Chemical shift of solvated La(III) (in Hz);

c, Chemical shift of complexed La(III) (in Hz);

d, Calculated from equation 6.4. The average value is 1.3±0.1 $\times 10^4$ s^{-1}.

The regressions were done for several spectra obtained with different ρ values. As examples, figure 6.2 shows the experimental and calculated spectra for two ρ's. The sum of the pseudo-first order rate constants, $k_a + k_b$ described in equation 6.1, were obtained from the lineshape analyses of the experimental spectra and are reported in table 6.2.

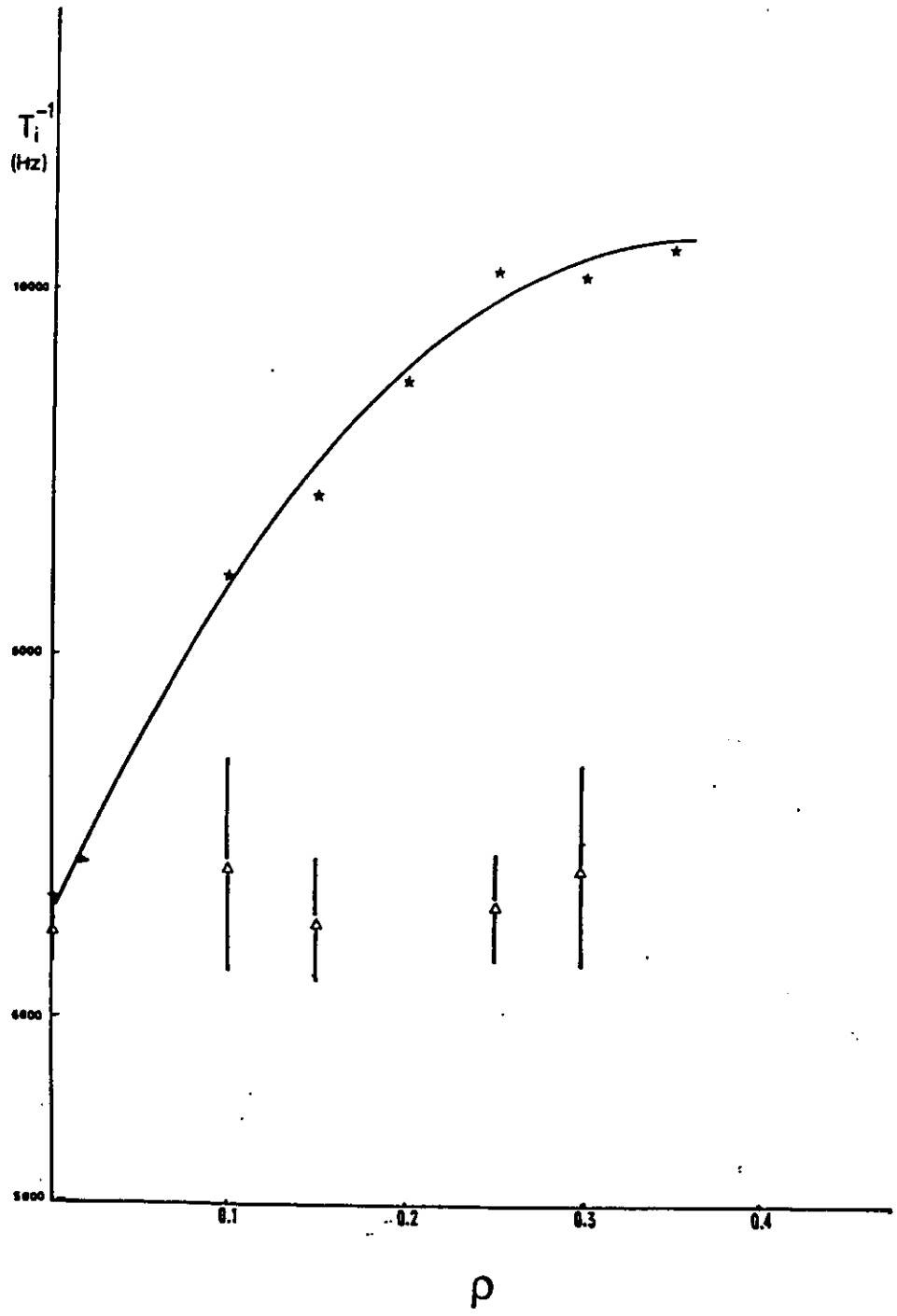

Figure 6.1: ^{139}La relaxation rates as a function of ρ for $La(NO_3)_3$ - B15C5 in acetonitrile. * (i = 2) transverse relaxation rate and Δ (i = 1) longitudinal relaxation rate. $[La(III)]_o$ = 0.020 M. T = 300 K.

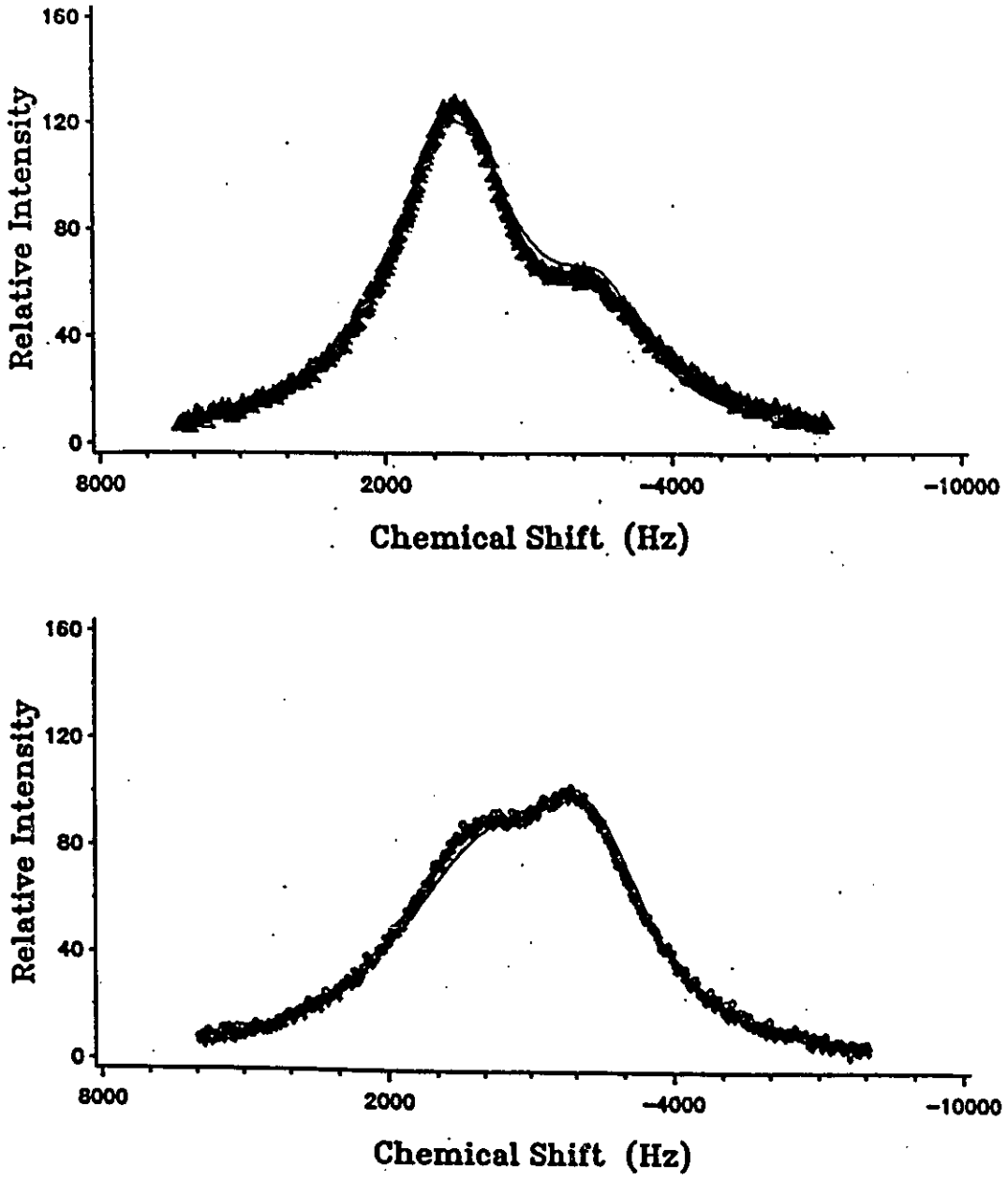

Figure 6.2: ^{139}La NMR spectra of $La(NO_3)_3$ - B15C5 in acetonitrile. The points are experimental and the curves were calculated from the non-linear regression of lineshape analysis. Top: $\rho = 0.18$. Bottom $\rho = 0.40$. $[La(III)]_o = 0.0050$ M. T = 300 K.

Table 6.2. Rate Constants for La(III) Exchange in Acetonitrile[a]

$P_B(\rho)$	$k_a + k_b$[b] ($\times 10^3$ s^{-1})
0.18	3.10 ± 0.17
0.30	3.70 ± 0.18
0.40	4.20 ± 0.20
0.60	5.30 ± 0.20

a, Crown ether = B15C5, $[La]_o$= 0.0050 M, T = 300 K;

b, Determined from lineshape analyses of the ^{139}La experimental spectra.

6.2.2 B15C5 Chemical Exchange in the complex B15C5-La(III) in AN: ^{13}C NMR Studies.

The ligand exchange has been investigated on this system by ^{13}C NMR of B15C5. The ^{13}C NMR spectra of the ligand were recorded on the samples with various R values (R = $[La(III)]_o$ / $[B15C5]_o$). As described in chapter 4, four signals resulting from the nonequivalent carbon atoms of the crown ether ring were observed at R = 0 and R > 1, respectively characterizing the B15C5 ligand in the solvated and the complexed states. Table 6.3 gives the chemical shifts of these ^{13}C peaks. In the range 0 < R < 1, the ^{13}C NMR spectra exhibit the characteristics of B15C5 undergoing a relatively fast exchange between the sites A and B of equation 6.5 (see figure 4.17). Similarly to the case of the La(III) cation discussed previously, the exchange of B15C5

also involves two sites and can be described by the following equation.

$$\underset{(A)}{(B15C5)_s} \underset{k_b'}{\overset{k_a'}{\rightleftharpoons}} \underset{(B)}{(B15C5)_c} \qquad (6.5)$$

Here, $(B15C5)_s$ and $(B15C5)_c$ represent respectively the solvated and the complexed crown ethers. k_a' and k_b' are the pseudo-first order rate constants or the reciprocal of the resident time for the B15C5 respectively in these two sites.

However, in this case, the process is no longer a simple two site exchange since there are four NMR peaks corresponding to the four ethereal carbon atoms of B15C5 in each site. The exchange described in equation 6.5 actually involves 4 pairs of carbon atoms. Before doing any kinetic treatments of the experimental NMR spectra, we have to find out the chemical shift correlation for these four pairs.

Scheme I is a diagram of B15C5 with a numbering of the carbon and proton positions.

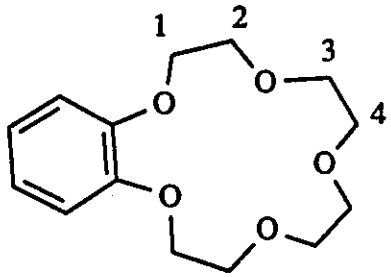

Scheme I: B15C5, the numbers represent carbon and proton positions.

The assignment of the carbon resonances was achieved by heteronuclear chemical shift correlation experiments (HETCOR). Figure 6.3 shows the HETCOR contour plots of B15C5 (R = 0) and of (La : B15C5)$^{3+}$ (R >1). For the free (solvated)

B15C5, the ^{13}C chemical shifts are in the following order: $C_3 > C_4 > C_2 > C_1$, as seen in figure 6.3 A. This assignment was based on the corresponding proton chemical shifts ($H_1 > H_2 > H_3 > H_4$), resulting from the effects of ring current anisotropy of the aromatic substituent and confirmed by a long-range HETCOR experiment[129]. In the case of complexed B15C5, only C_1 might be assigned to the resonance at the highest frequency. The assignment of the rest of the carbons cannot be made through the HETCOR experiment because the correlated proton signals are superposed (see figure 6.3 B). Therefore, the correlation of carbon atoms between the two different B15C5 species cannot be obtained through the HETCOR experiments. We then tried another way to solve this problem.

Table 6.3. ^{13}C NMR Chemical Shifts of the Etherel Carbons for Solvated and Coordinated B15C5 in Acetonitrile[a].

Carbon Atoms[b]	B15C5 (ppm)	(B15C5 La(III)) (ppm)
C-1	69.13	71.42
C-2	69.58	70.34
C-3	70.96	70.72
C-4	70.42	69.48

a, [B15C5] = 0.015 M, T = 300 K;

b, Numbering of the carbon atoms is given on Scheme I.

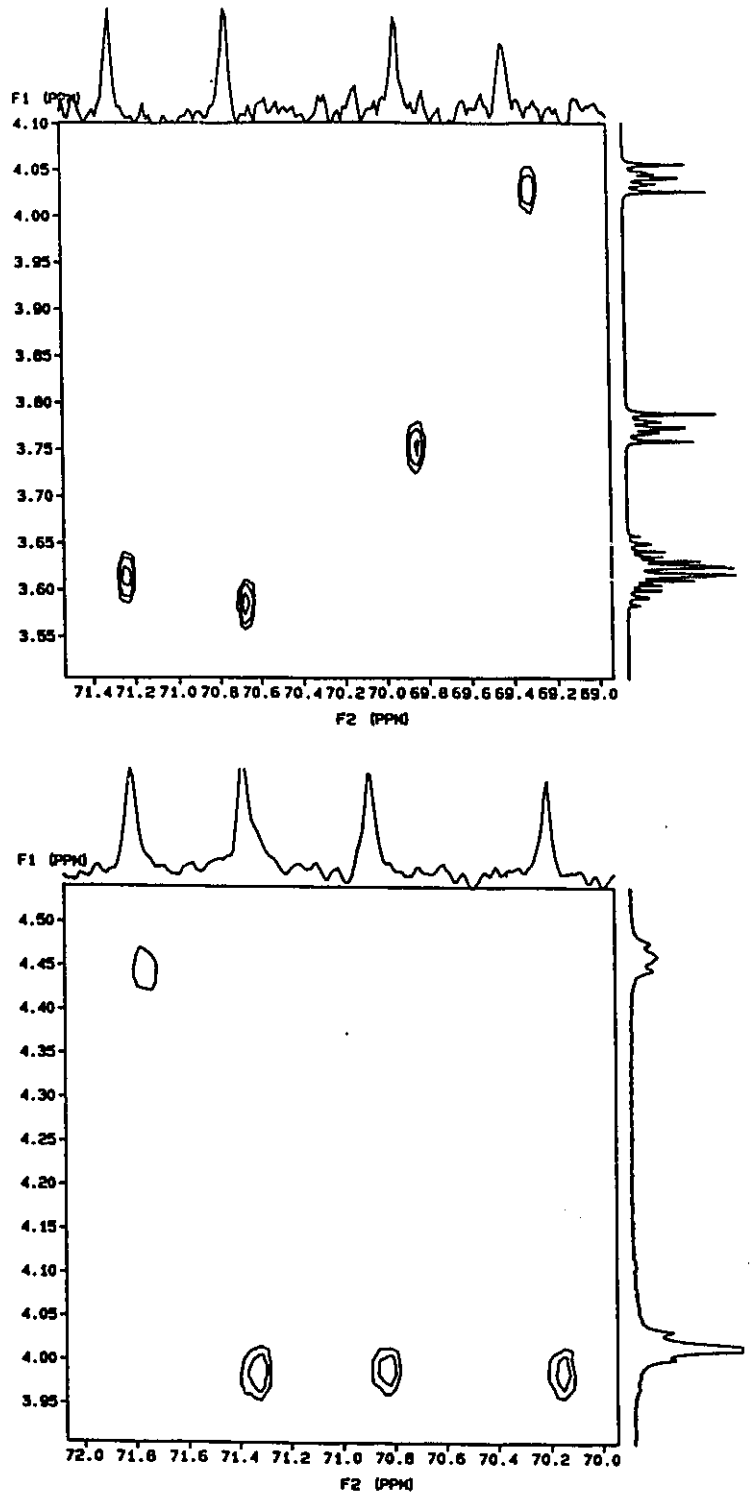

Figure 6.3: HETCOR contour plot of (A) free B15C5 and (B) coordinated B15C5 in CD_3CN at 300 K.

Since the chemical shifts for the carbons of B15C5 are different in the solvated site and in the complexed site, an individual ^{13}C NMR peak should shift smoothly from its position in the solvated state to that in the complexed site, in the range $0 < R < 1$. A plot of the ^{13}C NMR chemical shifts as a function of R might be helpful to figure out the correlation of these carbon atoms. Figure 6.4 shows these plots. From figure 6.4, one might conclude that the ^{13}C chemical shifts of B15C5 in the complexed site are in a order of $C_1 > C_3 > C_2 > C_4$. Even if some precipitation occurred when $R > 0.4$, this order of chemical shifts for the complexed B15C5 was used in the analyses of the experimental NMR spectra.

In order to obtain the rate constants of the exchange reaction described in equation 6.5, the observed ^{13}C NMR spectra in the range $0 < R < 0.3$ were simulated, taking the chemical shifts from table 6.3 and using $k_a' + k_b'$ as a variable. The simulations were made through two computer programs. One of them is "Simulation of NMR Spectra of Exchange Systems". This program was written by Dr. R. E. D. McClung (Chemistry Department, University of Alberta) and kindly given to us by Dr. M. J. McGlinchey (Chemistry Department, University of McMaster). The other one is a FORTRAN program written by ourselves, based on the equations describing a chemical exchange of two sites. These equations can be found in Appendix I. The same results for $k_a' + k_b'$ were obtained by these two programs and are reported in table 6.4. Figure 6.5 shows the experimental and the simulated ^{13}C NMR spectra. The successful simulation of the experimental spectra (as seen in figure 6.5) confirmed the carbon correlations given in figure 6.4.

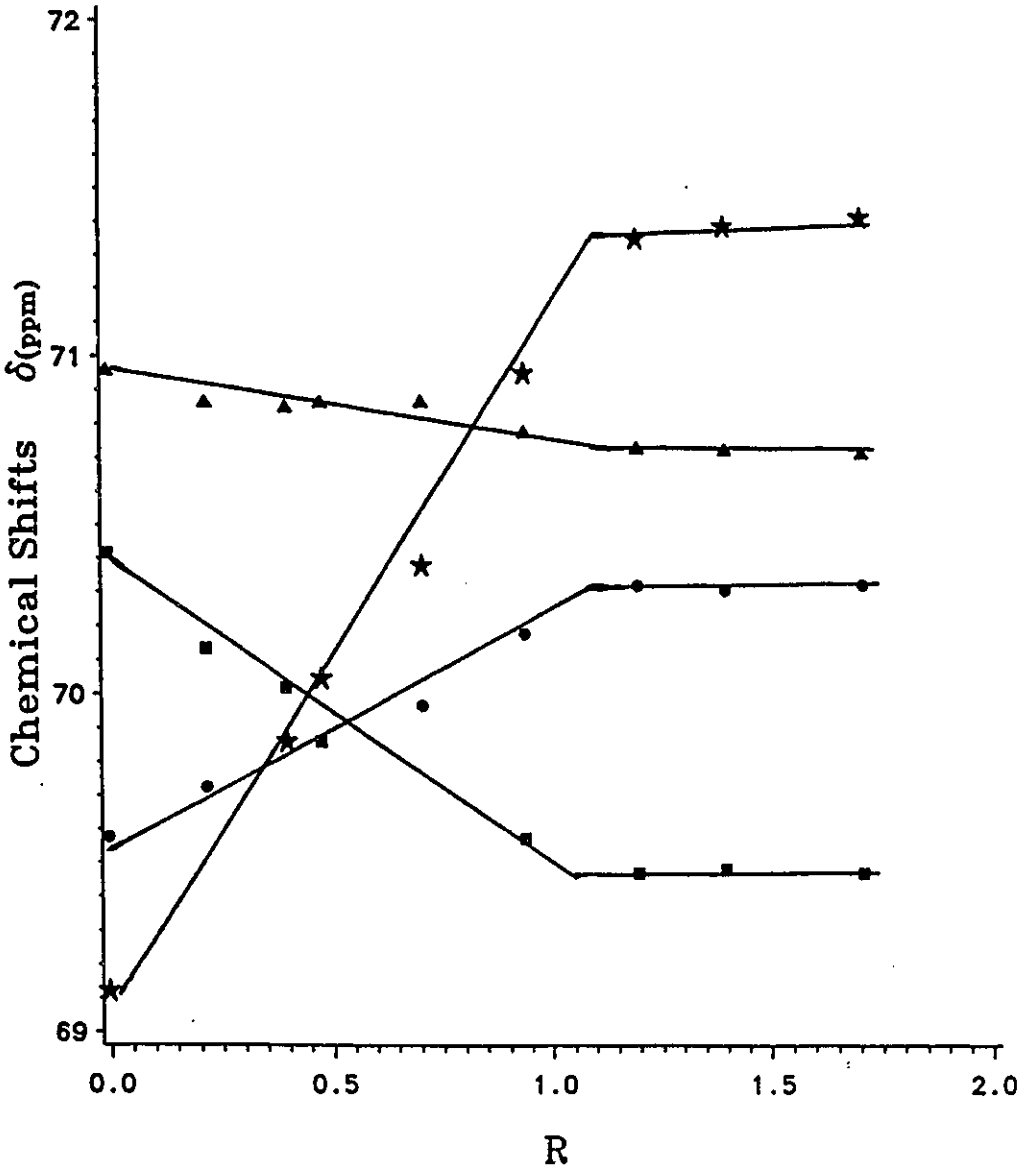

Figure 6.4: ^{13}C chemical shifts as a function of R for $La(NO_3)_3$ - B15C5 in acetonitrile. $[B15C5]_o = 0.015$ M. T = 300 K.

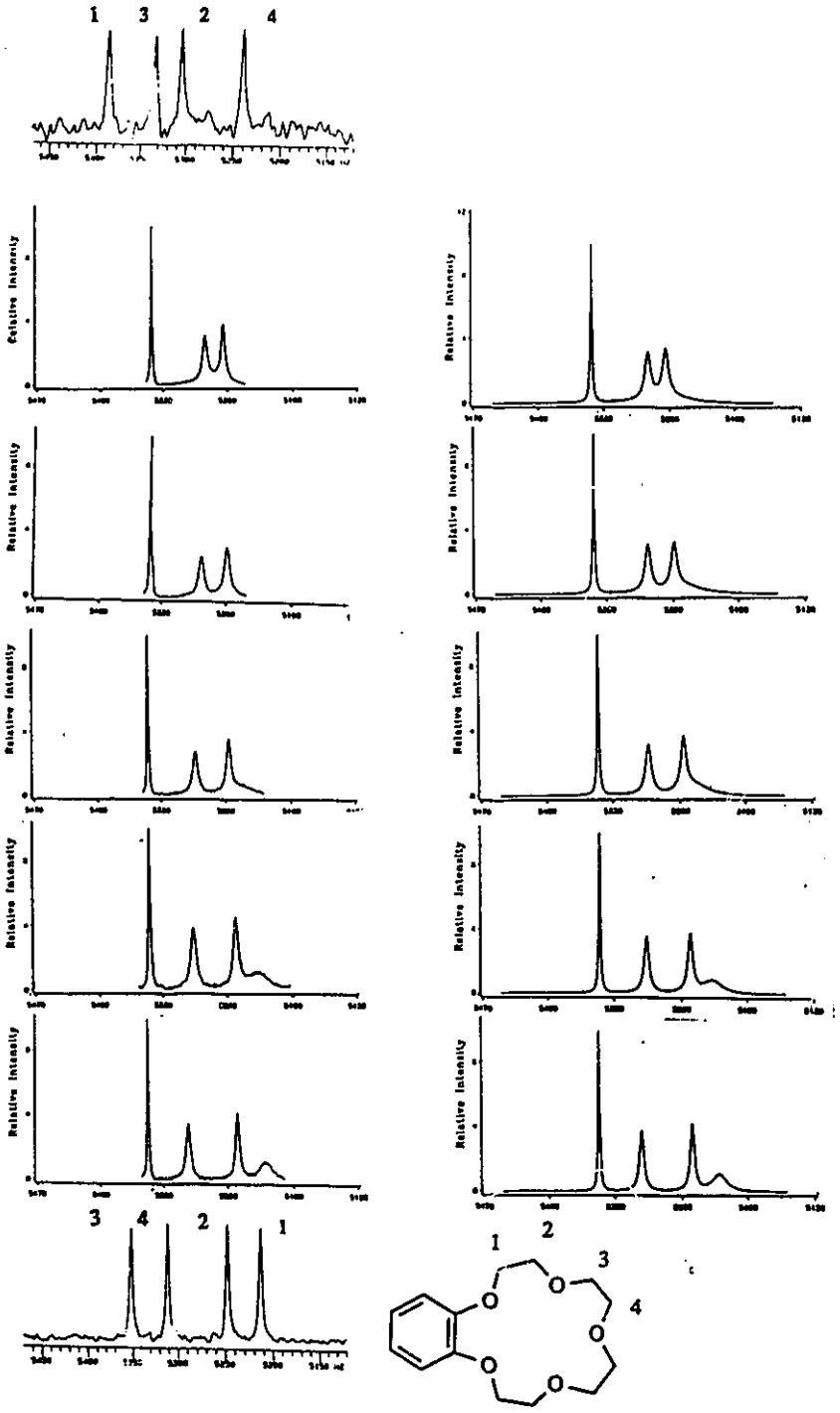

Figure 6.5: Experimental and simulated ^{13}C NMR spectra of B15C5 for $La(NO_3)_3$ - B15C5 in acetonitrile. Left: the experimental spectra, top to bottom $R >$ 1, = 0.32, 0.256, 0.196, 0.136, 0.096, and 0. Right: the simulated spectra corresponding respectively to the experimental ones. $[B15C5]_o = 0.015$ M. T = 300 K.

The proton NMR spectra of B15C5 in the same system also exhibit the characteristics of a ligand undergoing a fast chemical exchange (see figure 4.15). Because more complicated situations, such as ^1H - ^1H coupling, have to be taken into account, a kinetic analysis of these spectra is extremely difficult to perform. However, some characteristics of the observed ^1H NMR spectra are worth to be pointed out: the line broadenings were still observed for the methylene protons of the B15C5 in the cases of $R \geq 1$. This may indicate the presence of another kind of ligand exchange. This feature can be seen more clearly in the system involving 15C5, which will be discussed in the next section.

Table 6.4. Kinetic Data for B15C5 Chemical Exchange in Acetonitrile.

$[B15C5]_o$ (M)	R^a	$(k_a' + k_b')^b$ ($\times 10^3\ s^{-1}$)
0.015	0.096	1.25 ± 0.05
	0.136	1.30 ± 0.10
	0.196	1.40 ± 0.12
	0.256	1.58 ± 0.14
	0.320	1.75 ± 0.15

a, $R = [La(III)]_o / [B15C5]_o$;

b, Determined from a simulation of the ^{13}C experimental spectra.

6.2.3. 15C5 Chemical Exchange in the Complex La(III)-15C5 in AN: ^{13}C and ^{1}H NMR Studies.

The ^{13}C NMR spectra of 15C5 in solution show a single peak for all the samples, while some line broadening is observed in the region $0 < R < 1$ (see figure 4.19). The analysis of these spectra is relatively easy since the exchange reaction involves only two sites. An equation similar to 6.5 is used to describe this exchange process.

$$\underset{(A)}{(15C5)_s} \underset{k_b'}{\overset{k_a'}{\rightleftharpoons}} \underset{(B)}{(15C5)_c} \qquad (6.6)$$

Here, similarly to equation 6.5, $(15C5)_s$ and $(15C5)_c$ are the 15C5 respectively in the solvated and the complexed sites. k_a' and k_b' are the respective rate constants for these two sites.

Based on equation 6.6 and through a non-linear regression procedure, full lineshape analyses were performed for the ^{13}C NMR spectra obtained in the range of $0 < R < 1$. The NMR parameters used in the calculation were taken from the spectra at $R = 0$ and $R > 1$, which characterize the 15C5 ligand in the solvated and in the complexed sites respectively. The sum of the pseudo-first order rate constants, $k_a' + k_b'$, were obtained from the non-linear regression and are given in table 6.5. The experimental and calculated NMR spectra are shown in figure 6.6.

The characteristics of the 15C5 exchange were also shown in the proton NMR spectra. These spectra have previously been given in figure 4.18. The 15C5 exchange rate is not very fast on the ^{1}H NMR chemical shift time scale. Consequently, separated signals respectively for solvated and complexed 15C5 were obtained. The line

broadenings observed in the cases of $0 < R < 1$ are an indication of the occurrence of an exchange of 15C5 ligand between the sites A and B described in equation 6.6. These observations are consistent with the ^{13}C NMR results shown previously, and the rate constants for the exchange process have been obtained through the analyses of the ^{13}C NMR spectra.

Table 6.5. Kinetic Results of 15C5 Chemical Exchange in Acetonitrile[a]

ν^b_a (Hz)	$\nu_b{}^c$ (Hz)	P_B (R)	$(k_a' + k_b')^d$ (s^{-1})
5334.3	5323.2	0.15	60 ± 1
		0.30	67 ± 1
		0.44	91 ± 3
		0.59	119 ± 5
		0.76	211 ± 10

a, $[15C5]_o = 0.0043$ M, T = 300 K;

b, Chemical shift of free 15C5 (in Hz);

c, Chemical shift of coordinating 15C5 (in Hz);

d, Obtained from full lineshape analyses of ^{13}C experimental NMR spectra.

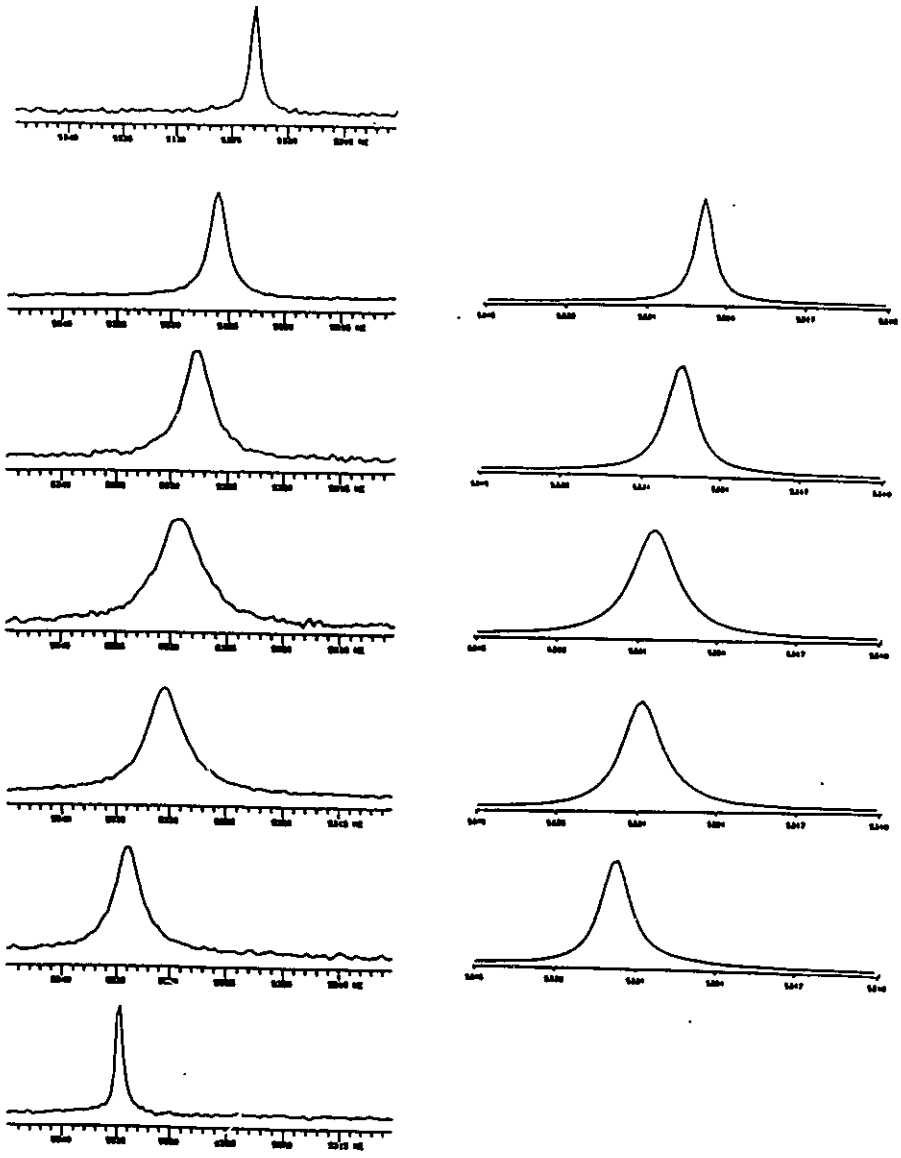

Figure 6.6: Experimental and calculated ^{13}C NMR spectra of 15C5 for $La(NO_3)_3$ - 15C5 in acetonitrile. Left: the experimental spectra, top to bottom $R > 1$, $R = 0.76$, 0.59, 0.44, 0.30, 0.15, and 0. Right: the spectra calculated from the non-linear regression for lineshape analysis, top to bottom: $R = 0.76$, 0.59, 0.44, 0.30, and 0.15. $[15C5]_o = 0.0043$ M. T = 300 K.

In addition to what is described above, a very interesting feature was found on the ^1H NMR spectra of the complexed 15C5 ligand. Instead of a single peak, multiple ^1H signals were observed. This can result from two situations: (i) the complexed 15C5 is in different conformations; (ii) the protons in the complexed 15C5 are not equivalent. The former case is less plausible since the corresponding ^{13}C NMR spectra exhibit only a single peak (see figure 6.6). Therefore, the characteristics observed on the ^1H NMR spectra for the complexed 15C5 should result from the nonequivalence of the protons. As mentioned in the discussion given in chapter 4, in the La(III) - 15C5 complex, the 15C5 ligand should be located on one side of La(III) cation. Therefore, the protons closer to the La(III) are different from those apart from the La(III) cation. Since the chemical exchange features were observed on the ^1H NMR spectra of 15C5 even in the cases of $R > 1$, the following model was proposed based on the above discussions to describe this process (equation 6.7).

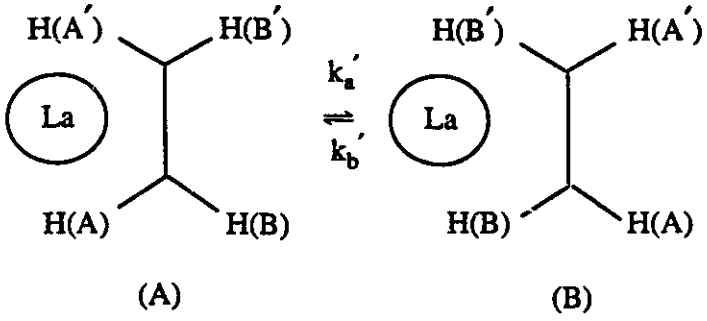

(6.7)

The equation 6.7 implies that the protons of the 15C5 ethyleneoxy fragments are an AA′BB′ system. This model is supported by the ^1H NMR spectra of the complexed 15C5 obtained at lower temperatures, in which an AA′BB′ pattern can be clearly observed (see figure 6.7).

In order to obtain the rate constants for the process shown in equation 6.7, the

^{1}H NMR spectra of the complexed 15C5 ligand (R > 1) were recorded at various temperatures and simulated on the basis of the model of equation 6.7, through the DNMR3 program. The related coupling constants of the protons were obtained from the simulation of the ^{1}H NMR spectra obtained at 239 K, since the spectrum at this temperature has a high resolution feature. These coupling constants, reported in table 6.6, were used as fixed values during the simulation procedures for other temperatures. Table 6.7 lists the calculated rate constants. The experimental and the simulated ^{1}H NMR spectra are shown in figure 6.7 for various temperatures.

Table 6.6. ^{1}H NMR Parameters of Coordinated 15C5 in Acetonitrile[a]

Chemical Shifts (ppm)		Coupling Constants[b] (Hz)		
$\delta_A(\delta_{A'})$	$\delta_B(\delta_{B'})$	J_{trans}[c]	J_{gem}[c]	J_{cis}[c]
4.032	3.935	3.6	-10.6	6.1

a, $[15C5]_o = 0.0041$ M;

b, Coupling constants for the 15C5 OCH_2CH_2O fragment as shown in equation 6.7;

c, $J_{trans} = J_{AB'} = J_{A'B}$, $J_{gem} = J_{AB} = J_{A'B'}$, and $J_{cis} = J_{AB'} = J_{A'B}$.

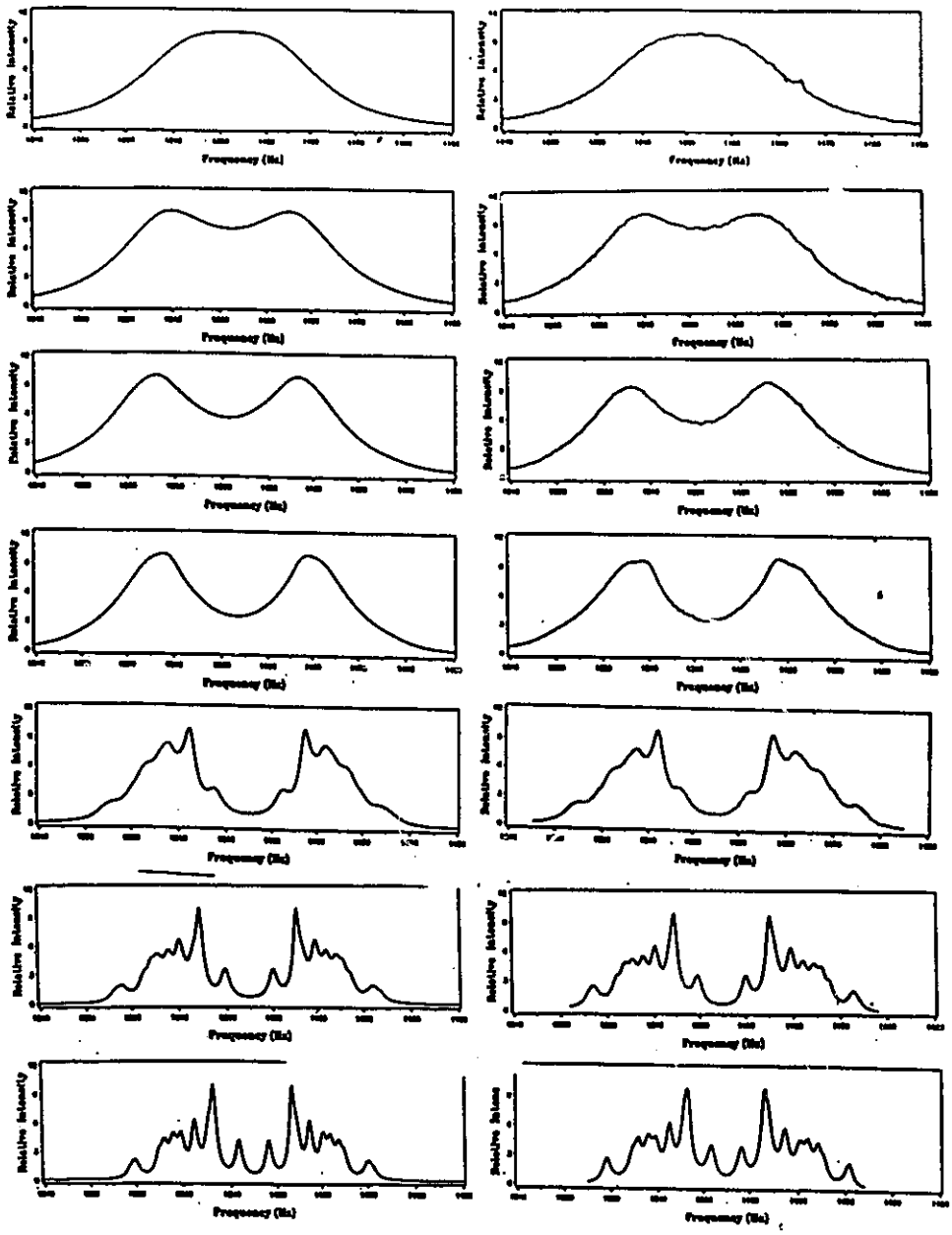

Figure 6.7: Experimental and calculated ^1H NMR spectra of the coordinated 15C5 for complex $La(NO_3)_3$ - 15C5 in CD_3CN at various temperatures. $[15C5]_o$ = 0.0041 M. R = 1.08. Right: the experimental spectra. Left: the corresponding spectra calculated from DNMR3 based on the AA'BB' proton system undergoing a chemical exchange. Top to bottom: T = 331.9, 313.2, 303.8, 297.3, 277.8, 258.4, and 239.0 K.

Table 6.7.

Kinetic Data on the Coordinated 15C5 Internal Exchange in Acetonitrile for Various Temperatures[a] (equation 6.7).

Temperatures (K)	k (s^{-1})[b]
239.0	2.5
258.4	5.6
277.8	12
297.3	35
303.8	42
313.2	55
331.9	114

a, $[15C5]_o = 0.0032$ M, $R = 1.08$;

b, Obtained from the simulations of the 15C5 ^1H NMR spectra.

6.2.4 18C6 Chemical Exchange in the complex La(III)-18C6 in AN: A ^{1}H NMR Study

The ^{139}La NMR spectra obtained on the system of $La(NO_3)_3$ 6 H_2O - 18C6 - AN indicate that the cation exchange is slow (see figure 4.9). The ligand exchange is also slow on the proton and ^{13}C NMR chemical shift time scales (see figure 4.10 and 4.11). The kinetic study on this system cannot be done by linebroadening measurements. Magnetization transfer offers another NMR method for studying slow exchanges. This technique is most useful in the region where the exchange rates are similar or somewhat slower than the relaxation rates. The theoretical description of this method can be made through an energy level diagram (figure 6.8).

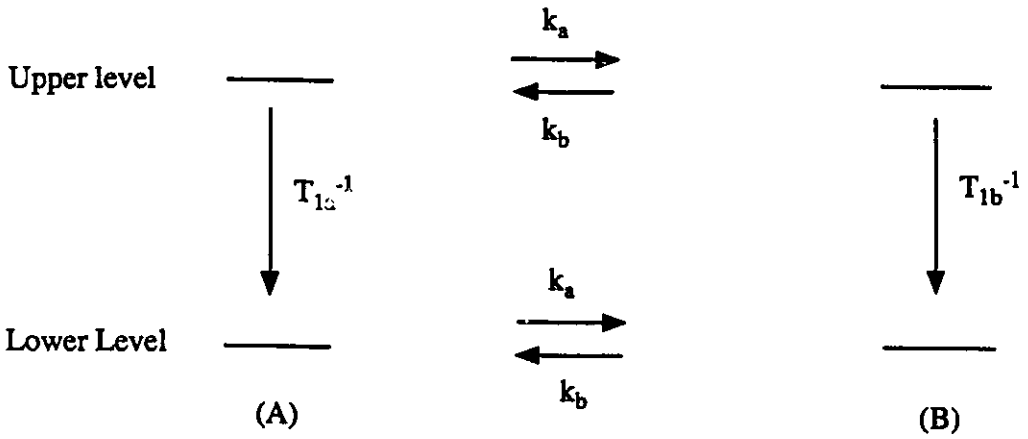

Figure 6.8. Energy level diagram for magnetization transfer.

Figure 6.8 shows a such diagram for two species undergoing a chemical exchange. Because the chemical exchange takes place without change of spin state, an equilibrium will be established for both higher and lower levels. If the Boltzmann distribution of one species is perturbed, the effects will transfer to another species through the process of chemical exchange. For example, continuously selective

saturation of the B resonance will increase the transfer of spins to the upper level of A and decrease the transfer to its lower level. However, the longitudinal relaxation of A will always tend to return the population distribution back to normal. Therefore, there is a competition between magnetization transfer at a rate k_b and relaxation at a rate T_{1a}^{-1}. When the chemical exchange rate, k_b, is much faster than the relaxation, the resonance of A will eventually be saturated. In the case of $T_{1a}^{-1} >> k_b$, the population distribution of A will remain unchanged. If k_b is comparable to T_{1a}^{-1}, a decreased intensity of A signal is expected to be observed. The rate constant for the chemical exchange can be derived by measuring the reduction in intensity of the monitored signal[148].

$$(I_o^a - I^a) / I_o^a = T_{1a} / (1 + k_a T_{1a}) \qquad (6.8)$$

Where I_o^a and I^a represent the intensities of the A resonance, respectively in the absence and in the presence of a saturating field on the resonance of B. T_{1a} is the longitudinal relaxation time for the site A.

This method has been mainly used in the kinetic study of biological systems[149-151]. In the present work, this technique was applied to investigate the 18C6 exchange in the system of $La(NO_3)_3\ 6\ H_2O$ - 18C6 - AN. Again, the chemical exchange in this system involves two sites (equation 6.9).

$$\begin{array}{ccccc} & & k_a' & & \\ (18C6)_s & & \rightleftharpoons & & (18C6)_c \\ (A) & & k_b' & & (B) \end{array} \qquad (6.9)$$

Where again $(18C6)_s$ and $(18C6)_c$ are the crown ether respectively in the solvated and complexed sites. k_a' and k_b' are the exchange rate constants respectively for these two sites.

The proton NMR observations were made on a sample of $R = 0.5$; in this case, $k_a' = k_b'$. At temperatures < 60 ^{0}C, no reduction in intensity of the monitored signal could be observed. However, a significant decrease of the intensity was found on a saturation transfer experiment performed at 333 K. Figure 6.9 shows the ^{1}H NMR spectra of 18C6 at this temperature. In figure 6.9, the spectrum (B) was recorded upon saturation of the complexed 18C6 signal; the spectrum (A) was taken by placing the saturation field on the other side of the complexed 18C6 peak; and (C) is a differential spectrum between (A) and (B). The intensities of the free 18C6 signal in spectra (A) and (C) were determined from a integration. T_1 for the free 18C6 was measured at R = 0 where there is no chemical exchange. The rate constant, k_a', could be calculated on the basis of equation 6.8, which was found to be 0.15 ± 0.03 s^{-1}. A similar experiment was done by saturating the signal of the free 18C6 and following the complexed 18C6 peak. The longitudinal relaxation time for the complexed 18C6, T_b was measured at R > 1. k_b' was then calculated through an equation similar to the equation 6.8. A value identical to k_a' was obtained for k_b'. The determination of the rate constant for 18C6 chemical exchange was also checked by measuring the free 18C6 longitudinal relaxation in the presence of the saturation field on B resonance (the complexed 18C6), $(T_{1a})^{sat}$. The measurement was made on a sample of $R = 0.50$ and the rate constant, k_a', was calculated through equation 6.10. Again, the same result for k_a' was obtained.

$$(I_o^a - I^a) / I_o^a = k_a' (T_{1a})^{sat} \qquad (6.10)$$

An alternative experimental approach for this kind of investigation is inversion transfer. It involves placing a magnetic label at one resonance by inverting its spin population and following the intensity of the other signal as the inverted resonance relaxes back[148,149]. The detailed description of this technique has been given in Chapter 2. The inversion transfer observations were made on the same sample as that used in the saturation transfer study. Again, it is only for temperature ≥ 60 ^{0}C, that the

intensity variations could be observed on the monitored signal. This was done for different mixing times, τ_{mix}, indicating that 18C6 undergoes a chemical exchange between the free and the coordinated sites, at a rate measurable by the inversion transfer technique. The results are consistent with those obtained previously by the saturation transfer study. Figure 6.10 shows the proton NMR spectra of 18C6 at 333 K, for various values of τ_{mix}. The experiment was performed (i) by inverting the complexed 18C6 ^{1}H NMR signal, and following the intensity variations of the free 18C6 signals and (ii) by inverting the free 18C6 signal and following the perturbation of the complexed 18C6 resonance. The description of the behavior of two exchanging sites in an inversion magnetization transfer experiment has been given by Morris and Freeman[154]. The following equations were used for the calculation of the exchange rate constants[154].

$$I^a / I_o^a = 1 - (2k_a'/\beta)\{\exp[-1/2(\alpha - \beta)\tau_{mix}] - \exp[-1/2(\alpha + \beta)\tau_{mix}]\} \quad (6.11)$$

$$\alpha = R_a + R_b \quad (6.12)$$

$$\beta = [R_a - R_b)^2 + 4k_a'k_b']^{1/2} \quad (6.13)$$

$$R_a = k_a' + T_{1a}^{-1} \quad (6.14)$$

$$R_b = k_b' + T_{1b}^{-1} \quad (6.15)$$

k_a' was calculated from a non-linear regression procedure, through equations 6.11 to 6.15 (experiment (i)). Very similar equations (not shown) with the equations 6.11 - 6.15 can be obtained for the calculation of k_b' and the value of k_b' was determined (experiment (ii)). The same result was found for k_a' and k_b', 0.17 ± 0.04 s^{-1}. Figure 6.11 shows the reduced intensity (I / I_o) of the free 18C6 ^{1}H NMR signals as a function of τ_{mix}. In the figure 6.11, the solid line has been calculated from the non-linear regression described above. It is noteworthy that the same results for the exchange rate were obtained by the inversion transfer experiment and by the saturation transfer method.

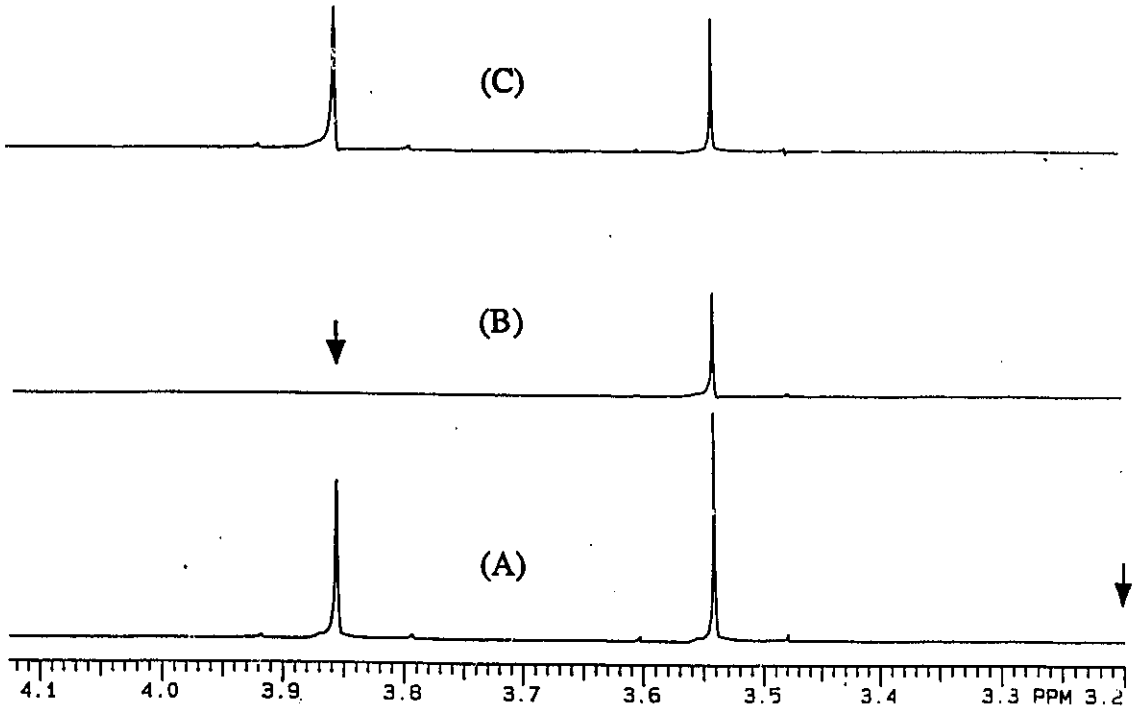

Figure 6.9. ^{1}H NMR spectra of 18C6 for 18C6 - $La(NO_3)_3$ in CD_3CN recorded by saturation transfer method. (B), the complexed 18C6 signal was saturated; (A), the saturation field was placed on the other side of the complexed 18C6 peak; (C) is a differential spectrum between (A) and (B). The arrow indicates the frequency of irradiation in cases (A) and(B). $R = 0.50$. T = 333 K.

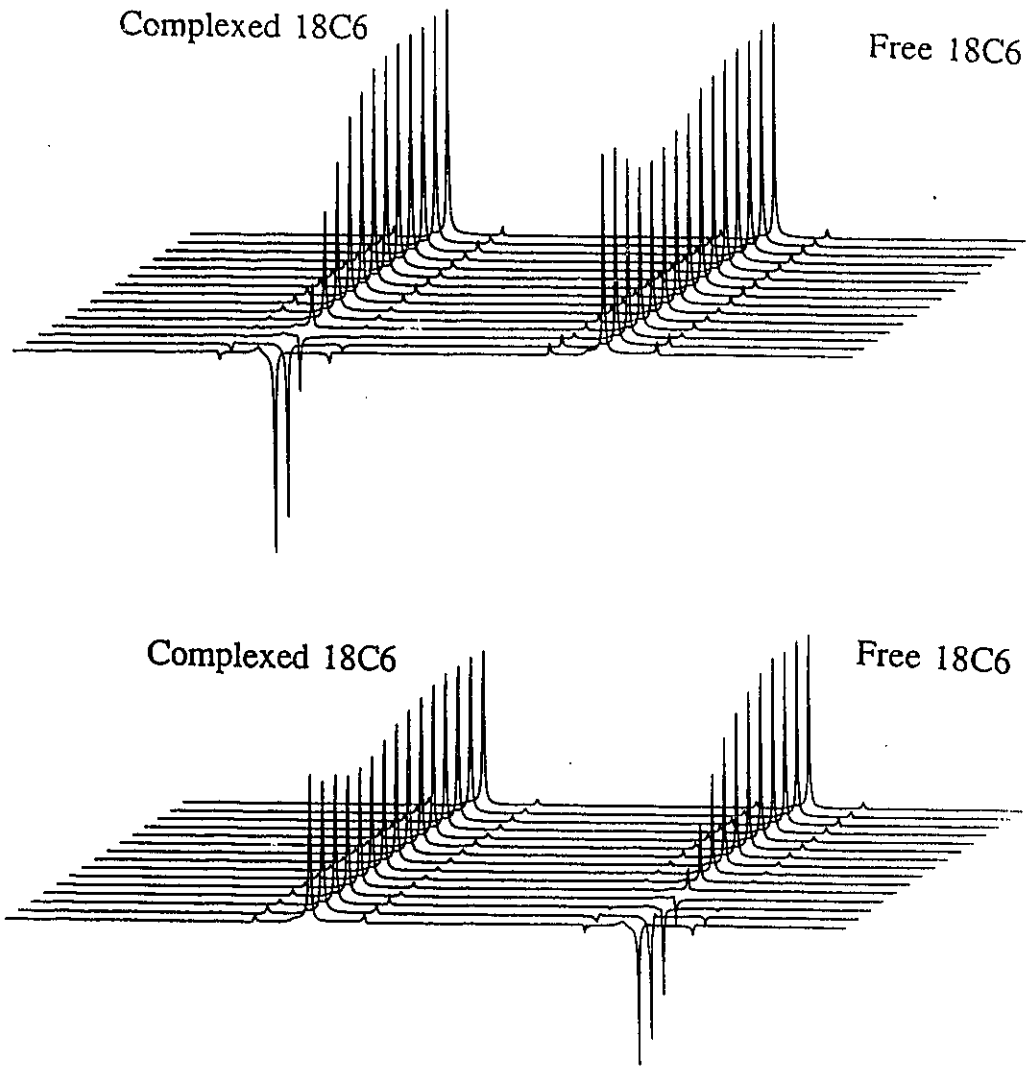

Figure 6.10: ^{1}H NMR spectra of 18C6 for 18C6 - $La(NO_3)_3$ in CD_3CN recorded for various τ_{mix} values by inversion transfer technique. Top: the signal of coordinated 18C6 was inverted and the resonance of free 18C6 was monitored; Bottom: inverting the free 18C6 signal and following the resonance of coordinated 18C6. Front to back: τ_{mix} = 0.0, 0.1, 0.5, 1.0, 1.5, 2.0, 3.0, 4.0, 5.0, 6.0, 8.0, 10.0, 12.0, 15.0, and 20.0 s.

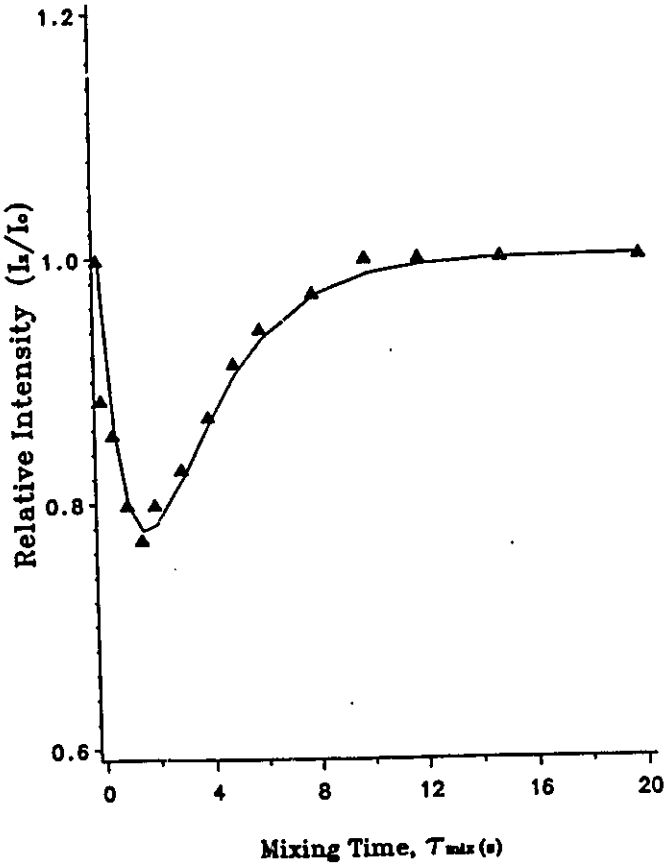

Figure 6.11: Reduced intensities of the free 18C6 ^{1}H NMR signals as a function of τ_{mix}. The solid line was calculated from a non-linear regression through equations 6.11 - 6.15. The points are experimental. T = 333 K. R = 0.50.

6.3. Mechanisms of the Chemical Exchange

An NMR kinetic study is based on the lifetime measurement of an observed nucleus in specific sites. The reciprocal of these measured life time values were presented as the pseudo-first-order rate constants in the previous section. Since NMR gives access only to pseudo-first-order rate constants, the mechanisms of the exchange have to be known, in order to obtain the actual rate constants for the chemical exchange processes.

One can identify two possible mechanisms, originally postulated by Shchori et al.[155,156], for a two site exchange involving cation and crown ethers in solution. These two mechanisms, which have been successful in accounting for the NMR results obtained in sodium - crown ether systems[157-159], are considered here for the purpose of the interpretation of the NMR data obtained in the La(III) - crown ether systems. This approach is logical, since, except for the nature of the cations involved, the situations are similar in both cases. The first mechanism is referred to as *dissociative exchange* and can be described by the following equations:

$$(MC)^{3+} \underset{k_1}{\overset{k_{-1}}{\rightleftharpoons}} M^{3+} + C \qquad C + M^{3+} \underset{k_{-1}}{\overset{k_1}{\rightleftharpoons}} (MC)^{3+} \qquad (6.16)$$

Where $(MC)^{3+}$, M^{3+}, and C represent respectively La(III)-crown ether complex, La(III) cation, and the crown ethers.

This mechanism is initiated by the dissociation of the complex to give a free metal ion and a free ligand and is followed by a recombination process to reform the complex. The rates of disappearance of the solvated and complexed metal cation can be expressed as:

$$-d[M]/dt = [M]/\tau_A = k_a [M] = k_1 [M] [C] \qquad (6.17)$$

$$-d[MC]/dt = [MC]/\tau_B = k_b\,[MC] = k_{-1}\,[MC] \qquad (6.18)$$

The sum of the inverse lifetimes, $k_a + k_b$, determined from the NMR kinetic studies described previously, is:

$$k_a + k_b = k_1\,[C] + k_{-1} \qquad (6.19)$$

Since $k_1 = k_{-1} \times K_c = k_{-1}\,[MC]/[M]/[C]$ and since K_c is usually large enough for $[MC] \cong [C]_o$, equation 6.20 can be derived from equation 6.19:

$$k_a + k_b = k_{-1}\,(1 - \rho)^{-1} \qquad (6.20)$$

Where $\rho = [C]_o / [M]_o$, the ratio of ligand total concentration over metal cation total concentration.

The equation 6.16 can also be used to describe a ligand exchange through a dissociative mechanism. Similarly, the rates of disappearance of free and coordinated crown ethers can be expressed as:

$$-d[C]/dt = [C]/\tau_A' = k_a'\,[C] = k_1\,[M]\,[C] \qquad (6.21)$$

$$-d[MC]/dt = [MC]/\tau_B' = k_b'\,[MC] = k_{-1}\,[MC] \qquad (6.22)$$

And:

$$k_a' + k_b' = k_{-1}\,(1 - R)^{-1} \qquad (6.23)$$

Where $R = [M]_o / [C]_o$, the ratio of metal cation and ligand total concentration in the solutions. $k_a' + k_b'$ were determined from the NMR kinetic studies of the ligand exchange as described previously.

The second mechanism by which the chemical exchange may proceed is usually called *associative exchange*. In this mechanism, the chemical exchange is achieved through an interaction of another metal cation with the complex and can be described by equation 6.24 (cation association exchange):

$$M^* + MC \overset{k_2}{\rightleftharpoons} M^*C + M \qquad (6.24)$$

In this case, the rates of disappearance of the metal cation respectively from its solvated and complexed states are equal and can be expressed as:

$$-d[MC]/dt = -d[M]/dt = k_2 [M] [MC] \qquad (6.25)$$

Since $-d[MC]/dt = k_a [M]$ and $-d[M]/dt = k_b [MC]$, therefore:

$$k_a + k_b = k_2 ([M] + [MC]) = k_2 [M]_o \qquad (6.26)$$

If the ligand exchange proceeds through a ligand association, the equation 6.24 becomes (ligand association exchange):

$$C^* + MC \overset{k_2'}{\rightleftharpoons} MC^* + C \qquad (6.27)$$

The related equations are:

$$-d[MC]/dt = -d[C]/dt = k_2' [C] [MC] \qquad (6.28)$$

$$k_a' + k_b' = k_2' ([C] + [MC]) = k_2' [C]_o \qquad (6.29)$$

If the two mechanisms of equations 6.16 and 6.24 were the only ones contributing to the La(III) cation chemical exchange, then the overall sum of the pseudo-first order rate constants measured by NMR, can be expressed as:

$$k_a + k_b = k_{-1} (1 - \rho)^{-1} + k_2 [M]_o \qquad (6.30)$$

Similarly, for the crown ether chemical exchange, equation 6.30 becomes:

$$k_a' + k_b' = k_{-1} (1 - R)^{-1} + k_2' [C]_o \qquad (6.31)$$

The relationships given in equations 6.30 and 6.31 allow us to test mechanistic hypotheses. The actual constants corresponding to the mechanism can then be extracted from the experimental data. Based on equation 6.30, a plot of $k_a + k_b$ against $(1 - \rho)^{-1}$ for $[M]_o$ constant, or a plot of $k_a + k_b$ as a function of $[M]_o$ for ρ constant should be a straight line. The slope and intercept of the plot of $k_a + k_b$ against $(1 - \rho)^{-1}$ should be related respectively to the rate constants of k_{-1} and k_2. Similarly, the mechanism and rate constants for a ligand exchange can be obtained from equation 6.31.

Figure 6.12 shows a plot of $k_a + k_b$, obtained by ^{139}La NMR at total La(III) concentration of 0.0050 M in the system consisting of $La(NO_3)_3$ 6 H_2O - B15C5 -AN, as a function of $(1 - \rho)^{-1}$. The solid line in figure 6.12 was obtained from a linear regression analysis of the experimental data points. The relationship between $k_a + k_b$ and $(1 - \rho)^{-1}$ shown in figure 6.12 may suggest that the La(III) cation chemical exchange is through both dissociative and associative mechanisms since the obtained straight line has non-zero values of slope and of intercept. The dissociative nature of the exchange of La(III) is confirmed by the ^{13}C NMR studies. This will be discussed later in this section. The La(III) cation associative exchange in this system is indicated also by the dependence of the exchange rate upon $[La(III)]_o$, the total lanthanum

concentration. As shown previously, a single ^{139}La NMR peak was obtained in the case of $[La(III)]_o$ = 0.020 M while two separated signals characterizing the La(III) cation respectively in the solvated and the complexed states were observed in the case of $[La(III)]_o$ = 0.0050 M, indicating that the rate of the lanthanum cation exchange is different in these two cases. However, taking into consideration the fact that nitrate anions have a strong ability to coordinate with the La(III) cation and may also play a role in the cation chemical exchange, it would be safe to state that the La(III) cation exchange is catalyzed by the presence of lanthanum nitrate. Even so, the rate constants k_{-1} and k_2 were calculated from the slope and the intercept of the plot given in figure 6.12. These values are listed in table 6.8.

As mentioned previously, the ligand crown ether chemical exchange may also be interpreted on the basis of the associative and dissociative mechanism models. Figure 6.13 gives plots of $k_a' + k_b'$, obtained by ^{13}C NMR on B15C5 (see table 6.4), as a function of $(1 - R)^{-1}$ at several temperatures. All these plots are linear and extrapolate to the origin. This is a good indication that the ligand exchange occurs only via the dissociative pathway. The rate constant k_{-1} for the B15C5 exchange can be determined from the slopes of these lines. As an example, the calculated k_{-1} value is 1150 ± 20 s^{-1} at 300 K. It is noteworthy that the equations describing the ligand exchange and the cation exchange via a dissociative mechanism are the same (see equation 6.16) and the dissociation of the complex La(III)-B15C5 will contribute to the ligand exchange and to the cation exchange. Therefore, the result obtained by the ^{13}C NMR on the B15C5 exchange confirms the contribution of dissociative mechanism to the La(III) cation exchange process. Moreover, the rate constants k_{-1}, determined independently from the ligand and the cation kinetic studies, are in good agreement (see table 6.8; k_{-1} = 1600 ± 200 s^{-1} (^{139}La); k_{-1} = 1150 ± 20 s^{-1} (^{13}C)).

A similar procedure for the kinetic data analysis can be done for the 15C5 chemical exchange. Figure 6.14 shows a plot of $k_a' + k_b'$, obtained from the ^{13}C NMR

spectra of 15C5, as a function of $(1 - R)^{-1}$, Again, the relationship between $k_a' + k_b'$ and $(1 - R)^{-1}$ is linear. The rate constant for the 15C5 dissociation process can be calculated from the slope of the plot: $k_{-1} = 50 \pm 10\ s^{-1}$ at 300 K.

The fact that k_{-1} is much larger in the case of B15C5 than in the case of 15C5 seems very interesting. Usually, at least for the few cases where a comparison is possible, the reverse is observed or both rates are comparable for the cases involving a crown ether and its benzo-substituted analogue. For example, k_{-1}, determined from the ^{23}Na NMR on a $NaBPh_4$ solution in AN, is $3.8 \pm 0.5 \times 10^3\ s^{-1}$ in the case of 18C6 and $4 \times 10^3\ s^{-1}$ for the case of DB18C6[157]. Another example can be found for the potassium dissociative exchange in the systems involving 18C6 and DB18C6: k_{-1}, determined from ^{39}K NMR on a KI solution in MeOH, is $6.8 \pm 2.7 \times 10^4\ s^{-1}$ in the case of 18C6[160] whereas it is $610\ s^{-1}$ in the case of DB18C6[161]. One can only speculate on the origin of the behavior observed in the present work. Plausibly, the 15C5 complex is better stabilized in solution than the more bulky B15C5 one, in which the three nitrate groups are in close proximity to the electron-rich aromatic ring.

Table 6.8.

Rate Constants of the Chemical Exchange in the La(III) - Crown Ether Systems

Type of Exchange	Nucleus Observed	k_{-1} (s^{-1})	k_2 (s^{-1})
Cation (La(III)	^{139}La	1600±200[a]	2.6±0.7x10^{5}[a]
Ligand (B15C5)	^{13}C	1150±20[b]	----[f]
Ligand (15C5)	^{13}C	50±10[c]	----[f]
Ligand (15C5)	^{1}H	35±5[d]	----[f]
Ligand (18C6)	^{1}H	0.15[e]	-----

a, Determined from lineshape analysis of ^{139}La NMR spectra recorded at $[La(III)]_o = 0.0050$ M;

b, Obtained from simulation of the B15C5 ^{13}C NMR spectra;

c, Determined from lineshape analysis of 15C5 ^{13}C NMR spectra;

d, The value obtained from simulation of the coordinated 15C5 ^{1}H NMR spectra at 297.3 K and $R = 1.08$;

e, Calculated by magnetization transfer technique, assuming that the 18C6 exchange occurs via a dissociative pathway. T = 333 K;

f, No associative exchange was detected.

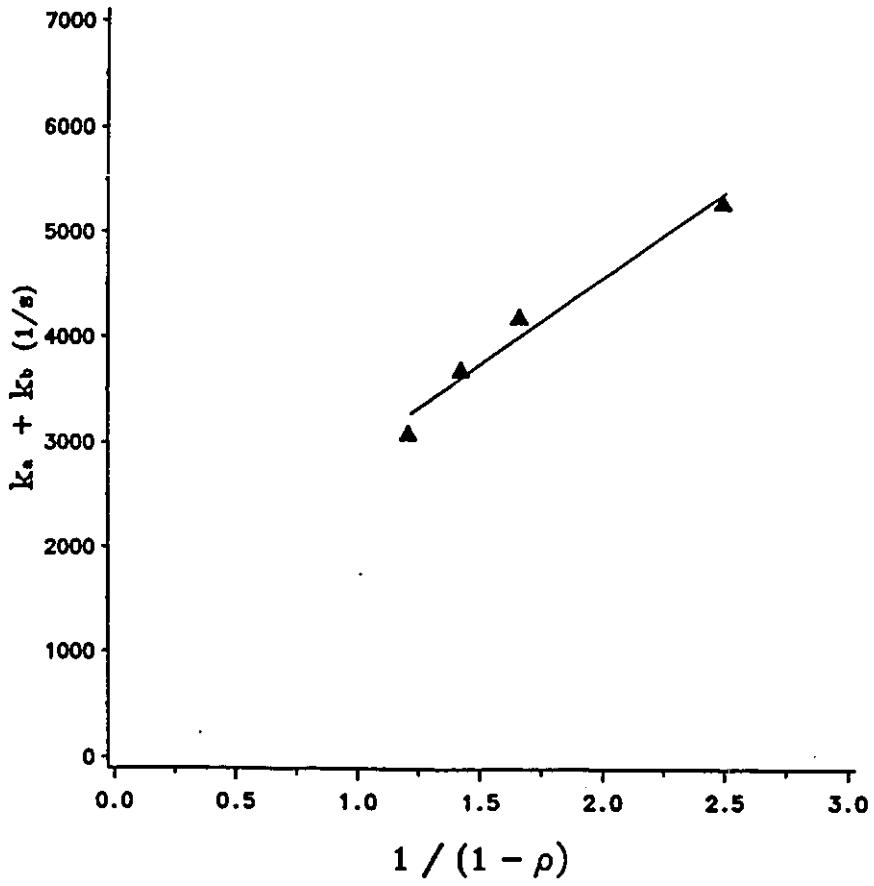

Figure 6.12. ($k_a + k_b$), obtained from ^{139}La NMR lineshape analysis, as a function of $(1-\rho)^{-1}$ for $La(NO_3)_3$ - B15C5 in AN. The points are experimental and the line is calculated from linear regression of the experimental data. $[La(III)]_o$ = 0.0050 M and T = 300 K.

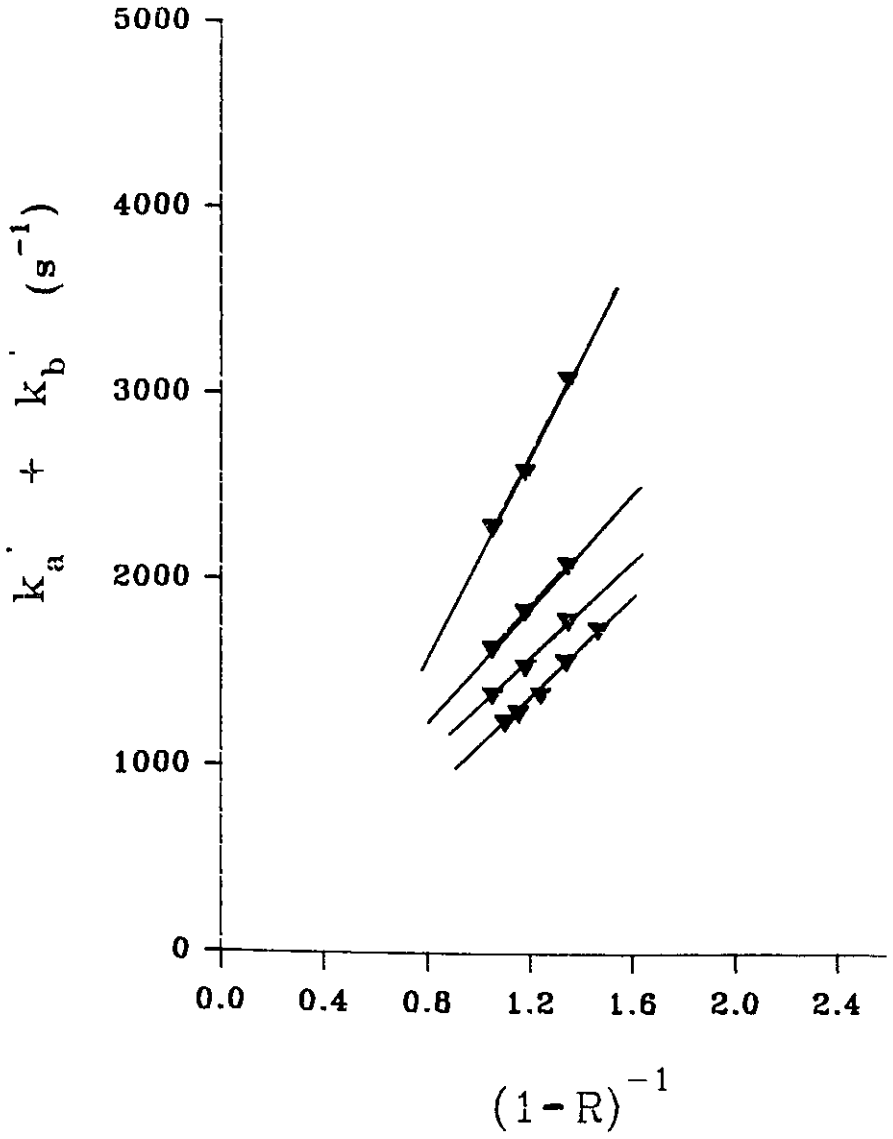

Figure 6.13: ($k_a' + k_b'$), obtained from ^{13}C NMR lineshape analysis, as a function of $(1\text{-}R)^{-1}$ for $La(NO_3)_3$ - B15C5 in AN. The points are experimental and the line is calculated from linear regression of the experimental data. $[B15C5]_o$ = 0.015 M. Top to bottom: T = 331, 318, 308, and 300 K.

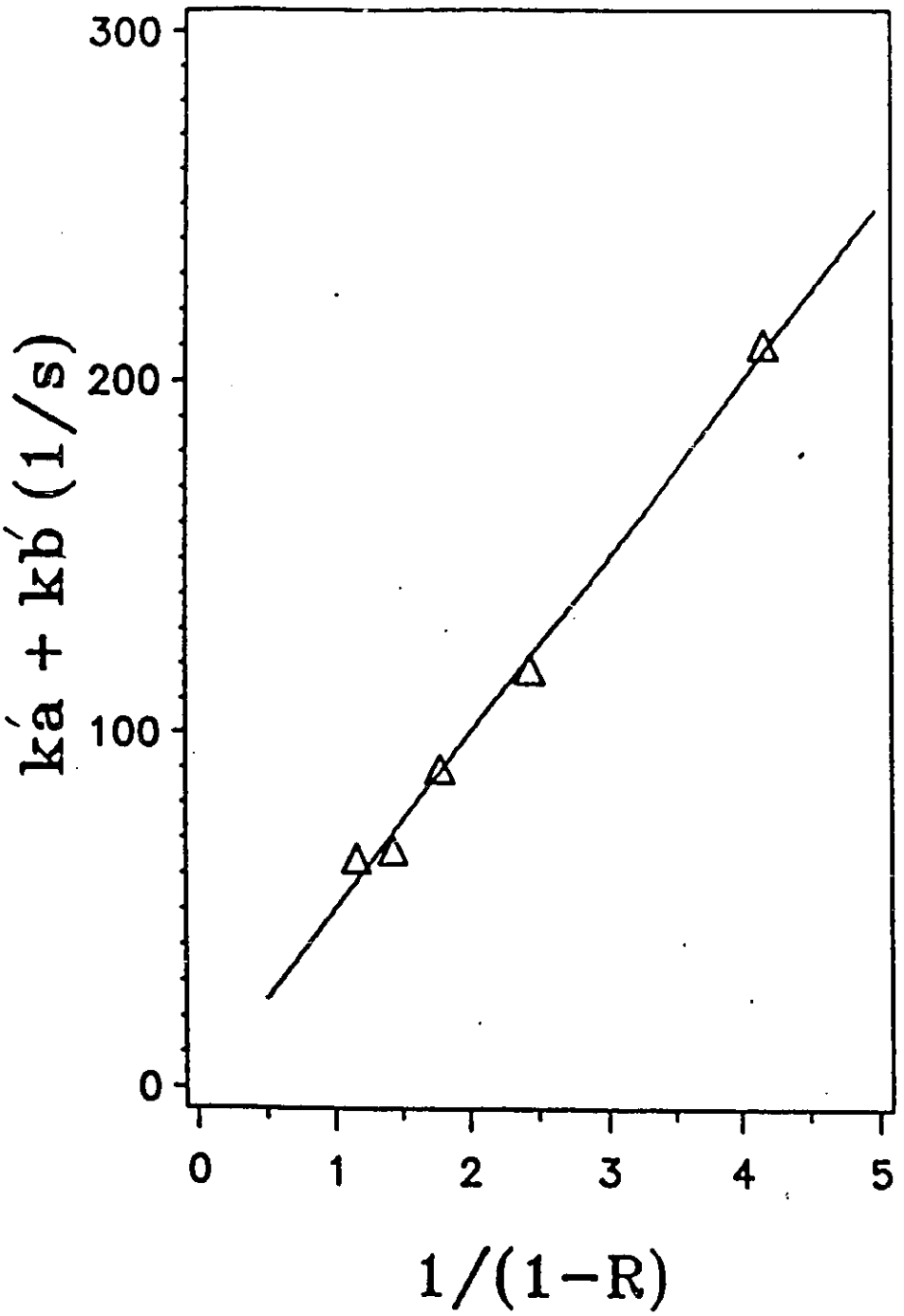

Figure 6.14: $(k_a' + k_b')$, obtained from ^{13}C NMR lineshape analysis, as a function of $(1\text{-}R)^{-1}$ for $La(NO_3)_3$ - 15C5 in AN. The points are experimental and the line is calculated from linear regression of the experimental data. $[15C5]_o$ = 0.0043 M and T = 300 K.

The activation parameters for the ligand dissociative exchange were determined from temperature variation studies. The Eyring equation was used to describe the relationship between the calculated rate constants and the activation parameters:

$$k = (k_B T / h) \exp(-\Delta G^{\neq} / RT) \qquad (6.26)$$

$$k = (k_B T / h) \exp(-(\Delta H^{\neq} - T\Delta S^{\neq})/RT \qquad (6.27)$$

Where k_B is the Boltzmann constant and h is Planck's constant. $\Delta G^{\neq}$, $\Delta H^{\neq}$, and $\Delta S^{\neq}$ are the free energy, enthalpy, and entropy of activation respectively. Figure 6.15 and 6.16 are the Eyring plots respectively for B15C5 and 15C5 exchanges studied by their ^{13}C NMR investigations. In both cases, the plots are linear, indicating that equation 6.27 is valid in the range of temperatures studied. The activation parameters were obtained from the plots and are reported in table 6.9.

From the above discussions, one can see that the ligand exchange in the systems of La(III) - crown ethers occurs mainly via a dissociative mechanism. However, large negative entropies of activation were obtained for this kind of exchange (see table 4.9). This may be understood by considering the solvation of the transition sate for the exchange reaction. It is impossible to compare the activation results obtained in the present work with the literature values since kinetic studies on these systems have not so far been reported. However, large negative values of entropy of activation were found for the dissociation of the complexes Eu(III)-(2.2.1) and Eu(III)-(2,2,2) in aqueous solution: $\Delta S^{\neq} = -106.7$ J K^{-1} mol^{-1} for the dissociation of Eu(III)-(2,2,1) and -108.8 J K^{-1} mol^{-1} for the case of Eu(III)-(2,2,2) have been reported[162]. Negative entropies of activation were also found for the dissociation of complexes of the sodium cation with crown ethers in non-aqueous solution. For example, a $\Delta S^{\neq} = -78 \pm 8$ J $K^{-1}mol^{-1}$ was reported for the sodium cation dissociative exchange in nitromethane solution of $NaBPh_4$ in the presence of DB18C6[163].

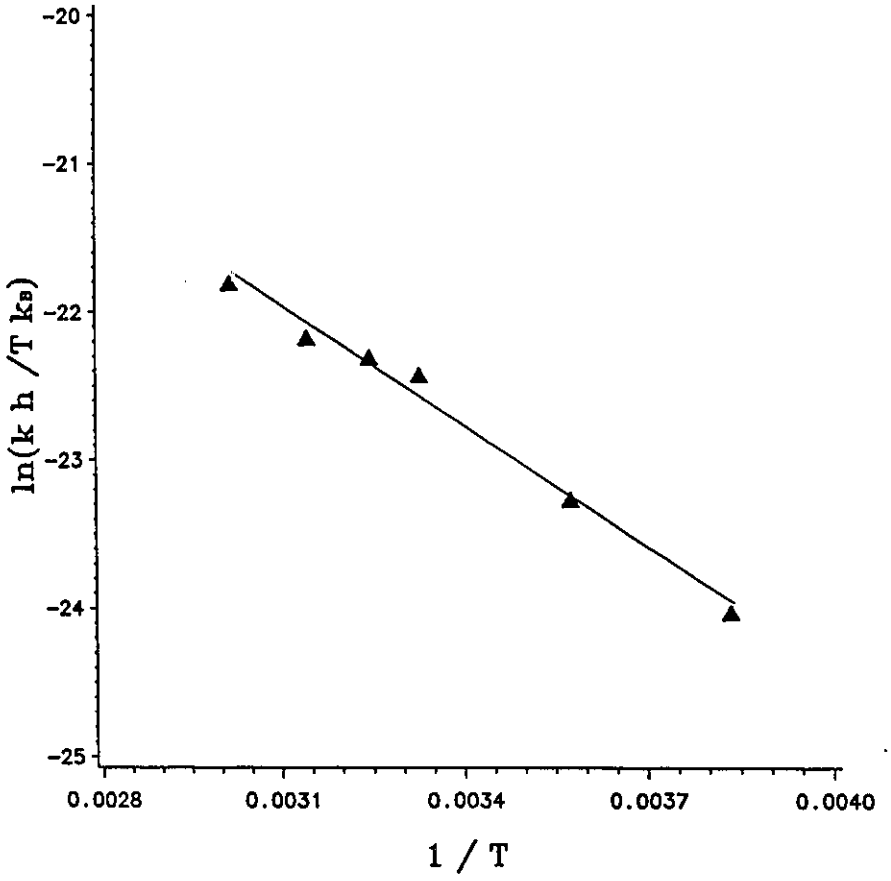

Figure 6.15: ln(k h / k_B T) as a function of T^{-1}. Crown ether = B15C5. $[B15C5]_o$ = 0.015 M. The points are experimental and the line is calculated from linear regression of the experimental data. k at each temperature was obtained from the analysis of the B15C5 ^{13}C NMR results.

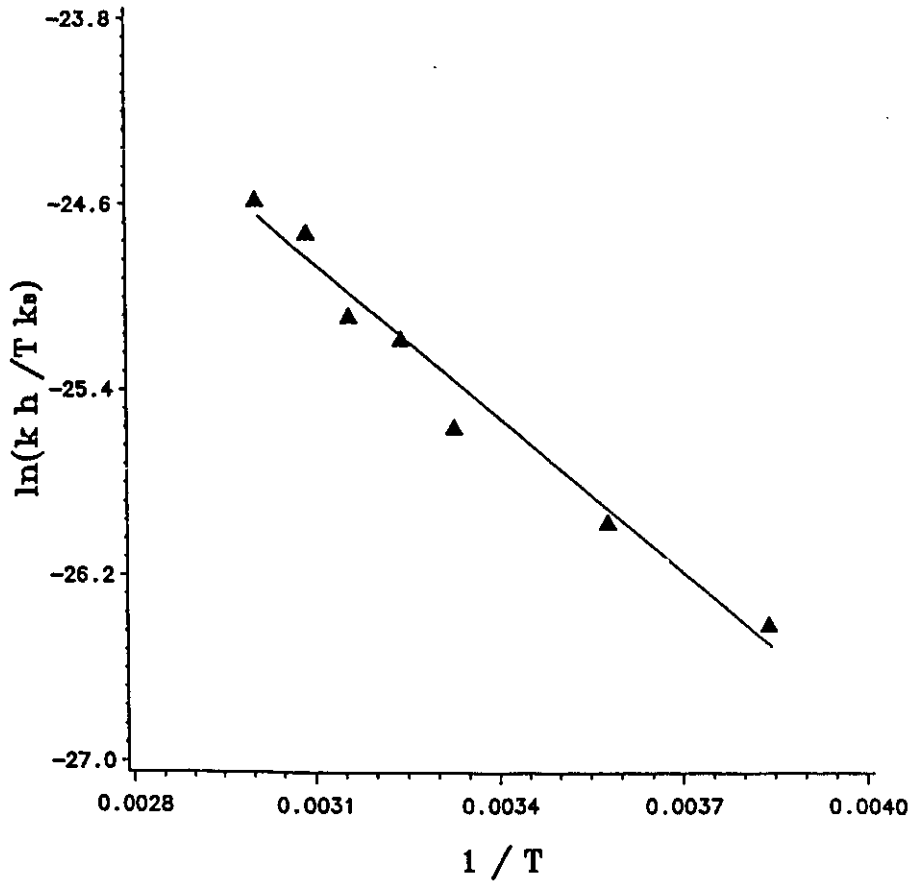

Figure 6.16: ln(k h / k_B T) as a function of T^{-1}. Crown ether = 15C5. $[15C5]_o$ = 0.0043 M. The points are experimental and the line is calculated from linear regression of the experimental data. k at each temperature was obtained from the analysis of the 15C5 ^{13}C NMR results.

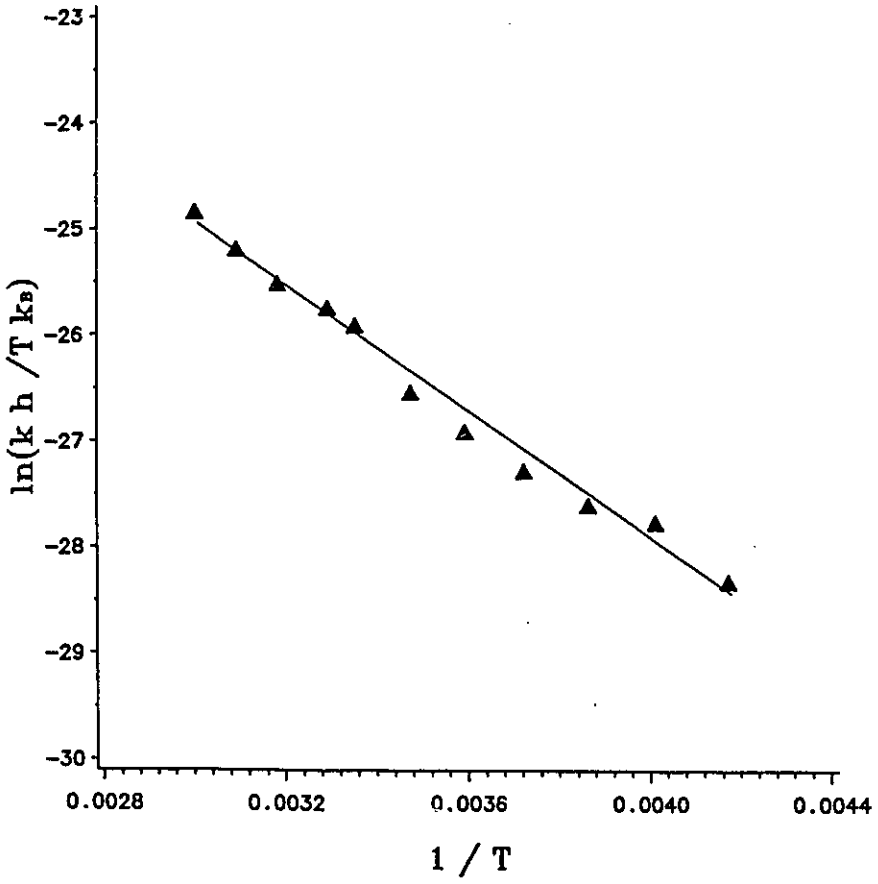

Figure 6.17: ln(k h / k_B T) as a function of T^{-1}. Crown ether = 15C5. $[15C5]_o$ = 0.0041 M. The points are experimental and the line is calculated from linear regression of the experimental data. k at each temperature was obtained from the analysis of ^1H NMR spectra of the coordinated 15C5 (see table 6.7).

Table 6.9. Activation Parameters for the Ligand Exchange.

Crown Ethers	$\Delta H^{\neq}$ (kJ.mol^{-1})	$\Delta S^{\neq}$ (J.mol^{-1})	$\Delta G^{\neq}$ (kJ.mol^{-1})
15C5[a]	20 ± 2	-140 ± 6	64 ± 2[b]
15C5[c]	25 ± 1	-133 ± 4	64 ± 1[d]
B15C5	23 ± 1	-112 ± 4	56 ± 1[b]
18C6	----	----	87[e]

a, Determined from ^{13}C NMR of 15C5;

b, T=300.0 ± 0.5 K;

c, Obtained from the ^{1}H NMR observations on the coordinated 15C5;

d, T = 297.3 ± 0.5 K;

e, T = 333 ± 1 K, only free energy was calculated from k = 0.15 s^{-1} at 333 K.

A kinetic phenomenon is still observable in the case of 15C5 from its ^{1}H NMR for values of R > 1 (see figures 4.18 and 6.7). This was discussed earlier in section 6.2.3. Since, under the same conditions, no similar kinetic behavior was detected from ^{13}C NMR, the different ^{1}H resonances for the coordinated 15C5 ligand were attributed to the presence of two chemically different types of protons belonging to the same type of 15C5 - La(III) complex. The equation 6.7 shown previously was used to describe this kind of exchange. The possible mechanisms that could account for this experimental observation are given in scheme II.

Scheme II

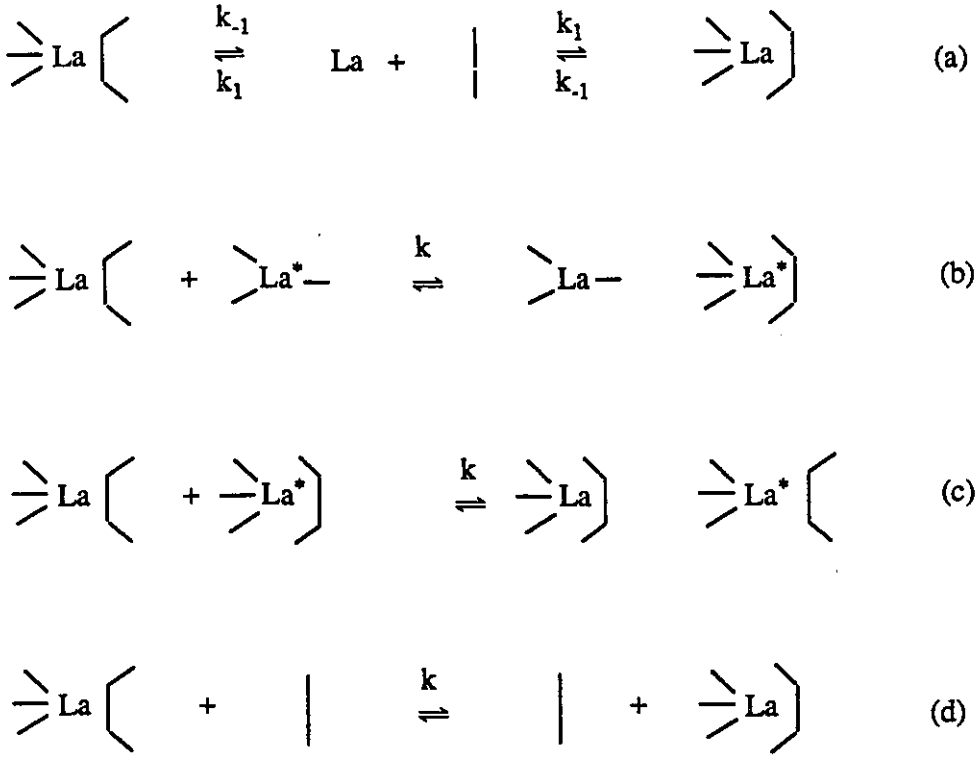

$\big|$ represents the solvated 15C5, $\big\rangle$ and $\big\langle$ are the complexed 15C5 with its protons in the "inner" ($\big\rangle$) and in the "outer" ($\big\langle$) states, and — indicates NO_3^{-1}

All four reactions shown in scheme II can cause the rearrangement of the complexed 15C5. Therefore, each of them may be responsibile for the complexed 15C5 exchange. In scheme II, the reaction (a) is dissociative and the reactions (b), (c), and (d) take place via associative pathways. The mechanisms described by reactions (c) and (d) are excluded for the coordinated 15C5 exchange since the exchange rate is independent on both the concentrations of the 1:1 complex and of the free ligand (see the spectra shown in figure 4.18). As shown in figure 4.18, the behavior of the complexed 15C5 exchange was observable in the cases of $R > 1$ where there is no free ligand in solution, indicating that the reaction (d) does not account for the exchange process. Similarly, the ^1H spectra in the region $0 < R < 1$ are the same, implying that the exchange rate of the complexed 15C5 is independent of the complex concentration which will increase with increase of R. Therefore, reaction (c) is not responsible for the process described in equation 6.7. In the reaction (b) of Scheme II, the exchange rate would depend on the concentration of the free lanthanum cation. Since the exchange behavior of the coordinated 15C5 was also observed in the cases of $R < 1$ where the concentrations of the free La(III) were equal to zero, the most plausible mechanism for the exchange of the complexed 15C5 is reaction (a).

It should be pointed out that if the coordinated 15C5 exchange occurs via the mechanism described in reaction (a) the rate constants determined respectively from the ^{13}C NMR studies at $0 < R < 1$ and from the ^1H NMR investigations at $R > 1$ should be the same, since equation 6.16 described a ligand dissociation exchange between its solvated and complexed sites, and reaction (a) represents the same process. The results reported in table 6.8 indicate that this is indeed the case. The fact that the dissociative

mechanism is the dominant contribution to the coordinated 15C5 exchange can be further checked by the activation parameters. The Eyring plot of the data given in table 6.7 is also a straight line (see figure 6.15). The activation parameters were calculated from the slope and the intercept of the plot. These values are given in table 6.9. One can see from table 6.9 that the activation parameters obtained respectively from the ^{13}C NMR studies on the ligand exchange and from the ^{1}H NMR observations on the intramolecular rearrangement are the same.

The reaction (b) in scheme II cannot be completely ruled out from the mechanisms for the exchange of the complexed 15C5. It should be noted that reaction (b) describes the process of the La(III) cation association exchange. As shown previously in this section, the La(III) cation association exchange was detected from the ^{139}La NMR studies on the system of $La(NO_3)_3$ 6 H_2O - B15C5 - AN. It is reasonable to believe that this exchange also plays a role in the system involving 15C5. Indeed, the ^{1}H NMR spectra given in figure 4.18 were different for different values of R in the cases of $R > 1$, indicating that the exchange of the complexed 15C5 is also catalyzed by the concentration of the free La(III) cation. However, considering the condition (R = 1.08) under which the ^{1}H NMR studies for the complexed 15C5 exchange were carried out, the fact that the dissociative exchange is the main mechanism is not surprising since in this case, the concentration of free La(III) is very small. In this case, the contribution of the cation association to the exchange of the complexed 15C5 may be negligible.

The kinetic studies discussed above might also help in understanding the complex structure in solution. As mentioned previously, the model postulated on the basis of the solid state structure of the complex 15C5-La(III) successfully accounted for the ^{1}H NMR data on the complexed 15C5 chemical exchange. This might indicate that the structures for this complex in solution and in the solid state are similar. Moreover, the solid state structures of the La(III) cation complexes with crown ethers may also be used to interpret the different kinetic behaviors observed in cases involving different

crown ethers. For example, the cation exchange in the system involving B15C5 is measurable by ^{139}La NMR whereas the La(III) exchange is very slow for 18C6. The different rates for the cation exchange in these two cases may be understood by considering the structures of the complexes La(III)-18C6 and La(III)-B15C5. As seen previously, the associative pathway is an important contribution for the La(III) cation exchange in the system of B15C5, plausibly because the free La(III) can make contact with the complex from the crown ether side. This contribution, however, is expected to be much smaller for the system involving 18C6. Assuming that the structures of the complex 18C6-La(III) in solution and in the solid state are the same or very similar, the approach of a free lanthanum cation to the complex is hindered from both directions: it has to face the coordinated nitrates. Furthermore, the dissociation of the complex 18C6-La(III) is also expected to be much slower than that of the La(III) complexes with 15C5 or with B15C5. Therefore, the ligand and the cation dissociation exchange in the case of 18C6 should be slower than for the cases of B15C5 or of 15C5. Finally, as shown previously, the ligand (B15C5 or 15C5) exchange was detected only through a dissociation mechanism. If the structures of these complexes are considered, this result becomes logical since the crown ether cannot easily contact the complexed La(III) cation in either case (complexes La(III)-B15C5 and La(III)-15C5).

GENERAL CONCLUSIONS

^{139}La NMR has proven to be a very sensitive technique for studying the La(III) complexation in solution. In Chapter 3 of this thesis, ^{139}La NMR spectroscopy was used to investigate the cation and anion interactions in aqueous solutions of lanthanum nitrate, chloride, and perchlorate. The ^{139}La NMR data were accounted for by the presence of 1:1 inner sphere complexes of La(III) with these three anions. The thermodynamic stability constants for these contact ion pairs were determined by introducing activity coefficient effects to the data analyses. The quadrupolar relaxation mechanism of ^{139}La in the solutions was discussed. Instead of the usual reorientational time fluctuations, fast solvent exchange in the La(III) solvation shell is believed to be the major contribution to the ^{139}La quadrupolar relaxation. The nature of the La(III) first coordination sphere in acetonitrile solution of $La(NO_3)_3$ 6 H_2O was examined by ^{139}La and ^{17}O NMR. The following model accounted for the experimental data.

$$\{La(NO_3)_3\,(AN)_x\} + H_2O \rightleftharpoons \{La(NO_3)_3\,H_2O(AN)_y\}$$

Significant line broadening was observed in the ^{17}O NMR spectra when the $H_2{}^{17}O$ molecule was coordinated to La(III). Besides a quadrupolar relaxation contribution, the indirect coupling between the ^{17}O nucleus of the coordinated water and ^{139}La is thought to contribute also to the line broadening. The coupling constant was estimated by analysis of the ^{17}O NMR spectra.

In Chapter 4, the thermodynamic study of La(III) complexes with crown ethers in non-aqueous solutions was carried out by multinuclear magnetic resonance spectroscopy. In the methanol solutions of $LaCl_3$ 7 H_2O, a 1:1 complex of La(III) with

18C6 was formed. The formation constant for the complex was determined from the lineshape analyses of the experimental ^{139}La NMR spectra. The ^{139}La NMR study on the system of $LaCl_3$ 7 H_2O - B15C5 - Methanol indicated that no complex between La(III) and the crown ether was formed in solution. In the acetonitrile solutions of $La(NO_3)_3$ 6 H_2O, 1:1 cation : crown ether complexes were quantitatively formed for La(III) with 18C6, B15C5, and 15C5. Multinuclear magnetic resonance studies on these systems indicate that the crown ethers coordinate directly to La(III) while the coordinated water and most probably the solvent (AN) molecules are expelled out from the first coordination shell of La(III) upon the complex formation.

The crystals of these complexes were prepared and their structures were determined by X-ray crystallography. These results were reported in chapter 5. In the solid states of these complexes, the first coordination spheres of La(III) were occupied by the oxygen atoms of three bidentate nitrate anions and of the crown ethers. Structural similarities were found for the La(III) complexes with crown ethers in the solution and in the solid state.

The kinetic studies of La(III) - crown ether complexes were discussed in chapter 6. Both cation and ligand exchanges are slow in the system of $La(NO_3)_3$ 6 H_2O - 18C6 - AN. 18C6 chemical exchange was only measurable by the magnetization transfer technique at high temperature. The rate constant obtained for the exchange is $k = 0.15$ s^{-1} at 333 K. When the crown ether is B15C5, the cation chemical exchange was detectable by ^{139}La NMR. The La(III) exchange occurs definitely through a dissociative mechanism. However, an associative process (involving a second cation or the nitrate counteranion) might also contribute to the cation exchange since the La(III) exchange rate is salt concentration dependent. The crown ether exchange mechanism is accessible by ^{13}C and ^{1}H NMR. The dissociative pathway is the only mechanism for the ligand (B15C5 and 15C5) exchange. Considering the structures of La(III) complexes with B15C5 and with 15C5 in solution, the dissociative mechanism must be the major contributor to the crown ether chemical exchange since the ligand cannot

make contact with La(III) from both sides of the complexes.

A kinetic process involving coordinated B15C5 and/or 15C5 was detected from the ^1H NMR spectra of the ligands. Detailed ^1H NMR observations were made on the system involving 15C5. On the basis of the La(III) - 15C5 crystal structure, a model involving "inner" and "outer" proton exchange was postulated to account for the ^1H NMR experimental data. The mechanistic study showed that this proton exchange occurs through a dissociation and recombination of the complex.

The activation parameters for B15C5 and 15C5 chemical exchanges were determined through temperature variation studies. Although the ligand exchange occurs through a dissociation process, large negative entropies of activation were obtained, suggesting a complete reorganization of the La(III) solvation shell during the exchange process.

APPENDIX I:

Equations describing the simulation of B15C5 ^{13}C NMR spectra.

For each pair of carbons in free and in coordinated sites of B15C5, the intensity of ^{13}C NMR signal can be expressed as:

$$I_i = -C \times \{P \times [1 + \tau \times (P_B \times (T_{2A}^{-1})_i + P_A \times (T_{2B}^{-1})_i)] + Q \times R\} / P^2 + R^2$$

$$P = \tau \times ((T_{2B}^{-1})_i \times (T_{2A}^{-1}) - 4\pi^2 V^2 + \pi^2 D^2) + P_A \times (T_{2A}^{-1})_i + P_B \times (T_{2B}^{-1})_i$$

$$Q = \tau \times (2\pi V - \pi D(P_A - P_B))$$

$$R = 2\pi V \times (1 + \tau((T_{2B}^{-1})_i + (T_{2A}^{-1}))) + \pi D\tau((T_{2B}^{-1})_i - (T_{2A}^{-1})) + \pi D(P_A - P_B)$$

Where $D = \nu_A - \nu_B$

$$V = 0.5 (\nu_A + \nu_B) - \nu$$

$$\tau = (k_A + k_B)^{-1}$$

and ν_A, ν_B are the ^{13}C chemical shift in Hz respectively for site A and B.

The above equations are also suitable for the La(III) cation exchange between the solvated site and the site complexed by a crown ether.

In the case of B15C5 exchange, since there are four pairs of carbons, the total intensity of the ^{13}C NMR spectra will be the sum of contributions from each pair:

$$I = \Sigma I_i \qquad (i = 1 - 4)$$

APPENDIX II:

A FORTRAN program corresponding to the equations given in Appendix I.

```
REAL Y1(1600), X(1600), V(10), Y2(1600), Y3(1600), Y4(1600), Y(1600)
C=1E3
R=1400.0
T=1.0/R
PA=0.804
PB=1.0-PA
READ(5,*,END=999) (V(I), =1, 8)
READ(5,*,END=999) PI
DO 10 I=1, 800
X(I)=5100.0+0.5*
F1=V(1) -V(8)
T2A1=1.0/PI/1.0
T2B1=1.0//1.0
DF1=0.5*(V(1)+V(8))-X(I)
P1=T*(1/T2A1/T2B1-4*PI**2*DF1**2+**2*F1**2)+PA/T2A1+PB/T2B1
Q1=T*(2*PI*DF1-PI*F1*(PA-PB))
RM1=2*PI*DF1*(1+T*(1/T2A1+1/T2B1))+PI*F1*(PA-PB)
RH1=PI*T*F1*(1/T2B1-1/T2A1)
R1=RM1+RH1
Y1(I)=C*(P1*(1+T*(PB/T2A1+PA/T2B1))+Q1*R1)/(P1*P1+R1*R1)
F2=V(2) -V(6)
DF2=0.5*(V(2)+V(6))-X(I)
T2A2=1.0/PI/1.0
T2B2=1.0//1.0
```

```
P2=T*(1/T2A2/T2B2-4*PI**2*DF2**2+PI**2*F2**2)+PA/T2A2+PB/T2B2
Q2=T*(2*PI*DF2-PI*F2*(PA-PB))
RM2=2*PI*DF2*(1+T*(1/T2A2+1/T2B2))+PI*F2*(PA-PB)
RH2=T*PI*F2*(1/T2B2-1/T2A2)
R2=RM2+RH2
Y2(I)=C*(P2*(1+T*(PB/T2A2+PA/T2B2))+Q2*R2)/(P2*P2+R2*R2)
F3=V(3)-V(5)
DF3=0.5*(V(3)+V(5))-X(I)
T2A3=1.0/PI/1.0
T2B3=1.0//1.0
P3=T*(1/T2A3/T2B3-4*PI**2*DF3*DF3+PI**2*F3*F3)+PA/T2A3+PB/T2B3

Q3=T*(2*PI*DF3-PI*F3*(PA-PB))
RM3=2*PI*DF3*(1+T*(1/T2A3+1/T2B3))+PI*F3*(PA-PB)
RH3=PI*T*F3*(1/T2B3-1/T2A3)
R3=RM3+RH3
Y3(I)=C*(P3*(1+T*(PB/T2A3+PA/T2B3))+Q3*R3)/(P3*P3+R3*R3)
F4=V(4)-V(7)
DF4=0.5*(V(4)+V(7))-X(I)
T2A4=1.0/PI/1.0
T2B4=1.0//1.0
P4=T*(1/T2A4/T2B4-4*PI**2*DF4*DF4+PI**2*F4*F4)+PA/T2A4+PB/T2B4

Q4=T*(2*PI*DF4-PI*F4*(PA-PB))
RM4=2*PI*DF4*(1+T*(1/T2A4+1/T2B4))+PI*F4*(PA-PB)
RH4=PI*T*F4*(1/T2B4-1/T2A4)
R4=RH4+RM4
Y4(I)=C*(P4*(1+T*(PB/T2A4+PA/T2B4))+Q4*R4)/(P4*P4+R4*R4)
```

```
      Y(I)=Y1(I)+Y2(I)+Y3(I)+Y4(I)
10    CONTINUE
      YMAX=Y(1)
      DO 50 I=2,800
      IF(YMAX.GE.Y(I)) GO TO 50
      YMAX=Y(I)
50    CONTINUE
      DO 40 I=1,800
      Y(I)=Y(I)/YMAX*10.0
40  WRITE(6,300) X(I), Y(I)
300   FORMAT(6F10.4)
999   STOP
      END
```

Note: A data file for this program contains ^{13}C chemical shifts (in Hz) and π value.

APPENDIX III:

An execution program for running a FORTRAN program on a mainframe computer.

```
/* this program will run a VS FORTRAN program.
It is invoked by typing:
F <program name> [( [Nocompile] [Single] [Data=< file name>]
[Result=<file name>]
[Library=<text library name>] ]
where optional arguments are:
Nocompile: Used if a compiled TEXT version exists.
Single: Specifies that the single precision IMSL library should be used. The
default is double precision.
Data: Gives the name of the input disk file, of filetype DATA.
The default is the program name.
Result: Gives the name of the result file, of filetype RESULT. The default is the
program name.
Library: Gives the name of a user supplied text library.
In a fortran program, the file numbers used must be: 5 for input from disk data
file; 6 for output to disk data file; 7 for input/output with the terminal.*/
PARSE UPPER ARG programname '(' op.1 op.2 op.3 op.4 op.5
dataname=programname
resultname=programname
imsllibrary='IMSLDLIB'
userlibrary=''
DO i=1 TO 5
PARSE VAR op.i option '=' argument
```

```
IF ABBREV('NOCOMPILE',option,1) THEN compile='no'
IF ABBREV('DATA',option,1) THEN dataname=argument
IF ABBREV('RESULT',option,1) THEN resultname=argument
IF ABBREV('SINGLE',option,1) THEN imsllibrary='IMSLSLIB'
IF ABBREV('LIBRARY',option,1) THEN userlibrary=argument
END
IF compile /= 'no' THEN 'FORTVS' programname '(SDUMP'
'GLOBAL TXTLIB VLNKMLIB VFORTLIB CMSLIB PLOTLIB' imsllibrary
'FILEDEF 3 DISK' DATANAME 'DATA A'
'FILEDEF 5 DISK' DATANAME 'DATA A'
'FILEDEF 6 DISK' RESULTNAME 'RESULT A (LRECL 130'
'FILEDEF 7 DISK' RESULTNAME 'OUTPUT A(LRECL 130'
'FILEDEF 8 TERMINAL'
'ERASE' PROGRAMNAME 'LISTING'
'LOAD' PROGRAMNAME '(START'
```

Note: The name for this program is F EXEC. To run a FORTRAN program, type: F filename. A FORTRAN program to be run must be saved as <filename fortran>.

REFERENCES:

1, K. B. Yatsimirskii and N. K. Davidenko, *Coord. Chem. Rev.* , **27,** 223 (1979).

2, A. D. Sherry and C. F. G. C. Geraldes, in *"Lanthanide Probes in Life, Chemical and Earth Sciences"*, Ed., J.-C. G. Bunzli and G. R. Choppin, **Chap. 4,** Elsevier, New York, (1989).

3, M. M. Probst, T. Radnai, K. Heinzinger, P. Bopp, and B. M. Rode, *J. Chem. Phys.*, **89,** 753 (1985).

4, S. F. Lincoln, Adv. *Inorg. Bioinorg. Mechanisms,* **4,** 217 (1986).

5, C. Cossy and A. E. Merbach, *Pure & Appl. Chem.*, **60,** 1785 (1988).

6, B. W. Matthews and L. H. Weaver, *Biochemistry,* **13,** 1719 (1974).

7, L. Lee and B. D. Sykes, *Biochem.*, **19,** 3208 (1980).

8, W. DeW. Horrocks Jr., *Adv. Inorg. Biochem.*, **4,** 201 (1982).

9, C.-L. A. Wang, R. R. Aquaron, P. C. Leavis, and J. Gergely, *Eur. J. Biochem.*, **124,** 7 (1982).

10, R. J. P. Williams, *Struture and Bonding,* **50,** 79 (1982).

11, M. T. Henzl, W. D. McCubbin, C. M. Kay, and E. R. Birnbaun, *J. Biol. Chem.*, **260,** 8447 (1985).

12, a, J. Reuben, *Naturwissenschaften,* **62,** 172(1975).

b, J. Reuben, *"Handbook on the Physics and Chemistry of Rare Earths"*, **Vol. 4, Chap. 39,** 515 (1979).

13, E. Nieboer, *Structure and Bonding,* **22,** 1 (1975).

14, K. J. Ellis, *Inorg. Perspect. Biol. Med.*, **1,** 101 (1977).

15, M. E. Switzer, *Sci. Prog. Oxford,* **65,** 19 (1978).

16, R. B. Martin and F. S. Richardson, *Quat. Rev. Biophys.*, **12,** 181 (1979).

17, C. H. Evans, *Trends Biol. Sci.*, **445** (1983).

18, D. M. Dooley and J. H. Dawson, *Coord. Chem. Rev.*, **60,** 1 (1984).

19, F. S. Richardson, *Chem. Rev.*, **82,** 541 (1982).

20, C. F. Meares and T. G. Wensel, *Acc. Chem. Res.*, **17**, 202 (1984).

21, a, W. DeW. Horrocks Jr. and D. R. Sudnick, *Acc. Chem. Res.*, **14,** 384 (1981).

b, W. DeW. Horrocks Jr. and M. Albin, *Prog. Inorg. Chem.*, **31**, 1 (1984).

22, J.-C. G. Bunzli, in *"Lanthanide Probes in Life, Chemical and Earth Sciences"*, Ed., J.-C. G. Bunzli and G. R. Choppin, **Ch. 7**, Elsevier, New York, (1989).

23, C. J. Pederson, *J. Am. Chem. Soc.*, **89**, 7071 (1967).

24, B. Dietrich, J. M. Lehn, and J. P. Sauvage, *Tetrahedron Lett.*, 2885 (1969).

25, E. P. Kyba, M. G. Siegel, L. R. Sousa, G. Sogah, and D. J. Cram, *J. Am. Chem. Soc.*, **95**, 2691 (1973).

26, E. Weber and F. Vogtel, *Top. Curr. Chem.*, **98,** 1 (1981).

27, A. V. Bajaj and N. S. Poonia, *Coord. Chem. Rev.*, **87**, 55 (1988).

28, J.-C. G. Bunzli and D. Wessner, *Coord. Chem. Rev.*, **60,** 191 (1984).

29, C. J. Pedersen, *J. Am. Chem. Soc.*, **89,** 2495 (1967).

30, A. Cassol, A. Seminara, and G. De Paoli, *Inorg. Nucl. Chem. Lett.*, **9,** 1163 (1973).

31, F. Nicolo, D. Plancherel, J.-C. G. Bunzli, and G. Chapuis, *Helv. Chim. Acta,* **70,** 1798 (1984).

32, R. D. Rogers and L. K. Kurihama, *Inorg. Chem.*, **26,** 1498 (1987).

33, R. D. Rogers and L. K. Kurihama, *Inorg. Chim. Acta,* **130,** 131 (1987).

34, J.-C. G. Bunzli and D. Wessner, *Helv. Chim. Acta,* 64, 582 (1981).

35, J.-C. G. Bunzli, *"Handbook on the Physics and Chemistry of Rare Earths"*, Ed., K. A. Gschneidner, Jr. and L. Eyring, **Chap. 60,** Elsevier, New York, (1987).

36, J.-C. G. Bunzli and D. Wessner, *Helv. Chim. Acta*, **61**, 1454 (1978).

37, J. D. J. Backer-Dirks, J. E. Cooke, A. M. R. Galas, J. S. Ghotra, C. J. Gray, F. A. Hart, and M. B. Hursthouse, *J. Chem. Soc. Dalton Trans.*, 2191 (1980).

38, A. Seminara and A. Musumeci, *Inorg. Chim. Acta*, **39**, 9 (1980).

39, J. D. Simon, W. R. Moomaw, and T. M. Ceckler, *J. Phys. Chem.*, **89**, 5659 (1985).

40, M. C. Almasio, F. Arnaud-Neu, and M. J. Schwing-Weill, *Helv. Chim. Acta*, **66**, 1296 (1983).

41, R. M. Izatt, J. S. Brasdshaw, S. A. Nielsen, J. D. Lamb, and J. J. Christensen, *Chem. Rev.*, **85**, 271 (1985).

42, C. Detellier, H. P. Graves, and K. M. Briere, *" Alkali Metal NMR Studies of Synthetic and Natural Inophore Complexes"*, **Chap. 4**, Ed., E. Buncel and J. Jones, Elsevier, New York, (1991).

43, R. K. Harris, *"Nuclear Magnetic Resonance Spectroscopy "*, Second Edition, Longman Froup UK Limited, England, (1986).

44, J. Mason, *"Multinuclear NMR"*, Plenum Press, New York, (1987).

45, T. C. Farrar and E. D. Becker, *"Pulse and Fourier Transform NMR"*, Acad. Press, New York, (1971).

46, A. Abragam, *"The principles of Nuclear Magnetism"*, Oxford University Press, New York, (1985).

47, J. K. M. Sanders and B. K. Hunter, *"Modern NMR Spectroscopy: A Guide for Chemists"*, Oxford University Press, New York, (1987).

48, a, F. Bloch, *Phys. Rev.*, **70**, 460 (1946).

b, F. Bloch, W. W. Hansen, and M. Packard, *Phys. Rev.*, **70**, 474 (1946).

49, F. A. Bovey, *"Nuclear Magnetic Spin Resonance"*, Second Edition, Academic Press, San Diego, (1987).

50, R. K. Harris and B. E. Mann, *"NMR and the Periodic Table"*, Academic Press, London, (1979).

51, J. Sandstrom, *"Dynamic NMR Spectroscopy"*, Academic Press, New York, (1982).

52, P. Laszlo, *Progr. NMR Spectr.*, **13,** 257 (1979).

53, S. F. Lincoln, *Progr. Reaction Kinetics*, **9,** 1 (1977).

54, C. Brevard and P. Granger, *"Handbook of High Resolution Multinuclear NMR"*, John Wiley and Sons, New York, (1981).

55, D. Rehder, in *"Multinuclear NMR"*, Ed. J. Mason, Chap. 9, Plenum Press, New York, (1987).

56, W. H. Chambers and D. Williams, *Phys. Rev.*, **76,** 461 (1949).

57, W. Dickinson, *Phys. Rev.*, **76,** 1414 (1949).

58, K. Nakamura and K. Kawamura, *Bull. Chem. Soc. Japan*, **44,** 330 (1971).

59, J. Reuben, *J. Phys. Chem.*, **79,** 2154 (1975).

60, J. Reuben and Z. Luz, *J. Phys. Chem.*, **80,** 1357 (1976)

61, L. S. Smith, Jr., D. C. McCain, and D. L. Wertz, *J. Am. Chem. Soc.*, **98,** 5125 (1976).

62, D. C. McCain, *J. Inorg. Nucl. Chem.*, **42,** 1185 (1980).

63, O. Lutz and H. Oehler, *J. Magn. Resonance*, **37**, 261 (1980).

64, V. P. Tarasov, G. A. Kirakosyan, S. V. Trots, Yu. A. Buslaev, and V. T. Panyushkin, *Koord. Khim.*, **9,** 205 (1983).

65, D. F. Evans and P. H. Missen, *J. Chem. Soc., Dalton Trans.*, 1929 (1982).

66, P. L. Rinaldi, S. A. Khan, G. R. Choppin, and G. C. Levy, *J. Am. Chem. Soc.*, **101,** 1350 (1979).

67, C. F. G. C. Geraldes and A. D. Sherry, *J. Magn. Resonance*, **66,** 274 (1986).

68, J. C. G. Bünzli, A. E. Merbach, and R. M. Nielson, *Inorg. Chim. Acta*, **139,** 151 (1987).

69, Y. Ducommun, L. Helm, G. Laurenczy, and A. E. Merbach, *Magn. Reson. Chem.*, **26,** 1023 (1988).

70, A. Fratiello, V. Kubo-Anderson, T. Bolinger, C. Cordero, B. DeMerit, T. Flores, and R. Perrigan, *J. Solution Chem.*, **18,** 313 (1989).

71, S. J. Lyle and M. Rahman, *Talanta,* **10,** 1177 (1963).

72, G. W. Gokel, D. J. Cram, C. L. Liotta, H. P. Harris, and F. L. Cook, *Org. Synth.*, **57,** 30 (1977).

73, F. G. Riddell, S. Arumugam, and B. G. Cox, *J. Chem. Soc., Chem. Commun.*, 1890 (1987).

74, D. C. Shungu and R. W. Brigga, *J. Magn. Reson.*, **77,** 491 (1988).

75, G. Robinson, P. W. Kuchel, and B. E. Chapman, *J. Magn. Reson.*, **63,** 314 (1985).

76, *SAS User's Guide: Statistics,* **Version 5,** 198X, Chap. 25, p. 575.

77, D. A. Kleier and G. Binsch, DNMR3, Program 165, *Quantum Chemistry Program Exchange,* Indiana University, U.S.A. (1970).

78, *SAS/GRAPH Software,* **Version 6,** (1990).

79, F. H. Spedding, M. J. Pikal, and B. O. Ayers, *J. Phys. Chem.*, **70,** 2440 (1966).

80, F. H. Spedding, L. E. Shiers, M. A. Brown, J. L. Derer, D. L. Swanson, A. J. Habenschuss, *J. Chem. Eng. Data,* **20,** 8 (1975).

81, F. H. Spedding, P. F. Cullen, and A. Habenschuss, *J. Phys. Chem.*, **78,** 1106 (1974).

82, (a) A. Habenschuss and F. H. Spedding, *J. Chem. Phys.*, **70,** 2797 (1979);
(b) *Ibid* **70,** 3758 (1979);
(c) *Ibid* **73,** 442 (1980).

83, (a) A. H. Narten and R. L. Hahn, *J. Phys. Chem.*, **87,** 3193 (1983).
(b) B. K. Annis, R. L. Hahn, and A. H. Narten, *J. Chem. Phys.*, **82,** 2086 (1985).

84, (a) L. S. Smith and D. L. Wertz, *J. Am. Chem. Soc.*, **97,** 2365 (1975);
(b) M. L. Steele and D. L. Wertz, *Ibid* **98,** 4424 (1976);

(c) M. L. Steele and D. L. Wertz, *Inorg. Chem.*, **16,** 1225 (1977).

85, P. J. Breen and W. deW. Horrocks Jr., *Inorg. Chem.*, **22,** 536 (1983).

86, C. Cossy, L. Helm, and A. E. Merbach, *Inorg Chem.*, **27,** 1973 (1988).

87, H. B. Silber, R. Bakhshandehfar, L. A. Contreras, F. Gaizer, M. Gonsalves, and S. Ismail, *Inorg. Chem.*, **29,** 4473 (1990).

88, J.-C. G. Bunzli and J.-R. Yersin, *Inorg. Chem.*, **18,** 605 (1979).

89, H. B. Silber and R. L. Campbell, *J. Less - Common Met.*, **149,** 265 (1989).

90, A. Fratiello, V. Kubo-Anderson, S. Azimi, T. Flores, E. Marinez, D. Matejka, R. Perrigan, and M. Vigil, *J. Solution Chem.*, **19,** 811 (1990).

91, A. Fratiello, V. Kubo-Anderson, T. Bolinger, C. Cordero, B. DeMerit, T. Flores, D. Matejka, and R. Perrigan, *J. Magn. Resonance,* **83,** 358 (1989).

92, C. Detellier, in"NMR of Newly Accessible Nuclei", Vol2, Ed. by P. Laszlo, Chapter 5, Acad. Press, New York, (1983).

93, J. Reuben and D. Fiat, *J. Chem. Phys.*, **51,** 4909 (1969).

94, L. A. Bromley, J. Chem. Thermod., 4, 669 (1972).

95, "Handbook of aqueous Electrolyte Thermodynamics" J. F. Zemaitis, Jr., D. M. Clark, M. Rafal, and N. C. Scrivner, DIPPR Pul., New york, (1986).

96, Z. Kollarik, *Coll. Czech. Chem. Comm.*, **32,** 435 (1967)

97, A Anagnostopoulos and P. O. Sakellaridis, *J. Inorg. Nucl. Chem.*, **32,** 1740 (1970)

98, G. Kasabov, L. Genov, and I. Dukov, *Godishn. Vyssh. Khim.-Tekhnol. Inst., Sofiya,* **24,** 265 (1978); *Chem. Abstr.*, **96,** 111080c (1982).

99, R. V. Southwood-Jones, W. L. Earl, K. E. Newman, and A. E. Merbach, *J. Chem. Phys.*, **73,** 5909 (1980)

100, D. P. Fay, D. Litchinsky, and N. Purdie, *J. Phys. Chem.*, **73,** 544 (1969)

101, A. Gierer, K. Wirtz, and *Z. Naturforsch., Teil A* **8,** 532 (1953)

102, J. Reuben, *Biochemistry*, **10,** 2834 (1971).

103, a, J.-C. G. Bunzli and M. M. Vuckovic, *Inorg. Chim. Acta,* **73,** 53 (1983).

b, J.-C. G. Bunzli and M. M. Vuckovic, *Ibid*, **90**, 105 (1984).

c, J.-C. G. Bunzli and J.-R. Yersin, *Ibid*, **94**, 301 (1984).

d, J.-C. G. Bunzli, J.-R. Yersin, and C. Mabillard, *Inorg. Chem.*, **21**, 1471 (1982).

e, J.-C. G. Bunzli, C. Mabillard, and J.-R. Yersin, *Ibid*, **21**, 4214 (1982).

f, J.-C. G. Bunzli and J.-R. Yersin, *Helv.Chim. Acta.*, **65**, 2498 (1982).

104, J.-C. G. Bunzli and C. Mabillard, *Inorg. Chem.*, **25**, 2750 (1986).

105, D. L. Wertz and S. T. Finch, *Inorg. Chem.*, **18**, 1590 (1979).

106, H. B. Silber and T. Mioduski, *Inorg. Chem.*, **23**, 1577 (1984).

107, M. Frechette, I. R. Butler, R. Hynes, and C Detellier, *Inorg. Chem.*, (1992).

108, J. P. Kintzinger in " *NMR 17, Basic Principles and Progress*", Ed. by P. Diehl, E. Fluck, and R. Kosfeld, Springer-Verlag Berlin Heidelberg Press, New York, (1981).

109, Z. Luz and G. Yagil, *J. Phys. Chem.*, **70**, 554 (1966).

110, D. Hugi-Cleary, L. Helm, and A. E. Merbach, *Helv. Chim. Acta*, **68**, 545 (1985).

111, L. Helm, L. I. Elding, and A. E. Merbach, *Helv. Chim. Acta*, **67**, 1453 (1984).

112, S. Aygen, H. Hanssum, and R. Van Eldik, *Inorg. Chem.*, **24**, 2853 (1985).

113, O. Lutz, W. Nepple, and A. Nolle, *Z. Naturforsch.*, **31 a**, 1046 (1976).

114, J. Virlet and G. Tantot, *Chem. Phys. Lett.*, **44**, 296 (1976).

115, O. Howarth in " *Multinuclear NMR* " Ed. J. Mason, **Chap. 5**, Plenum Press, New York, (1987).

116, C. Detellier, H. P. Graves, and K. M. Briere, " *Alkali Metal NMR Studies of Systhetic and Natural Ionophore Complexes*", Chapter 4, Ed., E. Buncel and J. R. Jones, Elsevier, (1992).

117, R. M. Izatt, J. D. Lamb, J. J. Christensen, and B. L. Haymore, *J. Am. Chem. Soc.*, **99**, 8344 (1977).

118, S. F. Lincoln, *Prog. Reac. Kinetics*, **9**, 1 (1979).

119, V. Gold and L. Z. Zdunek, *J. Chem. Soc., Faraday Trans. 2*, **78**, 1835 (1982).

120, L. S. Smith, Jr., D. C. McCain, and D. L. Wertz, *J. Am. Chem. Soc.*, **98**, 5125 (1976).

121. D. L. Wertz and S. T. Finch, *Inorg. Chem.*, **18**, 1590 (1979).

122, E. Ohyoshi and S. Kohata, *Polyhedron*, **8**, 1562 (1989).

123, J. Zhou and X. Wu, *He Huaxue Yu Fangsshi Huaxue*, **6**, 78 (1984).

124, J.C. G. Bunzli and F. Pilloud, *Inorg. Chem.*, **28**, 2638 (1989).

125, M. Bisnaire, C. Detellier, and D. Nadon, *Can. J. Chem.*, **60**, 3071 (1982).

126, H. D. H. Stover, A. Delville, and C. Detellier, *J. Am. Chem. Soc.*, **107**, 4167 (1985).

127, A. Delville, H. D. H. Stover, and C. Detellier, *J. Am. Chem. Soc.*, **107**, 4172 (1985).

128, H. D. H. Stover and C. Detellier, *J. Phys. Chem.*, **93**, 3174 (1989).

129, K. M. Briere, *"Thesis for Ph. D. Degree"*, Chemistry Department, University of Ottawa, (1990).

130, R. B. King and P. R. Hechley, *J. Am. Chem. Soc.*, **96**, 3118 (1974).

131, P. Lu, C. Shen, Y. Fan, S. Jin, S. Zhang, and F. Yu, *Fenzi Kexue Yu Huaxue Yanjiu*, **3**, 77 (1983).

132, J.-C. G. Bunzli, B. Klein, G. Chapuis, and K. J. Schenk, *Inorg. Chem.*, **21**, 808 (1982).

133, R. D. Shannon, *Acta Crystallogr.*, **A 32**, 751, 1976.

134, J.-C. G. Bunzli, D. Wessner, and H. T. T. Oahn, *Inorg. Chim. Acta*, **32**, L33 (1979).

135, J.-C. G. Bunzli and A. Giorgetti, *J. Less-Common Met.*, **112**, 355 (1985).

136, N. K. Dally, *" Synthetic Multidentate Macrocyclic Compounds"*, Ckapter 4, Ed. R. E. Izatt and J. J. Christensen, Academic Press, New York, (1978).

137, D. F. Grant and E. J. Gabe, *J. Appl. Crystallogr.*, **11**, 114 (1978).

138, E. J. Gabe, F. L. Lee, and Y. Lepage, *J. Appl. Crystallogr.*, **22,** 384 (1989).

139, Y. Lepage, E. J. Gabe, and G. J. Gainsford, *J. Appl. Crystallogr.*, in press.

140, C. A. Chang and V. C. Sekhar, *Inorg. Chem.*, **26,** 1982 (1987).

141, V. C. Sekhar and C. A. Chang, *Inorg. Chem.*, **25,** 2061 (1986).

142, E. Brucher and A. D. Sherry, *Inorg. Chem.*, **29,** 1555 (1990).

143, M. De Jonghe and W. D'Olieslager, *Inorg. Chim. Acta,* **109,** 7 (1985).

144, E. L. Yee, O. A. Gansow, and M. J. Weaver, *J. Am. Chem. Soc.*, **102,** 2278 (1980).

145, J.-C. G. Bunzli, H. T. T. Oanh, and B. Gillet, *Inorg. Chim. Acta,* **53,** L219 (1981).

146, D. E. Woessner, *J. Chem. Phys.*, **35,** 41(1961).

147, V. Gold and L. Zdunek, *J. Chem. Soc. Faraday Trans.*, **78,** 1835 (1982).

148, P. W. Kuchel, B. T. Bulliman, B. E. Chapman, and K. Kirk, *J. Magn. Reson.*, **74,** 1 (1987).

149, J. R. Alger and R. G. Shulman, *Quart. Rev. Biophys.*, **17,** 83 (1984).

150, S. L. Campbell-Burk, J. A. den Hollander, J. R. Alger, and R. G. Shulman, Biochem., 26, 7493 (1987).

151, G. Robinson, B. E. Chapman, and P. W. Kuchel, *Eur. J. Biochem.*, **143,** 643 (1984).

152, F. G. Riddell, S. Arumugam, and B. G. Cox, *J. Chem. Soc., Chem. Commun.*, 1890 (1987).

153, D. C. Shungu and R. W. Briggs, *J. Magn. Reson.*, **77,** 491 (1988).

154, G. A. Morris and R. Freeman, *J. Magn. Resonance,* **29,** 433 (1978).

155, E. Shchori, J. Jagur-Grodinski, Z. Luz, and M. Shporer, *J. Am. Chem. Soc.*, **93,** 7133 (1971).

156, E. Shchori, J. Jagur-Grodinski, and M. Shporer, *J. Am. Chem. Soc.*, **95,** 3842 (1973).

157, H. P. Graves and C. Detellier, *J. Am. Chem. Soc.*, **110,** 6091 (1988).

158, A. Delville, H. D. H. Stover, and C. Detellier, *J. Am. Chem. Soc.*, **109,** 7293 (1987).

159, K. M. Briere and C. Detellier, *New J. Chem.*, **13,** 145 (1989).

160, E. Schmidt and A. I. Popov, *J. Am. Chem. Soc.*, **105,** 1873 (1983).

161, M. Shporer and Z. Luz, *J. Am. Chem. Soc.*, **97,** 665 (1973).

162, E. L. Yee, O. A. Gansow, and M. J. Weaver, *J. Am. Chem. Soc.*, **102,** 2278 (1980).

163, A. Delville, H. D. H. Stover, and C. Detellier, *J. Am. Chem. Soc.*, **109,** 7293 (1987).